

**SYNTHETIC AND ANALYTICAL STUDIES**

**OF**

**BIOMIMETIC METAL COMPLEXES**

**THESIS**

Submitted in fulfilment of the requirements for the Degree of

**DOCTOR OF PHILOSOPHY**

of Rhodes University

by

**KEVIN WAYNE WELLINGTON**

**Department of Chemistry**

**Rhodes University**

**June 1999**

## TABLE OF CONTENTS

	page
<b>1 INTRODUCTION</b>	1
<b>1.1 METALLOENZYMES</b>	1
1.1.1 Background	1
1.1.2 The structure of metalloenzymes	2
1.1.3 Functions of metalloenzymes	3
<b>1.2 TYROSINASE</b>	5
1.2.1 Background	5
1.2.2 The active sites of tyrosinase and haemocyanin	8
1.2.3 Studies of the active site of haemocyanin	9
1.2.3.1 <i>Early studies</i>	9
1.2.3.2 <i>More recent studies</i>	10
1.2.4 Similarities between tyrosinase and haemocyanin	11
1.2.5 A possible mechanism of oxidation by tyrosinase	13
1.2.6 Applications of the enzyme tyrosinase	15
<b>1.3 THE BIOMIMETIC APPROACH TO TYROSINASE ANALOGUES</b>	16
1.3.1 The selection of ligands for dinuclear copper complexes	18
1.3.2 Coordination considerations in the reaction of copper complexes with dioxygen	20
1.3.3 The mode of binding of dioxygen in oxyhaemocyanin and oxytyrosinase	22
1.3.4 Synthetic biomimetic models of haemocyanin and tyrosinase	24
<b>1.4 THE IMPORTANCE OF METAL-DIOXYGEN BONDING</b>	37
<b>1.5 OBJECTIVES OF THE PRESENT INVESTIGATION</b>	41

<b>2 DISCUSSION</b>	42
<b>2.1 LIGAND DESIGN AND RATIONALE</b>	42
<b>2.2 LIGAND SYNTHESSES</b>	43
2.2.1 Biphenyl ligands	44
2.2.2 1,10-Phenanthroline ligands	54
2.2.3 Schiff base ligands prepared from diketones	59
2.2.4 The Baylis-Hillman approach to ligand syntheses	64
2.2.5 Macrocyclic syntheses	70
2.2.6 Dendrimer synthesis	73
<b>2.3 COMPLEXATION AND COMPUTER MODELLING STUDIES</b>	78
2.3.1 Complexation Studies	78
2.3.2 Copper Complexes	80
2.3.3 Computer Modelling Studies	90
2.3.4 Other Transition Metal Complexes	101
2.3.4.1 Cobalt Complexes	101
2.3.4.2 Nickel Complexes	114
2.3.4.3 Platinum Complexes	127
<b>2.4 ELECTROCHEMICAL STUDIES: CYCLIC VOLTAMMETRY<sup>1</sup></b>	136
2.4.1 Copper Complexes	137
2.4.2 Cobalt Complexes	142
2.4.3 Nickel Complexes	145
<b>2.5 BIOMIMETIC EVALUATION OF THE CATALYTIC ACTIVITY OF     COPPER COMPLEXES</b>	150
<b>2.6 CONCLUSIONS</b>	155

<b>3 EXPERIMENTAL</b>	157
<b>3.1 GENERAL</b>	157
<b>3.2 PROCEDURES FOR LIGAND SYNTHESSES</b>	158
3.2.1 Biphenyl ligands	158
3.2.2 1,10-Phenanthroline ligands	167
3.2.3 Schiff base ligands prepared from diketones and 2-(2-aminoethyl)pyridine	172
3.2.4 The Baylis-Hillman approach to ligand synthesis	177
3.2.5 Macrocyclic syntheses	181
3.2.6 Dendrimer synthesis	185
<b>3.3 SYNTHETIC PROCEDURES FOR THE PREPARATION OF     COMPLEXES</b>	185
3.3.1 Copper Complexes	185
3.3.2 Cobalt Complexes	190
3.3.3 Nickel Complexes	193
3.3.5 Platinum Complexes	195
<b>3.4 PROCEDURE FOR THE COMPUTER MODELLING OF     COMPLEXES</b>	198
<b>3.5 ELECTROCHEMICAL STUDIES: CYCLIC VOLTAMMETRY</b>	199
<b>3.6 METHOD FOR THE EVALUATION OF THE CATALYTIC     ACTIVITY OF COPPER COMPLEXES</b>	205
<b>4 REFERENCES</b>	206
<b>5 APPENDIX: CRYSTAL STRUCTURE DATA</b>	220

## ACKNOWLEDGEMENTS

I am grateful to my supervisor Prof. Perry Kaye for granting me the opportunity to work with him and also for the advice, support and encouragement over the years. Also to Prof. Nyokong, my co-supervisor who has, over the years, been a source of inspiration and encouragement, for her support and advice with the electrochemistry. I would also like to thank Dr. Cheryl Sacht for informative discussions concerning coordination chemistry. Special thanks go to Dr. Gary Watkins, also for informative discussions, but most of all for his generous support and guidance with the coordination chemistry section despite not being one of my supervisors.

I am also grateful to my colleagues, who over the years, have made my stay in the department a pleasant one, for their support and encouragement. I want to thank, in particular, Andre Daubinet who has always been very willing to assist with the molecular modelling programme Cerius<sup>2</sup>.

I am very grateful to Mintek and, also to the FRD and DAAD for their financial support. I want, in particular, to thank Mr. Bob Tait, Dr. Kathy Sole and Dr. Brian Green at Mintek.

I also want to thank the technical staff (Mr Aubrey Sonneman and Mr. Andre Adriaan), the secretaries (Mrs. Margie Kent and Mrs. Bernita Tarr), and the storeman (Mr. Johan Buys) for their support, and Ms Leanne Cook (University of the Witwatersrand) for X-ray structure determinations.

Most of all, I would like to thank my parents for their support and encouragement over the years. I dedicate this thesis to my parents in appreciation of their support and encouragement.

## ABSTRACT

Several series of novel diamido, diamino and diimino ligands containing different spacers and heterocyclic donors have been synthesised. The spacers include the flexible biphenyl, the rigid 1,10-phenanthroline and various acyclic moieties, while the heterocyclic donors comprise pyridine, imidazole or benzimidazole groups. These ligands have been designed to complex copper and act as biomimetic models of the active site of the enzyme, tyrosinase, and their complexes with copper, cobalt, nickel and platinum have been analysed using microanalytical, IR, UV-Visible and cyclic voltammetric techniques. Attempted reduction of the biphenyl-based diimino ligands resulted in an unexpected intramolecular cyclisation affording azepine derivatives, the structures of which were elucidated with the aid of single crystal X-ray analysis of cobalt and nickel complexes. Computer modelling methods have been used to explore the conformational options of the copper complexes, and to assess the accessibility of the dinuclear copper site to substrate molecules. Computer modelling has also been used, in conjunction with the available analytical data, to visualise the possible structures of selected ligands and complexes.

The copper complexes, although predominantly polymeric, were evaluated as biomimetic catalysts using 3,5-di-*t*-butylphenol and 3,5-di-*t*-butylcatechol as substrates. Some of the complexes clearly displayed biomimetic potential, exhibiting both phenolase and catecholase activity.

**ABBREVIATIONS**

CDI	carbonyldiimidazole
CH <sub>2</sub> Cl <sub>2</sub>	dichloromethane
CHCl <sub>3</sub>	chloroform
CT	charge transfer
CV	cyclic voltammetry
DTBC	3,5-di- <i>tert</i> -butylcatechol
DTBP	3,5-di- <i>tert</i> -butylphenol
DMF	<i>N, N</i> -dimethylformamide
DMSO	dimethylsulfoxide
Et <sub>3</sub> N	triethylamine
Et <sub>2</sub> O	diethyl ether
EPR	electron paramagnetic resonance
EXAFS	extended X-ray absorption fine structure
HCBD	hexachlorobutadiene
IR	infrared
MeCN	acetonitrile
NMR	nuclear magnetic resonance
THF	tetrahydrofuran
UV	ultraviolet

## INTRODUCTION

### 1.1. METALLOENZYMES

#### 1.1.1. Background

Metal ions are often found as constituents of proteins and enzymes. In fact, approximately one third of enzymes known require metal ions for activity,<sup>1</sup> and it is apparent that nature has utilized the special properties of metal ions to perform a wide variety of specific functions which may be crucial in life processes. In Australia, for example, the deficiency of copper in certain areas adversely affected the nervous system of sheep and caused anaemia and wool deterioration.<sup>1</sup>

Metal ions in proteins and enzymes can be roughly divided into two classes, *viz.*, chemical and structural metals. Metals which enter directly into biological reactions in a chemical manner are referred to as chemical metals, e.g. iron(II) in its role in the oxidation-reduction reactions catalysed by peroxidases and ferredoxins or the bonding of oxygen by haemoglobin. Those metals that stabilise the protein for biological function (e.g. calcium(II) in thermolysin) or indirectly promote catalysis by inducing a required orientation of the substrate or catalytic group in the protein (e.g. magnesium(II) in phosphoglucomutase) are referred to as structural metals.<sup>1</sup>

It has also been observed<sup>2</sup> that metal ions in proteins and enzymes are able to perform in two ways: i) as an integral part of the protein, removable only by extreme chemical attack and exhibiting high metal-ion specificity in function, or ii) loosely bound to the substrate or enzyme, readily dialysable and exhibiting low metal-ion specificity in catalytic function.

### 1.1.2. The Structure of Metalloenzymes

Metalloenzymes contain metal ions that are tightly bound and always isolated with the protein. The structure of the enzyme is destroyed upon removal of the metal ions. The metal ions are mainly responsible for electron transfer. Alcohol dehydrogenase (containing  $Zn^{2+}$ ),<sup>3</sup> arginase (containing  $Mn^{2+}$ ),<sup>4</sup> ferredoxin (containing  $Fe^{2+}$ ),<sup>5</sup> haemocyanin (containing  $Cu^{2+}$ )<sup>5</sup> and urease (containing  $Ni^{2+}$ )<sup>6</sup> are all metalloenzymes. In the case of the proteins, haemoglobin and the cytochromes, however, the metal ( $Fe^{2+}$  or  $Fe^{3+}$ ) is part of the haeme prosthetic group (non-protein). Metal ions frequently occur within the active site of the enzyme and resemble protons in that they are electrophiles, which are able to accept an electron pair for the formation of a coordinate-covalent bond with anionic or neutral ligands to yield complexes of various geometries, e.g., linear, square planar, tetrahedral or octahedral.<sup>7</sup>

The ability of free amino and carboxyl groups in proteins to bind to metals allows for the establishment of an active conformation, as in the case of carboxypeptidase A.<sup>8</sup> This enzyme, which promotes hydrolysis, has  $Zn^{2+}$  in its active site. When the ester substrate fits into the hydrophobic pocket of the enzyme, the zinc stabilises the enzyme-substrate complex by coordinating to the developing oxygen anion as the water attacks the carbonyl carbon of the ester substrate. In carbonic anhydrase, zinc binds to water making it sufficiently acidic to permit the loss of a proton and formation of a nucleophilic-hydroxyl group.

It is known that the biological role of metals in metalloenzymes is highly specific, and that the same metal ion in a different protein is able to perform different functions. The range of functions promoted, however, is largely dictated by the protein environment.

### 1.1.3. Functions of Metalloenzymes

Metalloenzymes function in many essential physiological processes. They effect a variety of important chemical transformations, often involving small molecule substrates or products such as molecular oxygen, hydrogen, nitrogen and water. The transformations occur with exceptional substrate regio- and stereoselectivity under mild conditions. Various metal clusters or ions have been observed at the active sites, and living systems have utilised rudimentary recurring, structures that have been modified or adapted for particular purposes. The role of metalloenzymes is to perform specific catalytic functions. Dioxygen metabolism is vital to aerobic organisms, mainly as a primary energy source having a thermodynamically favourable reduction to water [standard potential,  $E^{\circ} = 0.82 \text{ V}$  (1 atm  $\text{O}_2$ , pH = 7)], and metalloenzymes have been used for the insertion of dioxygen into biological substrates.<sup>9</sup> This insertion occurs through mono- or dioxygenation processes. The functions of various metalloproteins and metalloenzymes are summarised in Table 1.<sup>10</sup>

Metalloenzymes may be controlled by changing the pH, thus disrupting the flow of electrons which the enzyme would normally regulate. Metalloenzymes can also be inhibited by using transition state analogs which mimic the structure of the transition state in the reaction of the enzyme with a particular substrate.

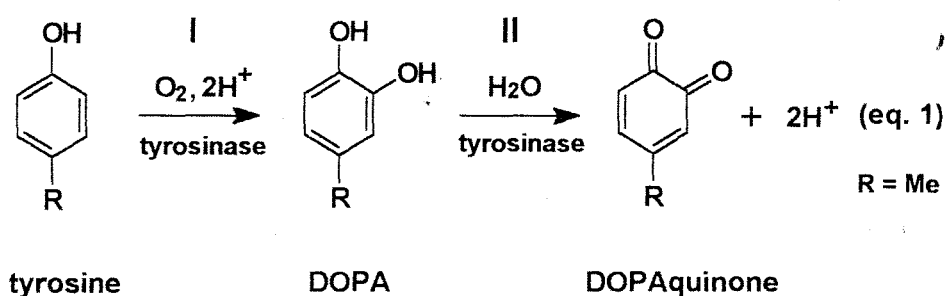
**Table 1:** Functions of various metalloenzymes and metalloproteins.<sup>10</sup>

Metal	Protein	Source	Function
Mo	nitrogenase	<i>Cl.pasteurium</i>	electron transfer
	nitrate reductase	<i>N. crassa</i>	electron transfer
Co	methionine synthetase	micro-organisms	methionine biosynthesis, transfer of a methyl group
Fe	haemerythrin	blood cells of marine worms	oxygen storage and/or transport
	haemoglobin	mammalian erythrocytes	oxygen storage and/or transport
	myoglobin	mammalian muscle	oxygen storage and/or transport
	cytochrome b and c catalase	animal and plant tissue, liver, erythrocytes	electron transfer in mitochondrial respiration
Fe, Cu	peroxidase	plant roots	oxidation of H <sub>2</sub> O <sub>2</sub> to O <sub>2</sub>
	cytochrome oxidase	yeast and animal tissue	reduction of H <sub>2</sub> O <sub>2</sub> to H <sub>2</sub> O
Fe, Cu	haemocyanin	blood of molluscs	electron transfer in O <sub>2</sub> reduction
Cu	tyrosinase	mushrooms	oxygen transport
	dopamine-β- hydroxylase	adrenal medulla	mixed function oxidase
Cu, Zn	erythrocuprein	erythrocytes	mixed function oxidase
Zn	carboxypeptidase	pancreas	superoxide dismutation
	carbonic anhydrase	erythrocytes	protein hydrolysis
	alcohol dehydrogenase	liver	acid-base control, CO <sub>2</sub> hydration- dehydration metabolism and oxidation of alcohols
Zn, Ca	thermolysin	<i>B. thermoproteolyticus</i>	Zn, protein hydrolysis; Ca, thermal stability
Mn	pyruvate carboxylase	liver	formation of pyruvic acid from Acetyl CoA
Mn, Ca	conconavalin A	jack bean	cell mitogen
Ca	α-amylase	<i>B.subtilis</i> , saliva	carbohydrate hydrolysis

## 1.2 TYROSINASE

### 1.2.1 Background

Tyrosinase is a metalloenzyme which was discovered in 1895, when a black pigment was observed in the mushroom, *Russulla nigricans*.<sup>11</sup> The enzyme was named tyrosinase in reference to the substrate tyrosine, oxidation which affords a black pigment. As the structures of most tyrosinases and their modes of action have not been fully elucidated, tyrosinase remains the subject of wide-ranging research by many biologists and chemists. Tyrosinase is found widely in microorganisms, plants and animals. In microorganisms and animals, tyrosinase catalyses the initial step in the biochemical formation of the highly coloured pigment, melanin, from tyrosine.<sup>11</sup> In plants, the physiological substrates comprise a variety of phenolics, which are oxidised by tyrosinase in the browning reaction observed when apples, bananas, mushrooms etc. are injured and exposed to dioxygen. Although the function of this reaction has not been established, it is believed that it may offer protection of the wound from pathogens or insects. It has also been suggested that tyrosinase may be involved in wound healing and, possibly, sclerotisation of the cuticle in insects.<sup>11</sup>



Tyrosinase catalyses both the *o*-hydroxylation of monophenols (cresolase activity) and the two-electron oxidation of the *o*-diphenol (catecholase activity) to the *o*-quinone using molecular O<sub>2</sub>.<sup>11</sup> The substrate supplies the two electrons required for the reduction of the second oxygen atom to H<sub>2</sub>O and, thus, functions as an internal monooxygenase. The hydroxylation reaction (I) is faster than the oxidation reaction

(II) ( $k_{(0)} = 10^3 \text{ s}^{-1}$ ,  $k_{(1)} = 10^7 \text{ s}^{-1}$ ; eqn.1).<sup>12</sup> The rate determining step is believed to be the hydroxylation of the substrate to DOPA (dihydroxyphenylalanine). The pigment, melanin, is obtained *via* a series of non-enzymatic polymerisation reactions of the DOPAquinone product. Other common names for tyrosinase are phenolase and polyphenol oxidase.

**Table 2:** Properties of some tyrosinases which have been well characterised.<sup>13</sup>

Source	No. of subunits	MW/subunits (KDa)	Absorption* nm ( $\times 10^{-3} \text{ M}^{-1} \text{ cm}^{-1}$ )	Circular dichroism* / nm ( $\times 10^{-3} \text{ M}^{-1} \text{ cm}^2 \text{ dmol}^{-1}$ )	Amino acid sequence
<i>Streptomyces glaucescens</i>	1	30.9	345 (17.4) 640 (1.5)	345 (-32.5) 470 (2.1) 575 (-1.7) 740 (5.0)	yes
<i>Neurospora crassa</i>	1	46	345 (18) 425 (0.5) 600 (1.0)	345 (-27) 520 (0.6) 600 (1.0) 750 (3)	yes
<i>Agaricus bisporus</i> (Mushroom)	2 2	13.4 43	345 (18) 600 (1.2)	353 }	no

\*Absorption and Circular Dichroism of oxy form

Tyrosinases isolated from the eubacteria *Streptomyces glaucescens* and the fungi *Neurospora crassa* and *Agaricus bisporus* are the best characterised (See Table 2). Although tyrosinase is the most widely studied multicopper oxygenase, there are many other important copper proteins (see Table 3) which are involved in the reactions of dioxygen or its derivatives.

**Table 3:** Other important copper proteins<sup>14, 15</sup>

Protein	Enzyme	Source	Function
"Blue" electron carriers	Azurin Plastocyanin Stellacyanin Urmecyanin	Algae, green leaves and other plants	Electron transfer (Photosynthesis)
"Blue" oxidases	Laccase	Tree, Fungal	Oxidation of phenols and diamines
	Ceruloplasmin	Human, animal serum	Weak oxidase activity Fe and Cu transport
	Ascorbate Oxidase	Plants	Oxidation of L-Ascorbic acid
Oxygen carrier	Haemocyanin	Molluscs and arthropods	Oxygen transport
Copper monooxygenases	Phenol o-monooxygenase	Animal skin, plants, insects, melanoma	tyrosine oxidation to melanin
	Dopamine beta-hydroxylase	Adrenals	Converts dopamine to norepinephrine

## 1.2.2 The active sites of tyrosinase and haemocyanin

There are inherent difficulties in purifying multi-subunit enzymes, and the elucidation of the protein structure of tyrosinases has been hampered by such multiplicity. As a result, there is no complete structure presently available for any tyrosinase enzyme. However, some understanding of the nature and function of the active site can be obtained by correlations with haemocyanins,<sup>16</sup> for which crystal structures of both the deoxy<sup>17</sup> and oxy<sup>18</sup> forms of the active sites have been obtained. Based on spectroscopic properties (mainly EPR), the copper proteins have been divided into three main groups (see Table 4).

**Table 4:** The groups of copper proteins and their characteristics.<sup>19</sup>

Group	Characteristics	Examples
Type I	Mononuclear copper having a trigonal basal plane with an N <sub>2</sub> S ligand donor set (S denotes thiolate sulfur from cysteine); exhibits unusual spectroscopic properties, viz., (1) a strong absorption band at ca. 600nm (an intense blue colour), (2) a small A <sub>  </sub> value (<70 G), and (3) a high reduction potential (generally >250 mV).	Plastocyanin Azurin
Type II	Mononuclear copper site exhibiting a normal EPR spectrum. Three sub-groups have been identified, viz., IIA, IIB and IIC.	Phenylalanine hydroxylase, galactose oxidase, superoxide dismutase.
Type IIA	The ligands comprise ordinary protein residues, such as histidine imidazole, cysteine thiolate and water (or hydroxide).	
Type IIB	The ligand donors include unusual protein side chains.	
Type IIC	The copper is bridged to another metal ion, forming a hetero-dinuclear metal site.	
Type III	EPR silent dinuclear site which binds dioxygen as peroxide and exhibits unusual physicochemical characteristics, viz., (1) diamagnetism, (2) two characteristic absorption bands at 350 and 580 nm, and (3) a low O-O vibration stretching frequency (ca. 750 cm <sup>-1</sup> ).	Tyrosinase and haemocyanin

Tyrosinase and haemocyanin have been classified as Type III copper proteins. Such proteins are characterised by a dinuclear copper active site, the copper atoms being anti-ferromagnetically coupled in the oxidised state and, therefore, EPR silent.<sup>20</sup>

### 1.2.3 Studies of the active site of haemocyanin

#### 1.2.3.1 Early studies

Haemocyanins function as oxygen carriers in the haemolymph of molluscs and arthropods. They have a dinuclear copper active site which bind oxygen, as a peroxide, to give oxyhaemocyanins. Volbeda and Hol<sup>21</sup> were the first to determine the three-dimensional structure of the deoxygenated form of haemocyanins from *Panulirus interruptus*, and found that the two Cu(I) ions of the active site are embedded in a protein matrix with three histidine residues coordinating each copper ion.

**Table 5:** Data for haemocyanin derivatives with different active site arrangements of the copper ions.<sup>29</sup>

Derivative	Name	Properties
Cu(I)..Cu(I)	deoxy	Coupled, colourless
Cu(II).O <sub>2</sub> .Cu(II)	oxy	Coupled, absorbs at 330 and 650 nm
Cu(II)..Cu(I)	half-met	EPR-active
Cu(II)..Cu(II)	met	Coupled, EPR-silent
Cu(II).. -	met-apo	Paramagnetic
Cu(II) Cu(II)	dimer	Paramagnetic, not coupled

Earlier, chemical and spectroscopic evidence suggested that each cuprous ion in deoxyhaemocyanin was coordinated to two or three imidazole ligands from histidine.<sup>22-28</sup> The spectral features of various forms of haemocyanin, generated with different active site arrangements, were investigated by Lang and Holde<sup>29</sup> (Table 5). The charge transfer spectra and magnetic properties of the oxy derivatives indicated

that oxygen was bound as an end-to-end peroxide ( $O^{2-}$ ) bridge across the two copper atoms. It was proposed that the oxygen bridge was positioned in the equatorial plane between the two copper atoms, as in Figure 1.

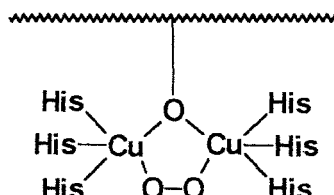


Figure 1

From an X-ray crystallographic study of *Panulirus interruptus* haemocyanin, the Cu(I)-Cu(I) distance in the deoxy form was found to be 3.8 Å.<sup>30</sup> Upon reaction of the deoxyhaemocyanin with  $O_2$ , significant coordination takes place giving rise to tetragonally coordinated copper(II) ions separated by 3.6 Å. These copper(II) ions are bridged by  $O_2^{2-}$  and an endogenous oxygen-containing group.<sup>31</sup>

### 1.2.3.2 More recent studies

Crystals of haemocyanin and oxyhaemocyanin from *Limulus polyphemus* have also been analysed.<sup>32,33</sup> High resolution X-ray crystal data for the oxyhaemocyanin indicated that each copper atom is tightly coordinated in a square planar geometry to both atoms of the oxygen molecule and to the nitrogen atoms of the two closer histidine ligands (Figure 2). Each copper atom is also weakly coordinated to the third histidine ligand which is in an axial position. Molecular oxygen lies in a side-on ( $\mu\text{-}\eta^2\text{:}\eta^2$ ) configuration with respect to the Cu-Cu axis. The two copper, the two oxygen, and the four nitrogen atoms lie approximately in the same plane. The two copper atoms are 3.54 Å apart while the two oxygen atoms are 1.41 Å apart. The relative positions of the copper atoms and histidine residues in this structure are very similar to those found by Volbeda and Hol.<sup>21</sup>

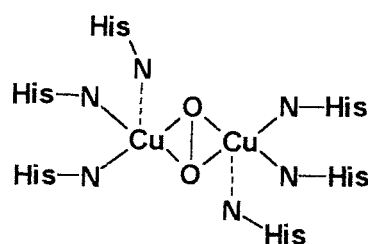


Figure 2

The data obtained for the deoxygenated form of the haemocyanin obtained from *L. poliphemus*, however, are rather different from those reported for the *P. interruptus* protein. Each copper atom exhibits trigonal geometry and is coordinated to three histidines, while the two copper atoms are 4.6 Å apart - a distance greater than the value found for the deoxygenated *P. interruptus* haemocyanin (3.8 Å).<sup>21</sup>

The structural difference between these two deoxy forms of haemocyanin has been explained in terms of a two-state model. The haemocyanin hexamer may adopt conformational states of high (R-state) or low (T-state) oxygen affinity, either of which may be oxygenated or deoxygenated. It has been postulated that the deoxygenated *L. poliphemus* haemocyanin is in the T-state, while that of *P. interruptus* haemocyanin assumes the deoxygenated R-state.<sup>32</sup>

#### 1.2.4 Similarities between tyrosinase and haemocyanin

Chemical and spectroscopic studies indicate that tyrosinase has a coupled dinuclear copper active site very similar to that of haemocyanin. Studies performed on a series of derivatives of mollusc and arthropod haemocyanins<sup>34-41</sup> and fungal tyrosinase,<sup>42-46</sup> have shown that the active sites of these proteins are remarkably similar and include examples of the deoxy [Cu(I) Cu(I)], oxy [Cu(II) O<sub>2</sub> Cu(II)], mixed-valent half-met [Cu(I)-Cu(II)], met [Cu(II)-Cu(II)] and the dimer [Cu(II)··Cu(II)] arrangements (see Table 5). The met derivative is considered to be the resting form of tyrosinase but,

unfortunately, there is currently no crystal structure available for the corresponding met haemocyanin. The EPR silence of the met form is due to antiferromagnetic coupling between the two copper(II) ions, which requires a super-exchange pathway involving a bridging ligand.<sup>40</sup> The crystal structure of *P. interruptus* haemocyanin reveals that it is not possible for the protein residues, in the vicinity of the copper site, to provide such bridging; in this case, the bridging ligand is presumed to be a water hydroxyl group.<sup>21</sup>

It is believed that a similar situation exists at the active site in met tyrosinase. It appears that only one water-derived ligand is bound terminally to the two copper(II) ions as the met tyrosinase Cu-Cu distance of 3.4 Å (as determined by EXAFS analysis) is too large for two, single atom hydroxide bridges.<sup>16</sup> Oxytyrosinase is produced from met tyrosinase by the addition of peroxide, or by two electron reduction to the deoxy state followed by the reversible binding of dioxygen.<sup>43,44,47</sup> As oxytyrosinase reacts with both the monophenol and the diphenol,<sup>17,18</sup> the geometric and electronic structures are important in understanding the hydroxylation chemistry of this enzyme. For oxyhaemocyanin, the following spectroscopic features are observed: (i) an intense absorption band at 350 nm ( $\epsilon \sim 20\,000\text{ M}^{-1}\text{ cm}^{-1}$ ),<sup>36</sup> (ii) a low O-O stretching frequency of ca.  $750\text{ cm}^{-1}$ ;<sup>19</sup> and (iii) a Cu-Cu distance of 3.6 Å (from EXAFS<sup>16</sup> and X-ray crystallography<sup>48</sup>). The spectral features observed for oxytyrosinase are essentially the same,<sup>16,43,44,46,47</sup> and are characteristic of the side-on  $\mu\text{-}\eta^2\text{:}\eta^2$  peroxide bridging mode (see Figure 3).

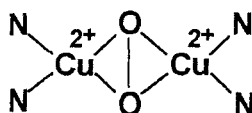


**Figure 3:** The geometric arrangement of the side-on  $\mu\text{-}\eta^2\text{:}\eta^2$  peroxide bridging mode in oxyhaemocyanin and oxytyrosinase.

In view of the similarities in the spectroscopic features of these oxy states, it is believed that oxytyrosinase has a similar dinuclear copper active site to that of oxyhaemocyanin. These spectroscopic features are quite well understood.<sup>21-23</sup> The intense absorption band at 350 nm indicates that the side-on peroxide is a very strong  $\sigma$ -donor ligand to the two copper(II) atoms, while the low O-O stretching frequency (at ca. 750 nm) indicates a weak O-O bond. The weakness of the O-O bond derives from the ability of the peroxide to act as a  $\pi$ -acceptor ligand; the  $\pi$ -back-bonding shifts electron density into the peroxide  $\sigma^*$  orbital, which is highly anti-bonding with respect to the O-O bond, thus activating it for cleavage.

### 1.2.5 The proposed mechanism of oxidation by tyrosinase

A mechanism, which takes into account the geometric and electronic characteristics of oxyhaemocyanin, has been proposed to account for the phenolase and catecholase activity of tyrosinase.<sup>18</sup> While earlier mechanisms have interpreted the complex kinetics of tyrosinase in terms of allosteric effects and two binding sites,<sup>44,48,49</sup> the mechanism outlined in Figure 4 accounts for all the kinetic and inhibition patterns observed for this enzyme.<sup>18</sup> In the first step of the phenolase cycle (A), a phenol binds in an axial position to one of the copper atoms of the oxy site. A trigonal bipyramidal rearrangement towards the equatorial plane then occurs, which orients the *ortho*-position of the phenol for hydroxylation by peroxide. The resulting *o*-diphenolate (met-D) is then oxidised to the quinone releasing the deoxy site for a further oxidation cycle. In the catecholase cycle (B), the *o*-catechol is oxidised to the quinone after reacting with the oxy site. From kinetic studies it has been found that bulky substituents on the phenol ring dramatically reduce the cresolase activity, but not the catecholase activity.<sup>18</sup> It has been deduced that monophenolic substrates require axial-to-equatorial rearrangement for *ortho*-hydroxylation, but this is not a necessity for diphenolic substrates undergoing simple electron transfer. The bridged bidentate coordination mode illustrated for the met-D form in Figure 4 is supported by the fact

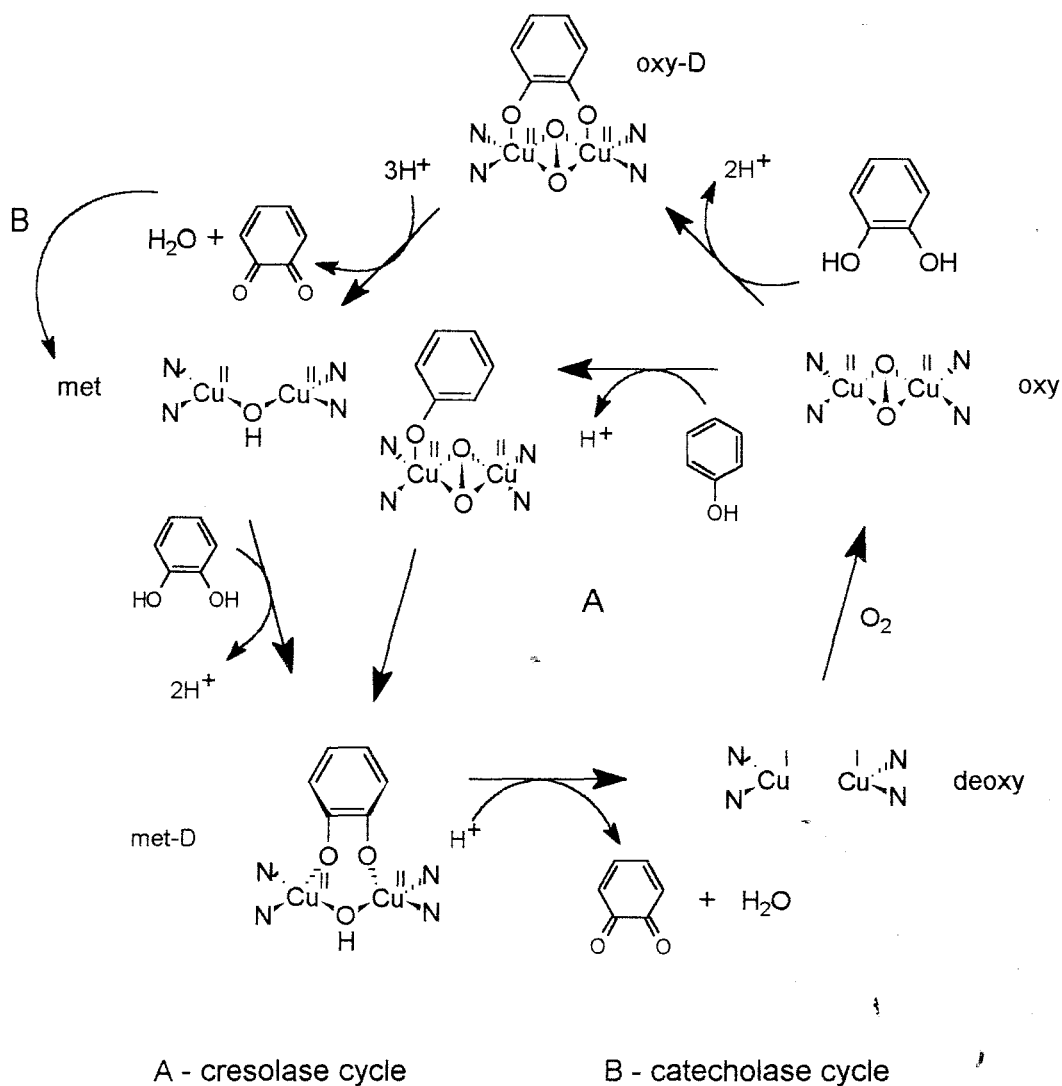


**Figure 4:** A mechanism proposed by Solomon *et al.* for the cresolase and catecholase activity of tyrosinase.<sup>50</sup>

that *o*-diphenol, but not the *m*- and *p*-diphenol (*o*- and *p*-diphenol have approximately the same redox potential) is oxidised by tyrosinase.<sup>50</sup> It has been noted that bidentate coordination to one copper atom is also a possibility.<sup>50</sup>

Notwithstanding the similarities, a major difference between the active sites of haemocyanin and tyrosinase is indicated by the fact that tyrosinase can react with

substrates whereas haemocyanin cannot. An explanation for this difference is provided by sequence comparisons of tyrosinases with the structurally defined haemocyanins, from which it is apparent that an additional domain in the larger haemocyanin protein blocks access to the dinuclear copper site.

### 1.2.6 Applications of the enzyme tyrosinase.

Current interest in applications of the tyrosinase enzyme is reflected in publications which have appeared in the recent literature. Atlow *et al.*<sup>51</sup> have reported use of the enzyme in the removal of phenols from industrial, aqueous effluents. The phenols are converted to the corresponding *o*-quinones, which then undergo non-enzymatic polymerisation to form water-insoluble aggregates. Another study has been concerned with the removal of aromatic amines from industrial waste-water.<sup>52</sup> Following treatment with the enzyme, a colour change from colourless to dark-brown was observed, but no precipitation occurred; however, treatment of the coloured compounds with a combination of tyrosinase and a cationic polymer coagulant, containing an amino group, resulted in the precipitation of the enzymatic reaction products. For heterogeneous applications, tyrosinase has been immobilised *via* free amino groups on cation exchange resins that can be used repeatedly,<sup>53</sup> a 100% removal of phenols being achieved after 2 h, with only marginal reduction in the activity even after 10 repeat treatments.

The development of new biosensors is a rapidly growing research field and the tyrosinase enzyme has been used as a biosensor for detecting several phenols and *o*-diphenols. Studies of this application were first undertaken by Schiller and co-workers,<sup>54,55</sup> and involved immobilising the enzyme in a polyacrylamide gel. An enzyme-spectrometric method was used initially but, subsequently, an enzyme-potentiometric method was developed. Campanella *et al.*<sup>56</sup> have reported an enzyme-amperometric method in which tyrosinase may be immobilised in three different ways

---

and coupled to an oxygen gas-diffusion electrode. This method has been used for the determination of phenol in several environmental matrices, and evaluated as a promising alternative to more conventional methods.

### 1.3 THE BIOMIMETIC APPROACH TO TYROSINASE ANALOGUES

Metalloenzymes effect a variety of important chemical transformations that often involve small molecule substrates, such as molecular oxygen, hydrogen, nitrogen and water. Metalloenzyme-catalysed reactions also function under very mild conditions, and affect transformations with exceptional efficiency and substrate regio- and stereoselectivity. As a result, extensive research has been undertaken in this field to design synthetic processes that approach this efficiency and selectivity and, thus, mimic the natural systems. A multidisciplinary bioinorganic approach has been adopted, which encompasses a variety of disciplines such as inorganic chemistry, synthetic organic chemistry, biochemistry and spectroscopy.

The basic objectives of the biomimetic approach, as applied to the modelling of metalloenzymes, can be outlined as follows:-

- (a) to develop a biomimetic model that will account for the spectroscopic characteristics and function of the metalloenzyme in terms of its structure;
- (b) to compare the observed metalloenzyme properties with those of the biomimetic model; and
- (c) to exploit the use of synthetic models which exhibit catalytic activity comparable to the metalloenzyme.<sup>57</sup>

Two principal strategies exist for the preparation of biomimetic models, viz., total synthesis and metal template condensation (the self-assembly approach). The total synthesis method allows for the incorporation of selected properties, such as geometry, polarity, hydrophilicity, hydrophobicity and steric characteristics; in this method, the metal is added after the ligand has been synthesised. In the metal template condensation method, on the other hand, the complex adopts an optimal geometry dictated by the nature of the metal ion. It is also important to consider the basic premise in bioinorganic chemistry, viz., that the chemistry of the metal-binding site is dependent on the immediate environment of the metal ion. In many metalloproteins, the amino acid side chains provide the coordination environment

and, at times, the coordination-sphere of the metal ion may be completed by a prosthetic group, such as a porphyrin ring.<sup>58</sup> Once synthesised, the synthetic model can be compared with the metalloprotein, with respect to spectral and physicochemical properties, coordination geometry, catalytic activity, and the mechanism of action. This may then provide information relating to the effects of the environment on the active site and/or to the intrinsic properties of the active site.

Besides providing a basis for postulating biological reaction pathways and possible metal-complex intermediates, extensive modelling efforts may yield small-molecule biomimetic catalysts capable of effecting transformations with practical applications. Such applications include the following:- (i) the removal of environmental pollutants, such as phosphate ester pesticides or nitrogen compounds; (ii) the hydrolysis of peptides or nucleic acids in biotechnological processes; or (iii) selective dioxygen-mediated oxidation in drug and chemical transformations.<sup>59</sup>

### **1.3.1 The selection of ligands for dinuclear copper complexes**

To design biomimetic models that will mimic the metalloenzyme, it is essential that the structure of the model be as similar as possible to that of the metalloenzyme. The ligands selected should be chemically similar to those in the enzyme and should also have the correct number of donor atoms required for coordination to the metal ions. For tyrosinase biomimetics, the ligands should be similar to the histidyl-imidazole moieties. The sizes of the ligands are also significant as they must be able to accommodate not only both copper ions, but also any additional bridging group essential for reactivity. Thus, the ligands used must be sufficiently flexible to adapt to different geometries, especially if there is a valence change, as is the case in dioxygen binding. The geometric and coordination requirements of Cu(I) and Cu(II) ions are quite different, as indicated in Table 2.<sup>60</sup> As six-membered chelate rings are more flexible than five-membered chelate rings, they can more

readily satisfy coordination changes in the redox process.<sup>61</sup>

When selecting ligands which will mimic histidyl-imidazole moieties, it is necessary that the nitrogen donors be aromatic or, at least,  $sp^2$  hybridised. As a result, imine nitrogens are preferred to amine - nitrogens. Ligands containing imine nitrogens can also stabilise copper complexes in the lower oxidation state better than amine nitrogens, because the unsaturated ligands can delocalise electron density from the metal ions *via*  $\pi$ -back-bonding.<sup>62</sup> Heterocycles containing nitrogen are particularly favoured.

Another aspect to be considered is the basicity of the donor group in the ligand, since the reactions under investigation involve electron transfer.<sup>58</sup> A list of ligands with their corresponding basicity is provided in Table 6.

**Table 6:** N-donor groups and their  $pK_b$  values.

Donor group	$pK_b$
Benzimidazole	8.5
Imidazole	7.0
Histidine	8.0
Pyridine	8.7
Pyrazole	11.5
Alkyl-NH <sub>2</sub>	3.0
Aryl-NH <sub>2</sub>	9.4

The use of imidazole groups has been hampered by cyclisation, encountered in the synthesis of ligands in which they have been included. Consequently, derivatives such as benzimidazole have been used as donor groups as they are less prone to cyclisation and, moreover, their increased steric bulk may be useful in controlling the metal ion stereochemistry.<sup>63</sup> A disadvantage, however, is that the aromatic ring (fused to the imidazole nucleus) can affect the spectroscopic properties of the resulting complex and mask the UV region, so important in

studying copper(I) complexes.<sup>58</sup>

Pyrazole groups have also been incorporated into ligands but, despite their easy preparation<sup>64</sup> and their spectroscopic similarity to imidazole, they are significantly less basic. Pyridine groups have the advantage that their basicity is similar to that of the histidyl-imidazole, and models in which pyridine has been incorporated have been successful in mimicking the reactivity<sup>65</sup> of copper proteins.

### 1.3.2 Coordination considerations in the reaction of copper complexes with dioxygen.

During the binding of dioxygen to copper, two charge-transfer processes can occur, *viz.*, metal- $\pi$ -to-dioxygen- $\pi^*$  back donation and donation from oxygen to the metal. This ultimately results in, at least partial, electron transfer to the metal and weakening of the O-O bond. The binding of dioxygen to copper is also accompanied by changes in both the oxidation state and coordination number of the metal. The observed coordination numbers and stereochemistry is dependent upon the oxidation state and, in the  $d^{10}$  Cu(I) ion, the coordination number of four dominates. The Cu(II)  $d^9$  ion, however, is the most prevalent oxidation state for copper and, in this state, an octahedral coordination environment dominates. In this coordination environment, there are four equatorial ligands that are strongly bound and two axial ligands that are less strongly bound (Jahn-Teller effect). The coordination numbers and geometries observed for the two oxidation states of copper are summarised in Table 7.

The coordination numbers and geometries of the Cu(I) and Cu(II) ions determine the resulting redox reactions for the two oxidation states. The redox process which occurs is also strongly affected by the type of ligand, the chelate ring size and the solvent. Six-membered chelate rings stabilise Cu(I),<sup>66</sup> while five-membered rings stabilise Cu(II).<sup>67</sup> When polar solvents are used, the Cu(II) oxidation state is favoured but, conversely, non-polar solvents favour the Cu(I) oxidation state.<sup>68,69</sup>

**Table 7:** Cu(I) and Cu(II) coordination numbers and geometries<sup>70</sup>

ION	Observed coordination number	Observed geometry
Cu(I)	2	Linear
	3	Trigonal
	4	Tetrahedral
Cu(II)	4	Square planar Tetrahedral
	5	Square pyramidal
	6	Trigonal bipyramidal Octahedral

### 1.3.3 The mode of binding of dioxygen in oxyhaemocyanin and oxytyrosinase

The dinuclear copper proteins, haemocyanin and tyrosinase, bind dioxygen reversibly at their active sites. It is believed that these proteins have very similar oxy active sites,<sup>42</sup> involving two copper(II) atoms (based on X-ray absorption data<sup>71,16</sup>) and bound peroxide (based on the unusually low Raman O-O stretching band<sup>72,73</sup> at 750 cm<sup>-1</sup>). The studies showed that a peroxide ion bridges the dinuclear copper active site of deoxyhaemocyanin and that oxidation of the metal ions from copper(I) to copper(II) occurs upon coordination of dioxygen. Intense absorption bands due to CT transitions have been observed for both oxyhaemocyanin and oxytyrosinase at 350 nm ( $\epsilon = 20\,000$ ) and 570 nm ( $\epsilon = 1000$ ). In a mononuclear copper-peroxide complex only two CT transitions are observed.<sup>23</sup> For oxyhaemocyanin, however, more than two peroxide-to-copper CT transitions are observed, which is further evidence that the pair of copper atoms are bridged. Because oxytyrosinase displays the same spectral features as oxyhaemocyanin, its active site has been ascribed a similar structure to that of oxyhaemocyanin.

Research has been focussed on elucidating the structure of the peroxide ion bridging the copper atoms. Initially, the three end-on peroxide bridging structures shown in Figure 5 were considered [(a)  $\mu$ -1,1; (b) *cis*  $\mu$ -1,2 and (c) *trans*  $\mu$ -1,2], but only the *cis*  $\mu$ -1,2 structure in (b) was expected to produce spectral features consistent with those observed for oxyhaemocyanin.<sup>36</sup> Several complexes have been synthesised to mimic the *cis*  $\mu$ -1,2 bridging in (b), but these were found to have a *trans*  $\mu$ -1,2 bridging mode and to exhibit spectral properties which differ widely from those of oxyhaemocyanin.<sup>74,75</sup>

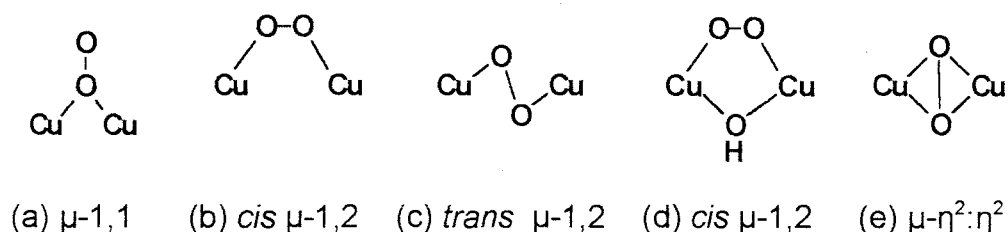


**Figure 5:** Possible structural models for the bridging peroxide ion in dicopper complexes.

Strong antiferromagnetic coupling has been observed for oxyhaemocyanin and oxytyrosinase, indicating that the copper ions are diamagnetic (EPR silent). To account for this coupling, a *cis*  $\mu$  1,2- arrangement [Figure 5 (d)] involving an endogenous bridge, originating from the protein, was proposed by Solomon.<sup>76</sup> The two copper atoms were considered to coordinate to two or three histidyl-imidazole ligands and were assumed to be in a copper(II) oxidation state (Figure 6). The endogenous bridge (OR) was thought to involve alkoxide, phenolate, sulphhydryl or hydroxyl groups in the protein or in the medium. The elucidation of the X-ray crystal structure of haemocyanin<sup>77</sup> from the spiny lobster (*Panulirus interruptus*) confirmed both the dinuclear nature of the active site and the presence of three histidine ligands per copper atom. However, the notion of an endogenous bridging group was discarded as there was no suitable candidate within 12 Å of the site.<sup>78</sup>

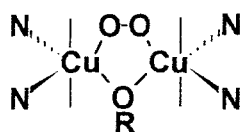


**Figure 6:** The dinuclear active site model proposed by Solomon.<sup>76</sup>

A model that binds dioxygen in a similar way to that exhibited by oxyhaemocyanin has been synthesised in the laboratory of Nobumasa Kitajima.<sup>79</sup> The structure of the complex (Figure 7) showed that the dioxygen was bound in the novel  $\mu$ - $\eta^2$ : $\eta^2$  bridging mode between the two copper atoms [Figure 5 (e)].<sup>79</sup> From the spectrochemical and magnetic properties it could be seen that this model closely

resembled the biosite in the protein. The controversy over the mode of dioxygen bridging was eventually resolved when a crystal structure of oxyhaemocyanin from the horseshoe crab was elucidated by Karen Magnus.<sup>80</sup> A  $\mu\text{-}\eta^2\text{:}\eta^2$  bridging mode for dioxygen was, in fact, observed between the two copper atoms, each of which is associated with three histidine nitrogens.

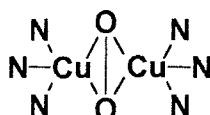


**Figure 7:** A model representing the  $\mu\text{-}\eta^2\text{:}\eta^2$  bridging mode of a complex which emerged from the laboratory of Nobumasa Kitajima.<sup>79</sup>

### 1.3.4 Synthetic biomimetic models of haemocyanin and tyrosinase

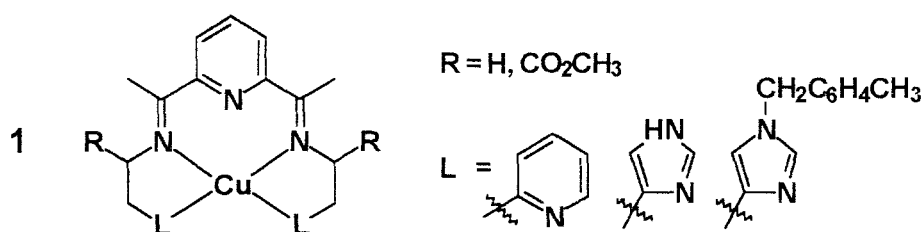
#### 1.3.4.1 Early work

Before the X-ray crystal structure elucidation of haemocyanin, research focussed on developing systems exhibiting the spectroscopic or physical features which characterise the biosite, the inference being that such systems reflect the structural characteristics. Once a good synthetic model (based on spectroscopic and physical features) was identified, then its X-ray crystal structure could be used to elucidate the structure of the biosite.

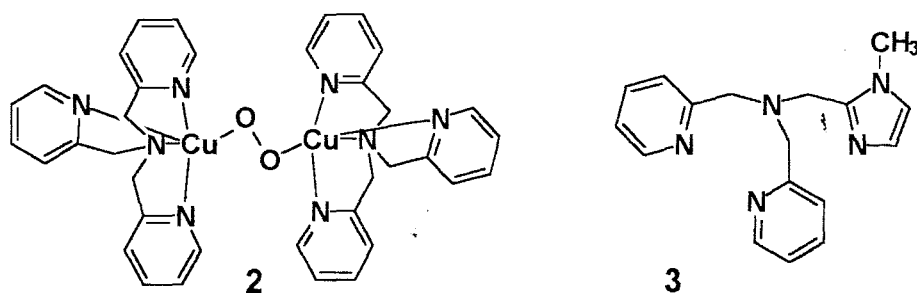
Thus, early research was based on an investigation of the physical and spectroscopic properties of dioxygen-bridged systems. Key issues addressed in this research included:- the structure of the deoxy-active site; the nature of the protein bridge; the nature and geometry of the Cu<sub>2</sub>O<sub>2</sub> unit; the factors responsible for the reversible binding of dioxygen; and the activation of molecular oxygen by tyrosinase.<sup>58</sup>

### 1.3.4.2 Mononuclear Complexes

Before the discovery that the active site of haemocyanin was dinuclear, research focussed on mononuclear copper complexes. The idea was that two mononuclear complexes could be brought together by dioxygen to produce a structural model of tyrosinase. Such systems were first reported by Wilson<sup>82-85</sup> and later by Casella,<sup>86</sup> complex **1** being an example of the complexes developed by Casella.

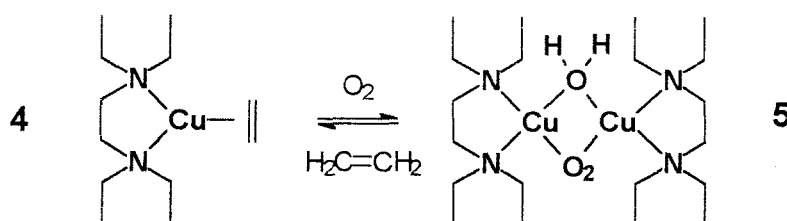


The red copper(I) complex **1** (R = H; L = pyridine) reacted with dioxygen in a 1:2 (Cu:O<sub>2</sub>) stoichiometry at room temperature to give a green product, formulated as a dinuclear copper(II)-peroxo species. This reaction may be partially reversed by purging the solution with nitrogen.

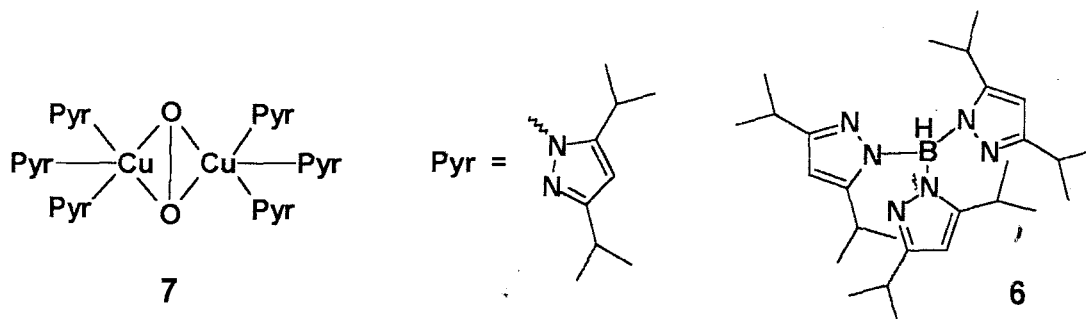


Complex **2**, developed by Jacobson *et al.*,<sup>87</sup> was one of the first completely characterised complexes in which two mononuclear units are bridged by dioxygen. The results of the spectroscopic analysis revealed that the structural features of the complex, i.e. the Cu-Cu separation and the geometry around the copper ions, were different to those in oxyhaemocyanin. It was also found that the peroxide bridge was *trans* rather than *cis*  $\mu$ -1,2. The fact that the complex is diamagnetic proves that an endogenous bridge is not a necessary requirement for coupling of the copper ions in the protein.

The copper complex of the ligand **3** is dimeric in solid form, but mononuclear in a solution of acetonitrile.<sup>88</sup> The complex binds dioxygen in a 2:1 ratio (Cu:O<sub>2</sub>) and, at -80°C, exhibits similar spectral features to those of complex **2**. It has, therefore, been proposed that the oxygenated dinuclear complex resulting from ligand **3** has dioxygen bound in a *trans*  $\mu$ -1,2 fashion. EPR measurements revealed that the copper ions in the oxygenated complex are magnetically coupled (EPR silent).



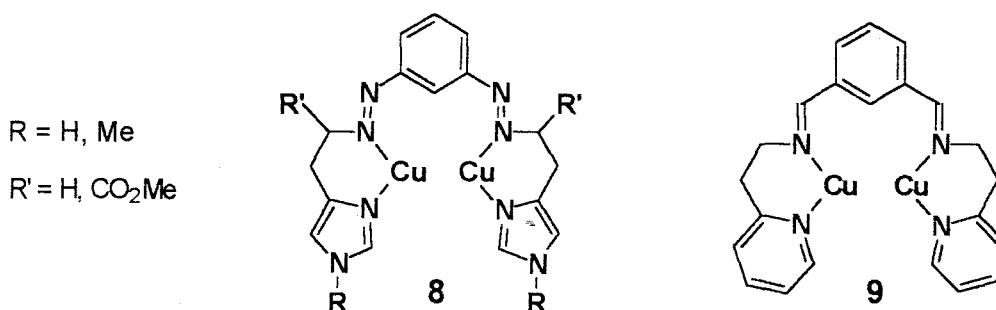
The mononuclear complex **4** has been found to bind dioxygen reversibly forming a  $\mu$ -peroxo copper(II) complex **5**;<sup>58</sup> from the IR spectrum it is apparent that the dioxygen is bound as peroxide. This reaction is reversible upon addition of ethylene, but no structural data was reported.



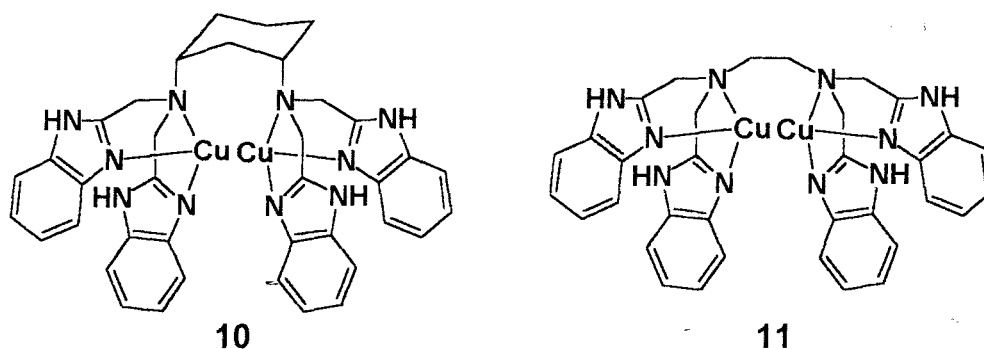
The synthesis of the dinuclear copper complex **7**, prepared from *tris*(pyrazolyl) borate ligands **6** by Kitajima and co-workers,<sup>79</sup> represented a major breakthrough in this field. The electronic spectra, magnetic character, Cu-Cu separation as well as the  $\mu$ -peroxo IR stretching frequency were all very similar to those observed for oxyhaemocyanin, and the  $\mu$ - $\eta^2$ : $\eta^2$  bridging mode was confirmed by X-ray crystallographic analysis.

### 1.3.4.3 Dinuclear complexes

Systems based on the model proposed by Solomon<sup>76</sup> (Figure 6) were designed so that a "reaction space" was provided in which the dioxygenated substrate could be bound and activated. It was expected that the chemical reactivity and the physicochemical characteristics of such complexes would be dependent upon the coordination environment. The ligands were designed to coordinate two copper atoms in sufficiently close positions to permit bridging by dioxygen.

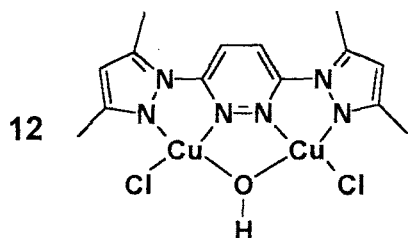


Complexes **8** and **9**, which reflect this strategy, have been reported by Casella.<sup>81</sup> For complex **8** (R = H and R' = H) oxidation of copper(I) to copper(II) occurs when the complex reacts with oxygen in dry acetonitrile. In methanol, however, the oxidation of copper(I) is inhibited by the hydroxylation of the aromatic nucleus at the C-2 position. In complex **9**, hydroxylation at C-2 occurs on treatment with oxygen, the resulting hydroxyl group acting as a bridge between the two copper atoms.

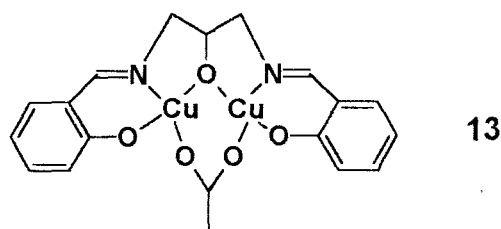


Complex **10** has been reported to react with dioxygen "semi-reversibly",<sup>81</sup> while complex **11**, which differs only in the nature of the spacer, reacts with oxygen

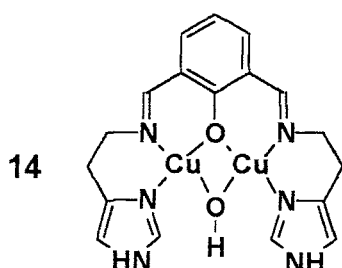
reversibly.



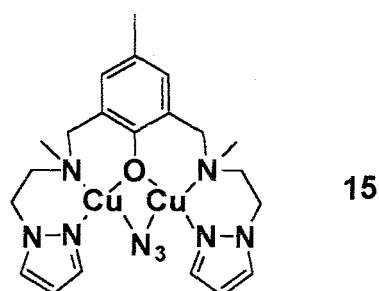
Hydroxide



Alkoxide



Phenoxide and alkoxide

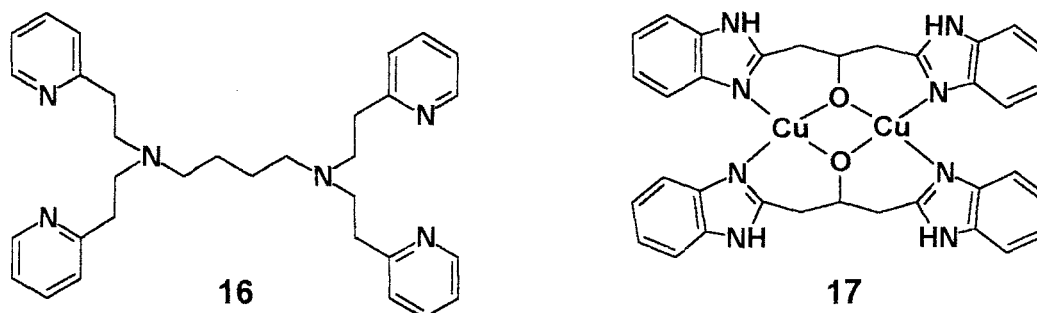


Phenoxide

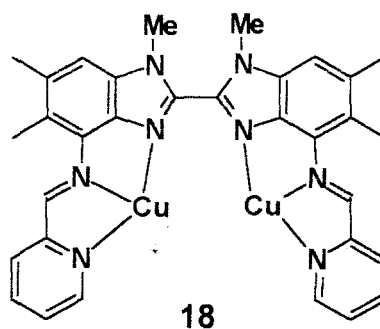
In some cases, the ligand has been designed to have a hydroxyl group as part of its structure, while in others an exogenous hydroxide bridge is inserted between the copper atoms upon reaction with dioxygen. Several synthetic complexes (12-15) with different peroxide bridges are shown above.<sup>58</sup>

Compared to their mononuclear analogues, dinuclear complexes have enhanced reactivity and specificity in catalytic oxidation.<sup>89</sup> Ligands that are binucleating have the advantage of offering greater control over electronic and magnetic properties than dimeric systems,<sup>90</sup> and this has led to attention being focussed on the design and synthesis of ligands that can coordinate two copper atoms. Karlin and co-workers<sup>91,92</sup> reported the synthesis of ligand **16**; the resulting copper complex reacts with dioxygen at low temperature quasi-reversibly. From EPR studies it could be seen that the copper complex was dinuclear and that it was EPR silent, due to strong anti-ferromagnetic coupling between the two cupric ions through the peroxide bridge. It was suggested that the dioxygen was bound in a *cis*  $\mu$ -peroxo or a bent  $\mu$ - $\eta^2$ : $\eta^2$  structure.<sup>93</sup> Although the crystal structure was not successfully

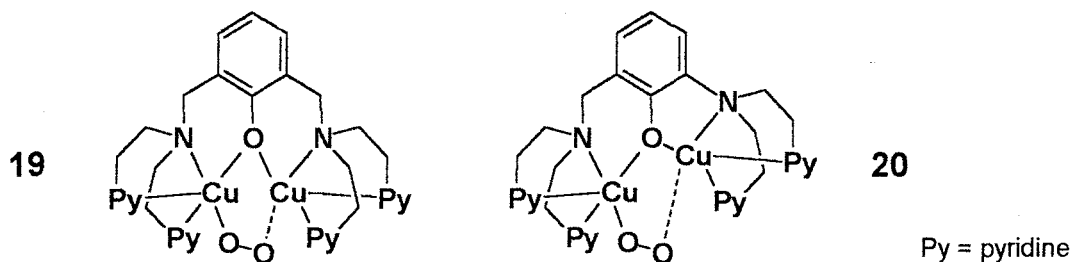
determined, a Cu-Cu distance of ca. 3.4 Å was estimated on the basis of EXAFS data,<sup>93</sup> and more recent studies have shown that the complex is virtually diamagnetic.<sup>94</sup>



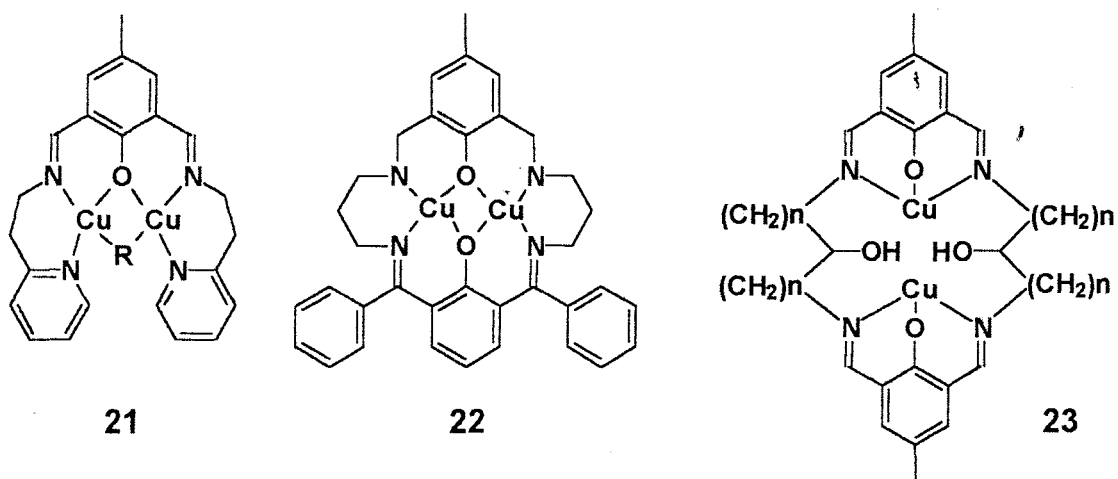
Complex **17**, reported by Zippel, displays antiferromagnetic coupling between the two copper(II) atoms, bridged by alkoxy groups.<sup>95</sup> From the X-ray crystal structure the Cu-Cu distance was found to be 3.033 Å. Studies on this complex revealed that the same structure is present in both the solid state and in solution, but that the complex does not show any tendency to effect oxidation of catechol.



Complex **18**, reported by Müller and co-workers,<sup>96</sup> adopts an open conformation resulting in a Cu-Cu distance of 6.16 Å in the crystal state. No antiferromagnetic coupling was observed for the two copper atoms because of the large Cu-Cu separation. The formation of an oxygenated complex was, however, precluded by the formation of a coordination polymer.

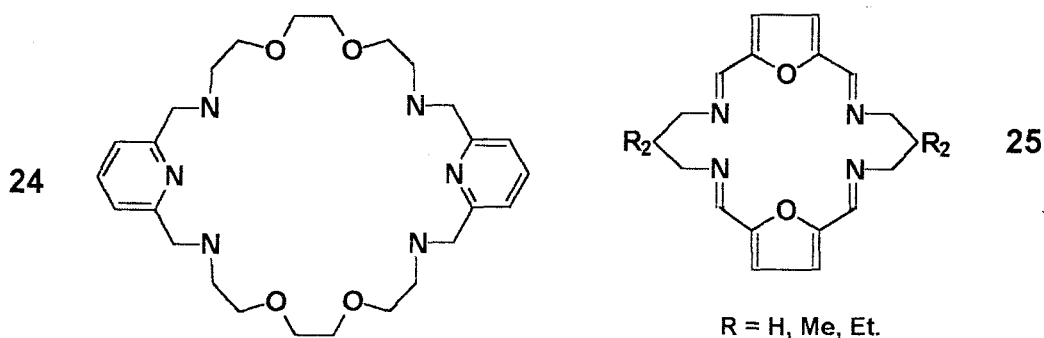


The symmetric dinuclear complex **19**, having a phenoxo bridging group, binds dioxygen quasi-reversibly at low temperature yielding an intensely purple coloured complex.<sup>97</sup> The suggestion that dioxygen is a peroxo adduct is based on Raman spectroscopy [ $\nu(\text{O-O}) = 803 \text{ cm}^{-1}$ ] and dioxygen absorption stoichiometry ( $\text{Cu}/\text{O}_2 = 2$ ) data. A Cu-Cu distance of 3.3 Å for complex **19** was determined by EXAFS analysis. Complex **20** is similar in structure to complex **19** but is unsymmetric; it has been shown that this complex reacts with dioxygen reversibly at  $-80^\circ\text{C}$  and is also intense purple in colour.<sup>97</sup> The coordination of dioxygen to the copper ions has been presumed to be the same in both complexes (**19** and **20**) because of their spectral similarity. Complex **20** is, however, more stable than complex **19** and, as a result, it has been possible to isolate it in solid form.

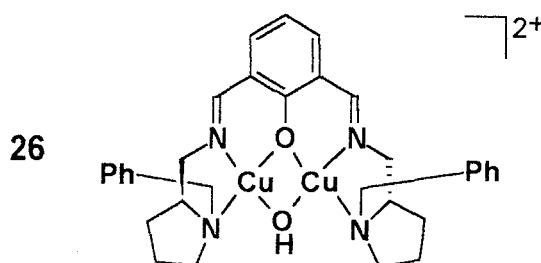


The peroxo adduct of complex **21**, reported by Nishida *et al.*, shows antiferromagnetic coupling.<sup>98</sup> From the X-ray crystal structure, it is apparent that the copper ions are coordinated in a trigonal bipyramidal geometry with the peroxide in an axial position. The copper(II) ions in complexes **22** and **23** also

exhibit antiferromagnetic coupling.<sup>99,100</sup>



The dinuclear copper complex of the macrocycle **24** is a bright yellow solid that changes to green when exposed to dioxygen in solution, and less rapidly in the solid state.<sup>15</sup> It has been proposed that a  $\mu$ -peroxo-dicopper(II) species is generated during the dioxygen uptake. Oxidative dehydrogenation occurs during this dioxygen uptake. The structures and properties of some dicopper(I) and dicopper(II) complexes of the macrocycle **25** have been reported. They function as catalysts for the oxidation of several organic substrates, including catechols, in the presence of oxygen.<sup>101</sup> In the  $[\text{Cu}_2(\mathbf{25})(\text{OEt})_2(\text{NCS})_2]$  complex, each copper(II) ion is bonded to two imino nitrogen atoms of the macrocycle, to the nitrogen of one terminally bound thiocyanate and to two bridging ethoxide groups in an approximate trigonal bipyramidal geometry. The Cu-Cu distance is 3.003 Å and the furan oxygen atoms are not coordinated. The copper(II) ions are strongly antiferromagnetically coupled in the bis( $\mu$ -alkoxo) complex and less strongly in the dihydroxo complex.<sup>15</sup>



Chiral dinuclear copper complexes have been relatively unexplored as catalysts for enantioselective oxidations. Feringa has reported the chiral dinuclear copper complex **26**,<sup>102</sup> which exhibits square planar geometry around each copper(II) ion and a normal Cu-Cu separation of 2.971 Å. A *trans*-orientation of the *N*-benzyl-

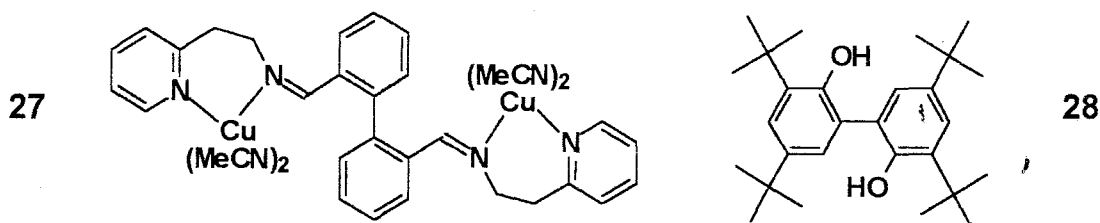
groups is found in complex **26** which, as a consequence, has  $C_2$ -symmetry.

### 1.3.5 Monooxygenase Models

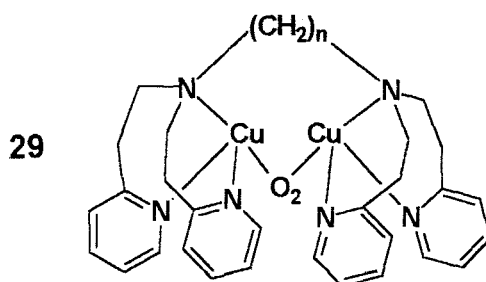
Since tyrosinase is a monooxygenase, a successful model of this enzyme would be one that can catalyse the hydroxylation of an aromatic ring. Models reported in the literature have done so in two ways, hydroxylating either an exogenous substrate or the ligand itself. In the section that follows, attention will focus on complexes that catalyse the hydroxylation of an exogenous substrate as well as those that hydroxylate the ligand itself.

#### Oxidation of exogenous substrates

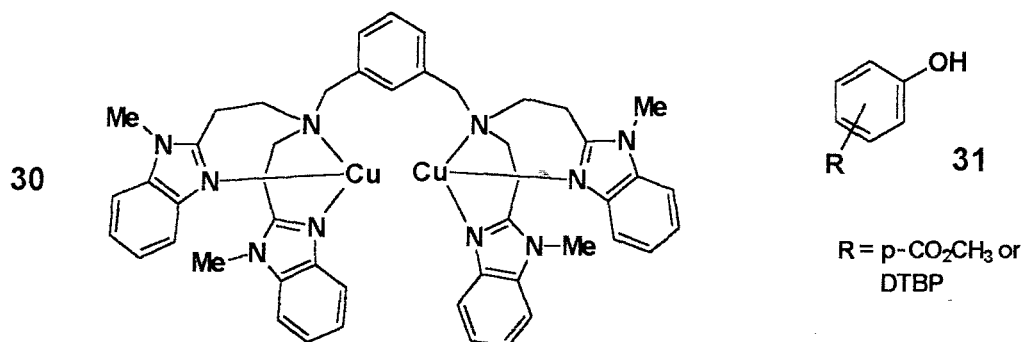
Several complexes have been reported that catalyse the oxidation of exogenous substrates. Kitajima's  $\mu$ -peroxo complex **7** which resembles the tyrosinase enzyme so closely in its spectroscopic features, has been reported to react with 3,5-di-*t*-butylphenol (DTBP) *via* a radical mechanism to afford coupled products.<sup>79</sup>



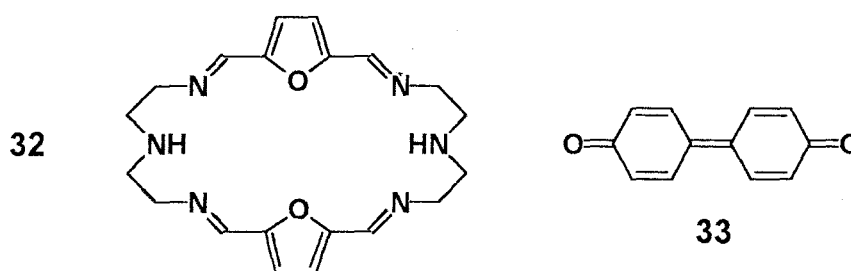
Reglier *et al.* reported the oxidation of DTBP (2,4-di-*t*-butylphenol) in the presence of triethylamine, by the biphenyl dinuclear copper complex **27**.<sup>103</sup> It is thought that deprotonation of the phenolic substrate promotes binding to the catalyst. A coupled product **28** is formed in the absence of triethylamine. Complex **29** ( $n = 4$ ), which reacts reversibly with dioxygen to form diamagnetic peroxide bridged structures,<sup>92</sup> has also been reported to give the coupled product **28** *via* a radical mechanism.



Complex **30** has been reported to catalyse the oxidation of DTBP to the quinone, and the phenolic substrates **31** to the dihydroxyphenols.<sup>104</sup> Evidence for the initial formation of an intermediate phenolate adduct was obtained.

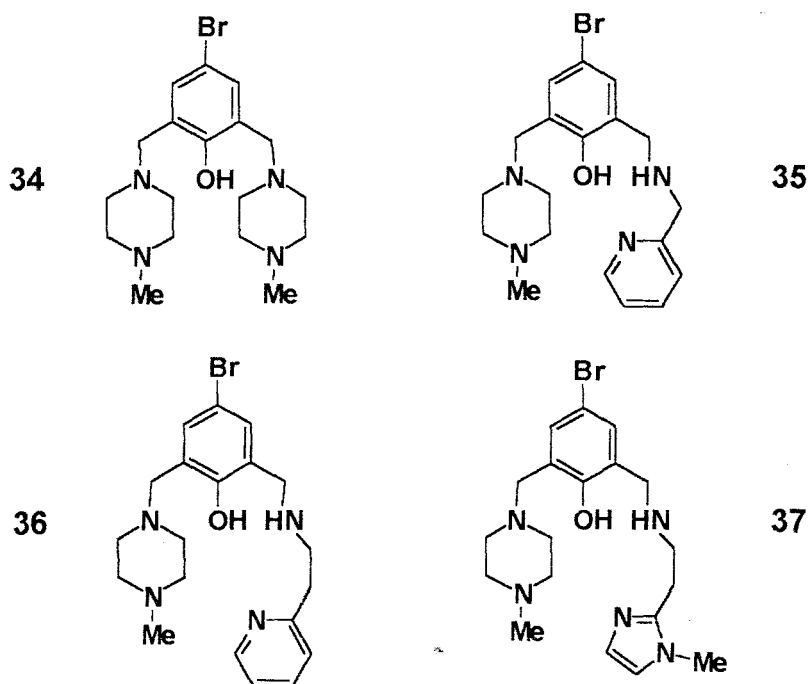


Complexes of the macrocyclic ligand **32** catalyse the oxidation of exogenous substrates, 2,6-di-*t*-butylphenol being oxidised to the coupled product **33**.



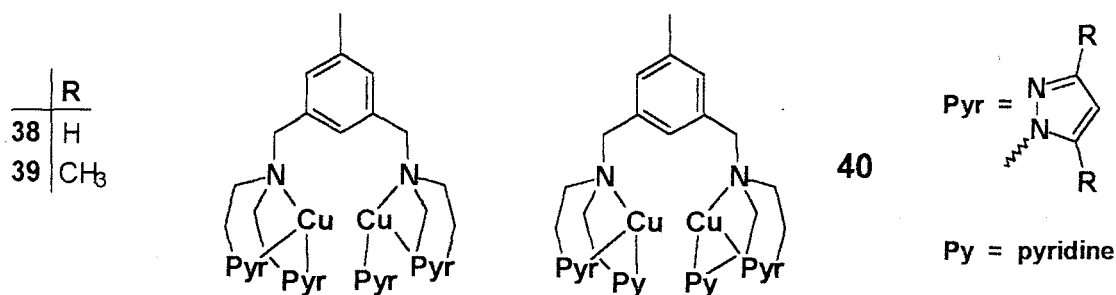
Reim *et al.* have reported symmetrical and unsymmetrical dinuclear copper complexes that catalyse the oxidation of 3,5-di-*t*-butylcatechol to the *o*-quinone.<sup>105</sup>

The complexes were prepared from ligands **34**, **35**, **36** and **37**. The dinuclear copper complex prepared from the symmetric ligand **34** displayed the highest catecholase activity of all the dinuclear copper complexes prepared from these ligands.

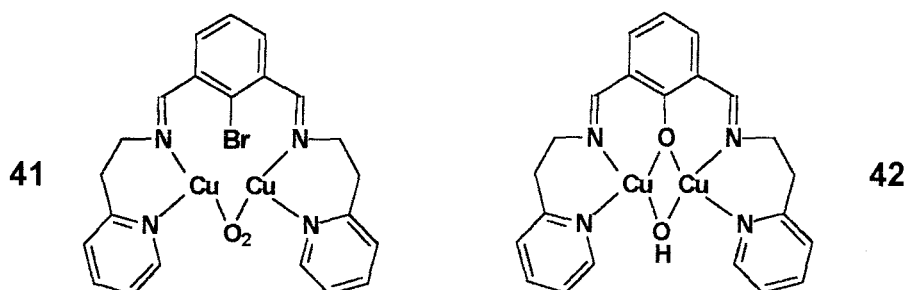


### Hydroxylation of the aromatic ring of the ligand.

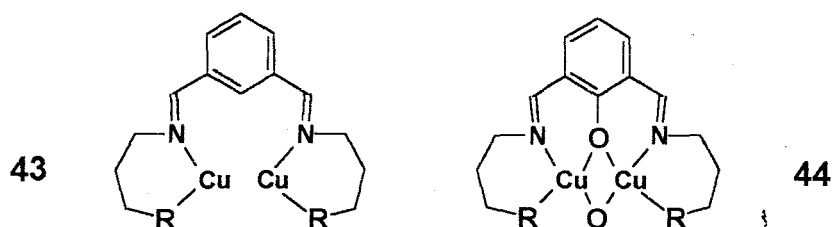
From studies conducted on the hydroxylation of the aromatic ring in dinuclear copper(I) complexes, it seems that the reaction is ligand dependent. Sorrel and his co-workers prepared complexes **38** and **39** and investigated their reaction with dioxygen.<sup>58</sup> They found that these copper(I) complexes neither catalyse the hydroxylation of the aromatic ring nor react with dioxygen in dichloromethane.



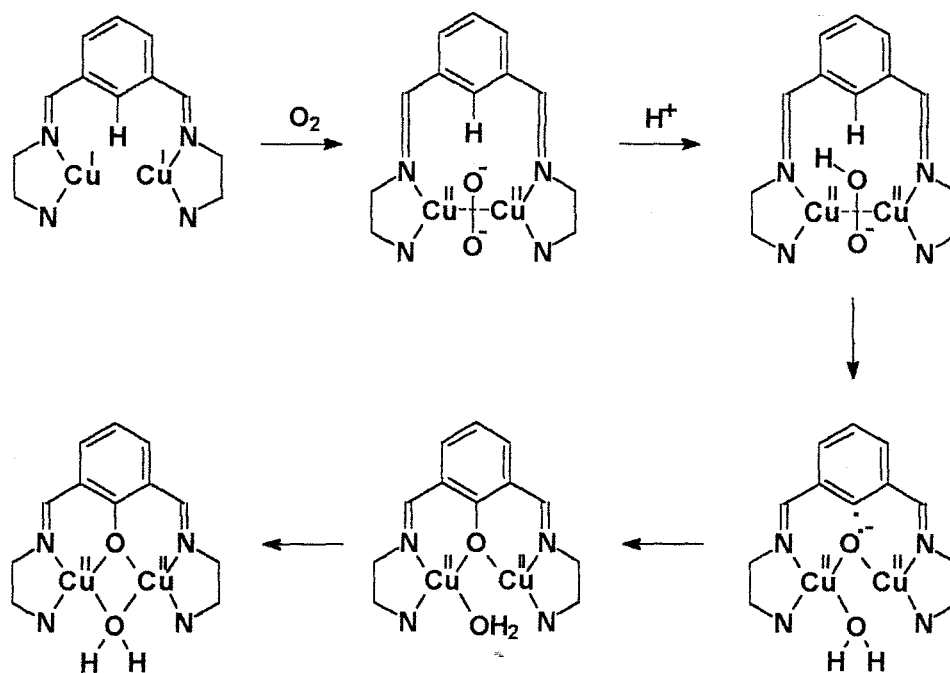
However, when the mixed pyrazole-pyridine copper(I) complex **40** was treated with dioxygen, a reaction was observed, but no aromatic hydroxylation occurred.



Dehalogenation reactions are catalysed by various enzymes using hydrolytic, reductive or oxidative pathways,<sup>106</sup> but only a few enzymes are capable of oxidative dehalogenation of aromatic compounds. The dinuclear copper(II) complex **41** has been reported to undergo oxidative debromination to afford complex **42** upon reaction with dioxygen at room temperature.

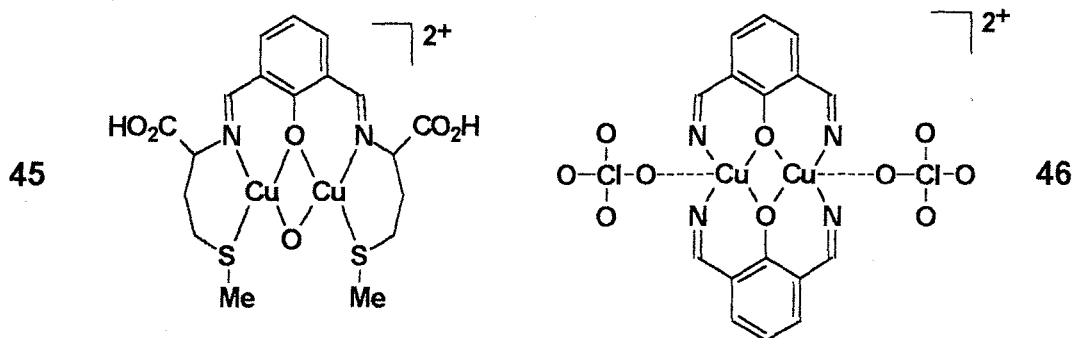


Casella and Gullotti have reported monooxygenase activity for complexes of type **43**, which are oxidised to the corresponding complexes **44**.<sup>107</sup> The hydroxylation of the ligand is affected by the solvent, the oxygenation reaction being partially or completely depressed in dry acetonitrile. Protons have been found to enhance the hydroxylation of some of these systems and, as a result, it has been suggested that an electrophilic copper-peroxo or copper-hydroperoxo complex is the active species in the hydroxylation process. A proposed mechanism for the hydroxylation reaction is illustrated in Scheme 1, and low-temperature spectral studies have been undertaken to characterise the intermediates.<sup>107</sup>



Scheme 1

Casella and co-workers have also reported aromatic hydroxylation to give the dinuclear copper(I) complex **45**, containing methionine sulfur groups.<sup>108</sup> The dinuclear copper(II) complex **46** forms as a result of hydrolytic cleavage of **45**, and has been characterised by X-ray crystallography.



## 1.4 THE IMPORTANCE OF METAL-DIOXYGEN BONDING

The flourishing interest in dinuclear and polynuclear complexes emanates from the fact that pairs or clusters of metal ions have the capacity to mediate certain chemical reactions of industrial significance either more efficiently than, or in a different manner to, isolated metal centres. Dinuclear complexes having metal centres in close proximity, have been the theme of much recent research since these structural units are believed to be involved in an array of crucial biochemical processes, especially oxygen transport and oxygen activation by metal - containing proteins and enzymes.<sup>109-120</sup> Reactions in which one or both atoms of dioxygen are catalytically inserted into an organic substrate are of significance in the synthesis of metabolic products and intermediates. Dioxygen also serves as an electron sink in the oxidation of a variety of small molecules such as ascorbic acid, catechol and amino acids.<sup>121,122</sup> Complexes, both synthetic and natural, which bind dioxygen reversibly have been termed oxygen carriers. In addition to their significance as models for natural oxygen carriers, synthetic dioxygen complexes have potential applications in dioxygen separation and storage, industrial processes and catalysis.<sup>122</sup> These complexes may act in catalytic or stoichiometric fashion. The concepts originating from these studies are expected to contribute to the evolution of practical synthetic systems for the reversible binding of oxygen and/or the oxidation of organic compounds.

The reduction of dioxygen is of major importance for biological systems and for oxygenation reactions. The free energy change for the four-electron reduction of dioxygen to two water molecules is  $-316 \text{ kJmol}^{-1}$  at pH 7 (eq. 1).



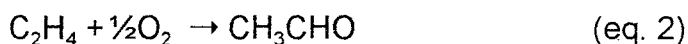
$$E^\circ = +0.815 \text{ V (vs. the normal hydrogen electrode)}$$

The reduction does not occur in a single step, but rather in a series of steps involving successive single - electron transfers. The usefulness of the reduction

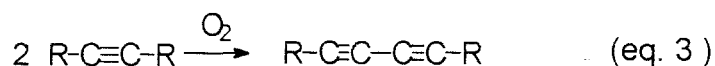
is, however, severely restricted. A common pathway for the reduction of dioxygen involves a one-electron reduction followed by disproportionation to form OH<sup>-</sup> (under basic conditions) or H<sub>2</sub>O<sub>2</sub> (under acidic conditions). The effective potential is pH independent and the single-electron reduction is endothermic by 128 kJmol<sup>-1</sup>.

It has been found that the oxidation of organic compounds is more efficient when dioxygen is directly involved with dinuclear rather than mononuclear complexes. The formation of metal hydroperoxides are of fundamental importance during these oxidations and, as a result, the formation of such species has been investigated.

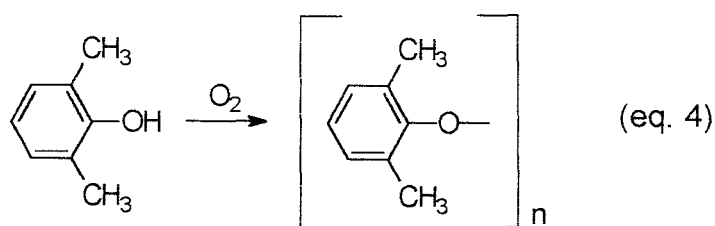
Copper is a metal which is particularly important in oxidation catalysis. It has been used extensively in the laboratory and in industry. The synthesis of acetaldehyde by catalytic oxidation of ethylene, the so-called Wacker process, is of major importance in the manufacture of organic chemicals from ethylene. The reaction is shown in equation 2.



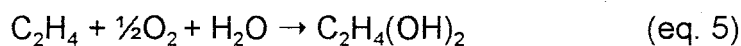
Although palladium is the main catalytic component responsible for the oxidation of acetaldehyde in the Wacker process, copper is the most effective co-catalyst to re-oxidise Pd<sup>0</sup> to Pd<sup>2+</sup> with dioxygen.<sup>123</sup> The oxidative coupling of acetylene to give diacetylenes, the Glaser reaction, is another well-known reaction catalysed by copper (eq. 3). This is synthetically useful<sup>124</sup> because many ethynyl compounds are coupled almost quantitatively. The coupling is effected by bubbling oxygen through an acetone solution of acetylene in the presence of a copper(I) chloride tetramethylethylenediamine complex.<sup>125</sup> This reaction is important in the commercial dimerisation of acetylene, which is then used as a precursor for chloroprene, the monomer for neoprene rubber.<sup>60</sup>



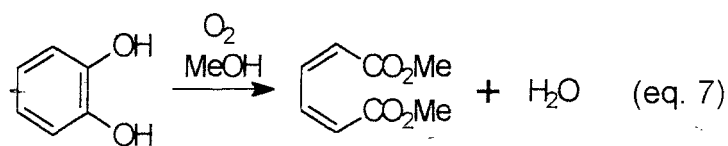
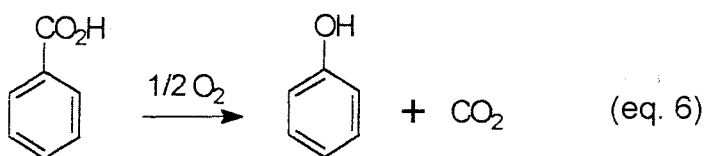
Aerobic oxidation of 2,6-xylenol with copper(I) in the presence of a N-donor ligand produces a *p*-phenylene oxide polymer which is widely used as an engineering thermoplastic under the trade name PPO (eq. 4).<sup>126</sup>



Ethylene glycol is produced directly from ethylene by oxidation in the Teijin process which utilises a CuBr system as a catalyst (eq. 5).<sup>127,128</sup> This oxidation process is important since ethylene glycol is a major intermediate in the synthesis of polyesters and polyurethanes.



The copper-mediated oxidative decarboxylation of benzoic acid to form phenol is an industrially useful reaction (eq. 6) as is the catalytic cleavage of catechol (eq. 7).<sup>129,130</sup>



Acrolein is manufactured by oxidising propene in the presence of heterogeneous catalysts containing copper or cuprous oxide, while methanol is produced from synthesis gas by a non-oxidative heterogeneous process using a CuO/ZnO catalyst. Hydroquinone, an important commodity chemical primarily used as an antioxidant and in photographic chemistry, is produced by the copper-catalysed oxidation of phenol with dioxygen to afford *p*-benzoquinone, which is then reduced.<sup>131</sup> The commercial production of trimethylhydroquinone, a vitamin E precursor, is based on the copper-catalysed oxidation of 2,3,5-trimethylphenol to the benzoquinone.<sup>131</sup> It is believed that copper-dioxygen complexes play important roles in these catalytic oxidation reactions. However, relatively few intermediates have been isolated and characterised. Furthermore, the structural factors which determine the catalytic effectiveness of the catalysts are not clearly understood.

There has also been considerable interest in the reactions of dioxygen and hydrogen peroxide with copper(I) complexes of 1,10-phenanthroline (phen),  $[\text{Cu}(\text{phen})_2]^+$  and substituted phen derivatives, following the discovery that  $[\text{Cu}(\text{phen})_2]^+$  cleaves deoxyribonucleic acid (DNA) in the presence of hydrogen peroxide.<sup>60</sup>

## 1.5 OBJECTIVES OF THE PRESENT INVESTIGATION

The primary aim of this study has been to design and prepare synthetic models of the enzyme, tyrosinase. In previous work in our group, synthetic models which contained an imine functionality were synthesised.<sup>138</sup> These synthetic models displayed some biomimetic activity but, unfortunately, the pure complexes could not be isolated, thus precluding unambiguous identification. It was suspected that the imine functionality was involved in intramolecular cyclisation resulting in formation of mixtures. In order to circumvent the problem of intramolecular cyclisation, attention in this study has been focussed on ligands which do not contain the imine functionality, and the following objectives were identified.

1. The design and synthesis of novel ligands capable of forming dinuclear copper complexes and acting as biomimetic models of the active site in tyrosinase.
2. The preparation and characterisation of copper complexes of these ligands.
3. An investigation of the copper oxidation state(s) in the resulting complexes using cyclic voltammetry.
4. Evaluation of the phenolase and catecholase activity of the copper complexes using 3,5-di-*t*-butylphenol and 3,5-di-*t*-butylcatechol as substrates respectively.
5. An investigation of complexes of the ligands with other metals, such as cobalt, nickel and platinum.

## 2 DISCUSSION

In the discussion that follows attention will be focussed on: - the synthesis of biphenyl ligands (Section 2.2.1); 1,10-phenanthroline ligands (Section 2.2.2); Schiff base ligands (Section 2.2.3); ligands prepared *via* the Baylis-Hillman reaction (Section 2.2.4); macrocyclic ligands (Section 2.2.5); and a dendrimer-based ligand (2.2.6). This is followed by complexation and computer modelling studies (Section 2.3). Electrochemical data, which help to elucidate the oxidation state(s) of the metal in copper, cobalt and nickel complexes, are considered in Section 2.4. Finally, the biomimetic evaluation of selected copper complexes is discussed in Section 2.5.

### 2.1 LIGAND DESIGN AND RATIONALE

The nature of the hydrocarbon groups (the "spacers") linking the coordinating units in dinuclear copper complexes had to be taken into account as this can markedly affect the reactivity of the copper complexes.<sup>132</sup> The ligands were designed, primarily, to incorporate copper(I) and copper(II) ions (Figure 8).

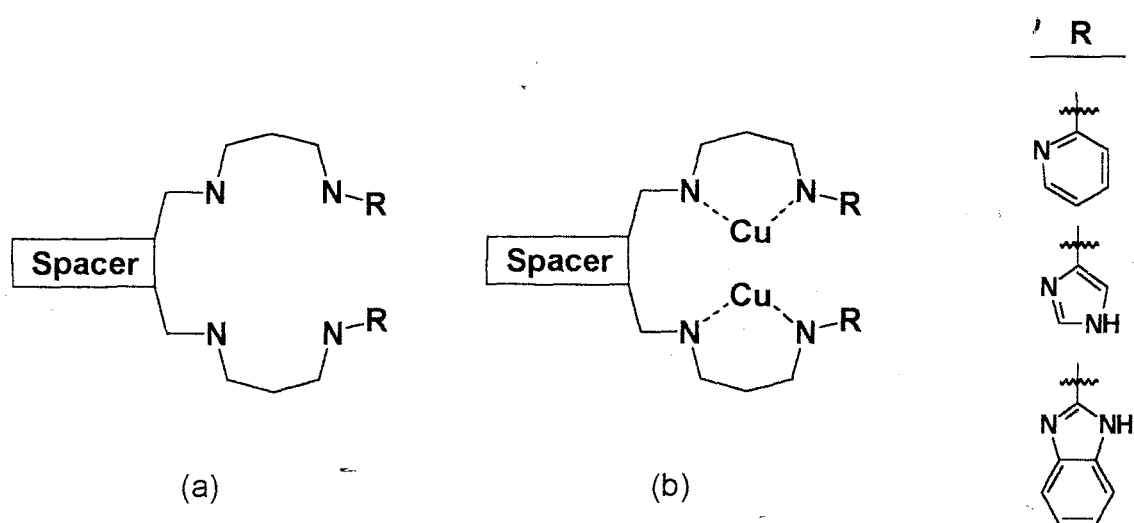


**Figure 8:** (a) The generalised ligand structure; (b) the complex after complexation with copper, but prior to oxygen bridging.

In these ligand systems, the spacer was varied to explore the effect of complex structure and geometry on biomimetic activity. For each of the ligands examined, there are at least two different types of nitrogen donor, one from an amide, amine or imine functionality attached to the "spacer", and the other from a heterocyclic system (R = pyridine, imidazole or benzimidazole; Figure 8). The electronic characteristics of the different nitrogen donors provide for variation in electron availability at the donor sites in the different complexes.

The incorporation of different nitrogen donor types is justified<sup>106</sup> by the fact that, in haemocyanin, one histidyl imidazole is situated further away from the copper ion than the other two;<sup>133</sup> it is believed that this is also likely to be the case in tyrosinase.<sup>134</sup> Additional support is provided by the activity shown by complexes containing different donor types.<sup>135,136</sup> The ligands have, typically, been designed to form 6-membered chelate rings on complexation, because this arrangement is stable for copper complexes and permits changes in the oxidation state.<sup>61</sup> For the ligands containing the planar 1,10-phenanthroline spacer, however, formation of a 5-membered chelate ring during complexation with copper is possible - an arrangement known to favour the stabilisation of the copper(II) oxidation state.<sup>137</sup> The substrate is expected to gain entry to the copper active site, in each case, by moving between the arms of the ligand.

In our attempts to develop synthetic models of the active site of the enzyme, tyrosinase, it was decided to prepare and isolate the organic ligand prior to complexation rather than use the template approach. This allows for the independent isolation and characterisation of the ligand without any interference from the metal ion.

## 2.2 LIGAND SYNTHESSES

### 2.2.1 Biphenyl ligands

The biphenyl unit has been used as a spacer to impart flexibility to the organic ligand and the resulting complex.<sup>138</sup> This spacer allows the complex to adopt a conformation in which the two copper atoms are sufficiently close together to permit bridging by dioxygen without imposing rigid planar geometry. It has been shown that if the spacer is too flexible, binding of the substrate may be inhibited.<sup>139</sup>

The synthetic routes used to prepare a series of ligands containing the biphenyl spacer are outlined in Scheme 2. Biphenyl-2,2'-dicarbaldehyde **48**<sup>140</sup> and biphenyl-2,2'-dicarboxylic acid **49**<sup>141</sup> were produced from phenanthrene **47** in separate reactions following reported methods. Thus, ozonolysis of phenanthrene **47** in methanol at low temperature [to inhibit formation of a stable peroxide **50** from the reaction of the intermediate with methanol (Scheme 3)] afforded biphenyl-2,2'-dicarbaldehyde **48** in high yield (93%). The <sup>1</sup>H NMR spectrum (Figure 9) of the dicarbaldehyde **48** is characterised by the aldehydic proton signal at  $\delta$ 9.83 ppm.

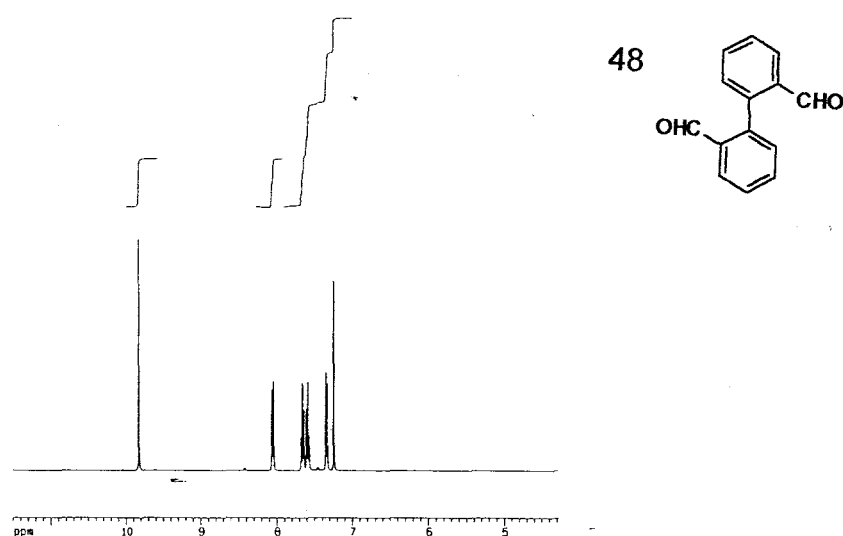
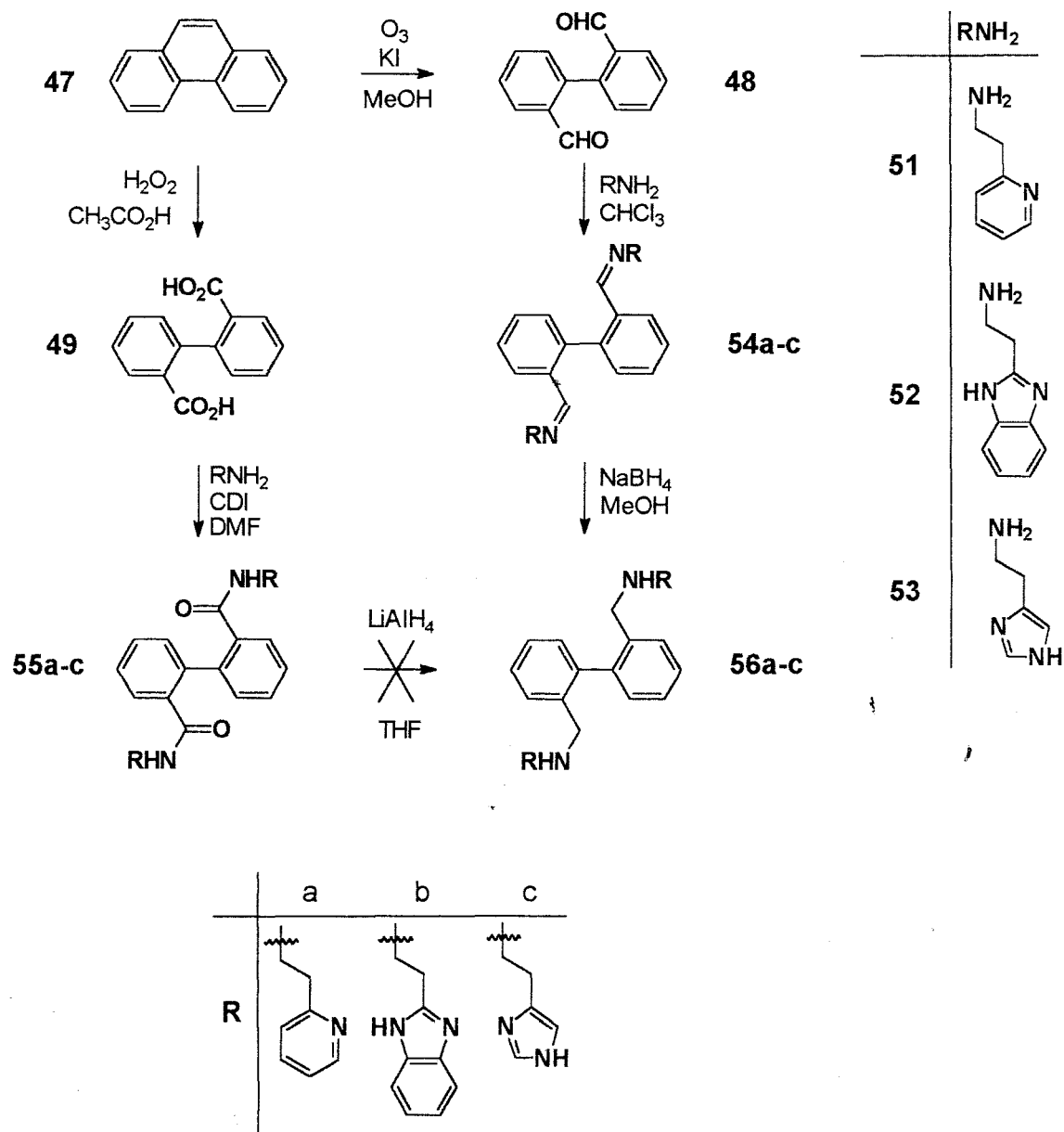
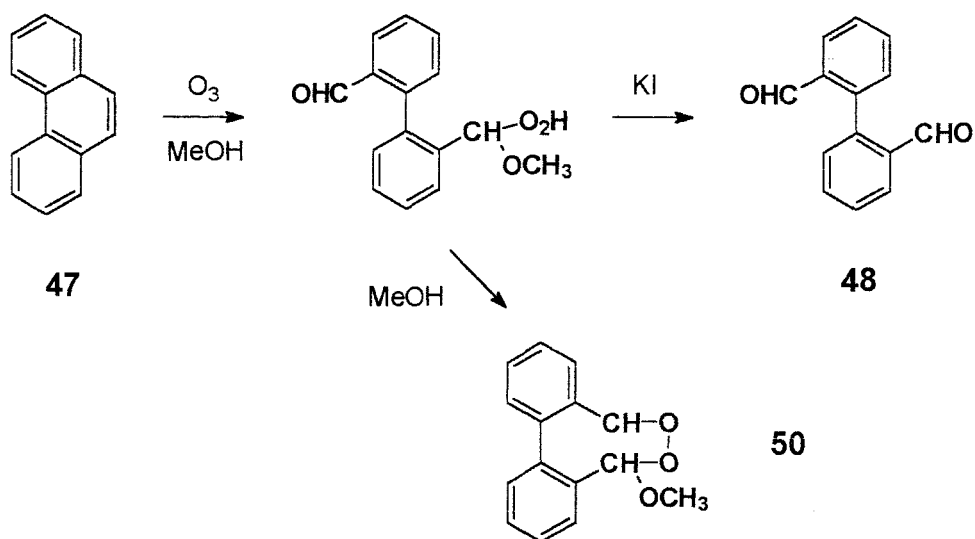


**Figure 9:** The 400 MHz <sup>1</sup>H NMR spectrum of biphenyl-2,2'-dicarbaldehyde **48** in CDCl<sub>3</sub>.

Access to the dicarboxylic acid **49** was achieved via  $\text{H}_2\text{O}_2$  oxidation of phenanthrene **47** in glacial acetic acid, the required product being isolated in 67% yield; the presence of the carboxylic acid group was confirmed by a  $^1\text{H}$  NMR signal at  $\delta 12.44$  ppm and a broad IR absorption band in the region  $2500\text{--}3500\text{ cm}^{-1}$ .

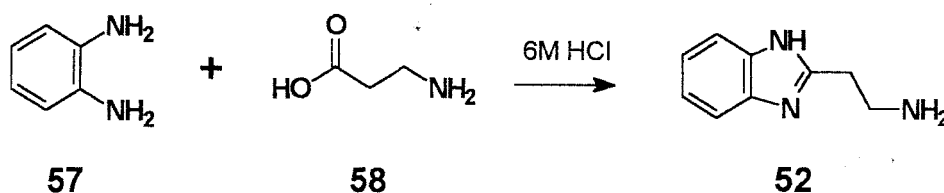


**Scheme 2:** Synthetic routes for obtaining ligands containing the biphenyl spacer.



**Scheme 3:** Synthesis of biphenyl-2,2'-dicarbaldehyde **48**.

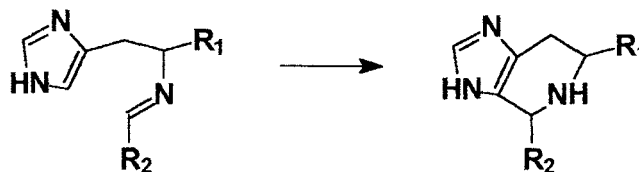
The chelating ligand system, 2-(2-aminoethyl)pyridine **51**, was available commercially, while histamine **53** had to be released from its dihydrochloride salt by treatment with sodium methoxide. 2-(2-Aminoethyl)benzimidazole **52** was obtained by reacting 1,2-diaminobenzene **57** with  $\beta$ -alanine **58** (Scheme 4).<sup>138</sup> The formation of the bis-substituted biphenyl derivatives **54a**, **54b** and **54c** containing these chelating systems, however, presented particular difficulties.



**Scheme 4:** Preparation of 2-(2-aminoethyl)benzimidazole **52**.

The formation and subsequent reduction of the diimino derivatives **54a**, **54b** and **54c** of the dialdehyde **48**, was expected to afford the required di-amino ligands **56a**, **56b** and **56c**. The tendency of imidazolyl imines to undergo intramolecular cyclisation, observed in our group<sup>138</sup> and reported by Casella *et al.*<sup>135</sup> (Scheme 5), had prompted us to target the diamines **56a**, **56b** and **56c** as model ligands rather

than their di-imino precursors **54a**, **54b** and **54c**. However, the reduction step proved more difficult than expected.



**Scheme 5:** An intramolecular cyclisation reaction proposed by Casella *et al.*<sup>135</sup>

The di-imino compound **54a**, containing pyridyl groups, was prepared using the procedure employed by Reglier *et al.*<sup>103</sup> Attempted reduction of this compound using sodium borohydride in methanol at room temperature, however, failed to afford the expected product, **56a**. The <sup>1</sup>H-NMR spectrum of the isolated product (Figure 10) are clearly inconsistent with structure **56a**. It was expected that the signals for the methylene protons at  $\delta$ 2.98,  $\delta$ 3.13 and  $\delta$ 3.48 ppm would each integrate for four protons but, instead, the integrals at  $\delta$ 2.98 and  $\delta$ 3.13 ppm are equivalent to two protons each, while only the signal at  $\delta$ 3.48 ppm integrates for four protons. The <sup>13</sup>C NMR spectrum (Figure 11), however, reveals the expected 14 signals (2 overlapping at ca. 55.5 ppm; 3 at ca. 127.5 ppm).

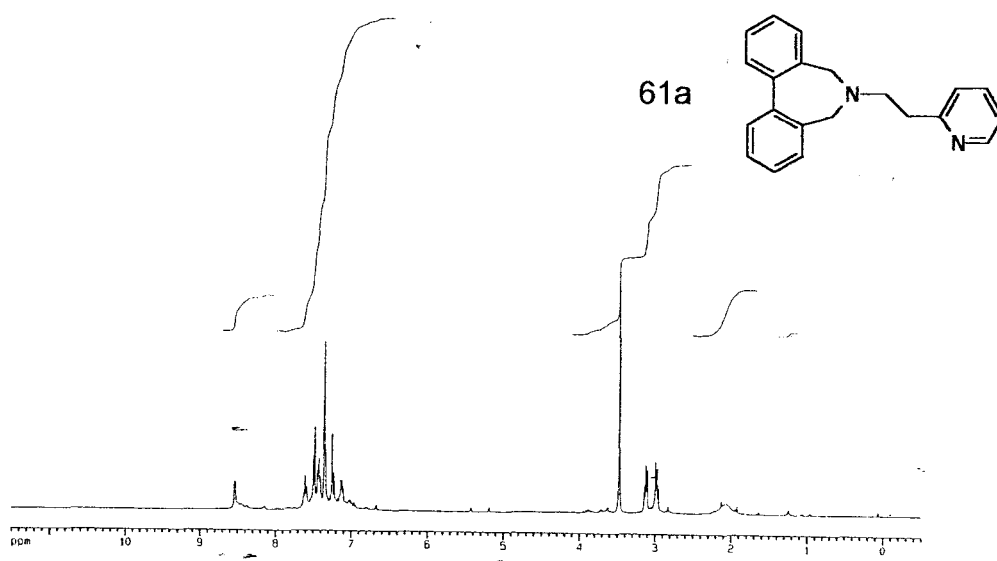


**Figure 10:** The 400 MHz <sup>1</sup>H NMR spectrum of ligand **61a** in CDCl<sub>3</sub>.

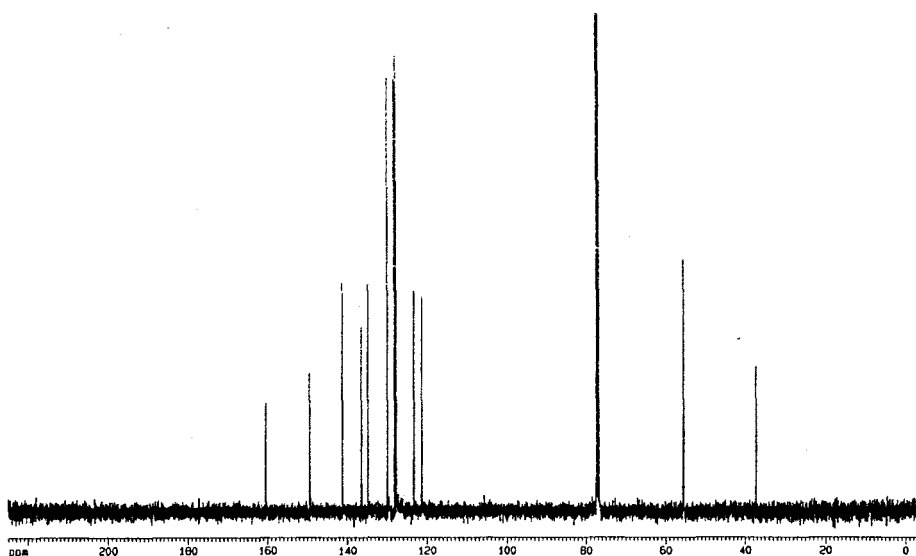
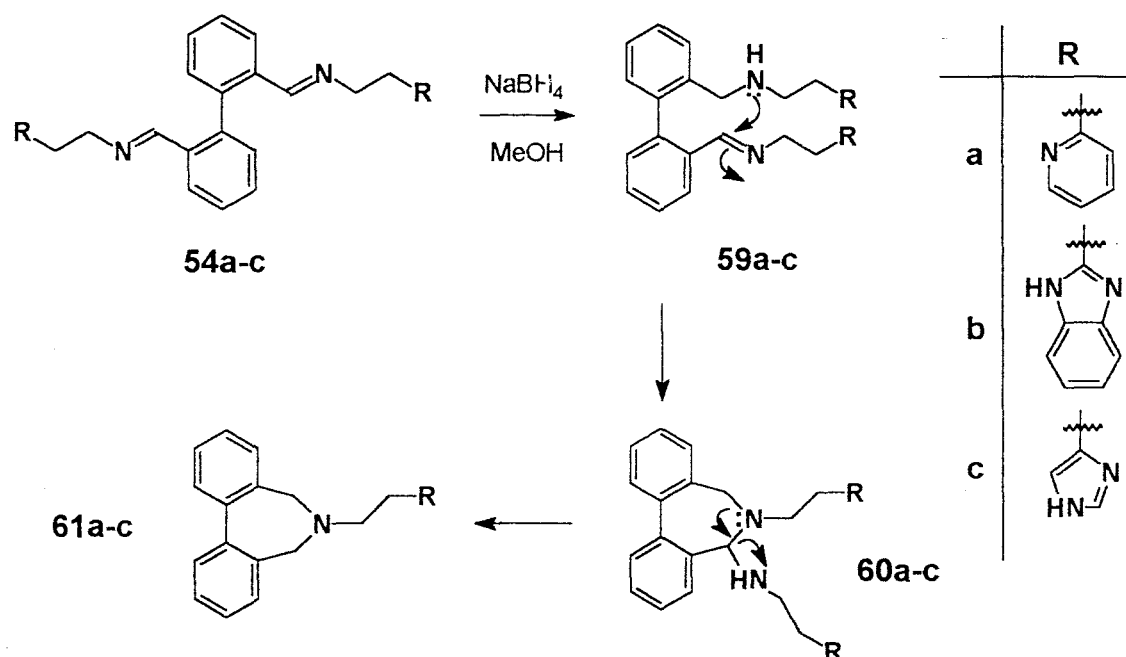


**Figure 11:** The  $^{13}\text{C}$  NMR spectrum of ligand **61a** in  $\text{CDCl}_3$ .

When the reaction was repeated at room temperature, the same product was isolated. Single crystal X-ray analysis (see sections 2.3.4.1.2, p.107, Figure 36 and 2.3.4.2.2, p.122, Figure 46) of the cobalt and nickel complexes of this compound revealed that the ligand was, in fact, the dibenzoazepine ( $\text{R} = \text{pyridine}$ ; Scheme 54), thus explaining the apparent anomalies in the NMR spectra.

Formation of ligand **61a** may be rationalised in terms of the mechanism outlined in Scheme 6. It is suggested that one imine functionality is first reduced during the reaction with  $\text{NaBH}_4$ . The lone pair on the nitrogen of the resulting amine functionality **59a** then attacks the remaining imine functionality, resulting in cyclisation and subsequent loss of one arm of the ligand from the intermediate amination **60a**. Similar reduction of diimines **54b** and **54c** also failed to yield the expected products **56b** and **56c**, affording, instead, the corresponding dibenzoazepines **61b** and **61c**. One- and two-dimensional analysis (illustrated for compound **61b** in Figures 12 and 13) provided unambiguous confirmation of the identity of these cyclised products.



**Scheme 6:** Proposed mechanism for the intramolecular cyclisation during  $\text{NaBH}_4$  reduction of the diimine **54a**.

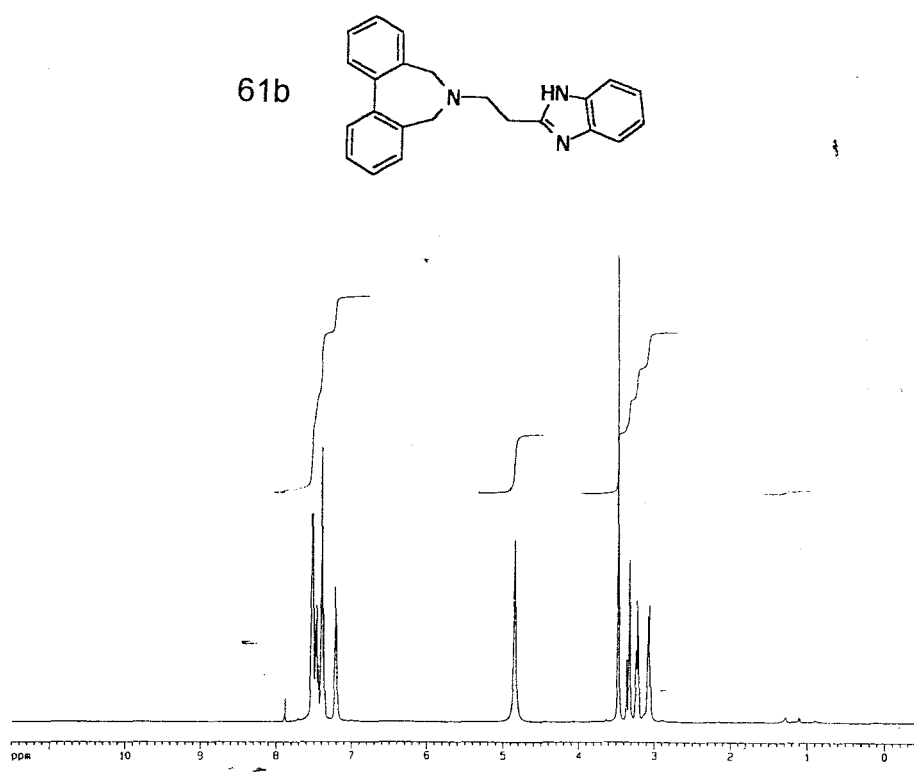


**Figure 12:** The 400 MHz  $^1\text{H}$  NMR spectrum of ligand **61b** in  $\text{MeOH-d}_4$ .

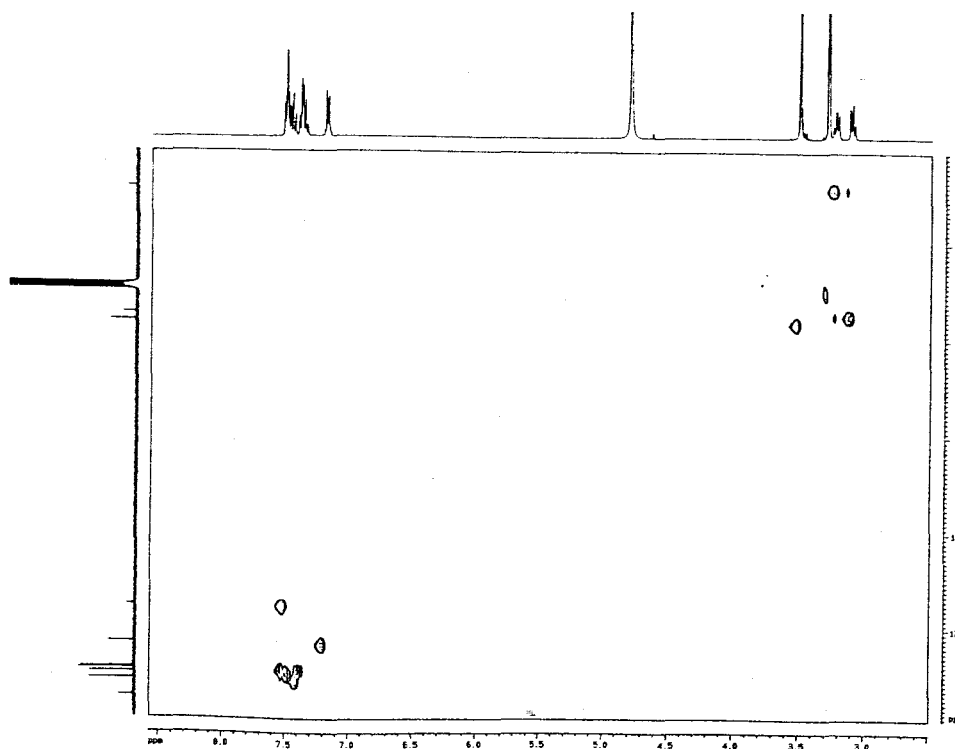


**Figure 13:** The HETCOR spectrum of ligand **61b** in MeOH- $d_4$ .

In an alternative approach, it was decided to focus attention on ligands containing amide rather than imine functions and to effect reduction to the corresponding amine ligands **56a**, **56b** and **56c** using lithium aluminium hydride (Scheme 2). The diamides were prepared by reacting the diacid **49** with the coupling agent carbonyl diimidazole (CDI),<sup>142</sup> at 40°C and then treating the resulting intermediate with the amines 2-(2-aminoethyl)pyridine **51**, 2-(2-aminoethyl)benzimidazole **52** and histamine **53**. The diamides were obtained in 54-82% yield and were fully characterised by elemental (high resolution MS) and spectroscopic analysis. Broadening and coalescence of certain signals is apparent in the  $^1\text{H}$  NMR spectra of ligands **55b** and **55c**. These effects are illustrated in the  $^1\text{H}$  NMR spectrum of diamide ligand **55c** where broad peaks are observed at  $\delta$ 2.51 and  $\delta$ 3.34 ppm (Figure 14). The broadening of the peaks are attributed to slow rotation of the bonds on the NMR time scale. Unfortunately, numerous attempts to reduce these diamides (**55a**, **55b** and **55c**) with reducing agents such as lithium aluminium hydride and Raney Nickel were unsuccessful.

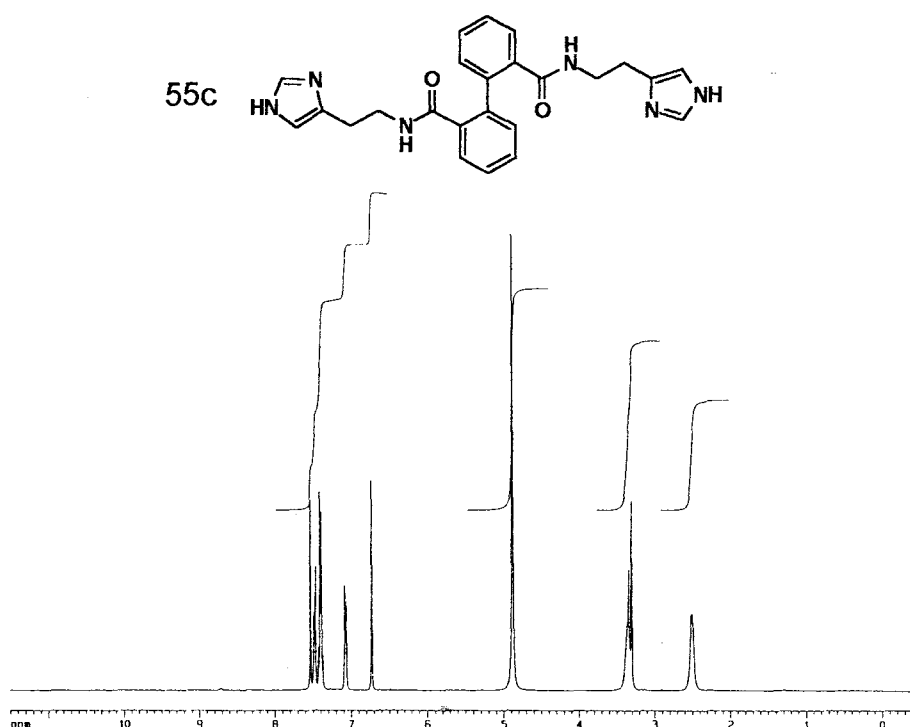
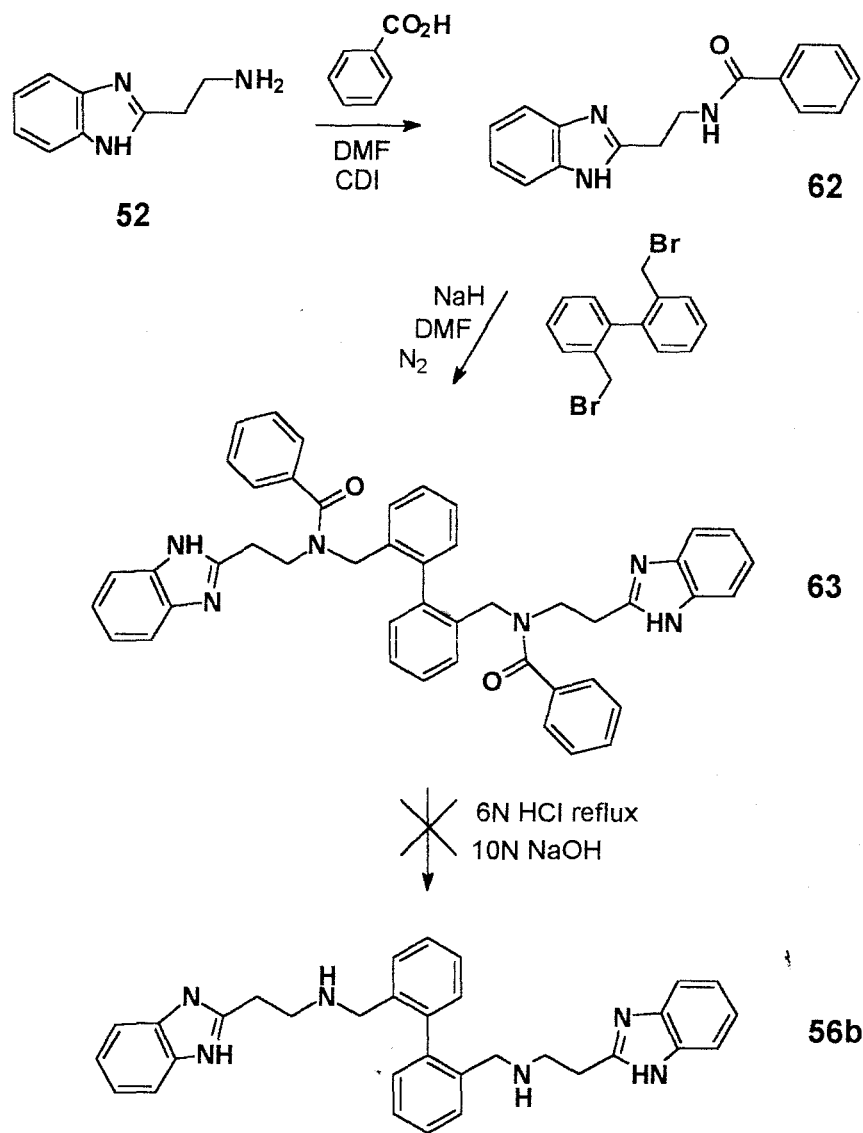


**Figure 14:** The 400 MHz <sup>1</sup>H NMR spectrum of diamide ligand **55c** in MeOH-*d*<sub>4</sub>.

In a third approach, a synthetic route reported by Sorrell and Garrity,<sup>143</sup> was explored. These authors had also been unsuccessful in their attempts to reduce similar amide derivatives and, as a result, they developed a synthetic route that involved initial protection of the amine as an amide, followed by deprotection using acid hydrolysis. A similar synthetic approach (Scheme 7) was investigated for generating the diamine ligand **56b**. The amide **62** was obtained by condensing 2-(2-aminoethyl)benzimidazole **52** with benzoic acid and using CDI as the coupling agent. This amide was then treated with NaH and 2,2'-dibromomethylbiphenyl to give the diamide ligand **63**. The structure of the ligand was confirmed by elemental and spectroscopic analysis; the complexity of the aromatic region in the <sup>13</sup>C NMR spectrum can be clearly seen in Figure 15. Attempts to remove the benzoyl protecting groups by acid hydrolysis proved unsuccessful. Given the unexpected difficulties in accessing the diamino ligands, we decided to examine the various amide ligands, which had been obtained, as potential ligands for complexing copper (see section 2.3.2).



**Scheme 7:** Attempted synthesis of ligand **56b**.

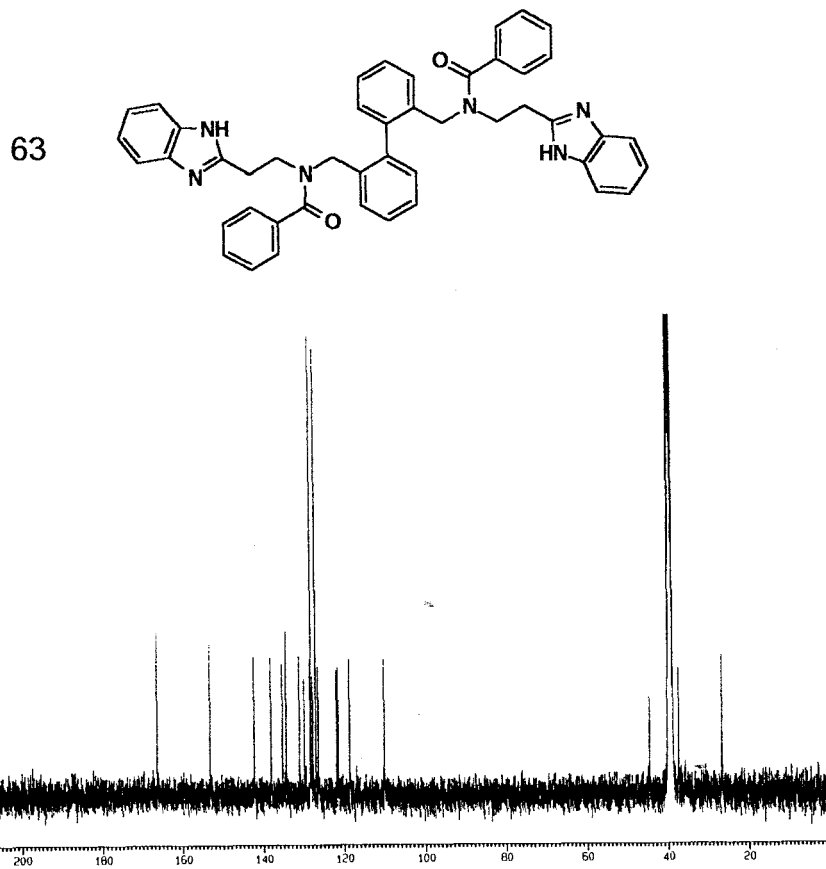


**Figure 15:** The 400 MHz  $^{13}\text{C}$  NMR spectrum of ligand **63** in  $\text{DMSO-}d_6$ .

### 2.2.2 1,10-Phenanthroline ligands

Ligands containing the 1,10-phenanthroline unit as spacer were expected to exhibit some rigidity and planarity. Such rigidity in copper complexes may well favour binding of the substrate and, thus, enhance their biomimetic potential. The synthetic routes followed to obtain 1,10-phenanthroline-containing ligands are outlined in Scheme 8.

Neocuproine **64** (2,9-dimethyl-1,10-phenanthroline) was used as the starting material. It has long been known that this compound is a useful analytical reagent for the determination of copper,<sup>144</sup> forming a bright red copper complex. The SeO<sub>2</sub> oxidation reactions of neocuproine **64** to 1,10-phenanthroline-2,9-dicarbaldehyde **65**<sup>145</sup> and the subsequent oxidation to 1,10-phenanthroline-2,9-dicarboxylic acid **66**<sup>145</sup> using 80% HNO<sub>3</sub>, occurred with relative ease. The <sup>1</sup>H NMR spectrum of 1,10-phenanthroline-2,9-dicarbaldehyde **65** (Figure 16) reveals the characteristic aldehydic proton signal at δ10.35 ppm.

Condensation of 1,10-phenanthroline-2,9-dicarbaldehyde **65** with the amines **51** and **52** gave the corresponding imines **67a** and **67b** which, without further purification, were reduced using NaBH<sub>4</sub> to afford the required diamino ligands **68a** and **68b**. These ligands were fully characterised, and 1- and 2-D NMR spectra for compound **68a** are illustrated in Figures 17 and 18 respectively. From the <sup>1</sup>H NMR spectrum it can be seen that the formation of the diamine ligand **68a** was successful, the singlet at δ4.32 ppm corresponding to the methylene groups. The HETCOR spectrum of ligand **68a** (Figure 18) reveals the requisite correlations between the carbons and their attached protons.



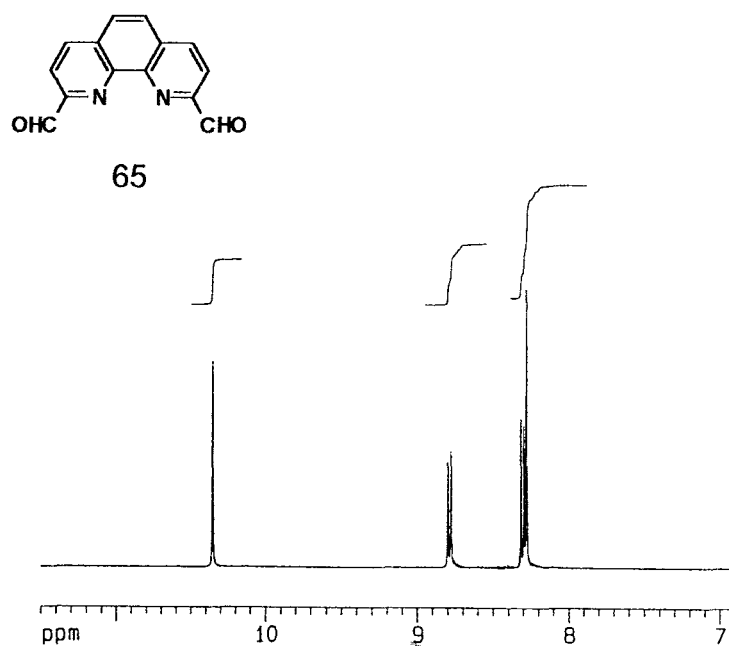


**Figure 16:** The 400 MHz <sup>1</sup>H NMR spectrum of 1,10-phenanthroline-2,9-dicarbaldehyde **65** in DMSO-*d*<sub>6</sub>.

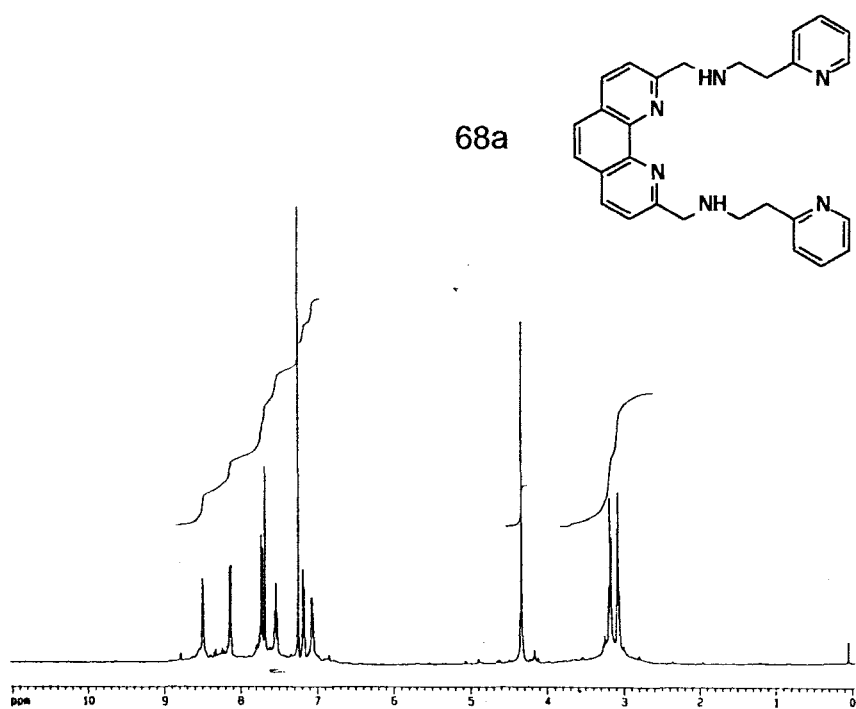


**Figure 17:** The 400 MHz <sup>1</sup>H NMR spectrum of ligand **68a** in CDCl<sub>3</sub>.

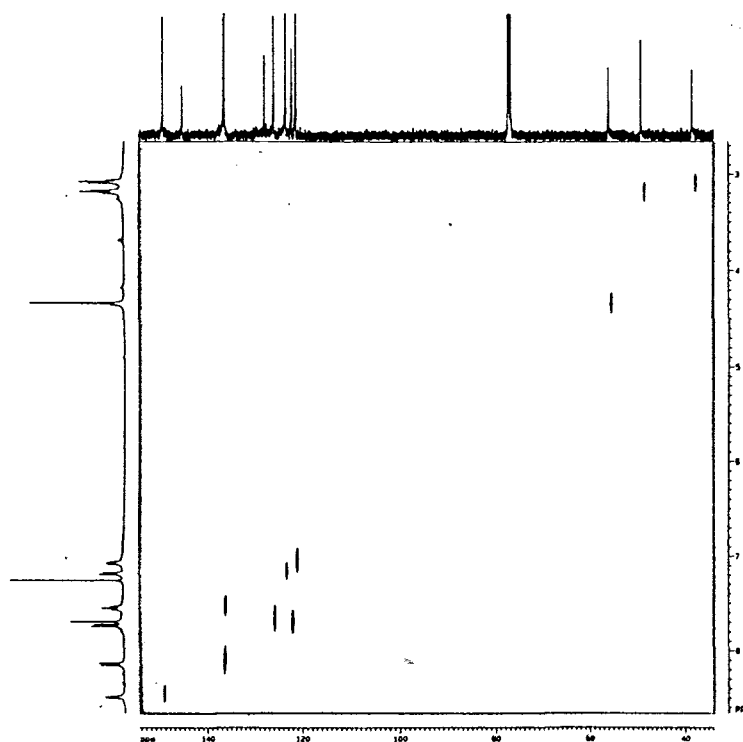


**Figure 18:** The HETCOR spectrum of ligand **68a** in  $\text{CDCl}_3$ .

In an alternative approach, the dicarboxylic acid **66** was condensed with each of the amines, 2-(2-aminoethyl)pyridine **51**, 2-(2-aminoethyl)benzimidazole **52** and histamine **53** using CDI as a condensing agent. The resulting diamides **69a**, **69b** and **69c** were isolated in yields ranging from 61 to 73% and, in each case, a signal corresponding to the amide proton was observed at  $\delta$ 9.5-9.8 ppm in the  $^1\text{H}$  NMR spectrum (illustrated for ligand **69b** in Figure 19). Access to the 1,10-phenanthroline-based diamino ligands **68b** and **68c** was then explored *via* the reduction of the intermediate diamides **69b** and **69c**. Amide carbonyl groups are commonly reduced using excess  $\text{LiAlH}_4$ . Unfortunately, as was the case with the biphenyl analogues, attempts to reduce the diamides **69b** and **69c** using  $\text{LiAlH}_4$  were unsuccessful. It was decided to evaluate the diamides as potential ligands for copper, the diamino analogues being available *via* the diimines.

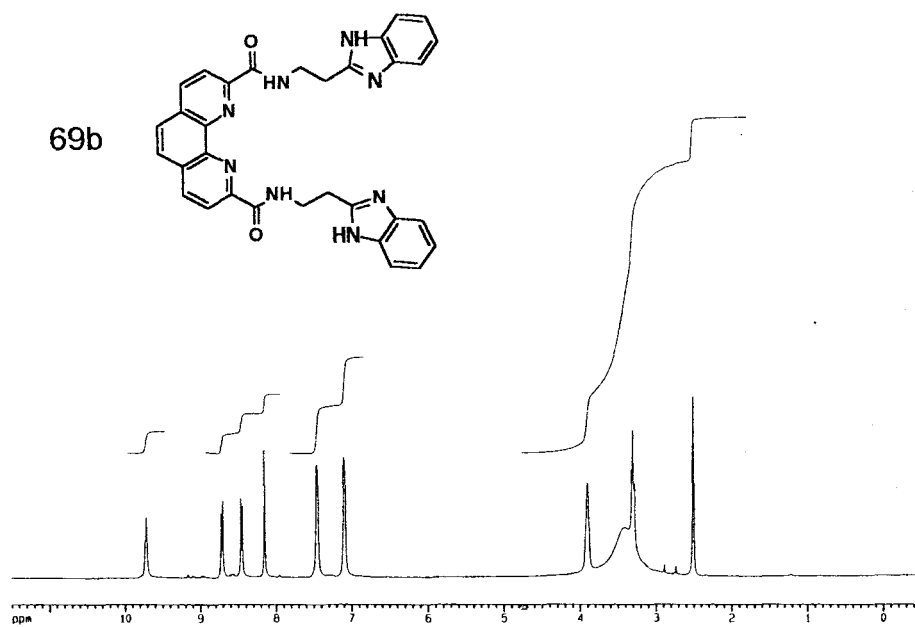


**Figure 19:** The 400 MHz  $^1\text{H}$  NMR spectrum of ligand **69b** in  $\text{DMSO-}d_6$ .

### 2.2.3 Schiff base ligands prepared from diketones

A series of novel diimine ligands were targeted, which contain acyclic spacers and which illustrate the effect of varying the length of the spacer chain and the substituents R<sup>1</sup>, R<sup>2</sup> and R<sup>3</sup> (Figure 20). As imidazole-containing imino ligands are prone to intramolecular cyclisation, 2-(2-aminoethyl)pyridine **51** was chosen to form the coordinating arms of the ligands. Various diketones were used to provide the required spacer moieties. Furthermore, the ligands were designed to complex copper *via* 6-membered chelate rings (see Figure 20b), thus allowing changes in the oxidation state of copper.<sup>61</sup> Additional advantages are that both the imine and pyridine moieties are able to stabilise copper in the lower oxidation state.

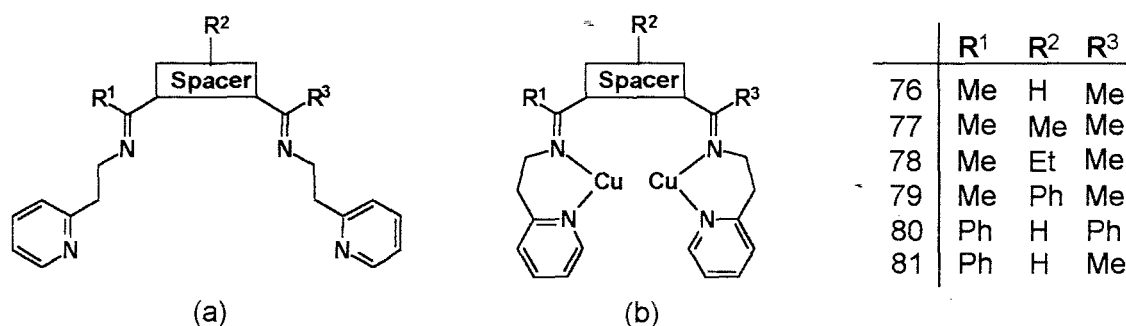
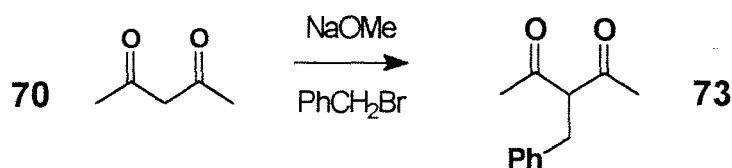


**Figure 20:** (a) Proposed Schiff base ligands and (b) their envisaged complexation with copper.

The synthesis of these ligands is outlined in Scheme 9. With the exception of the diketone **73**, which was prepared by the standard benzylation of acetylacetone (Scheme 10), the required diketones were available commercially. Reaction of these diketones with 2-(2-aminoethyl)pyridine **51** gave the expected diimines **76-81** in yields ranging from 25 to 61%. Similar condensation of the diketone **82** afforded the diimine **84**; numerous attempts to prepare the diphenyl analogue **85** from the diketone **83** proved unsuccessful. The ligands were purified by flash chromatography and characterised by NMR spectroscopy and by FAB-MS analysis.





**Scheme 10:** Synthesis of the diketone **73**.

The <sup>1</sup>H NMR spectra for ligands **76-81** in which the imine functionalities are separated by one carbon atom, reveal extensive tautomerism. A broad signal in the region δ12-13 ppm characterises the <sup>1</sup>H NMR spectra of these ligands (illustrated for ligand **78** in Figure 22) and is attributed to the hydrogen-bonded amino proton in the enamine tautomer (Figure 21). This interpretation is supported by deuterium exchange data. After the addition of D<sub>2</sub>O to a sample of ligand **78** in CDCl<sub>3</sub>, the <sup>1</sup>H NMR signal at δ12.37 ppm virtually disappeared (Figure 23); furthermore, the methylene signal at δ3.65 ppm (observed as a quartet before deuterium exchange) appeared as a triplet indicating coupling between the amino proton and the adjacent methylene protons. In the <sup>1</sup>H NMR spectrum of ligand **84** (in which the imine groups are separated by two methylene groups), however, the signal at ca. δ12 ppm is absent and the methylene signal at δ4.13 appears as a triplet, not as a quartet (Figure 24). Thus, it may be concluded that significant tautomerism only occurs when the imine functionalities are separated by one carbon atom.<sup>1</sup> This is not surprising since, only in these systems, is the enamine tautomer (Figure 21) stabilised by extensive conjugation and by a six-membered, H-bonded chelate.

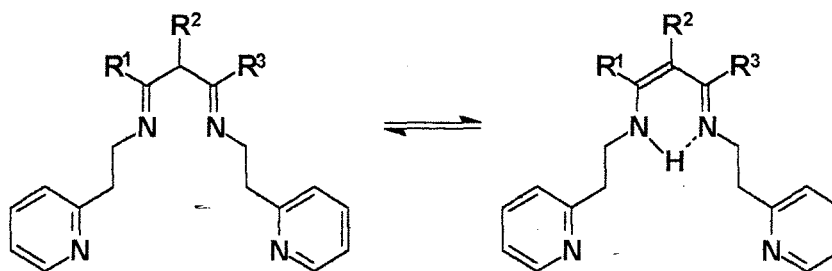


**Figure 21:** Tautomerism in the Schiff base ligands **76-81**.

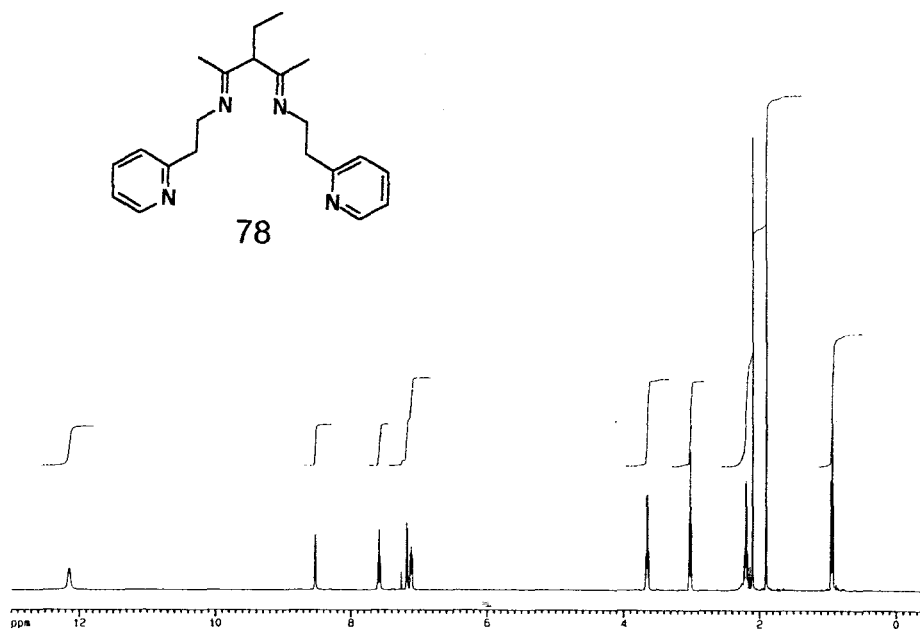


**Figure 22:** The 400 MHz  $^1\text{H}$  NMR spectrum of ligand **78** in  $\text{CDCl}_3$ .

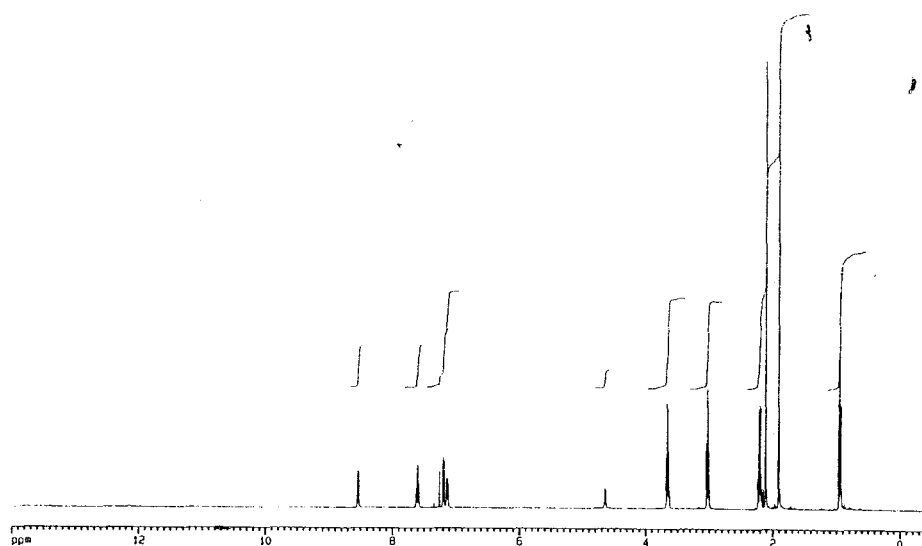


**Figure 23:** The 400 MHz  $^1\text{H}$  NMR spectrum of ligand **78** in  $\text{CDCl}_3$  after the addition of  $\text{D}_2\text{O}$ .

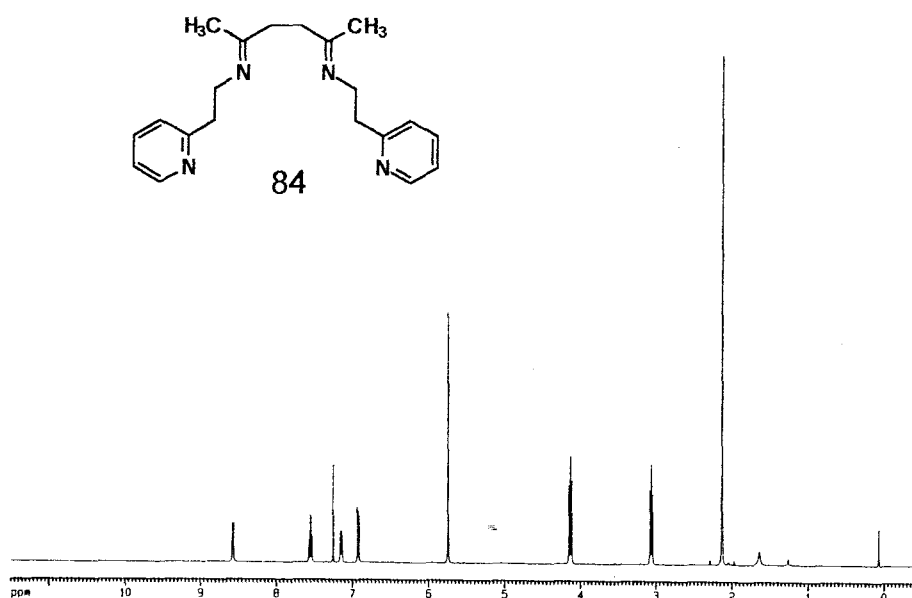
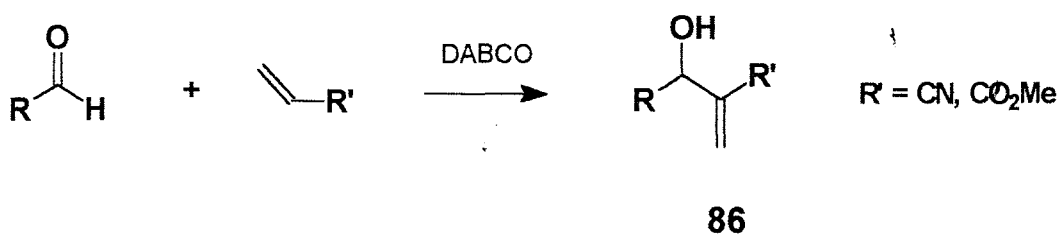


**Figure 24:** The 400 MHz <sup>1</sup>H NMR spectrum of ligand **84** in CDCl<sub>3</sub>.

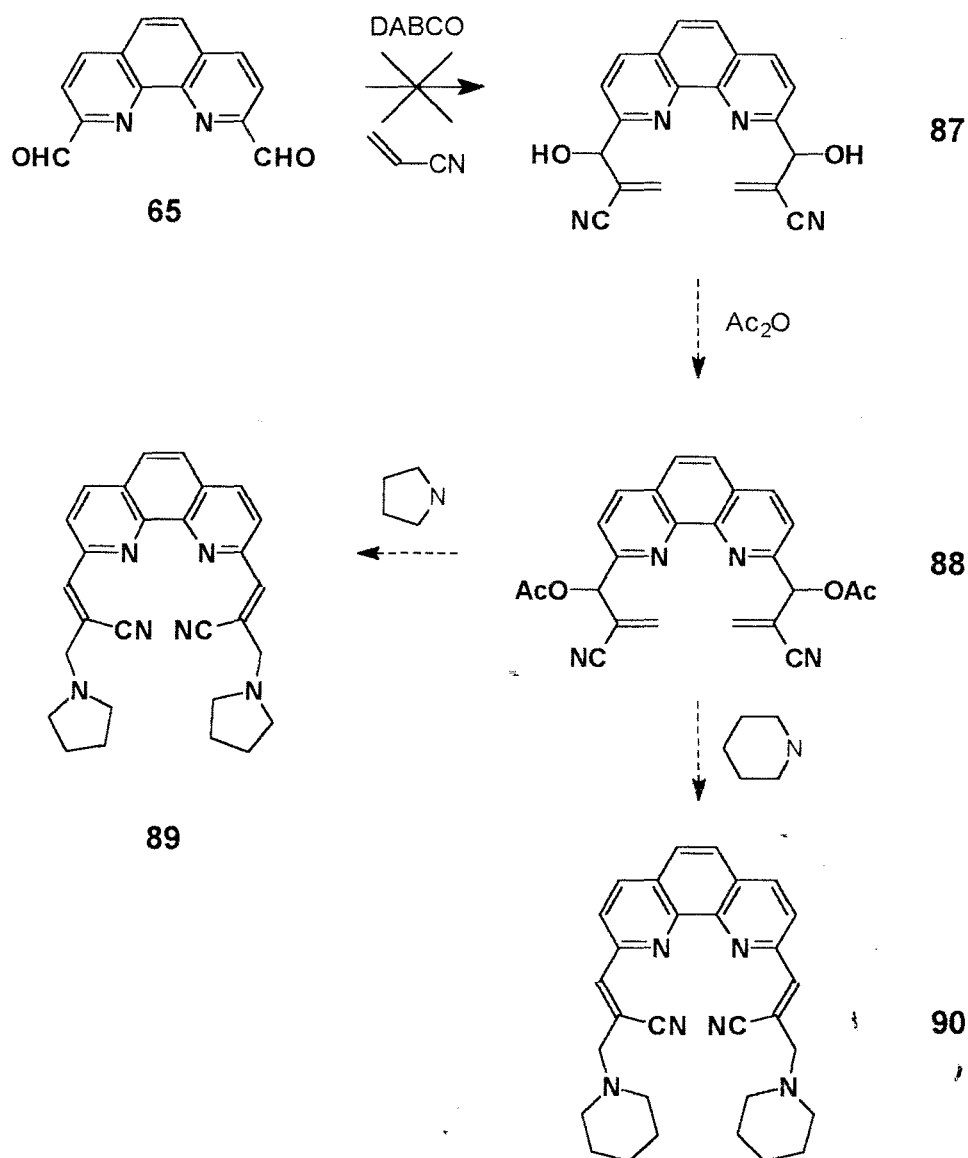
The Schiff base ligands, derived as they are from acyclic diketone spacers, are flexible, since rotation about the carbon-carbon bonds separating the two imine functionalities is possible. As a result, their copper complexes may be expected to readily adopt appropriate conformations for binding a substrate molecule. However, it was hoped that the copper complexes would not be too flexible as this could actually inhibit the binding of the substrate and result in an absence of catalytic activity.

## 2.2.4 The Baylis-Hillman approach to ligand synthesis

A further approach to the synthesis of ligand systems involved use of the Baylis-Hillman reaction,<sup>146</sup> in which activated alkenes (typically, acrylate esters) react with aldehydes in the presence of a nucleophilic catalyst, such as DABCO (diazabicyclo[2.2.2]octane), to afford multifunctional products **86** (Scheme 11). The reaction has been the subject of several reviews,<sup>147</sup> and has been applied in our research group to the synthesis of heterocyclic systems, *viz.*, indolizine,<sup>148</sup> quinoline,<sup>149</sup> coumarin and chromene derivatives.<sup>150</sup> In the present study, it was anticipated that application of the Baylis-Hillman reaction to a dialdehyde (e.g. 1,10-phenanthroline-2,9-dicarbaldehyde **65**; Scheme 12) would provide access to polydentate ligands such as **89** and **90**. Thus, reaction of the acetylated Baylis-Hillman product **88** with piperidine or pyrrolidine was expected to lead, *via* a conjugate addition-elimination sequence, to the ligands **89** and **90** respectively. Before applying the Baylis-Hillman reaction to the dialdehyde **66** it was decided to use pyridine-2-carboxaldehyde **91** (Scheme 13) as a model system to explore the feasibility of the proposed transformations.



**Scheme 11:** The Baylis-Hillman reaction.



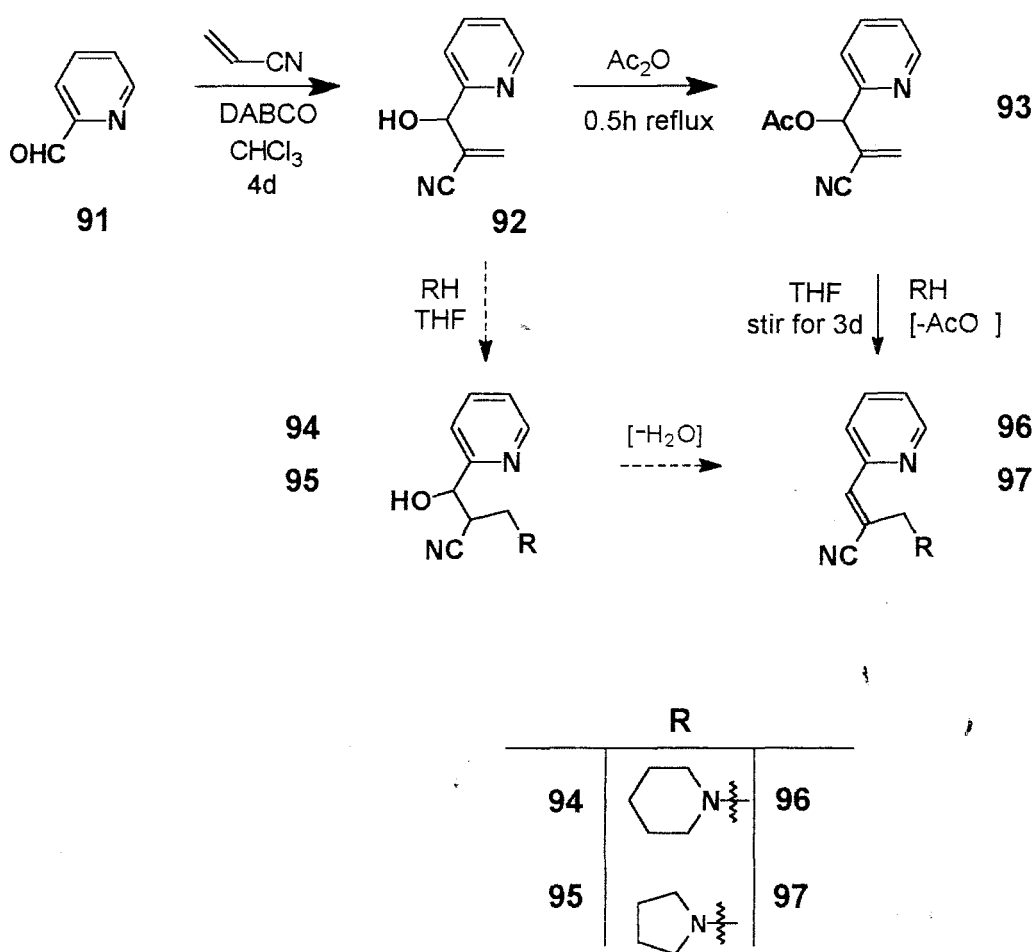
**Scheme 12:** Proposed Baylis-Hillman pathway to polydentate ligands.

#### 2.2.4.1 Pyridine-2-carboxaldehyde as a substrate

The Baylis-Hillman product **92** was obtained after 4 days by reacting pyridine-2-carboxaldehyde **91** with acrylonitrile in the presence of DABCO (Scheme 13).<sup>148</sup>

Once this product had been obtained, two routes to compounds **96** and **97** were considered. In the first, reaction of pyrrolidine or piperidine with the Baylis-Hillman product **92** was expected to give derivatives **94** and **95** via an addition reaction,

subsequent dehydration affording **96** and **97** respectively. Alternatively, acetylation of the Baylis-Hillman product **92**, followed by allylic ( $S_N$ ) displacement of acetate from the acetylated intermediate **93** by piperidine or pyrrolidine, was expected to afford compounds **96** and **97** respectively. In the event, the latter synthetic route involving the acetylated product **93** was attempted first and was found to work well; as a result, the alternative route was not attempted.



**Scheme 13:** Synthesis of model ligands using the Baylis-Hillman reaction.

The purpose of acetylating the hydroxyl group in the Baylis-Hillman product is, of course, to provide a better leaving group, thus facilitating allylic displacement by the nucleophilic 2° amine. One drawback of the acetylation approach, however, is that the acetylated product can cyclise at elevated temperature to form an

indolizine.<sup>148</sup> This cyclisation can be avoided by ensuring a reaction temperature of less than *ca.* 80°C. The acetylated product was obtained in 60% yield, and was readily identified by the characteristic acetate methyl signal at  $\delta$ 2.21 ppm in the  $^1\text{H}$  NMR spectrum (Figure 24).

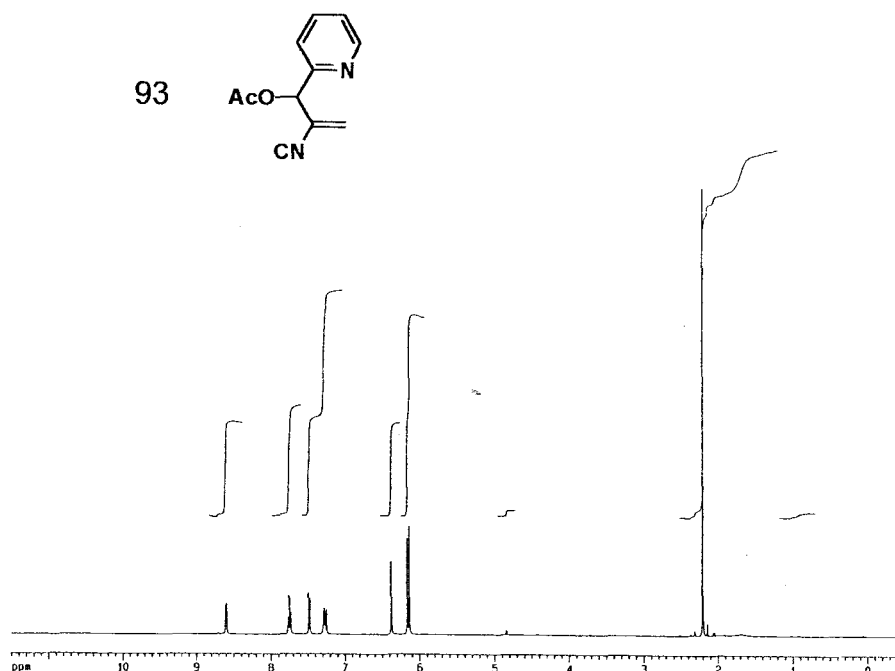


**Figure 24:** The 400 MHz  $^1\text{H}$  NMR spectrum of the acetylated product **93** in  $\text{CDCl}_3$ .

The  $^1\text{H}$  NMR spectrum of the substitution product **96**, on the other hand, (Figure 25) is characterised by the absence of the acetate methyl signal and the appearance of a signal at  $\delta$ 3.29 ppm corresponding to the allylic methylene protons; the piperidine methylene protons are responsible for the signals in the region  $\delta$ 1.4-3.3 ppm. The presence of the nitrile group is confirmed by an IR absorption band at  $2217\text{ cm}^{-1}$ . The analogous pyrrolidine derivative **97** was similarly characterised from the NMR and IR data.

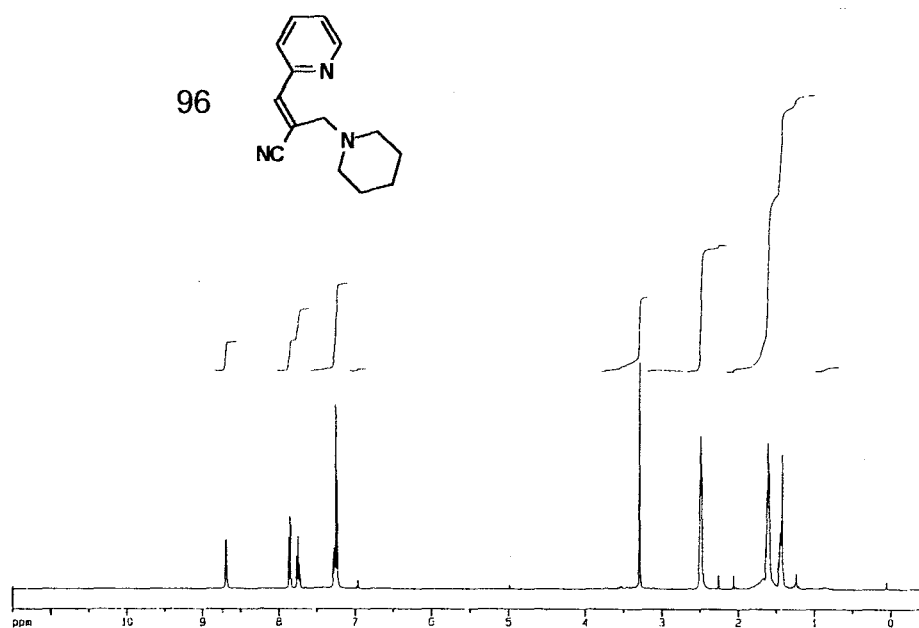


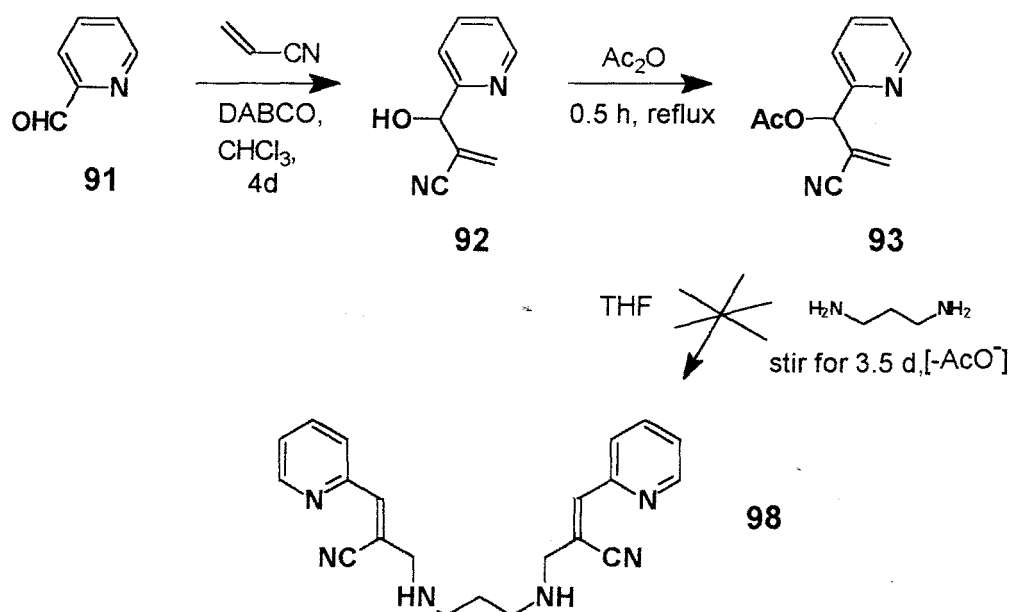
**Figure 25:** The 400 MHz <sup>1</sup>H NMR spectrum of compound **96** in CDCl<sub>3</sub>.

#### 2.2.4.2 1,10-Phenanthroline-2,9-dicarboxaldehyde **65** as a Baylis-Hillman substrate.

Given the success obtained with pyridine-2-carbaldehyde **91**, the use of 1,10-phenanthroline-2,9-dicarbaldehyde **65** as a substrate for the Baylis-Hillman reaction was investigated (see Scheme 12). Unfortunately, repeated attempts to react the dicarbaldehyde **65** with acrylonitrile in the presence of DABCO, at room temperature, in both chloroform and MeOH as solvent, proved unsuccessful. The substrate **65** is insoluble in both solvents and, consequently, the reactions were also attempted at reflux temperature in order to improve solubility. However, these attempts were also unsuccessful and this approach was abandoned.

An alternative strategy involving the Baylis-Hillman reaction was then explored (Scheme 13). In this approach, it was intended that the chelating arms of the ligand

should be attached to a 1,3-diaminopropane spacer rather than a 1,10-phenanthroline spacer. Unfortunately, attempted condensation of the acetylated Baylis-Hillman product **93** with 1,3-diaminopropane also proved unsuccessful, as indicated by the  $^1\text{H}$  NMR spectra of the reaction products isolated by chromatography.



**Scheme 13:** Attempted synthesis of the ligand **98**.

## 2.2.5 Macrocyclic Syntheses

Cyclic polydentate ligands, which exhibit conformational flexibility, have been found to act as effective hosts in binuclear and polynuclear complexes,<sup>151-155</sup> and such complexes are potential targets as supramolecular catalysts.<sup>156</sup> Macrocycles with large cavities, in particular, have received attention as inorganic and organic anion and cation receptors, affording complexes which participate in biological processes.<sup>157-160</sup>

Representations of a proposed macrocyclic system and possible dicopper complexes are shown in Figure 26. It is apparent that two coordination possibilities can occur, viz., tetradentate coordination with the copper atoms aligned “vertically” (b) and bidentate coordination (the remaining coordination sites being filled by solvent donors) in which the copper atoms are “horizontally” aligned (c).

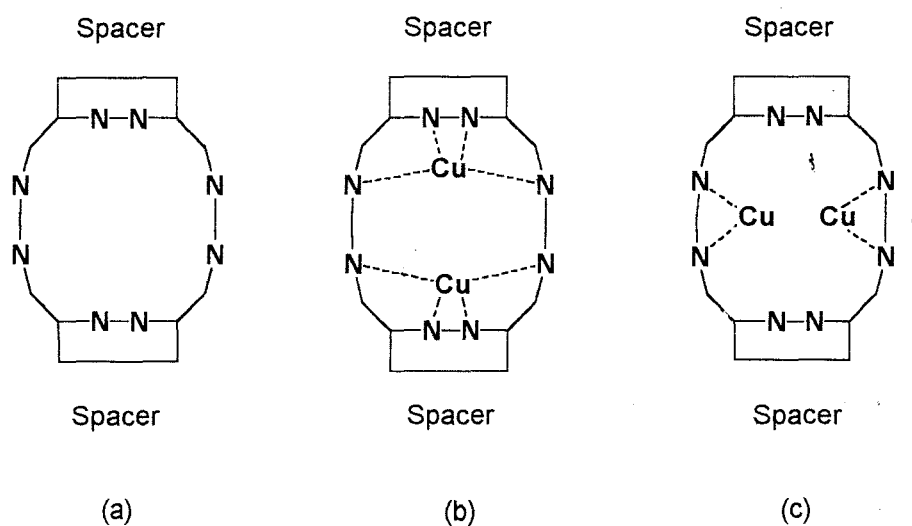
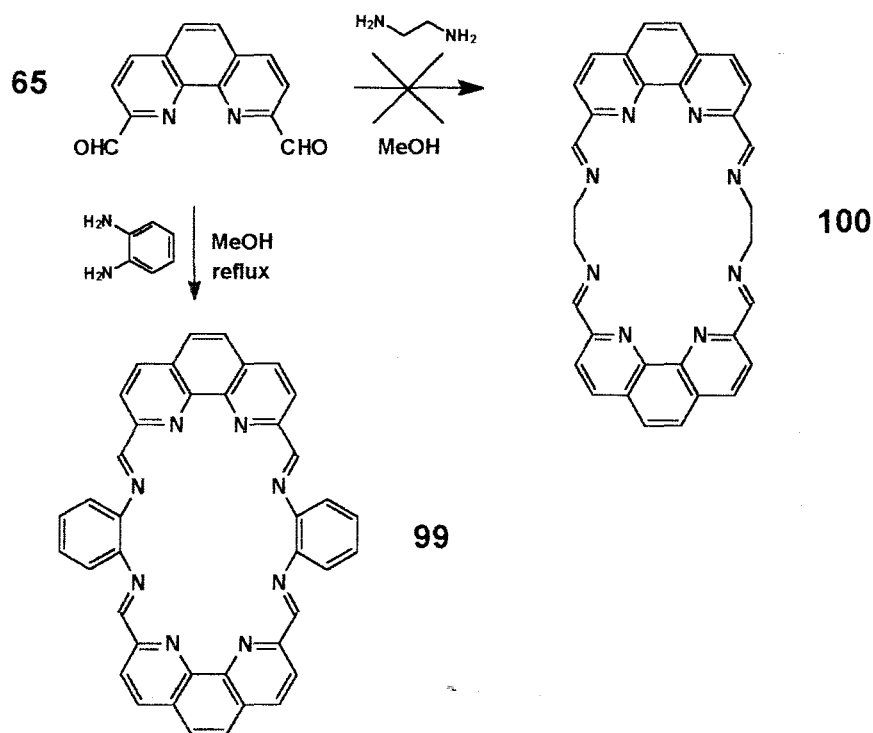


**Figure 26:** Representations of the proposed macrocyclic ligand (a) and possible dicopper coordination options, (b) and (c).



**Scheme 14:** Synthetic approaches to macrocyclic ligands.

The synthesis of the polydentate macrocycles **99** and **100** was explored, the former being more rigid and bulkier than the latter. The intention was to compare the catalytic activity of a rigid, bulky copper complex with that of a more flexible, less bulky system. 1,10-Phenanthroline-2,9-dicarbaldehyde **65** was used as a spacer and treated with 1,2-diaminobenzene and 1,2-diaminoethane with a view to obtaining Schiff base macrocycles **99** and **100** respectively (Scheme 14).

The novel dibenzo analogue **99** was isolated in 30% yield and characterised by MS and IR spectroscopy. The FAB mass spectrum clearly reveals the molecular ion peak at  $m/z$  616 (Figure 27), and high resolution MS analysis confirmed the atomic composition. The IR spectrum has a strong band at  $1619\text{ cm}^{-1}$ , characteristic of the imine functionality. Interestingly, the  $^{13}\text{C}$  NMR signals were unusually broad, possibly due to conformational flexions which are intermediate on the NMR time-scale.

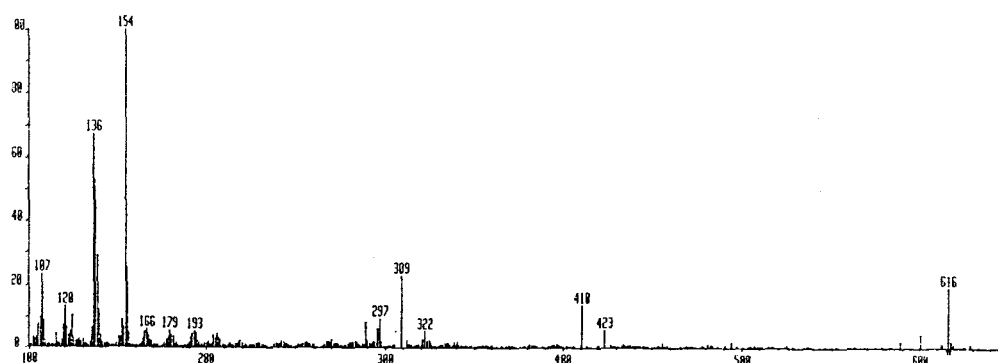


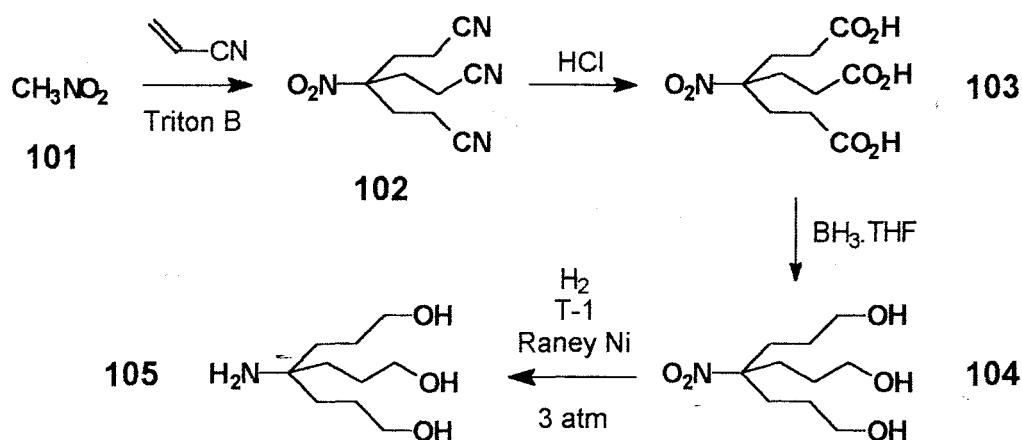
**Figure 27:** The FAB-MS spectrum of macrocycle **99** showing the molecular ion peak at  $m/z$  616.

Unfortunately, attempts to obtain the known ligand<sup>161</sup> **100** were unsuccessful; the products obtained in attempted preparations were insoluble in DMSO and are believed to be polymeric.

## 2.2.6 Dendrimer Synthesis

In the last few years, much attention has been given to the preparation and characterisation of dendrimer-based transition-metal complexes.<sup>162</sup> Such complexes provide a promising structural concept for new materials.<sup>163-168</sup> Unlike conventional metal-containing polymers, dendritic (from the Greek word meaning branched) cascade molecules have the advantage of offering a highly controlled architecture, which can act as a foundation for dendrimer-supported metal complexes.<sup>169</sup> Research in this area has blossomed and is currently concerned with exploring or developing various uses for dendritic molecules; these include: chemical sensors, magnetic resonance imaging agents, agents for delivering drugs or genes into cells, micelle mimics, nanoscale catalysts, reaction vessels, immuno-diagnostics, information-processing materials and high-performance polymers.<sup>170</sup>

In our investigation, it was anticipated that dendrimer moieties could be used to develop ligand systems which could mimic the macro characteristics of an enzymic active site, *viz.*, a hydrophilic exterior and a hydrophobic binding pocket. The account which follows details our first endeavours in this direction. The trihydroxyamine **105** was identified as a potentially useful dendrimer group, and its synthesis, following Newkome's method,<sup>171</sup> is outlined in Scheme 15.

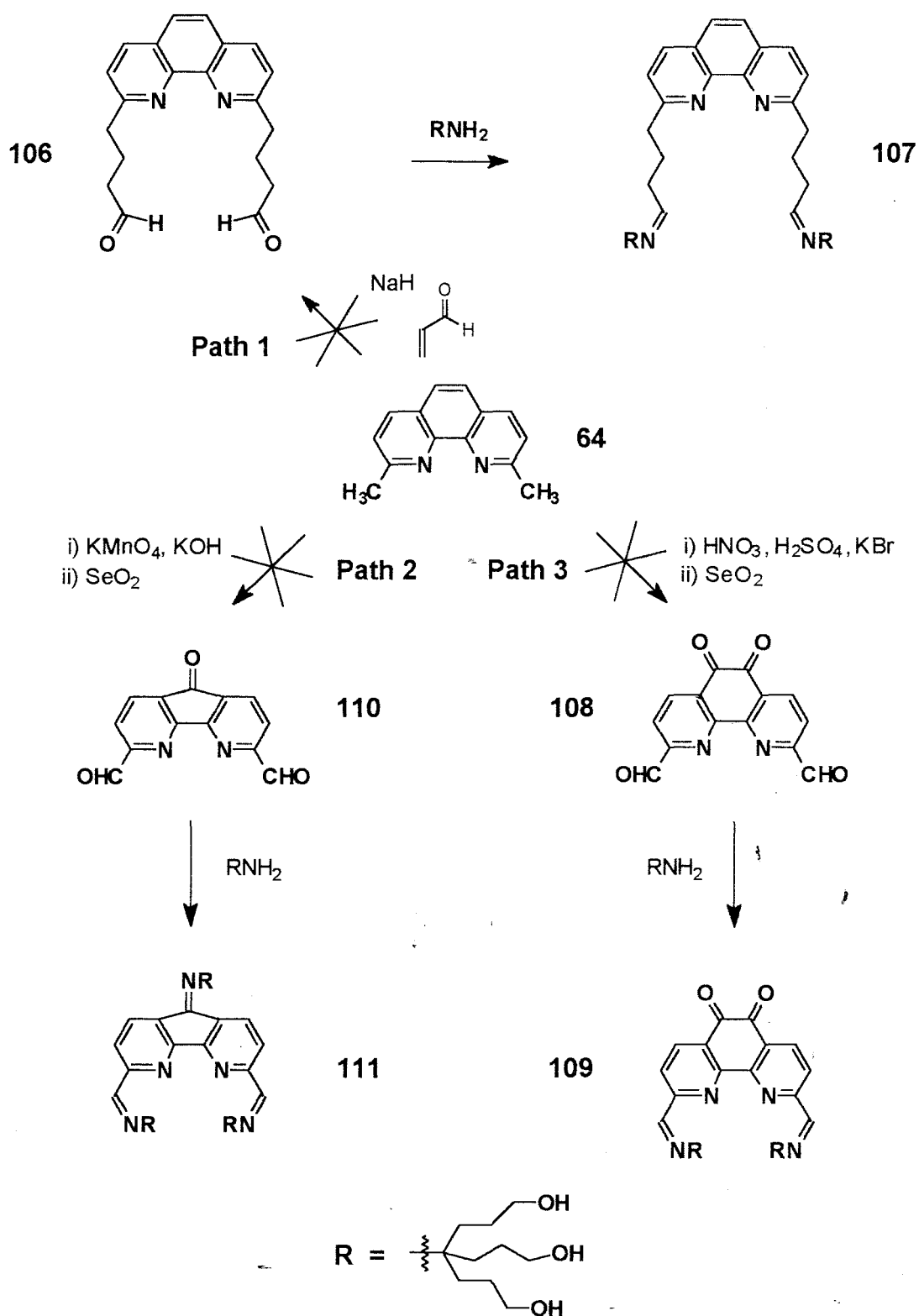


**Scheme 15:** Synthesis of the dendrimer moiety **105**.

Nitromethane **101** was reacted with acrylonitrile in the presence of Triton B (a surface active agent) to afford, *via* a Michael reaction, tris(2-cyanoethyl)-nitromethane **102**.<sup>171</sup> The nitro triacid **103**, prepared by acid-catalysed hydrolysis of the trinitrile **102**, was identified by the absence of a nitrile band (at ca. 2200  $\text{cm}^{-1}$ ) and the presence of a carbonyl band (at 1721  $\text{cm}^{-1}$ ) in the IR spectrum and the appearance of a carbonyl carbon signal at 175.6 ppm in the  $^{13}\text{C}$  NMR spectrum. The reduction of the triacid **103** to the triol **104** was achieved using the mild reducing system, borane-THF;<sup>171</sup> the absence of a carbonyl carbon signal and the presence of a signal at 60.3 ppm (corresponding to  $\text{CH}_2\text{OH}$ ) in the  $^{13}\text{C}$  NMR spectrum served as evidence for the formation of the triol **104**. The final reduction of the nitro functionality to obtain the amino triol **105** was achieved by hydrogenation using specially prepared T-1 Raney Nickel<sup>172</sup> as a reducing agent.<sup>171</sup> The success of this reduction was evidenced by the disappearance of the low-field (94.0 ppm) C- $\text{NO}_2$  signal in the  $^{13}\text{C}$  NMR spectrum.

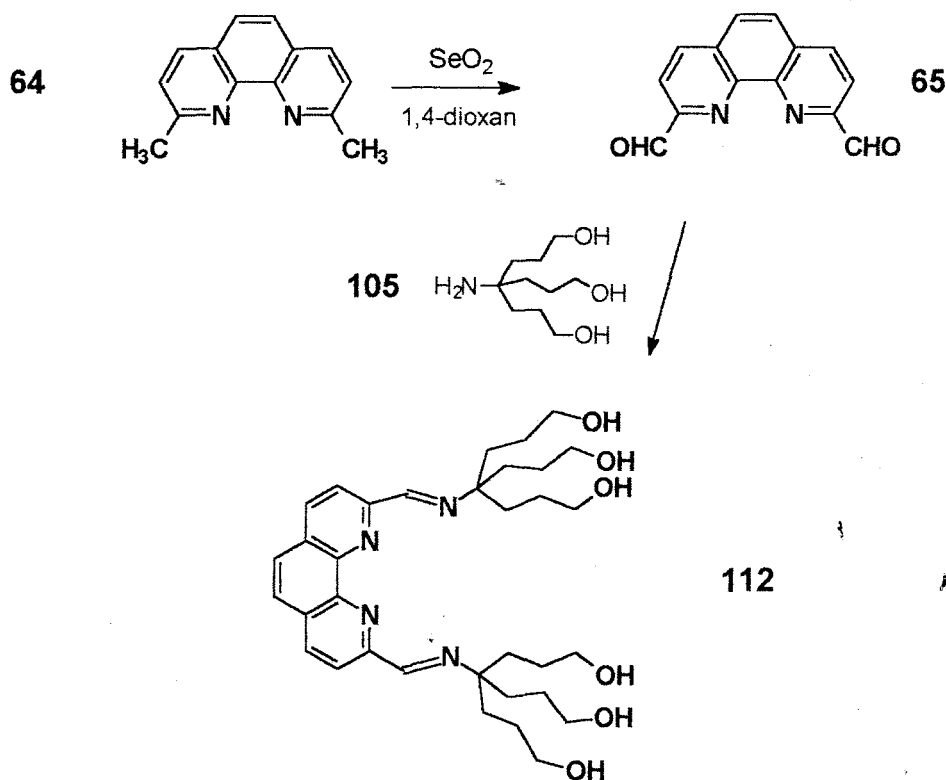
With the dendrimer moiety **105** in hand, attention was given to the construction of dendrimer-based ligands. Several approaches were explored (Scheme 16). The first route (Path 1) envisaged deprotonation of neocuproine **64**, using NaH to generate a dianion, for reaction with acrolein to produce the dialdehyde **106**. Subsequent reaction with the aminotriol **105** was then expected to afford the dendrimer ligand **107** *via* a Schiff base reaction. Unfortunately, this synthetic pathway was complicated by the formation of what appeared to be a polymeric product (insoluble in DMSO) during the reaction with acrolein.

In further approaches (Paths 2 and 3), the tri- and tetracarbonyl derivatives **108** and **110** were expected to react with the amino triol **105** to afford the corresponding dendrimer-based ligands **109** and **111**, respectively. Numerous attempts to oxidise the central ring in neocuproine **64**, using methods reported for 1,10-phenanthroline,<sup>173-175</sup> proved unsuccessful.



**Scheme 16:** Attempted pathways to dendrimer-based ligands containing the 1,10-phenanthroline spacer.

Finally, selenium dioxide oxidation of neocuproine **64** afforded the dialdehyde **65**, which on treatment with the amino triol **105**, gave the dendrimer-based ligand **112** in 96% yield (Scheme 17). This ligand was characterised by IR,  $^1\text{H}$  and  $^{13}\text{C}$  NMR spectroscopy. The  $^1\text{H}$  NMR spectrum (Figure 28) is characterised by the imine proton signal at  $\delta 8.09$  ppm and the broad upfield signals corresponding to the dendrimer methylene groups. The FAB mass spectrum of ligand **112** did not exhibit the expected molecular ion peak at  $m/z$  610 but, rather, a peak at  $m/z$  633 corresponding to attachment of a sodium cation ( $633.3627$ ;  $M + \text{Na}^+$ ); such ions are not unusual in the FAB-MS spectra.



**Scheme 17:** Synthesis of the dendrimer-based ligand **112**.

A mononuclear copper complex of this ligand was considered unlikely to be a good biomimetic model since two copper ions are found in the active site of the tyrosinase enzyme, whereas the coordination cavity in ligand **112** would probably only accommodate a single copper ion. Complexation with a metal would, however, establish whether coordination involves the aromatic nitrogen atoms or whether the

hydroxyl groups of the dendrimer moieties compete as donors.

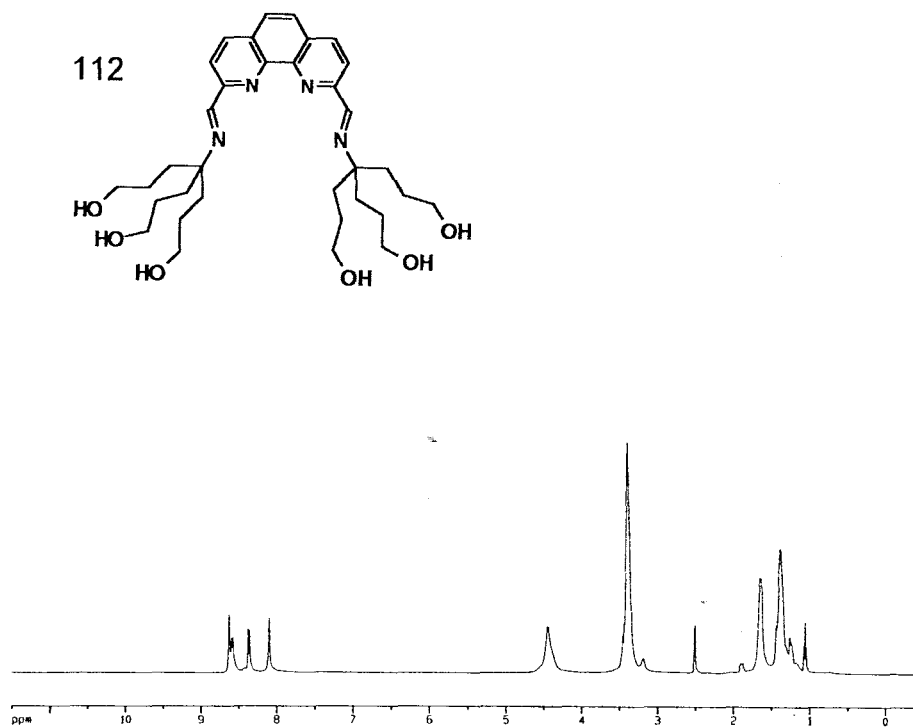


**Figure 28:** The 400 MHz <sup>1</sup>H NMR spectrum of the dendrimer-based ligand 112.

## 2.3 COMPLEXATION AND COMPUTER MODELLING STUDIES

### 2.3.1 Complexation Studies

While the ligands synthesised in this study were designed to form dinuclear copper complexes, they may also coordinate with metals other than copper, e.g. manganese(II), iron(II), cobalt(II), nickel(II), platinum(II), palladium(II) and lead(II). Consequently, some attention was also given to the complexation of ligands containing the biphenyl and 1,10-phenanthroline spacers (Schemes 2 and 8) with cobalt(II), nickel(II), platinum(II) and palladium(II).

Hard metals, which include copper(II), cobalt(II) and nickel(II) are known to coordinate with amide oxygen,<sup>176-178</sup> but the resulting metal-oxygen bonds are weaker than the corresponding metal-amide nitrogen bonds. Coordination of metals to nitrogen donors occurs over a wide pH range, but the ability of metals to deprotonate and complex with amide nitrogen is pH-dependent. From potentiometric titration studies of divalent metal ion-dipeptide systems, the following pH preferences have been obtained for the coordination of metals to peptide nitrogen donors:- copper(II), pH 5 - 6;<sup>179,180</sup> nickel(II), pH 8 - 9;<sup>181, 182</sup> platinum(II), pH < 5;<sup>183</sup> and palladium(II), pH 2.5 - 3.5.<sup>184, 185</sup>

It must, however, be emphasised that in the present complexation studies, the pH was not tuned to specifically achieve coordination of the metal with the amide nitrogen donors, and coordination of the metal could involve either the oxygen or nitrogen atom of the amide functionality.

The analysis of these complexes was expected to reveal:-

- (i) whether dinuclear complexes were formed;
- (ii) whether coordination of the metal occurs through the nitrogen or oxygen atom of the amide ligands; and
- (iii) the preferred geometry of the resulting complexes.

Ligands containing amide, imidazole and benzimidazole moieties should provide coordination environments that are similar to those in biological systems, such as enzymes, and the resulting complexes of cobalt and nickel could prove to be good synthetic models of metalloproteins in which these metals are found. The structures proposed for the various complexes, which have been isolated, are based on a consideration of the IR, NMR, UV-Vis, microanalytical and computer modelling data. Unfortunately in only two cases were crystals obtained which were suitable for X-ray crystallographic analysis.

### 2.3.2 Copper Complexes

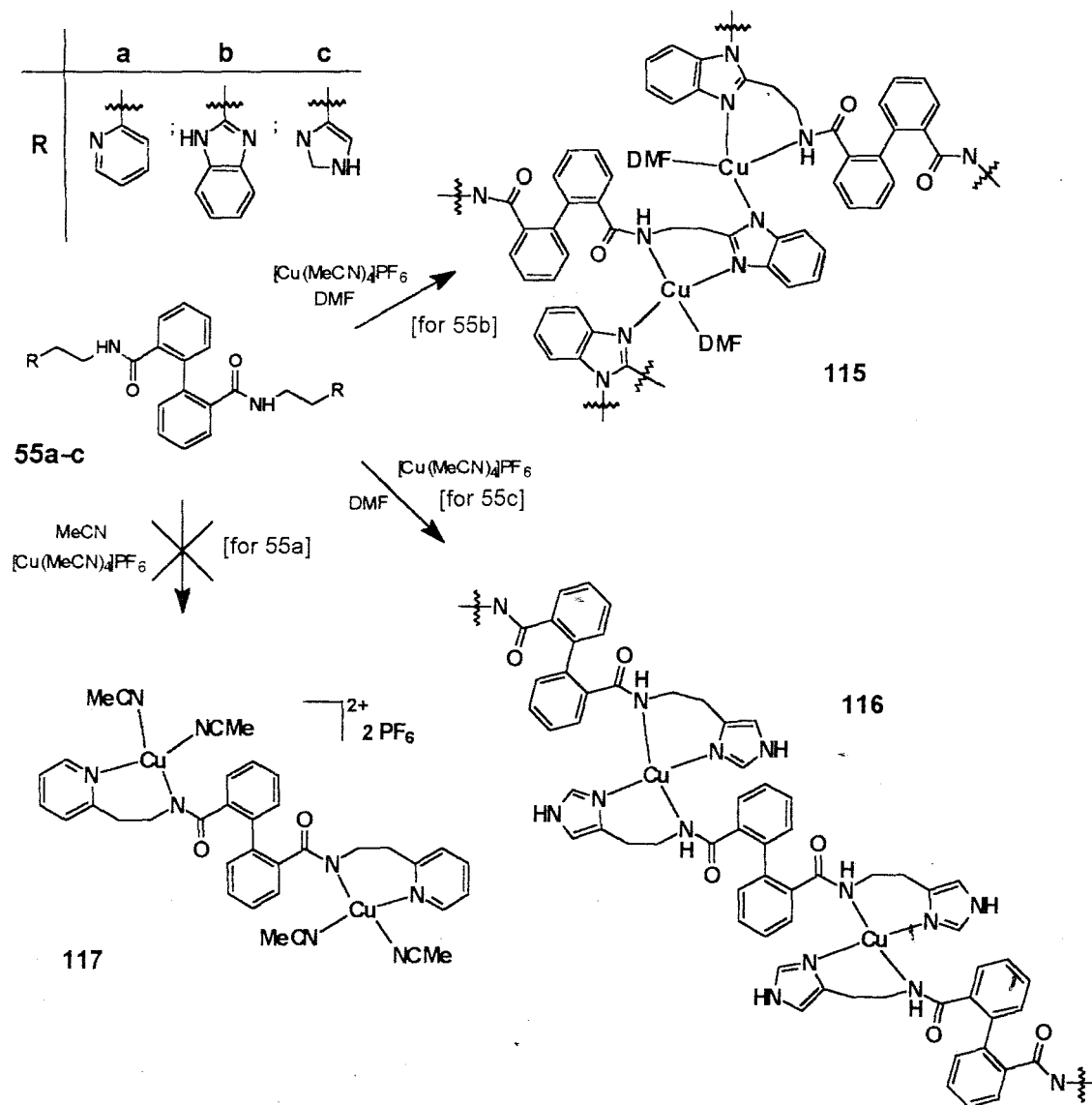
Copper is present at low concentrations in many enzymes and proteins.<sup>186</sup> In larger quantities, copper is toxic to humans and its salts are highly toxic to lower organisms.<sup>187</sup> Copper ions instantly form complexes with a wide variety of ligands and exhibit a range of oxidation states in the coordination compounds in which they occur. The copper(I) and (II) oxidation states are the most prevalent, but the copper(III) and (IV) oxidation states are also known. Copper(III) and copper(IV) oxidation states are, however, rare. Copper(I) is readily oxidised to copper(II), which is the most stable oxidation state of copper under standard conditions.<sup>188, 189</sup> A wealth of copper complexes have been generated,<sup>189</sup> and the crystal structures of many of these have been determined. These structures have permitted the characterisation of various regular and distorted geometries of the copper(II) ion,<sup>190, 191</sup> which are associated with the Jahn-Teller effect.<sup>192</sup> Copper(I), a  $d^{10}$  ion, behaves as a soft acid and favours coordination to soft sulfur and phosphorus bases,<sup>193</sup> whereas copper(II), a  $d^9$  ion, is considered to be a border-line hard acid which favours oxygen and nitrogen donors.<sup>194</sup> Diamagnetic, colourless complexes are formed by copper(I) with its closed shell configuration,<sup>190, 195</sup> while copper(II) produces highly coloured paramagnetic complexes.<sup>190, 194, 195</sup>

### 2.3.2.1 Synthesis of Copper complexes

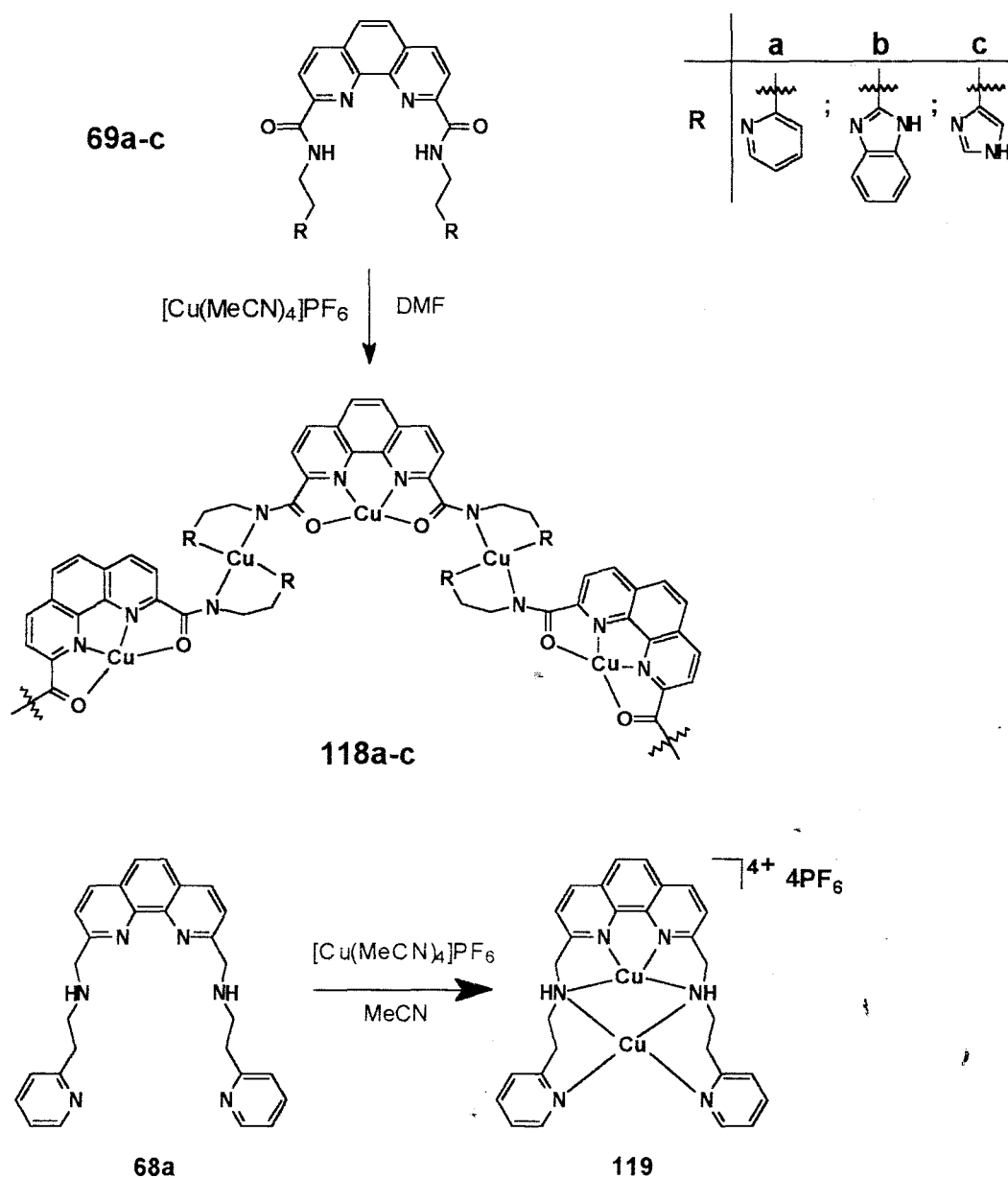
The complexation of copper with the various ligands occurred with ease [see Experimental section (3.3.1)]. Depending on the solubility of the ligand, dry DMF or dry MeCN were used as solvents in these complexation reactions.

#### *Biphenyl and 1,10-Phenanthroline Complexes*

The biphenyl (Scheme 18) and 1,10-phenanthroline (Scheme 19) ligands were reacted with  $[\text{Cu}(\text{MeCN})_4]\text{PF}_6$ , a Cu(I) reagent, at room temperature under  $\text{N}_2$  in dry, degassed solvent; in some cases, the solutions had to be heated to dissolve the ligands. The ligand solution was added dropwise to the solution of the copper(I) reagent to obtain dinuclear copper(I) complexes. The biphenyl complexes, obtained using this procedure, were green, indicating the copper(II) oxidation state. The 1,10-phenanthroline complexes, however, were brown in colour and there was some uncertainty as to whether this was an indication of the copper(I) or (II) oxidation state, since colourless complexes are formed for copper(I) and green complexes are formed for copper(II). Microanalysis data for these complexes (Table 8, p.85) show that the biphenyl and 1,10-phenanthroline complexes are, typically, dinuclear and of acceptable purity; the data for complex **117** appears to be a mixture of mononuclear and dinuclear complexes (data not included in Table 8). The results also indicate that two  $\text{PF}_6^-$  anions are present as counter ions- except for complex **119** which has four. This suggests either that protons from the amide, benzimidazole or imidazole moieties are generally removed during complexation, or that both copper atoms are in a copper(I) oxidation state in these complexes. All the complexes, except complex **119**, were insoluble in DMSO due, it is believed, to the formation of polymers. The structures proposed for the copper complexes detailed in Schemes 18 and 19, while necessarily tentative, are based on a consideration of the spectroscopic (Sections 2.3.2.2-4) and microanalytical data.



**Scheme 18:** Complexation of the biphenyl amide ligands with copper.

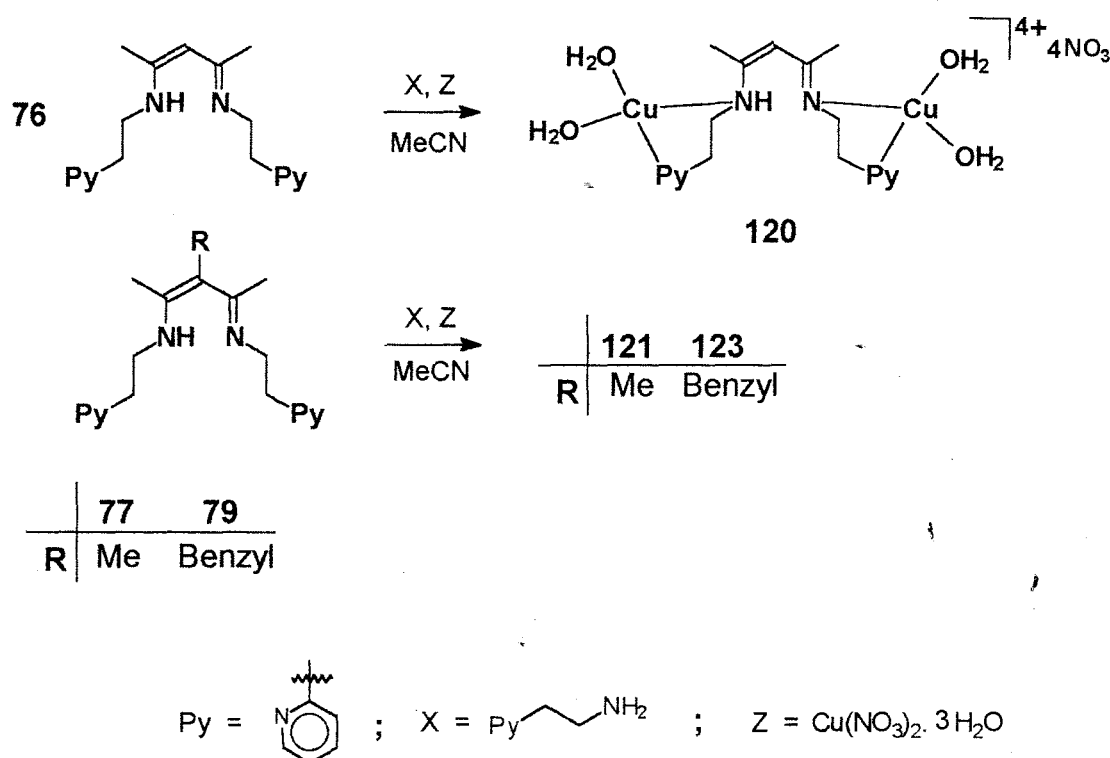


**Scheme 19:** Complexation of selected 1,10-phenanthroline ligands with copper.

#### *Schiff base complexes*

It was felt that it would be better to react the Schiff base ligands with a copper(II) reagent as the formation of mixtures of copper(I) or (II) complexes might have caused complications during the isolation and purification of the biphenyl- and the 1,10-phenanthroline-based complexes. Consequently, the ligands were treated with  $Cu(NO_3)_2 \cdot 3H_2O$  in MeCN (Scheme 20), without the precautions used

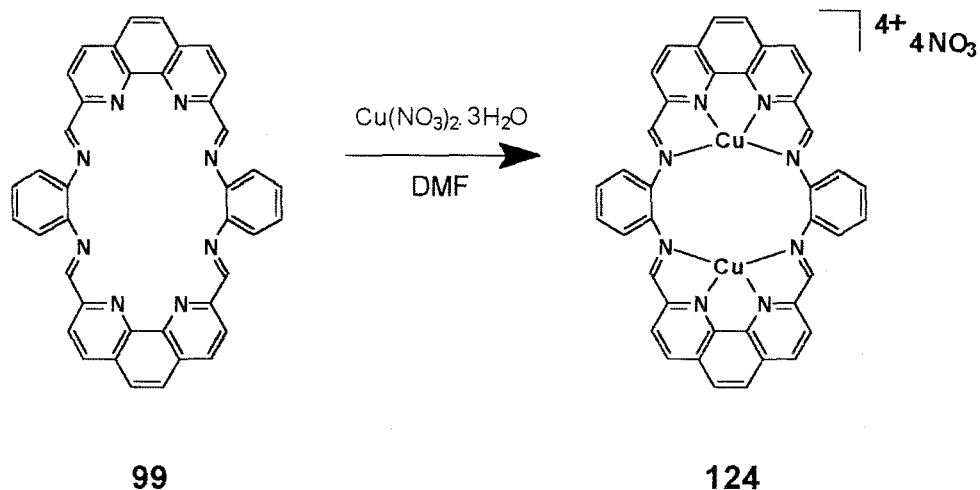
previously for the copper(I) complexes, viz., pre-drying and degassing the solvent and conducting the reaction under  $N_2$ . The resulting complexes **120**, **121** and **123** were green in colour and tended to be hygroscopic; from their microanalysis data (Table 8), it can be seen that these complexes were dinuclear. However, the data obtained for the complexes with ligands **74**, **75**, **78** and **84** (not included in Table 8) suggest formation of mixtures of mononuclear and dinuclear complexes. While a structure has been proposed for complex **120** (Scheme 20), the complexity of the spectroscopic data for complexes **121** and **123** preclude the confident assignment of structures.



**Scheme 20:** Complexation of the Schiff base ligands with copper.

#### *The Macrocyclic complex*

When a solution of the macrocycle **99** in DMF was added dropwise to a solution of the copper(II) reagent  $\text{Cu}(\text{NO}_3)_2 \cdot 3\text{H}_2\text{O}$ , the colour of the reaction mixture changed from turquoise to red-brown. Microanalysis of the resulting complex **124** (Table 8) indicated it to be dinuclear and of acceptable purity and, due to the presence of four nitrate anions, to contain two copper(II) cations.



**Scheme 21:** Complexation of macrocycle **99** with copper.

**Table 8:** Micro-analytical data for the copper complexes followed, in parentheses, by the calculated values.

Complex	Complex Stoichiometry	%Carbon	%Hydrogen	%Nitrogen
115	$\text{Cu}_2(55\text{b})(\text{PF}_6)_2 \cdot 2\text{DMF}$	41.9 (41.9)	3.9 (3.7)	10.0 (10.3)
116	$\text{Cu}_2(55\text{c})(\text{PF}_6)_2 \cdot 5\text{H}_2\text{O}$	30.8 (30.9)	3.4 (3.5)	8.8 (9.0)
118a	$\text{Cu}_2(69\text{a})(\text{PF}_6)_2 \cdot 5\text{H}_2\text{O}$	37.7 (37.3)	2.0 (2.7)	9.7 (9.4)
118b	$\text{Cu}_2(69\text{b})(\text{PF}_6)_2 \cdot 6\text{H}_2\text{O}$	35.4 (35.6)	3.2 (3.6)	10.3 (10.4)
118c	$\text{Cu}_2(69\text{c})(\text{PF}_6)_2 \cdot 5\text{H}_2\text{O}$	29.5 (30.0)	3.0 (3.2)	12.3 (11.7)
119	$\text{Cu}_2(69\text{a})(\text{PF}_6)_4$	30.2 (29.2)	2.7 (2.3)	7.4 (7.3)
120	$\text{Cu}_2(76)(\text{NO}_3)_4 \cdot 7\text{H}_2\text{O}$	28.2 (28.2)	3.9 (4.7)	13.7 (13.8)
121	$\text{Cu}_2(77)(\text{NO}_3)_4 \cdot 8\text{H}_2\text{O}$	29.0 (28.6)	4.1 (5.0)	13.0 (13.3)
123	$\text{Cu}_2(79)(\text{NO}_3)_4 \cdot 9\text{H}_2\text{O}$	32.8 (33.4)	3.6 (5.2)	12.0 (12.0)
124	$\text{Cu}_2(99)(\text{NO}_3)_4 \cdot \text{H}_2\text{O}$	47.5 (47.6)	3.0 (2.6)	16.6 (16.7)

### **2.3.2.2 NMR Studies of the copper complexes**

Upon coordination of copper the ligand nuclei are deshielded relative to the free ligand, and the magnitude of the downfield shift may reflect, to some extent, the proximity of a specific nucleus to the coordinated copper cation.<sup>92</sup> While copper(I) complexes can be readily analysed by NMR spectroscopy, copper(II) complexes are paramagnetic, and the signals for the nuclei close to the copper tend to be broadened, thus complicating analysis. This difference provides a quick and simple distinction between copper(I) and copper(II) complexes.

It was not possible to distinguish, on the basis of colour, whether copper(I) or (II) 1,10-phenanthroline complexes were obtained. From the <sup>1</sup>H NMR spectra of these complexes, however, it could be seen that the copper(I) oxidation state was not dominant as the signals in the <sup>1</sup>H NMR spectra were broad. Thus, it seems, that at least one copper atom in the 1,10-phenanthroline copper complexes may be in a copper(II) oxidation state; magnetic susceptibility studies will be required to determine whether copper(I) is present in these complexes.

### **2.3.2.3 IR studies of the copper complexes**

These studies were undertaken to determine whether coordination of the ligands with copper occurs through the nitrogen or oxygen of the amide functionality, or through the secondary or tertiary amine groups of the imidazole and benzimidazole units. The spectra were also expected to show whether the amide proton is removed during complexation. It was, however, not possible to establish whether coordination involves the 1,10-phenanthroline nitrogen donors because the aromatic bands overlap in the region of interest (1600-1500 cm<sup>-1</sup>).

#### ***Biphenyl- and 1,10-Phenanthroline-based complexes***

It can be seen from the data in Table 9 that copper coordinates with either the amide oxygen or nitrogen in the 1,10-phenanthroline- and biphenyl-based copper complexes. A negative carbonyl shift indicates coordination through the carbonyl

oxygen, while a positive NH shift indicates coordination through the nitrogen of the amide group. Thus, for complexes **118a** and **118b**, coordination involves the amide oxygen and, due to the absence of an amide NH band, through the amide nitrogen. For complexes **115** and **116** coordination appears to involve the amide nitrogen due to the positive NH shift. In the case of complex **118c**, coordination also involves the amide nitrogen since the amide NH band is absent indicating that deprotonation of the amide NH had occurred upon complexation with copper; the fact that  $\Delta\nu_{\text{C=O}}$  is zero, however, casts some doubt on the carbonyl oxygen coordination depicted in the structure proposed for complex **118c** (Scheme 19). For the  $\text{PF}_6^-$  anion a P-F stretching band between 840-850  $\text{cm}^{-1}$  is observed for each of these copper complexes.<sup>196</sup>

**Table 9:** Selected IR data for the amide copper complexes of the biphenyl- and 1,10-phenanthroline-based ligands.

Copper complexes	$\Delta\nu_{\text{NH}}^{\text{a}}/\text{cm}^{-1}$	$\Delta\nu_{\text{C=O}}^{\text{a}}/\text{cm}^{-1}$	$\nu_{\text{PF}_6}^{\text{b}}/\text{cm}^{-1}$
115	65	33	845
116	55	29	846
118a	-	-21	842
118b	-	-13	846
118c	-	0	845

<sup>a</sup> Frequency shift for amide absorption on complexation. A positive value indicates a frequency increment and a negative value a decrement relative to the free ligand.

<sup>b</sup> P-F stretching band for the  $\text{PF}_6^-$  counterion.

In the spectra of the biphenyl complex **115** and the 1,10-phenanthroline complex **118b**, the benzimidazole NH band (at ca. 3171  $\text{cm}^{-1}$ ) is absent, indicating that this proton has been removed suggesting that coordination with copper occurs through the secondary nitrogen donor of benzimidazole. The fact that the amide protons are not removed on formation of complex **115**, suggests that the  $\text{pK}_a$  of the benzimidazole protons in the ligand **55b** is lower than that of the  $\text{pK}_a$  of the amide protons. In the IR spectrum of the biphenyl complex **116** the imidazole NH band is present (at 3156  $\text{cm}^{-1}$ ), but the frequency of the amide NH band is increased by

55  $\text{cm}^{-1}$  to 3242  $\text{cm}^{-1}$  on complexation. The presence of the imidazole NH is an indication that the tertiary imidazole nitrogens as well as the amide nitrogens (see above) are coordinated to copper. For complex **116**, it seems that the reaction conditions do not favour deprotonation of either the imidazole secondary amine or the amide groups.

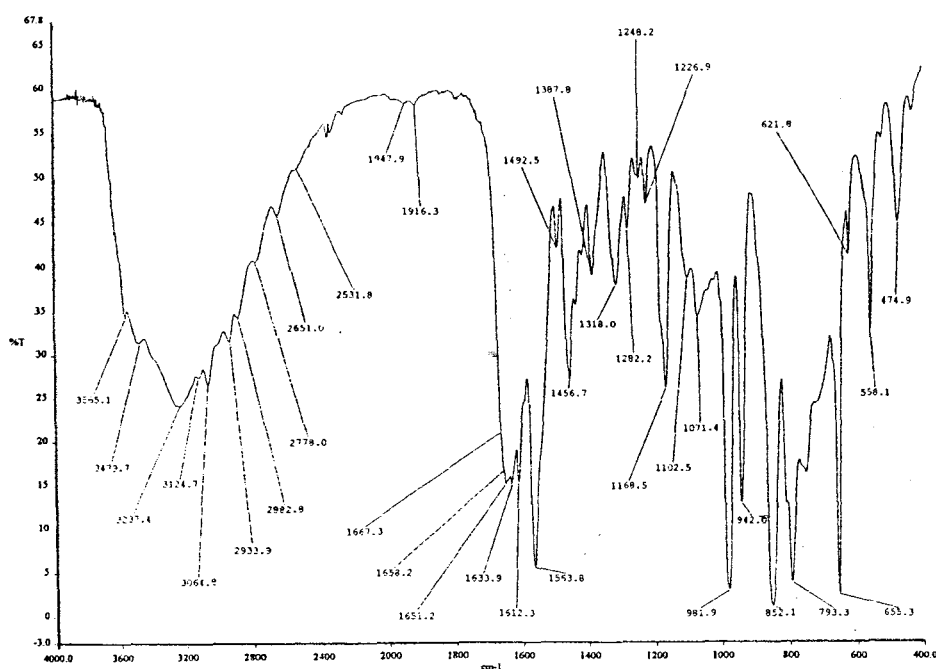


**Figure 29:** IR spectrum of complex **115** in hexachlorobutadiene.

A band at 3273  $\text{cm}^{-1}$  in the IR spectrum of the bis(amino) 1,10-phenanthroline complex **119** is attributed to the secondary amine NH stretch, indicating that the amine protons are not removed upon coordination with copper. A band at 853  $\text{cm}^{-1}$  is observed for the  $\text{PF}_6^-$  anions in this complex.

#### *Schiff base complexes*

The IR spectra of the copper complexes prepared from the Schiff base ligands are more complicated than expected. This complexity is attributed to the presence of the nitrate anion, which can act in its own right as an unidentate or bidentate ligand or simply be present as an uncoordinated counterion.<sup>202</sup> All these possibilities have

been found to occur in the Schiff base copper complexes.

The complex **121** exhibits a number of significant bands (Figure 30). These include:-

- i) the imine C=N band at  $1637\text{ cm}^{-1}$ ;
- ii) bands at  $1480$  and  $1283\text{ cm}^{-1}$  characteristic of the nitrate anion coordinated as a bidentate ligand;
- iii) a band at  $1445\text{ cm}^{-1}$  indicating unidentate coordination of nitrate; and
- iv) a band at  $1013\text{ cm}^{-1}$  which suggests that the nitrate anion is coordinated as a unidentate ligand;<sup>197</sup> a second band expected at ca.  $1315\text{ cm}^{-1}$  may be masked by the band occurring at  $1383\text{ cm}^{-1}$  and indicates the presence of free nitrate ion.

It is concluded that, in addition to the presence of the nitrate ion, unidentate and bidentate coordination of the nitrate ion occurs in this copper complex.

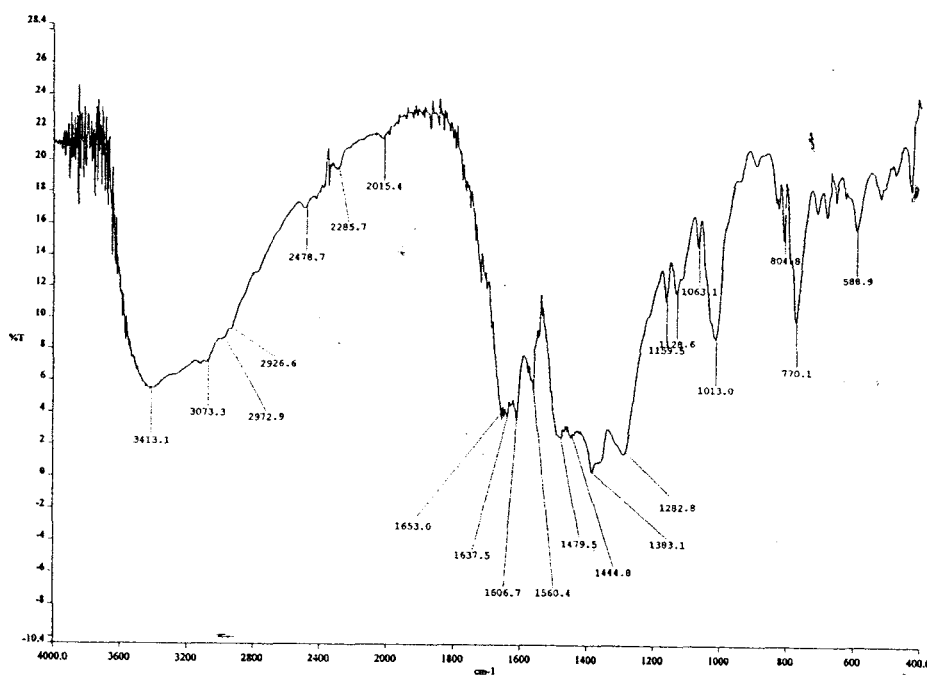


Figure 30: IR spectrum of complex **121** in KBr.

The IR spectrum of the copper complex **123** exhibits bands corresponding to the imine moiety and the free and bis-coordinated nitrate anion. In the case of the macrocyclic complex **124**, however, no unidentate or bidentate coordination of the nitrate anion is apparent; the band at  $1383\text{ cm}^{-1}$  reveals the presence of free nitrate anions, while the imine C=N band appears at  $1653\text{ cm}^{-1}$ . All of the Schiff base copper complexes examined proved to be hygroscopic and, consequently, the assignment of the NH band is precluded by the presence of a broad H<sub>2</sub>O hydroxyl band.

#### **2.3.2.4 UV-Vis studies of the copper complexes**

It was decided to use UV-Vis spectroscopy to detect whether the two copper atoms are in the same or different coordination environments within the dinuclear complexes. Different geometrical arrangements of the copper atom give rise to different absorption characteristics and, as the copper(I) and (II) oxidation states favour different geometries, it was expected that the UV-Visible absorption data would reflect the oxidation state(s) involved. Due to the insolubility of the complexes in DMF, DMSO was used as solvent but, unfortunately, the regions of interest were masked by solvent absorption bands, thus precluding comparison with the UV data reported for the enzyme, tyrosinase.

### 2.3.3 Computer Modelling Studies

Molecular mechanics is now a routine tool in organic chemistry,<sup>198,199</sup> and has become increasingly important in the field of drug design<sup>200</sup> and in studying the matching of bases in nucleic acids.<sup>201</sup> Its use is also well established in coordination chemistry,<sup>202,203</sup> where it has been used for the analysis of disordered structures,<sup>204</sup> the prediction of unknown structures,<sup>205</sup> the determination of isomer and conformer ratios<sup>206</sup> and metal ion selectivities.<sup>207</sup>

#### ***Molecular modelling and molecular mechanics***

The basis of molecular modelling is that all the important molecular properties (*i.e.* stabilities, reactivities and electronic properties) are related to the molecular structure. A computational study can only be carried out once a molecular model has been established, and because of its computational simplicity and efficiency, molecular mechanics is commonly used to construct such models. Typically, the energy-minimised model, which is obtained, represents an idealised gas-phase structure of the molecule that is independent of solvent effects in solution, or of lattice interactions in the solid state.

The molecular modelling of transition metal complexes is complicated, however, by the presence of partially filled, metal ion d-orbitals, which are responsible for the multifarious structures of coordination compounds, which exhibit a variety of coordination numbers and geometries. Moreover, metal-ligand bonds can become elongated during steric crowding, especially when small metal ions are coordinated. In cases where the ideal bond lengths have not been determined, it is considered acceptable to use an average force constant.<sup>203</sup>

In the computer models illustrated in this section, the following colour key applies: *carbon*: light-blue; *nitrogen*: dark-blue; *oxygen*: red; *hydrogen*: white; *copper*: yellow.

### 2.3.3.1 Computer modelling of the dinuclear copper complexes

Computer modelling studies were undertaken to explore the structures of proposed dinuclear copper complexes and their potential as biomimetic tyrosinase analogues. Bernhardt and Comba have published a force field for copper(II) in organometallic complexes.<sup>62</sup> This has been determined by modelling a series of amine and imine complexes and correlating the results with X-ray crystal structures. A close similarity was observed for these correlations, thus providing support for the validity of computer modelling of copper complexes. The discussion that follows focusses on the modelling of possible monomeric structures for the dinuclear copper complexes **120**, **128** and **130**<sup>†</sup>. The aim, in each case, was to determine:- (i) the most likely conformation for the ligand and the complex; (ii) the Cu-Cu distance in the complex; (iii) the feasibility of a dioxygen peroxide bridge between the two copper atoms; and (iv) the accessibility of the Cu-O<sub>2</sub>-Cu unit for binding phenolic substrates.

The distance between the copper atoms is, of course, crucial since the initial stage of the enzyme-catalysed reaction involves the binding of dioxygen across the dinuclear copper site. For rigid, planar molecules, a Cu-Cu distance of 5 Å is required for a good steric match; less for more flexible systems.<sup>208</sup> It is believed that the Cu-Cu distance in the tyrosinase enzyme is 3.5 Å,<sup>32,33</sup> and models reported to have displayed successful biomimetic activity have a similar Cu-Cu separation.<sup>101,217</sup> Initially, it was thought that the dioxygen in tyrosinase was bridged in a *cis*  $\mu$ -1,2 fashion<sup>209</sup> but, in fact, it is coordinated in a  $\mu$ - $\eta^2$ : $\eta^2$  side-on bridging mode.<sup>210,211</sup> The binding of the substrate appears to be accompanied by a change in coordination from tetragonal copper(I) to trigonal bipyramidal copper(II).<sup>212</sup> It is also believed that the peroxide moiety is in an equatorial plane when the phenolic substrate binds axially to one copper atom in the active site.<sup>213</sup> However, in order for the electron transfer to occur most readily at the active site of tyrosinase, the

<sup>†</sup> While the apparent polymeric nature of the copper complexes has already been indicated (p.81 and p.82) it is possible that, in solution, catalytically active monomeric complexes may exist in equilibrium with polymeric complexes.

phenolic substrate has to be in an equatorial plane to permit maximum overlap of the substrate donor orbitals with the half empty  $d_{x^2-y^2}$  orbitals of the copper(II) ions.<sup>211</sup> Such rearrangement from axial to equatorial binding is not required for catechols and, as a result, their oxidation is less geometrically and sterically demanding. Apparently, the protein pocket contributes to the stabilisation of the binding of either substrate through  $\pi$ -stacking interactions.<sup>213</sup>

In the present study, two modes of binding for dioxygen were modelled for each of the copper complexes **120**, **128** and **130**, i.e. a  $\mu$ -1,2 end-on and a  $\mu$ - $\eta^2$ : $\eta^2$  side-on bridging mode since these have been reported in the literature for copper complexes.<sup>214, 215, 216</sup>

Energy-minimised structures for the ligands, their dicopper complexes and oxygen-bridged derivatives were modelled using MSI Cerius<sup>2</sup> software on a Silicon-Graphics O<sup>2</sup> platform. Solvent molecules can coordinate to copper and, as a result, the binding of the solvent, acetonitrile, was taken into account during the modelling of these complexes. Pertinent data for the complexes are summarised in Tables 10 and 11. The ligands so examined (56b, 68b and 76) are depicted below.

**Table 10:** Cu-Cu separation in the modelled complexes before dioxygen binding.

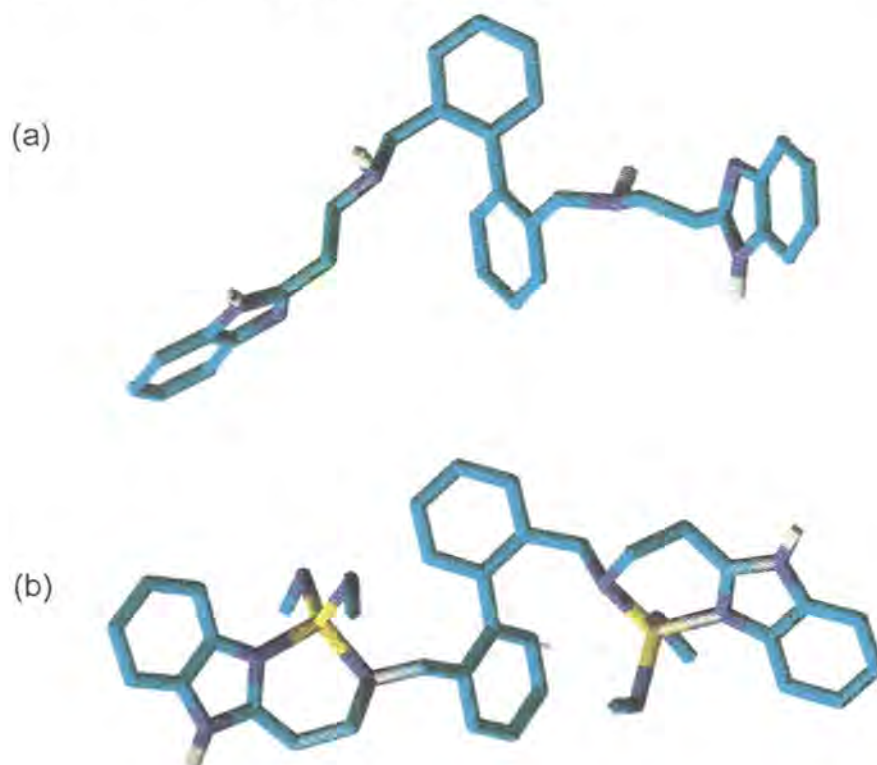
Ligand	Complex	Cu-Cu separation (Å)
76	120m	6.836
56b	128m	8.451
68b	130m	4.789

<sup>a</sup> m = monomeric form

**Table 11:** Cu-Cu separation and the potential energy in the modelled complexes after dioxygen binding.

Ligand	Complex <sup>a</sup>	Cu-Cu separation (Å) (after O <sub>2</sub> binding)	Potential Energy (kcalmol <sup>-1</sup> )
56b	129os	4.880	-246.9
56b	129oe	1.756	644.9
68b	131os	2.188	-38.2
68b	131oe	4.616	1030.3
76	132os	2.117	-687.8
76	132oe	4.642	48.0

os =  $\mu$ - $r_1^2$ : $r_2^2$  side-on dioxygen bridging;  
oe =  $\mu$ -1,2 end-on dioxygen bridging.

**Complexes containing the biphenyl spacer**

**Figure 31:** Energy-minimised conformations of the ligand **56b** (a) before and (b) after complexation with copper.

From the models in Figure 31 it can be seen that there is not a drastic change in conformation when ligand **56b** coordinates with copper. Upon binding to dioxygen, the copper atoms are, of course, brought much closer together. The models for the  $\mu-r^2:r^2$  side-on (complex **129os**) and  $\mu-1,2-trans$  bridging (complex **129oe**) of dioxygen are shown in Figure 32 (a) and (b) respectively. The  $\mu-1,2-trans$  bridging mode is expected to be favoured since this is the more stable arrangement for dioxygen in dinuclear copper complexes.<sup>210</sup> Complex **129oe** has a Cu-Cu distance of 1.756 Å, but it is less stable than complex **129os**, which has a Cu-Cu distance of 4.880 Å. It is apparent that there is a considerable change in conformation when dioxygen is bound to the dinuclear complex **128**, and that the geometry of the metal atoms changes from tetrahedral to octahedral in complex **129os**, and to trigonal bipyramidal in complex **129oe**.

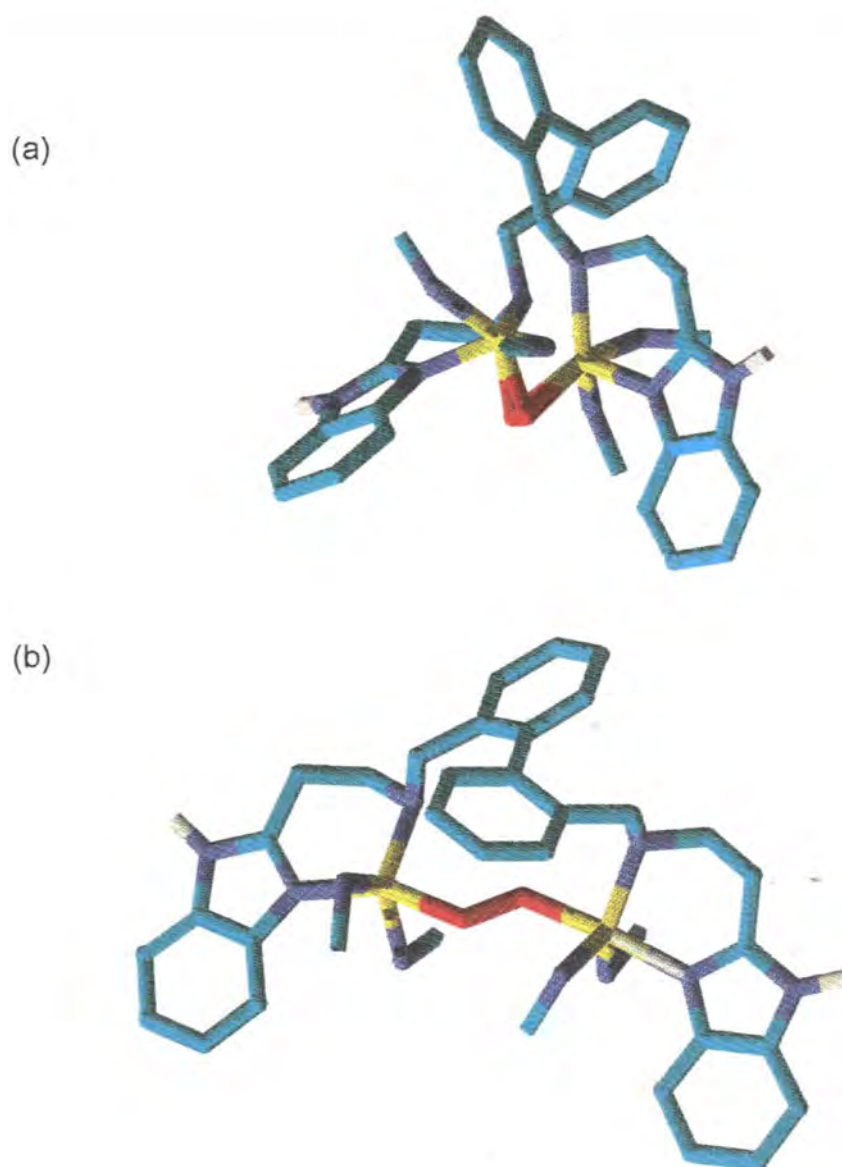


**Figure 32:** Energy-minimised conformations of the dioxygen-bridged copper complex **128**, showing (a) side-on and (b) *trans* bridging.

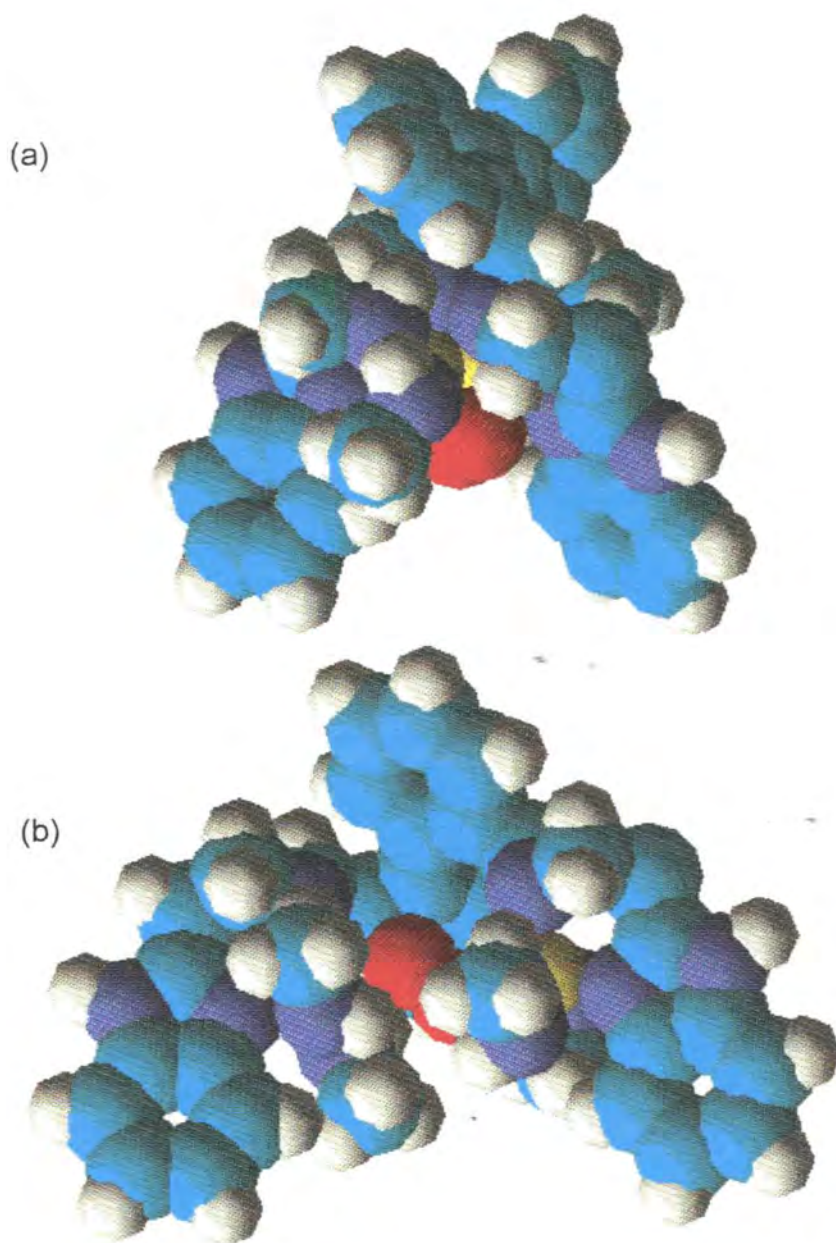


**Figure 33:** The space-filling models of the energy-minimised conformations of the dioxygen-bridged copper complex **128**, showing (a) side-on and (b) *trans* bridging.

In the dioxygenated system, the biphenyl arene rings remain out of the plane of the copper atoms and the binding site is seen to be concave. From the space filling models of complexes **129os** and **129oe** (Figure 33), it appears that, in both cases, the active site is readily accessible.

Reglier has reported a similar model of a complex that also features the flexible biphenyl spacer (see section 1.3.5 p.32) and displays both phenolase and catecholase activity when dioxygen is bound in the  $\mu$ -oxo form.<sup>103</sup> It has been shown, by means of molecular mechanics calculations using a BIOGROMOS program, that this model reflects a Cu-Cu distance of 3.6 Å when the deoxy form exhibits a biphenyl dihedral angle of 60°. <sup>217</sup> In the light of these results it is expected that the complex **128** should also be capable of attaining a Cu-Cu distance of ca. 3.6 Å and that it could also display phenolase and catecholase activity.

### ***Complexes containing the 1,10-phenanthroline spacer***

In the model of the dicopper deoxy complex **130** the tetrahedral geometry of copper(I) is apparent. Upon oxygenation, the geometry changes to a distorted octahedron in the case of the  $\mu$ - $\eta^2:\eta^2$  side-on bridged complex **131os**; in the  $\mu$ -1,2-*trans* complex **131oe** (Figure 34), however, the tetrahedral geometry changes to square pyramidal at the one coordination site and trigonal bipyramidal at the other. The Cu-Cu distance in complex **131os** is 2.188 Å, and 4.616 Å in complex **131oe**. From the potential energies it appears that complex **131os** is more stable than **131oe**, but in neither case does the oxygenated complex provide an obvious binding pocket to accommodate the substrate.

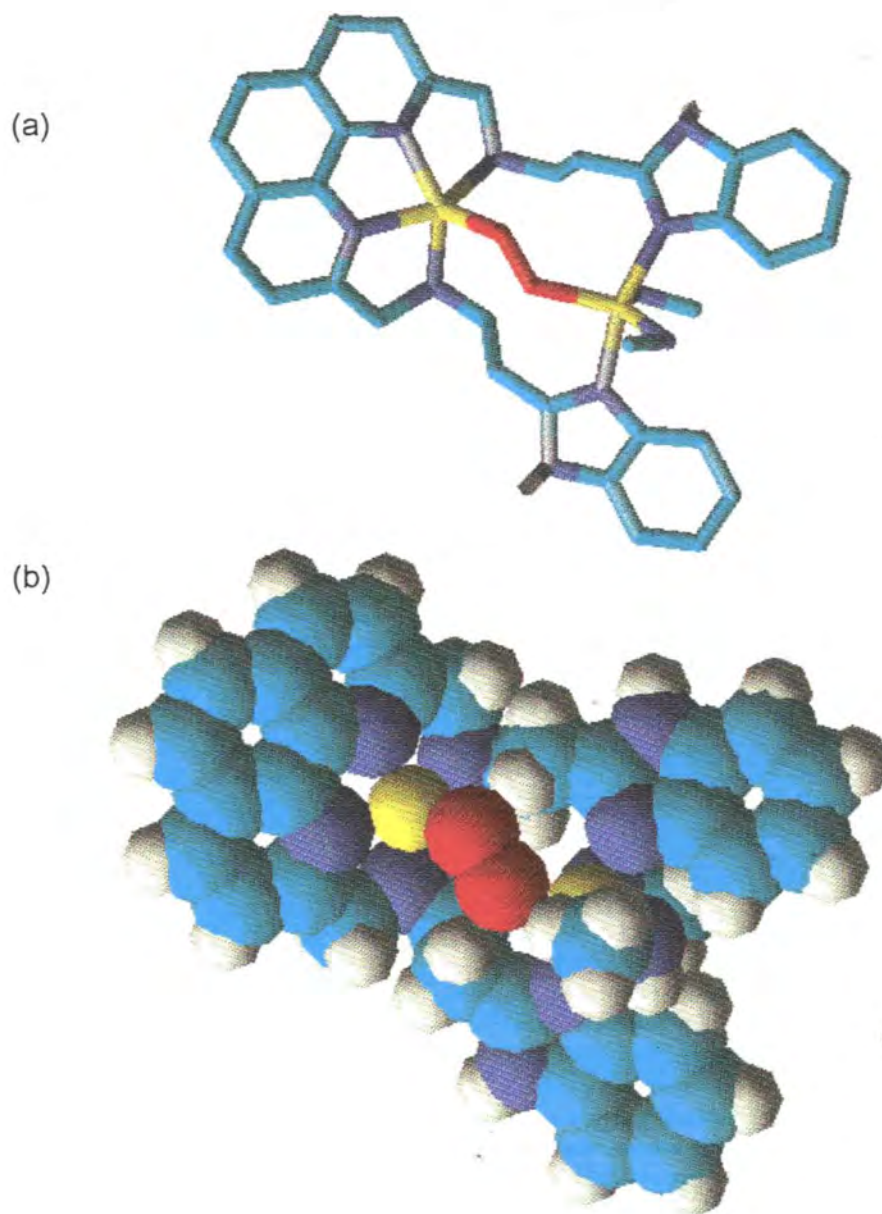


**Figure 34:** Energy-minimised conformations of the dioxygen-bridged copper complex 131oe: (a) a cylinder model and (b) a space-filling model.

In summary, the biphenyl spacer, due to its flexibility, should allow the oxygenated complex (**129os** or **129oe**) to adopt an optimal conformation that permits coordination of the substrate between the two copper ions. This may, however, be more difficult in the 1,10-phenanthroline complexes **131os** and **131oe** because of the rigidity imposed by the 1,10-phenanthroline spacer. In the latter complexes, the "active site" is peripheral, the dioxygen bridge being situated above the plane of the complex. The biphenyl analogues (**129os** and **129oe**), however, exhibit a concave region about the "active site" which could act as a binding pocket, providing access to a substrate molecule.

### ***Schiff base complexes***

The acyclic Schiff base ligands were expected to form complexes which would be considerably more conformationally flexible than the biphenyl or 1,10-phenanthroline analogues. For ligand **76**, a change in conformation occurs upon coordination with copper and tetrahedral geometry is observed for the copper atoms in the model of the resulting complex **120**. This tetrahedral geometry changes to distorted octahedral in the case of the  $\mu\text{-}\eta^2\text{:}\eta^2$  side-on bridged complex **132os** and, in complex **132oe**, where dioxygen is bound in a  $\mu\text{-}1,2\text{-trans}$  bridging mode, the geometry changes to trigonal bipyramidal (Figure 52). The Cu-Cu distance is 2.117 Å in complex **132os** and 4.642 Å in complex **132oe**. Comparison of the potential energies of these complexes reveal that complex **132os** is more stable. From the models of the complexes, it can be seen that, in each case, the active site lies in a concave region constituting a convenient binding site readily accessible to substrate molecules.

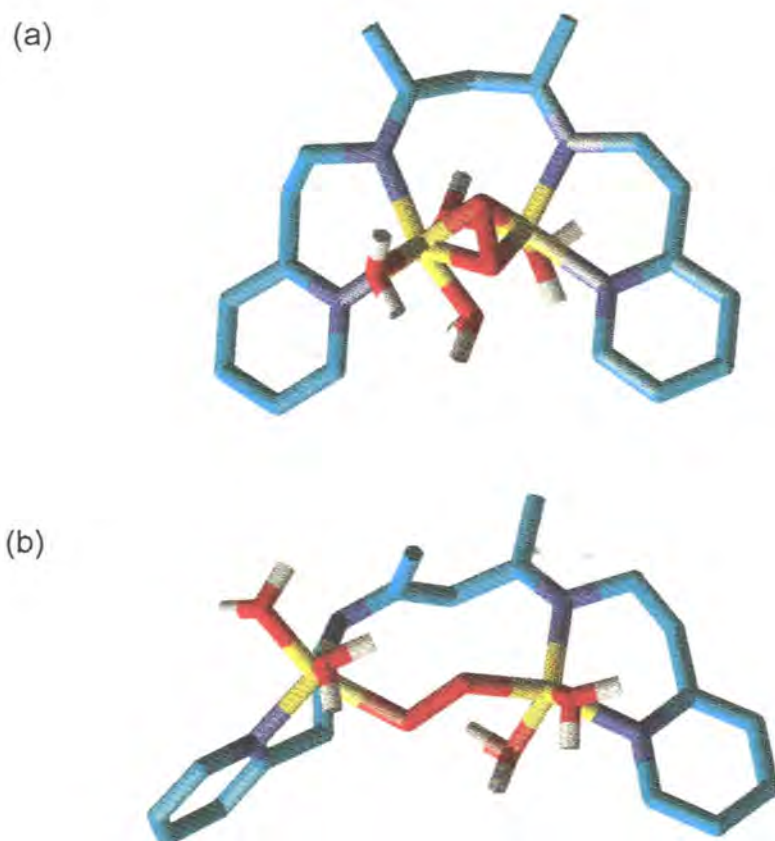


**Figure 35:** Energy-minimised models of (a) complex **132os**; and (b) complex **132oe**.

Unfortunately, none of the complexes afforded crystals suitable for single crystal X-ray analysis, thus precluding direct comparison of actual and computer-modelled structures. Moreover, in the case of the biphenyl- and 1,10-phenanthroline-based systems, the formation of polymeric complexes was observed.

## 2.3.4 Other Transition Metal Complexes

### 2.3.4.1 Cobalt Complexes

Cobalt may exist in various oxidation states, viz., cobalt(I), cobalt(II), cobalt(III) and cobalt(IV).<sup>218</sup> The cobalt(I) ion with its eight  $d$  electrons occurs in many complexes with  $\pi$ -bonded ligands. To make these complexes, in which the metal is trigonal bipyramidal or tetrahedral,  $\text{CoCl}_2$  is reduced with Zn or  $\text{N}_2\text{H}_4$  in the presence of the ligand.<sup>219</sup> The reduced form of Vitamin  $\text{B}_{12}$  is known to contain Co(I).<sup>220</sup> The cobalt(II) ion has a  $d^7$  configuration and typically exhibits four-coordinate tetrahedral or six-coordinate octahedral stereochemistry. A small difference in stability exists between these arrangements and, therefore, they may occur in equilibrium.

Cobalt(III), a  $d^6$  low spin, diamagnetic cation, is kinetically inert and displays octahedral stereochemistry. This is the most common oxidation state for cobalt in complexes, and cobalt(II) complexes are readily oxidised to cobalt(III). The oxidation of cobalt(II) to cobalt(III) is attributed to the higher crystal field stabilisation energy of cobalt(III).<sup>221</sup> Both cobalt(II) and (III) prefer nitrogen or oxygen donor ligands. The cobalt(IV) oxidation state is the highest oxidation state known for cobalt, but this is not as common as the cobalt(II) and (III) oxidation states.

Cobalt plays an important role in biological systems such as enzymes. The enzyme, glutamic mutase, is involved in the metabolism of amino acids, and ribonucleotide reductase in the biosynthesis of DNA.<sup>221</sup> Vitamin  $\text{B}_{12}$ , which was the first naturally occurring organometallic compound to be identified, is a cobalt complex which is involved in alkylation reactions.<sup>218, 222, 225</sup> In biological systems, iron(II) (e.g. haemoglobin and myoglobin) or copper(I) (haemocyanin) complexes serve as reversible oxygen carriers for the transport and storage of oxygen.<sup>223, 224</sup>

Since the discovery that Co(II) forms simple complexes that react reversibly with oxygen to give 1:1 and 2:1 metal complex-oxygen adducts,<sup>225, 226</sup> cobalt complexes

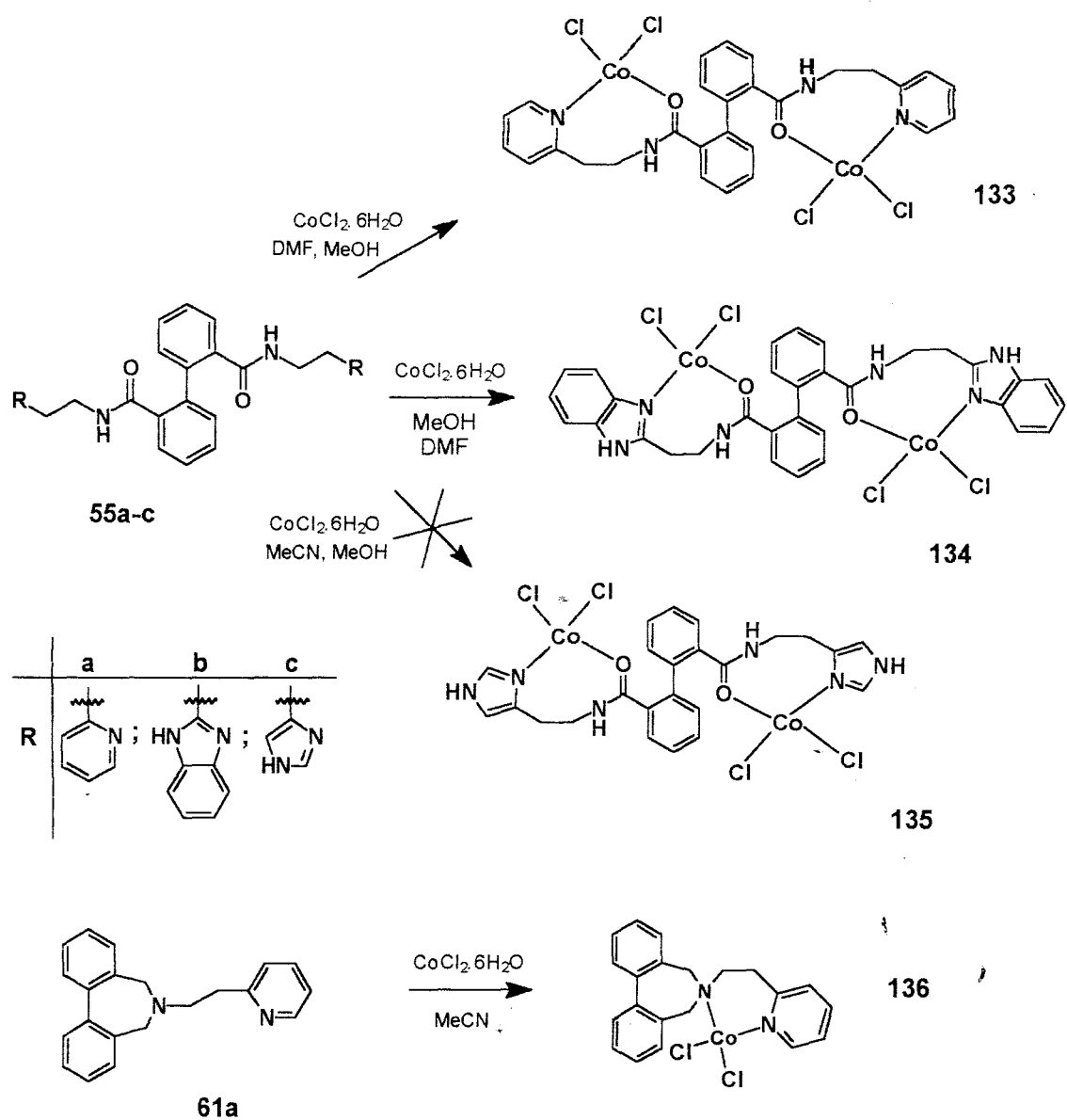
have been widely studied as models for biological processes.<sup>15, 227, 228</sup> Tetradentate Schiff base cobalt complexes have been used to study dioxygen activity and, since they undergo alkylation reactions, they have been used to mimic the reactions of Vitamin B<sub>12</sub>.

### 2.3.4.1.1 Synthesis of cobalt(II) complexes

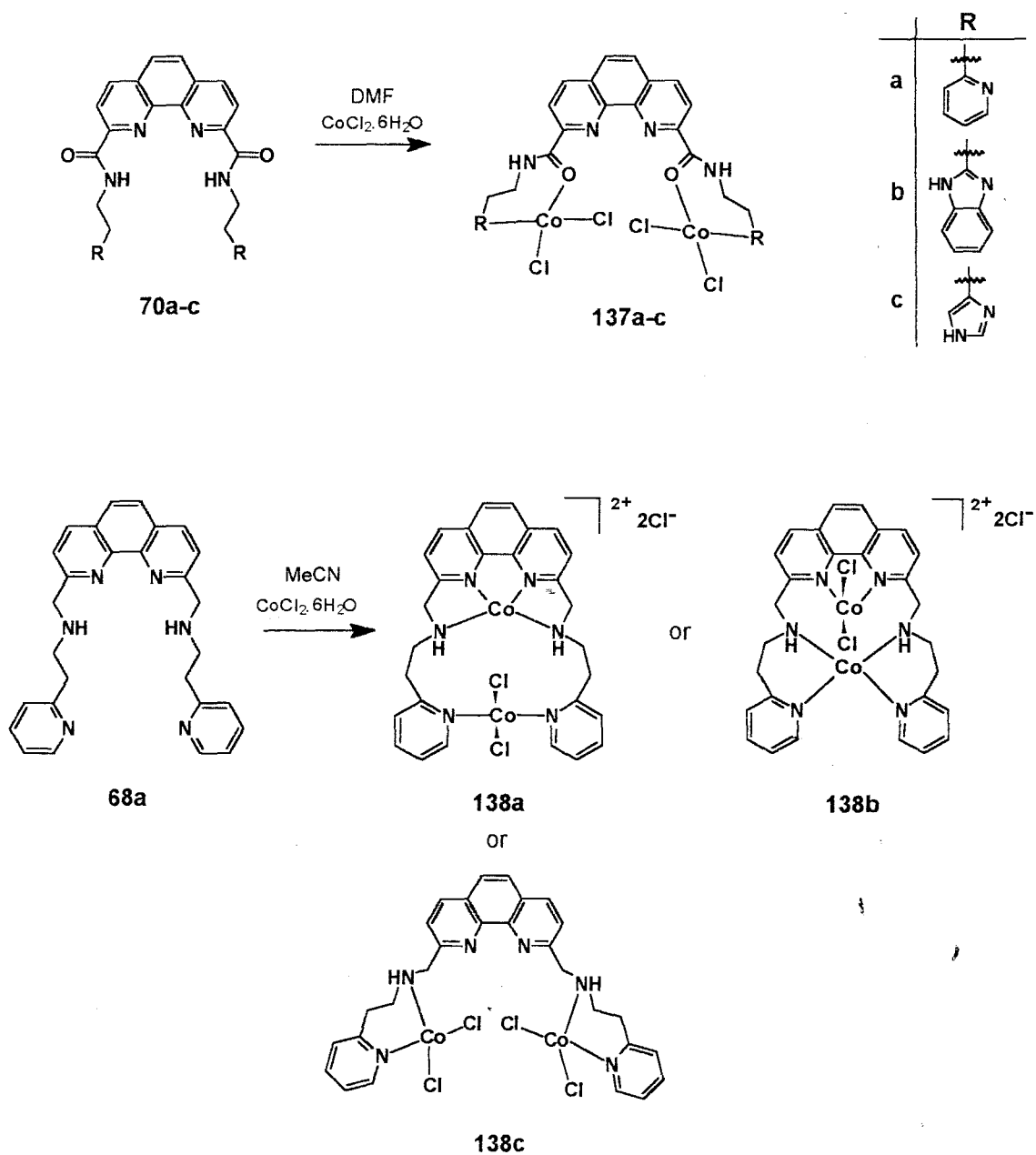
Cobaltous chloride hexahydrate (CoCl<sub>2</sub>·6H<sub>2</sub>O) was used to prepare the cobalt complexes, following the procedures detailed in the Experimental section (3.3.2). The microanalysis data for the resulting complexes, given in Table 10, indicate that four chloride anions are generally present and suggest that the amide, imidazole and benzimidazole protons are not removed during complexation with cobalt. The complexation of the biphenyl and 1,10-phenanthroline ligands with cobalt are outlined in Schemes 22 and 23. The formation of complex **135** (Scheme 22) was unsuccessful as could be seen from the microanalysis data which are not included in Table 12.

**Table 12:** Microanalytical data for the cobalt(II) complexes followed, in parentheses, by the calculated values.

Complex	Complex Stoichiometry	%Carbon	%Hydrogen	%Nitrogen
133	Co <sub>2</sub> (55a)Cl <sub>4</sub> ·H <sub>2</sub> O	46.3 (46.3)	3.7 (4.3)	7.5 (7.7)
134	Co <sub>2</sub> (55b)Cl <sub>4</sub> ·8H <sub>2</sub> O	41.5 (41.3)	4.0 (4.8)	9.5 (9.0)
136	Co(61a)Cl <sub>2</sub>	57.8 (58.7)	4.5 (4.7)	6.6 (6.5)
137a	Co <sub>2</sub> (69a)Cl <sub>4</sub> ·6H <sub>2</sub> O	39.1 (39.8)	3.3 (4.3)	10.3 (10.0)
137b	Co <sub>2</sub> (69b)Cl <sub>4</sub> ·8H <sub>2</sub> O	39.7 (40.2)	3.6 (4.4)	12.1 (11.7)
137c	Co <sub>2</sub> (69c)Cl <sub>4</sub> ·2H <sub>2</sub> O	38.1 (38.4)	3.6 (3.5)	14.8 (14.9)
138	Co <sub>2</sub> (68a)Cl <sub>4</sub> ·8H <sub>2</sub> O	41.8 (41.3)	3.8 (4.9)	10.1 (10.3)



Scheme 22: Complexation reactions of the biphenyl ligands with cobalt(II).



**Scheme 23:** Complexation reactions of the 1,10-phenanthroline ligands with cobalt(II).

### 2.3.4.1.2 Spectroscopic analysis of the cobalt(II) complexes

$^1\text{H}$  and  $^{13}\text{C}$  NMR spectra of the cobalt complexes were run to define the oxidation state of the metal ions. As cobalt can form both paramagnetic [Co(II)] and diamagnetic [Co(III)] complexes,  $^1\text{H}$  NMR spectroscopy was expected to establish the oxidation state of cobalt in the complexes. The  $^1\text{H}$  NMR spectra obtained for the biphenyl- and 1,10-phenanthroline complexes reveal broad, poorly resolved signals, indicating that *at least one* of the cobalt ions in each complex is paramagnetic.

IR spectra of the complexes were expected to establish whether the cobalt ions coordinate through the amide nitrogen or oxygen atoms. Determining whether coordination occurs through the aromatic nitrogen donors, however, was not possible, due to the congestion of bands in the aromatic region ( $1600\text{-}1500\text{ cm}^{-1}$ ) which makes detecting a band shift in this region rather difficult. Spectra were run in the far-IR region to determine whether the coordinated chloride anions are in a tetrahedral or octahedral environment. The IR frequencies for selected bands are shown in Table 13. From the negative IR frequency shifts of the amide carbonyl (amide I) bands, it is apparent that coordination occurs through the amide oxygen atom in both the biphenyl and 1,10-phenanthroline cobalt complexes. Although the benzimidazole NH band cannot be identified in the IR spectra of the biphenyl and 1,10-phenanthroline complexes **134** and **137b** respectively, it is assumed that coordination does not involve the secondary benzimidazole nitrogen as the microanalysis data show the presence of four chloride ions in each case. This is an indication that no deprotonation occurs on formation of these complexes, and it is believed that coordination involves the tertiary, benzimidazole nitrogen in both of these complexes. For the 1,10-phenanthroline complex **137c**, the imidazole NH bands are shifted, relative to the free ligand, indicating coordination through the tertiary, imidazole nitrogen.

**Table 13:** Summary of the IR frequencies ( $\nu_{\text{M-Cl}}$ ) and the amide frequency shifts ( $\Delta\nu_{\text{NH}}$  and  $\Delta\nu_{\text{C=O}}$ ) on formation of the amide cobalt complexes.

Cobalt Complex	$\Delta\nu_{\text{NH}}/\text{cm}^{-1}$	$\Delta\nu_{\text{C=O}}/\text{cm}^{-1}$	$\nu_{\text{M-Cl}}/\text{cm}^{-1}$
133	-	-19	306
134	13	-30	295
137a	18	-7	303
137b	-62	-7	311
137c	-38	-6	299

While the amide NH band cannot be seen in the IR spectrum of the biphenyl complex **133**, due to the presence of a strong, broad water band, the microanalysis data clearly indicates that formation of the complex does not involve deprotonation. An amide NH band is, however, observed at  $3274\text{ cm}^{-1}$  in the IR spectrum of the 1,10-phenanthroline complex **137a**, thus confirming the microanalysis data obtained for this complex which, due to the presence of four chloride ions, indicate that the amide functionality is not deprotonated.

Two Co-Cl bands characteristic of tetrahedral geometry are anticipated in the far-IR region (*ca.*  $301$  and *ca.*  $324\text{ cm}^{-1}$ ).<sup>229</sup> These bands are not observed for these amide complexes instead, a very strong, broad band, often with shoulders, is observed at *ca.*  $300\text{ cm}^{-1}$ . This may be due to accidental degeneracy of the symmetric and antisymmetric Co-Cl stretches, and it is suggested that the band at *ca.*  $300\text{ cm}^{-1}$  indicates a distorted tetrahedral cobalt geometry occurring within these complexes.

Coordination of the ligand with the tetrahedral cobalt ion in the amine complex **136** was unambiguously established by single crystal X-ray crystallography of this complex (Figure 36). A far-IR band at  $298\text{ cm}^{-1}$  is consistent with coordination of the chloride ion in a tetrahedral arrangement.

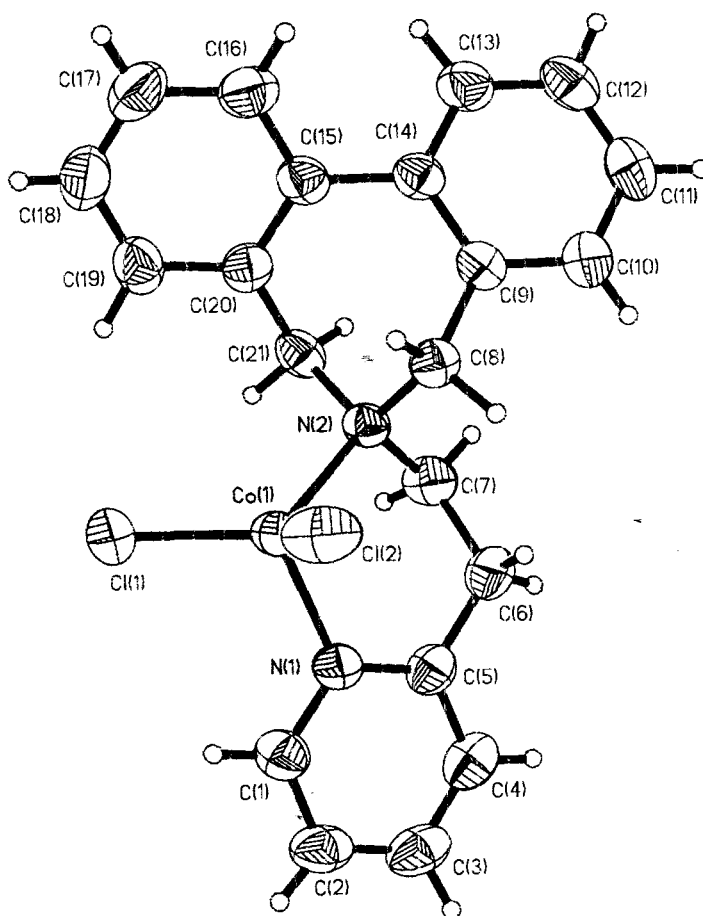


**Figure 36:** X-ray crystal structure of cobalt(II) complex 136, showing the crystallographic numbering.

An IR band at  $3398\text{ cm}^{-1}$  for complex **138** suggests that deprotonation of the secondary amine does not occur during complexation, while a shift of  $98\text{ cm}^{-1}$  for this NH band (relative to the free ligand) reflects coordination to the aliphatic amine nitrogen. In the far-IR region the strong, irregular band at  $311\text{ cm}^{-1}$  suggests that the chloride ions coordinate to cobalt in a tetrahedral arrangement.

Cobalt ions in tetrahedral or octahedral coordination environments give rise to characteristic absorption bands in the visible region. Absorption data for the cobalt complexes and their assigned geometry are summarised in Table 14, while the electronic spectrum for complex **137a** is illustrated in Figure 37.

**Table 14:** Electronic absorption bands with their assigned transition types and geometries for the cobalt complexes.

Complex	Absorption (nm)	Assignment	Geometry
133	600sh, 613, 657, 678	${}^4A_2 \rightarrow {}^4T_1(P)$	tetrahedral
134	579sh, 608, 628	${}^4A_2 \rightarrow {}^4T_1(P)$	tetrahedral
136	576, 621, 638	${}^4A_2 \rightarrow {}^4T_1(P)$	tetrahedral
137a	596sh, 604, 665, 677	${}^4A_2 \rightarrow {}^4T_1(P)$	tetrahedral
137b	597sh, 611, 656, 676	${}^4A_2 \rightarrow {}^4T_1(P)$	tetrahedral
137c	580sh, 608, 629, 677sh	${}^4A_2 \rightarrow {}^4T_1(P)$	† tetrahedral
138	597sh, 604, 666, 678	${}^4A_2 \rightarrow {}^4T_1(P)$	tetrahedral

In all cases, absorption spectra were observed corresponding to the  ${}^4A_2 \rightarrow {}^4T_1(P)$  transition, which is characteristic of tetrahedral cobalt coordination. The “fine structure” evident in Figure 37 is attributed to spin-orbit coupling effects and to transitions involving doublet states.<sup>230</sup>

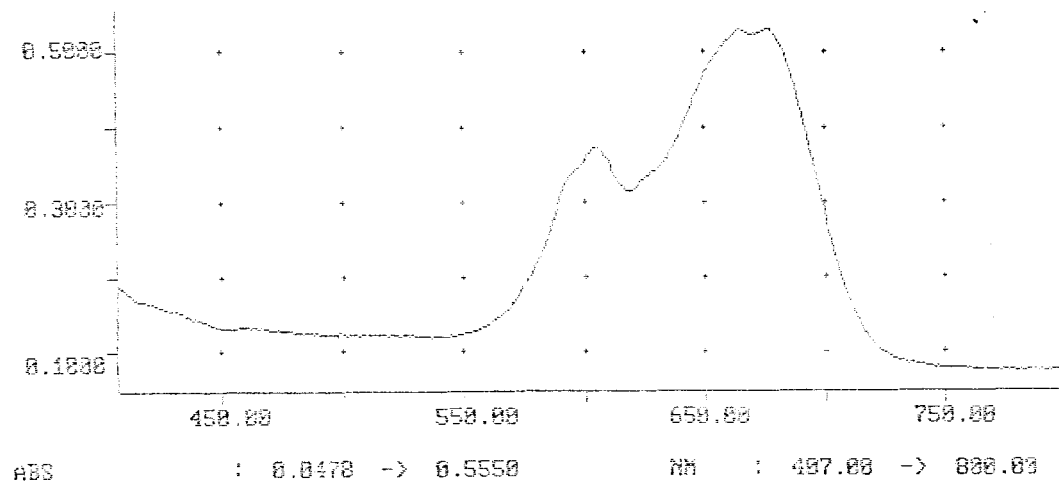


**Figure 37:** The electronic spectrum of complex **137a** in DMF.

### 2.3.4.1.3 Computer modelling of the cobalt complexes

These studies were undertaken to explore the possible 3-D structures of the dinuclear cobalt complexes because crystals suitable for single crystal X-ray analysis could not be obtained. Experimental IR and UV-Visible spectroscopic data has been taken into account in developing representative structures of the complexes detailed in Figure 38. For some of these complexes, isomeric structures of the product are possible and molecular mechanics calculations were used to predict the most likely structure. Thus, the symmetrical complex **138c**, is considered more likely than the isomeric systems **138a** or **138b**.

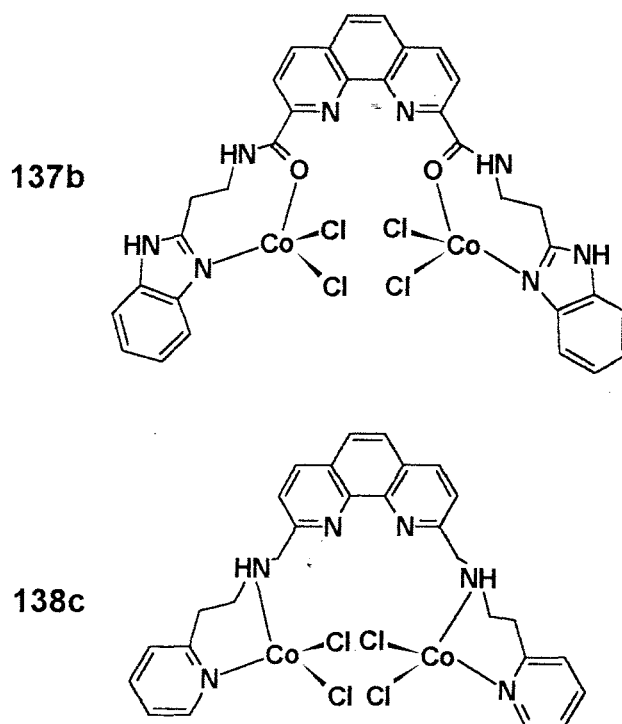


**Figure 38:** Cobalt complexes modelled.

The computer modelled structure of the 1,10-phenanthroline diamide cobalt complex **138c** is shown in [Figure 39(a)]. In this model, the distorted tetrahedral geometry of the metal ions can again be clearly seen. For the 1,10-phenanthroline diamide complexes coordination through the carbonyl oxygen of the amide functionality is indicated (see section 2.3.4.1.2). Complex **137b** was modelled on

this basis and the resulting structure illustrates the conformation expected to be typical of the analogous diamide cobalt complexes **137a** and **137c**. In this model, the distorted tetrahedral geometry of the metal ions can be seen [Figure 39(b)].

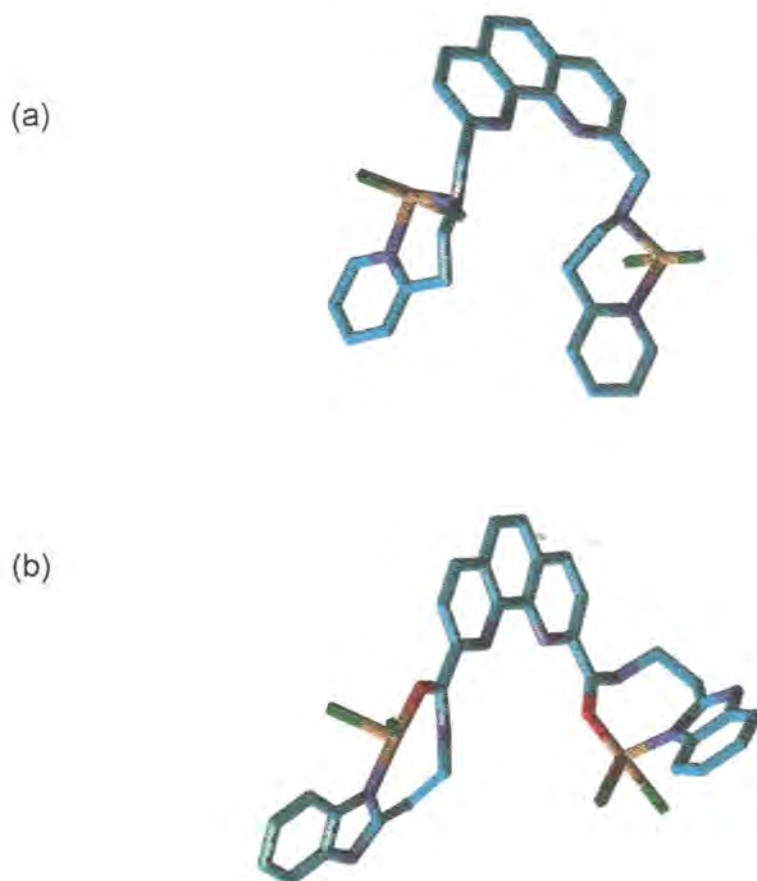


**Figure 39:** Computer-modelled structures of the 1,10-phenanthroline cobalt complexes: (a) complex **138c** and (b) complex **137b** for the biphenyl diamide cobalt complexes. Coloured atoms: *carbon*: light blue; *nitrogen*: dark blue; *oxygen*: red; *chlorine*: green; *cobalt*: light-brown.

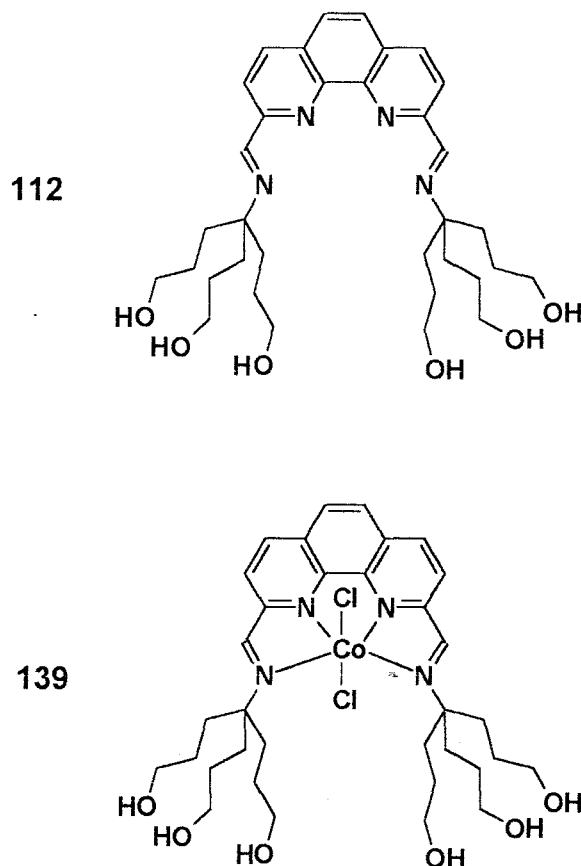


**Figure 40:** The dendrimer-based ligand **112** and the proposed structure of its cobalt(II) complex **139**.

It was also decided to model the dendrimer-based ligand **112** and the proposed cobalt(II) complex **139** (Figure 40). From the models shown in Figure 41, the 3-D arrangement of the dendrimer moieties in the ligand and the complex can be clearly seen. In the cobalt complex (Figure 41b), the 1,10-phenanthroline spacer is no longer planar, but slightly bent, while the octahedral geometry of the cobalt cation is also clearly apparent.

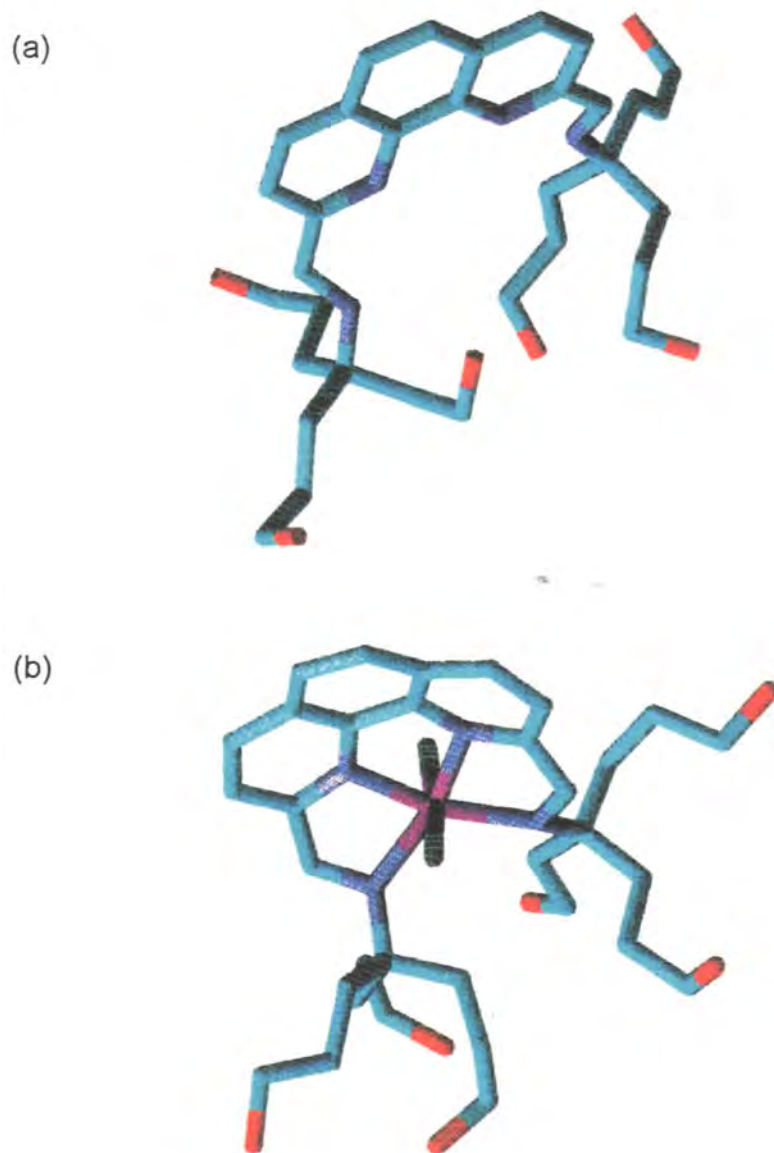
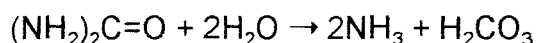


**Figure 41:** Computer modelled structures of: (a) the dendrimer ligand **112**;  
(b) the resulting cobalt(II) complex **139**.

### 2.3.4.2 Nickel Complexes

Various oxidation states have been observed for nickel ranging from (-I) to (+IV), but studies of the chemistry of nickel have concentrated on the (+II) oxidation state. The metal ion in nickel(II) complexes exhibits considerable variability in molecular geometry, e.g. four coordinate (tetrahedral or square planar), five coordinate (square pyramidal or trigonal bipyramidal) and six-coordinate (octahedral).<sup>231</sup> As a consequence, the chemistry of nickel(II) is quite complicated. Tetrahedral complexes are intensely blue in colour and paramagnetic;<sup>232</sup> square planar complexes are diamagnetic and usually red, brown or yellow in colour.<sup>232</sup> Thus, tetrahedral complexes may be distinguished from square planar complexes by their colour and their magnetic properties. Octahedral complexes may also be blue or purple in colour and paramagnetic due to the  $d^8$  ion having two unpaired electrons.<sup>232</sup> The nickel(III) oxidation state is rare and very few Ni(III) complexes are known; the (+IV) oxidation state, which is the highest for nickel, is also rare.

Nickel plays an important role in biological systems. The first such system to be discovered was the enzyme, urease, isolated from jack beans<sup>233,234</sup> and shown by UV-Visible spectroscopy and EXAFS studies to contain two octahedral nickel(II) ions in a nitrogen- and oxygen-donor environment. Urease is responsible for catalysing the hydrolysis of urea to ammonia and carbonic acid, thus:-



Nickel has subsequently been found in other enzymes, *viz.*, hydrogenases, CO dehydrogenases and coenzyme  $\text{F}_{430}$ .<sup>234</sup> Hydrogenases which occur in many bacteria, catalyse the oxidation of molecular hydrogen, while CO dehydrogenases interconvert carbon monoxide and carbon dioxide. It has been found that the hydrogenases and CO dehydrogenases have nickel(III) (low spin  $d^7$ ) and Fe-S clusters present in their structures.<sup>234</sup> Coenzyme  $\text{F}_{430}$ , which is a cofactor of methyl coenzyme M reductase and which contains nickel(II) in a square planar geometry,

is functional in a series of reactions in bacteria that result in the generation of methane gas.

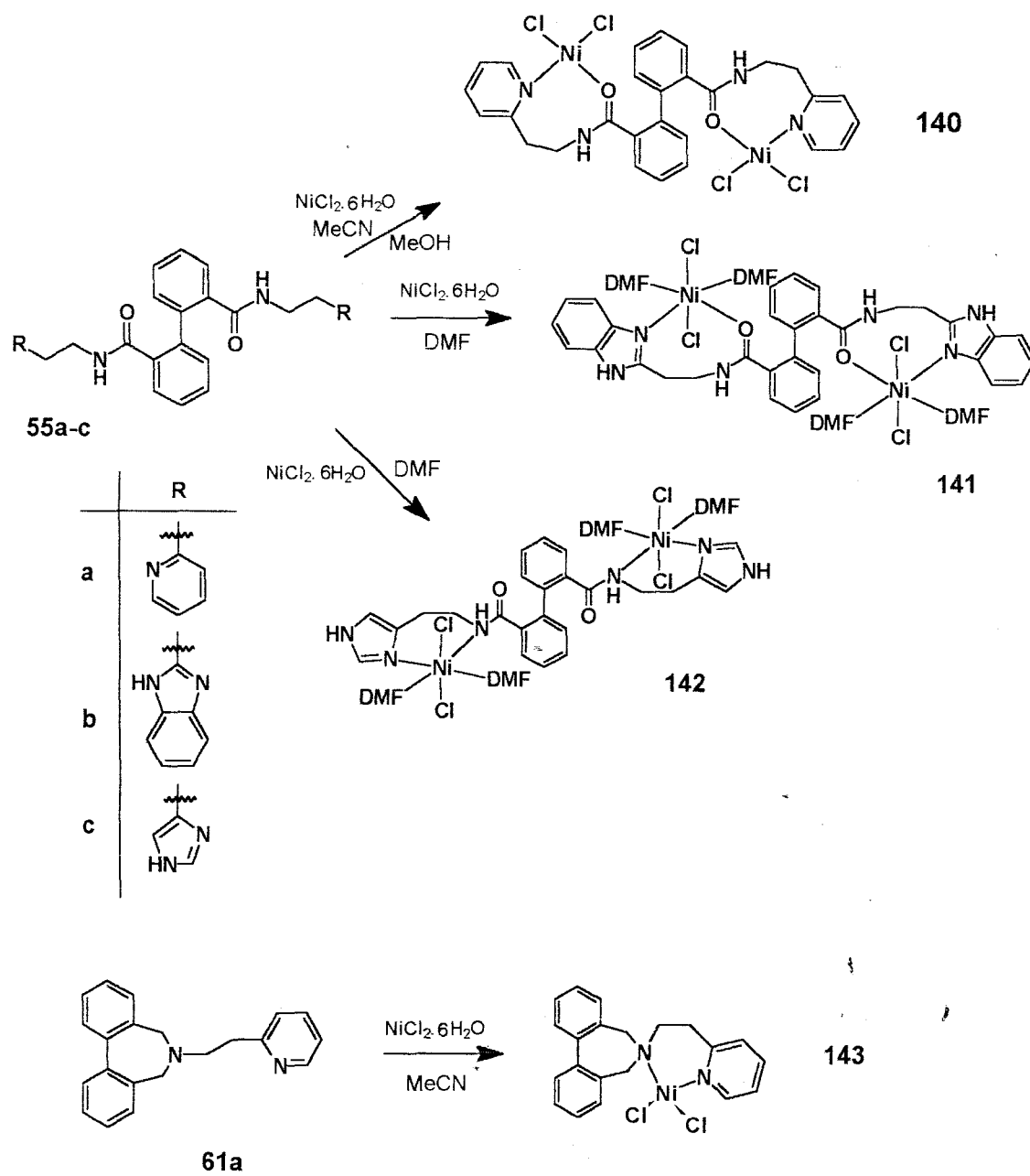
### 2.3.4.2.1 Synthesis of nickel complexes

Nickel chloride hexahydrate ( $\text{NiCl}_2 \cdot 6\text{H}_2\text{O}$ ) was used to prepare the nickel complexes (Schemes 24 and 25), following the procedure detailed in the Experimental section (3.3.3).

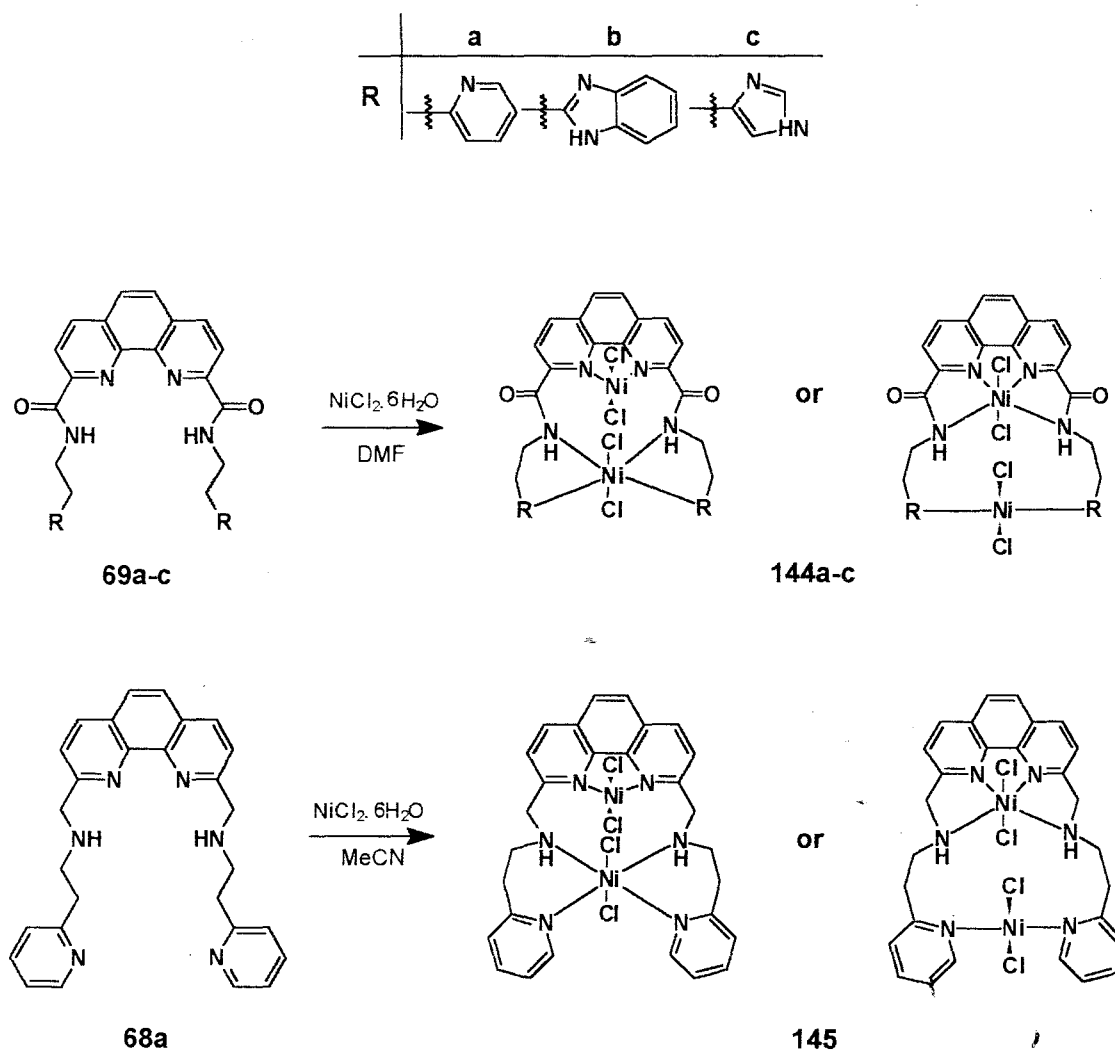
From the microanalysis data summarised in Table 15, it can be seen that: - i) most of the complexes examined are dinuclear; ii) most of the complexes have four chloride ions, except the mononuclear complex **143** for which there are two; iii) complexes **141** and **142**, appears to have DMF present, possibly as part of an octahedral coordination sphere; iv) deprotonation of the amide, amine, imidazole or benzimidazole groups has not occurred during formation of the dinuclear complexes.

**Table 15:** Microanalytical data for the nickel(II) complexes followed, in parentheses, by the calculated values.

Complex	Complex Stoichiometry	% Carbon	% Hydrogen	% Nitrogen
140	$\text{Ni}_2(55a)\text{Cl}_4 \cdot 6\text{H}_2\text{O}$	40.5 (41.1)	4.2 (4.7)	7.0 (6.9)
141	$\text{Ni}_2(55b)\text{Cl}_4(\text{DMF})_4 \cdot 9\text{H}_2\text{O}$	41.7 (42.6)	5.3 (5.9)	11.7 (11.3)
142	$\text{Ni}_2(55c)\text{Cl}_4(\text{DMF})_4 \cdot 3\text{H}_2\text{O}$	41.4 (41.8)	5.2 (5.7)	13.2 (13.5)
143	$\text{Ni}(61a)\text{Cl}_2 \cdot 1\text{H}_2\text{O}$	57.1 (56.5)	4.6 (5.0)	6.7 (6.3)
144a	$\text{Ni}_2(69a)\text{Cl}_4 \cdot 2\text{H}_2\text{O}$	42.6 (43.6)	4.0 (3.7)	11.3 (10.9)
144b	$\text{Ni}_2(69b)\text{Cl}_4(\text{DMF})_2 \cdot 8\text{H}_2\text{O}$	41.3 (42.1)	4.1 (4.8)	13.4 (12.9)
144c	$\text{Ni}_2(69c)\text{Cl}_4 \cdot 2\text{H}_2\text{O}$	37.6 (38.5)	4.2 (3.5)	14.5 (15.0)
145	$\text{Ni}_2(68a)\text{Cl}_4 \cdot 3\text{H}_2\text{O}$	44.1 (44.2)	4.0 (4.5)	11.0 (11.0)



**Scheme 24:** Complexation reactions of the biphenyl ligands with nickel(II).



**Scheme 25:** Complexation reactions of the 1,10-phenanthroline ligands with nickel(II).

### 2.3.4.2.2 Spectroscopic analysis of the nickel(II) complexes

The  $^1\text{H}$  NMR spectra of the biphenyl and the 1,10-phenanthroline nickel(II) complexes were expected to permit paramagnetic (tetrahedral and octahedral) and diamagnetic (square planar) nickel(II) complexes to be distinguished. However, the  $^1\text{H}$  NMR spectra of the 1,10-phenanthroline complexes typically reveal a combination of sharp and broad peaks as illustrated by the spectra of complex **144c** and the ligand **69c** (Figures 42 and 43). In the  $^1\text{H}$  NMR spectra of the biphenyl Ni(II) complexes, the peaks in the aromatic region ( $\delta 6\text{-}8$  ppm) were, typically, better resolved than in the spectra of the 1,10-phenanthroline Ni(II) complexes. Nevertheless, the signals for the biphenyl complexes are still broader than the corresponding free ligand signals (cf. Figures 44 and 45). These observations precluded unambiguous assignment of the metal ion geometries.

IR studies were undertaken to determine whether coordination with nickel occurred through the oxygen or the nitrogen of the amide group, since it is known that nickel coordinates with both oxygen and nitrogen donors. Pertinent IR data are summarised in Table 16.

**Table 16:** Summary of the IR frequencies ( $\nu_{\text{M-Cl}}$ ) and the amide frequency shifts ( $\Delta\nu_{\text{NH}}$  and  $\Delta\nu_{\text{C=O}}$ ) on formation of the nickel complexes.

Complex	$\Delta\nu_{\text{NH}}/\text{cm}^{-1}$	$\Delta\nu_{\text{C=O}}/\text{cm}^{-1}$	$\nu_{\text{M-Cl}}/\text{cm}^{-1}$
140	15	-11	276, 325
141	11	-6	387
142	61	13	378
144a	-33	2	253, 378
144b	-78	23	283, 384
144c	-61	0	310, 373

The 1,10-phenanthroline amide complexes **144a** and **144b**, exhibit negative shifts of the amide NH band and, positive shifts for the amide carbonyl bands indicating coordination through the amide nitrogen. In the case of complex **144c** no shift

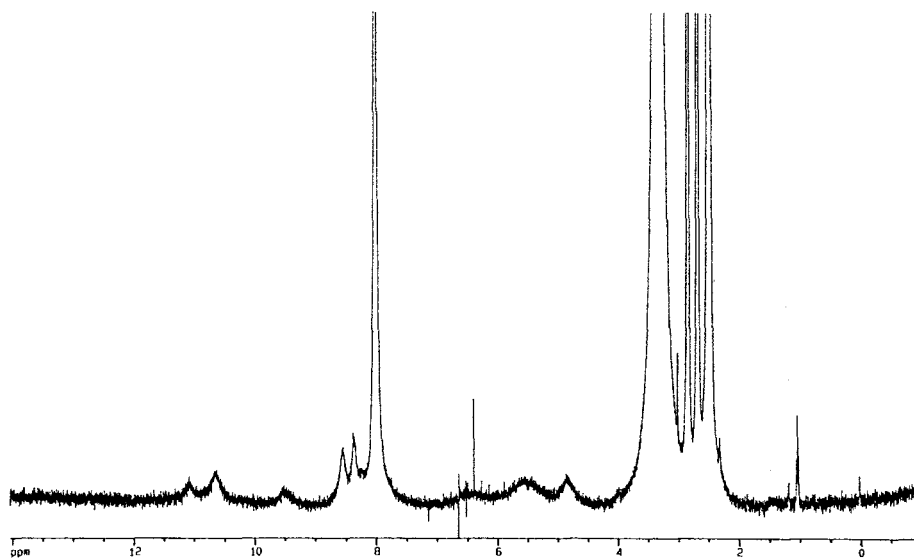


**Figure 42:** The 400 MHz <sup>1</sup>H NMR spectrum of the 1,10-phenanthroline complex **144c** in DMSO-d<sub>6</sub>.

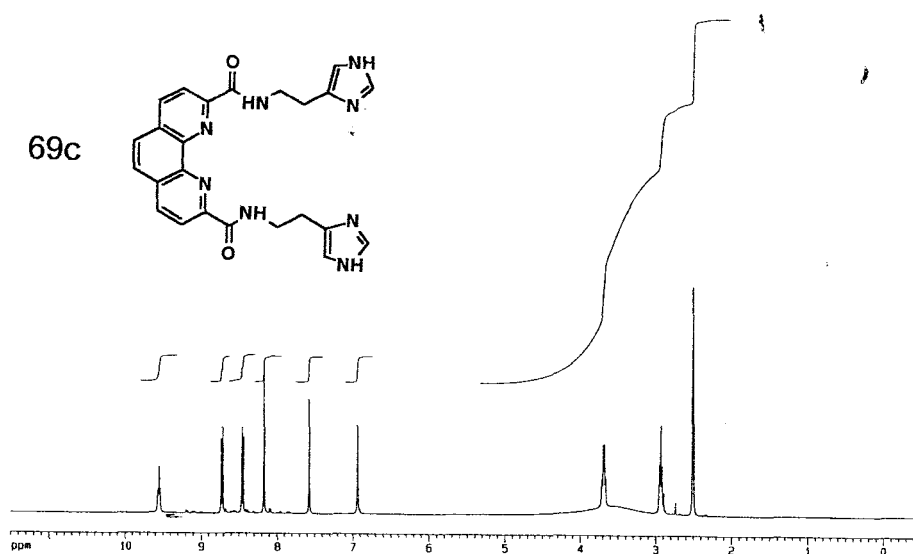


**Figure 43:** The 400 MHz <sup>1</sup>H NMR spectrum of the 1,10-phenanthroline ligand **69c** in DMSO-d<sub>6</sub>.

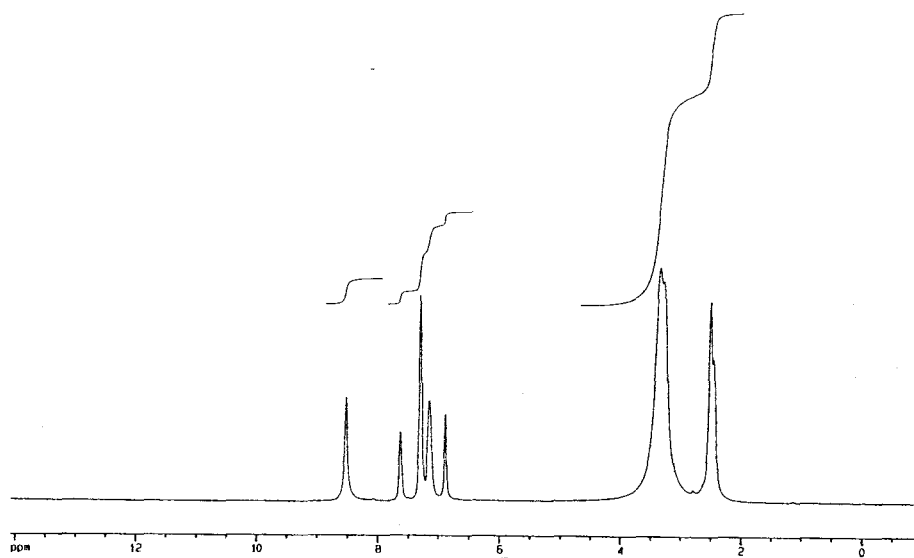


Figure 44: The 400 MHz <sup>1</sup>H NMR spectrum of the biphenyl complex **140** in DMSO-d<sub>6</sub>.

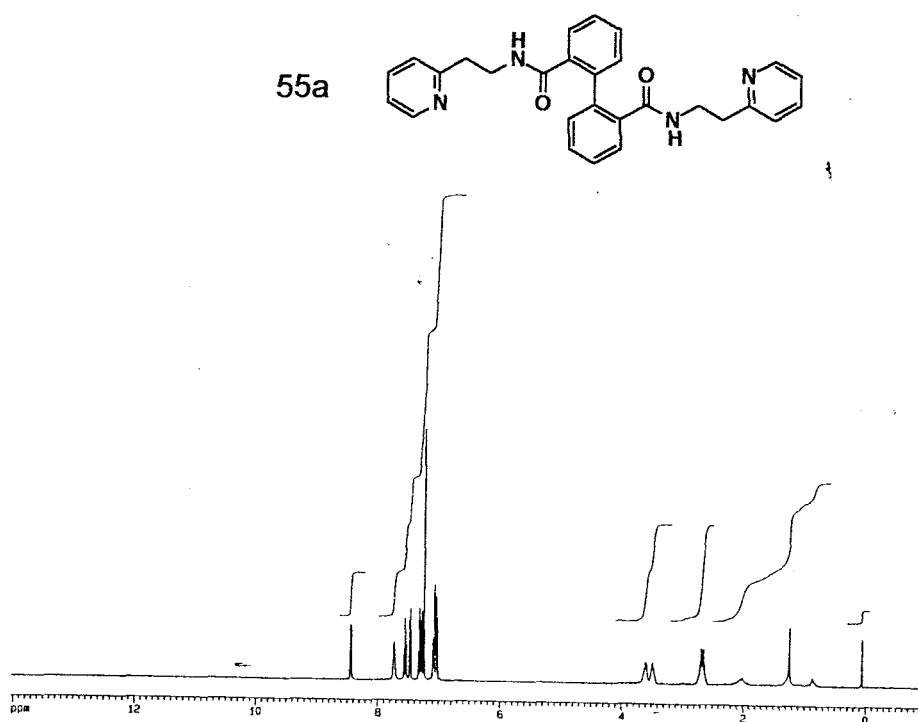
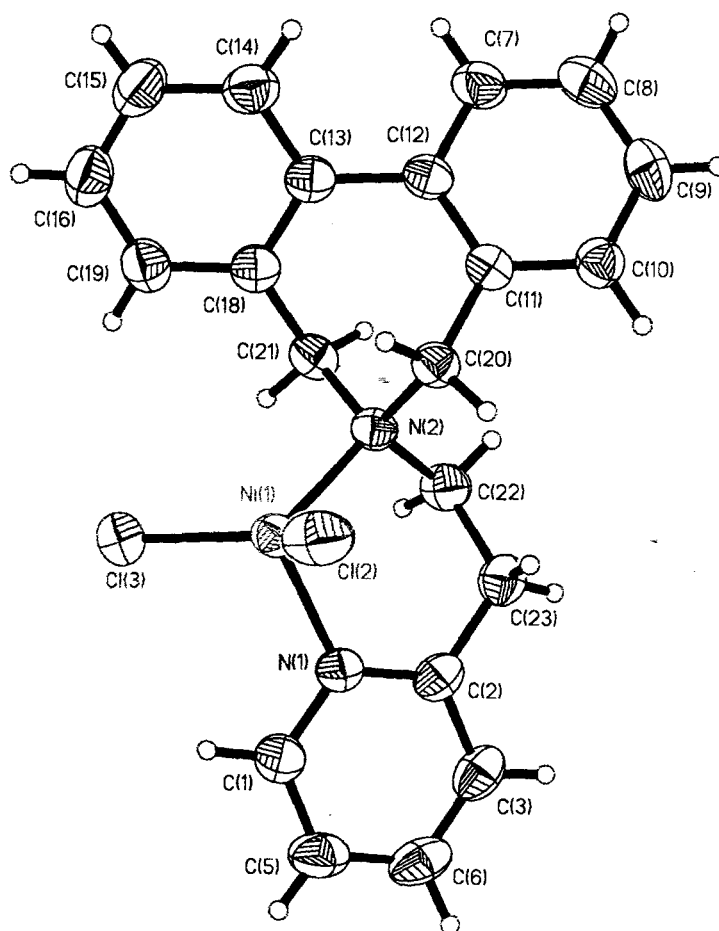


Figure 45: The 400 MHz <sup>1</sup>H NMR spectrum of the biphenyl ligand **55a** in DMSO-d<sub>6</sub>.

for the amide carbonyl is observed, but a negative shift of the amide NH band is an indication of coordination through the amide nitrogen. For the biphenyl amide complexes **140** and **141** coordination through the amide oxygen is indicated by positive NH shifts and negative carbonyl shifts; in the case of complex **142**, coordination through the amide nitrogen is suggested by the positive carbonyl shift, although  $\Delta\nu_{\text{NH}}$  is positive. The presence of the amide NH band in all cases shows that deprotonation of the amide nitrogen has not occurred, thus supporting the microanalysis data for these complexes.

A benzimidazole secondary amine NH stretching band was observed in the IR spectra of complexes **141** and **144b**; NH stretching bands for the imidazole secondary amine were also evident in the IR spectra of complexes **142** and **144c**, further supporting the microanalysis data which, in each case, indicated the presence of four chloride anions.

In the case of complexes **141** and **142** the strong bands in the 370-390  $\text{cm}^{-1}$  region are attributed to chloride anions coordinated in a *trans* geometry in an octahedral environment. For complex **143**, the two relatively strong bands observed at 289 and 329  $\text{cm}^{-1}$  are believed to be due to chloride ions coordinated within a tetrahedral environment, and the X-ray crystal structure for complex **143** (Figure 46) clearly confirms the tetrahedral geometry. Very weak bands at 276 and 325  $\text{cm}^{-1}$  in the far IR region were observed for **140** and have been tentatively assigned to Ni-Cl stretches. The low intensity of these bands suggests that the chloride anions are not in a tetrahedral environment (in contrast to those observed for complex **143**) and that the geometry of complex **140** is, in fact, square planar. In the case of complexes **144a-c**, the strong bands in the region 370-390  $\text{cm}^{-1}$  are attributed to *trans*-coordinated chloride ions in an octahedral environment, while others at 253, 283 and 310  $\text{cm}^{-1}$ , are indicative of chloride ions coordinated in a tetrahedral environment.<sup>235</sup> Similar bands for complex **145** (at 278 and 352  $\text{cm}^{-1}$ ) are also considered to indicate *trans*-coordinated chloride ions in tetrahedral and octahedral environments respectively.



**Figure 46:** X-ray crystal structure of complex **143** showing the crystallographic numbering.

Different UV-Vis absorption patterns characterise different geometries in nickel complexes,<sup>231,236,237,238</sup> and the absorption data, proposed transition types and geometries for some of the nickel complexes synthesised in this study are summarised in Table 17. The absorption bands for the complexes **144b** and **144c** appear to be masked by solvent bands (DMF and DMSO); for complex **145** a shoulder at 377 nm has been tentatively assigned as the main tetrahedral absorption band. The proposed geometries apply to at least one, but not necessarily both, Ni<sup>2+</sup> ions in each dinuclear complex.

**Table 17:** Electronic absorption bands with their assigned transition types and the proposed geometries for the nickel complexes.

Complex	Absorption (nm)	Assignment	Geometry
140	425	---	Square planar
141	412 590 619	${}^3A_{2g} \rightarrow {}^3T_{2g}$ ${}^3A_{2g} \rightarrow {}^3T_{1g}(F)$ ${}^3A_{2g} \rightarrow {}^3T_{1g}(P)$	Octahedral
142	410 525 576	${}^3A_{2g} \rightarrow {}^3T_{2g}$ ${}^3A_{2g} \rightarrow {}^3T_{1g}(F)$ ${}^3A_{2g} \rightarrow {}^3T_{1g}(P)$	Octahedral
143	514, 555	${}^3T_1 \rightarrow {}^3T_1(P)$	Tetrahedral
144a	363 582 621	${}^3A_{2g} \rightarrow {}^3T_{2g}$ ${}^3A_{2g} \rightarrow {}^3T_{1g}(F)$ ${}^3A_{2g} \rightarrow {}^3T_{1g}(P)$	Octahedral †
144b	masked	----	----
144c	masked	---	---
145	377sh	${}^3T_1 \rightarrow {}^3T_1(P)$	Tetrahedral

### 2.3.4.2.3 Computer modelling of the nickel complexes

In the absence of X-ray crystal structures, computer modelling was used to explore the possible 3-D structures of the dinuclear nickel complexes. The microanalytical, IR and UV-Visible spectroscopic data were again considered in developing structures for these complexes. In some cases, isomers are possible and molecular mechanics calculations have been used to predict the most likely structure. In this section, the discussion will focus on the computer modelling of the representative dinuclear nickel complexes shown in Figures 47 and 49.

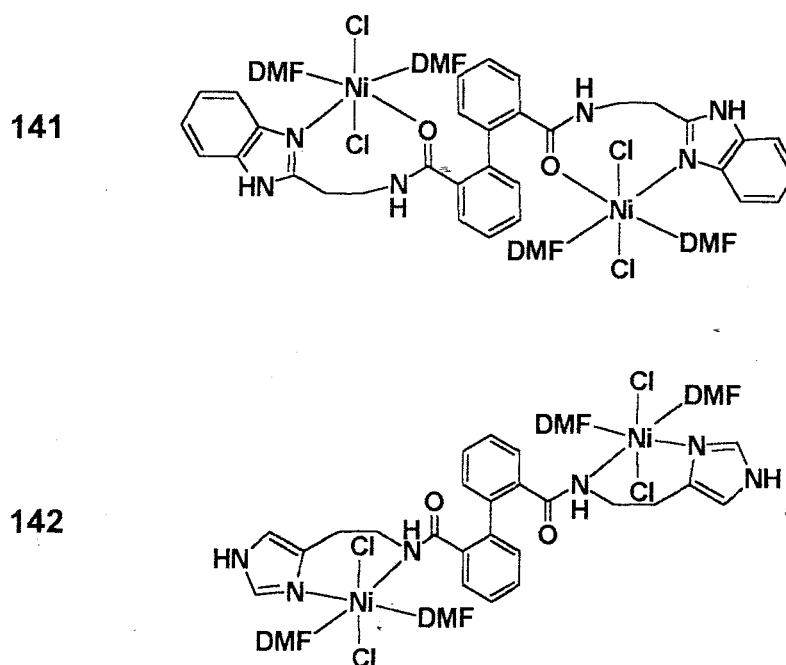
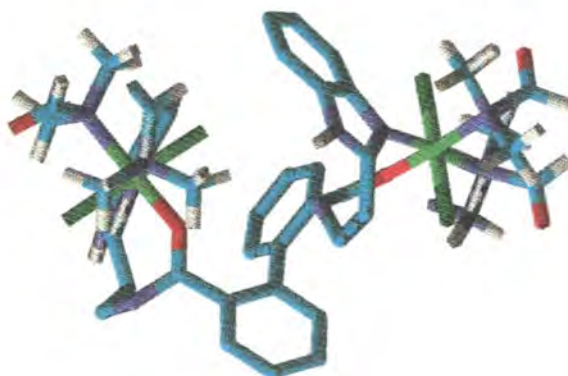


**Figure 47:** The representative biphenyl nickel complexes that have been modelled.

In the case of the biphenyl diamide complexes, coordination is presumed to involve amide oxygen in complex **141** (to give 8-membered chelate rings) and the amide nitrogen in complex **142** (to give 6-membered chelate rings). The energy-minimised models of these complexes are shown in Figure 48. The octahedral, metal ion geometry and the mutually perpendicular arrangement of the arene rings is apparent in these complexes.

(a)



(b)

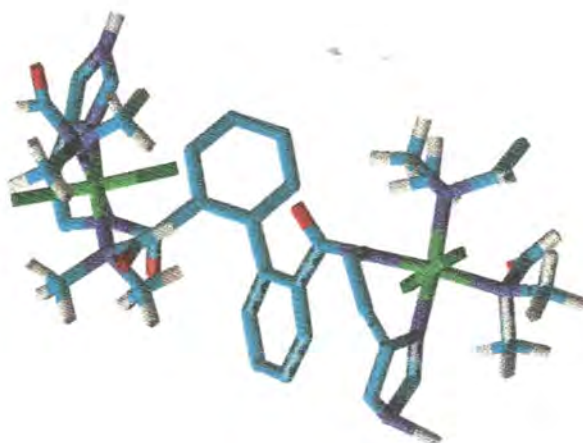


**Figure 48:** Energy-minimised models of (a) complex **141** and (b) complex **142**. Coloured atoms: Carbon: light-blue; nitrogen: dark-blue; oxygen: red; chlorine: green; nickel: light-green.

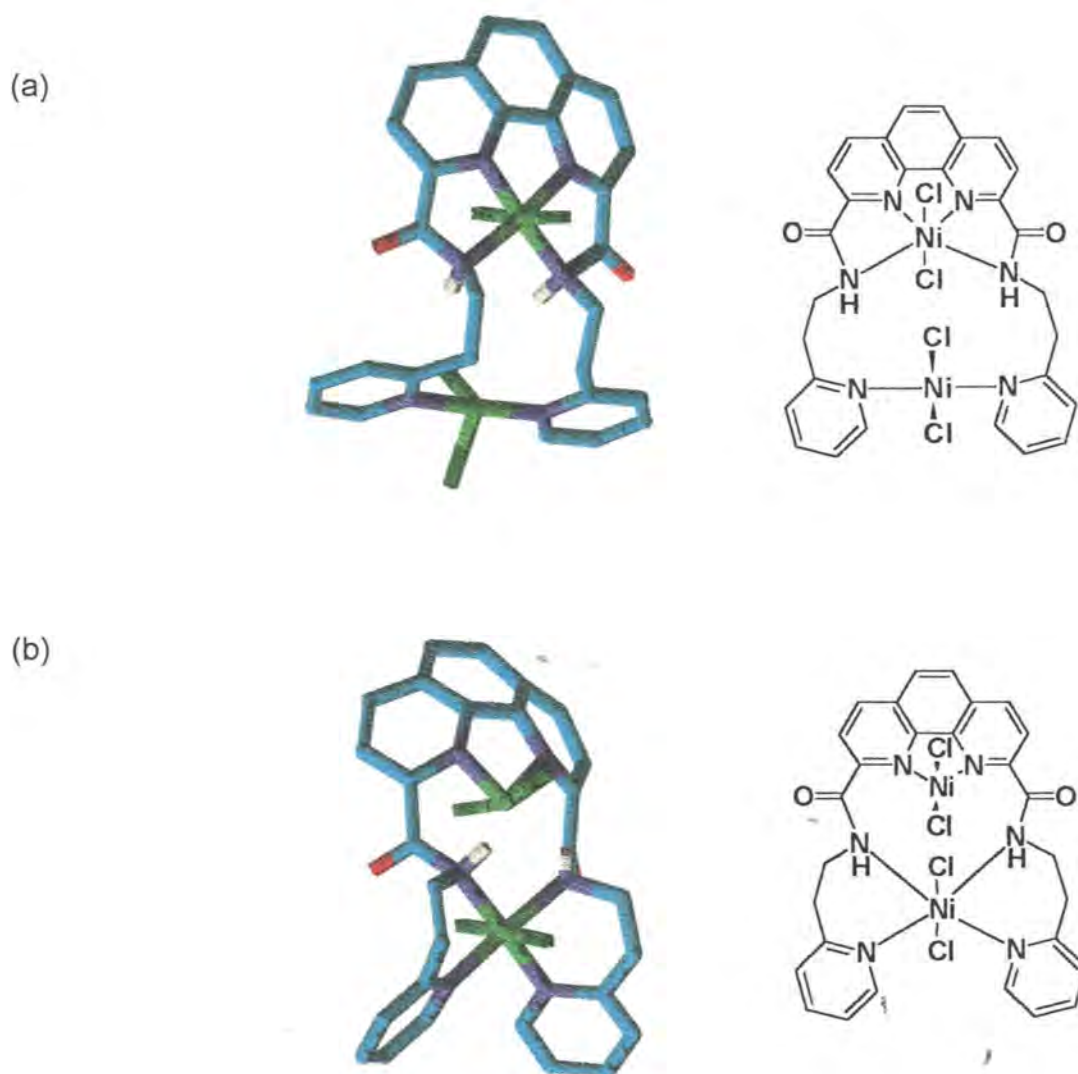


**Figure 49:** Computer-modelled structures of isomeric possibilities for the nickel(II) complex **144a**.

For the 1,10-phenanthroline complex **144a** two isomeric products are possible [(a) and (b); Figure 49]. These two complexes were modelled and the potential energy of each structure was calculated and found to be  $-89.6 \text{ kcalmol}^{-1}$  for isomer (a) and  $40.5 \text{ kcalmol}^{-1}$  for isomer (b), suggesting that isomer (a) is the favoured structure. In each case, one of the nickel(II) ions is octahedral, the other tetrahedral.

### 2.3.4.3 Platinum complexes

Platinum exhibits a very unusual pattern in transition metal chemistry. Although the other transition metals display a range of oxidation states, platinum is one of the few that display oxidation states differing by two electrons, viz., 0, II and IV.<sup>239</sup>

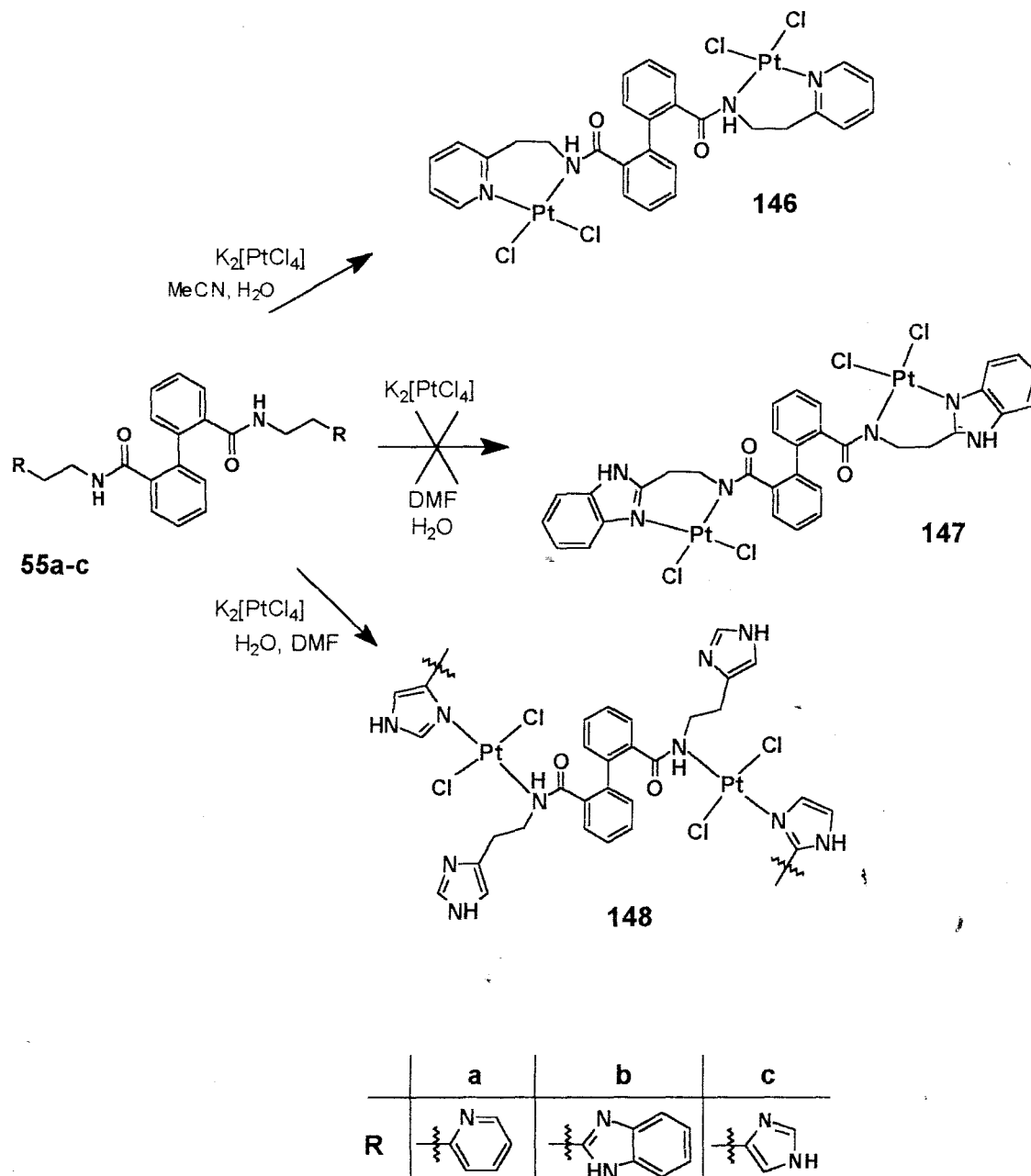
For Pt(IV), low-spin, kinetically inert  $d^6$  octahedral complexes are obtained,<sup>240</sup> while Pt(II) affords low-spin, kinetically inert  $d^8$  square planar, diamagnetic complexes.<sup>239</sup> Although very few complexes of Pt(0) are known, examples do exist in which platinum is two, three and four coordinate; in this oxidation state, the ground state can be considered to be  $d^{10}$  or  $d^9s^1$  and coordination with arsine, phosphine and isocyanide ligands has been reported.<sup>239</sup> The less common oxidation states (I) and (III) have assumed some importance due to their intermediacy in substitution reactions.<sup>239</sup>

In addition to its widespread use in catalysis, jewelry and electrical applications, platinum has assumed particular importance in the form of its complex, cisplatin, the *cis* isomer of  $[\text{Pt}(\text{NH}_3)_2(\text{Cl})_2]$ . Cisplatin is used as an anti-cancer drug for treating several kinds of malignant tumours.<sup>239</sup> It is highly biologically active, while the *trans* isomer is ineffective. The discovery of cisplatin as a chemotherapeutic agent has resulted in the rapid development of bio-platinum chemistry.<sup>241</sup>

#### 2.3.4.3.1 Synthesis of the Platinum Complexes

The platinum complexes of the biphenyl (Scheme 26) and 1,10-phenanthroline ligands (Scheme 27) were generally prepared by adding a solution of the ligand in DMF or MeCN, to a solution of  $\text{K}_2[\text{PtCl}_4]$  in water. The microanalysis results (Table 18) obtained for these platinum complexes show that they are dinuclear and that four chloride ions are present in all cases except complex **149** in which there are two, suggesting that the amide group is deprotonated in this complex. The expected benzimidazole complexes **147** and **150** did not appear to form, being

inconsistent with the structures depicted in Schemes 26 and 27.



**Scheme 26:** Complexation of the biphenyl ligands with platinum:



**Table 18:** Microanalytical data for the platinum complexes followed, in parentheses, by the calculated values.

Complex	Complex Stoichiometry	% Carbon	% Hydrogen	% Nitrogen
146	Pt <sub>2</sub> (55a)Cl <sub>4</sub> .3H <sub>2</sub> O	34.6 (34.4)	3.2 (3.4)	7.0 (7.5)
148	Pt <sub>2</sub> (55c)Cl <sub>4</sub> .2H <sub>2</sub> O	29.7 (28.9)	3.4 (2.8)	7.8 (8.4)
149	Pt <sub>2</sub> (69a)Cl <sub>2</sub> .3H <sub>2</sub> O	34.3 (34.6)	2.9 (2.8)	8.5 (8.7)
151	Pt <sub>2</sub> (69c)Cl <sub>4</sub>	25.0 (25.9)	2.4 (5.1)	9.8 (10.1)
152	Pt <sub>2</sub> (68a)Cl <sub>4</sub> .3H <sub>2</sub> O	31.8 (31.1)	2.8 (3.4)	7.3 (7.8)

### 2.3.4.3.2 NMR studies of the Platinum Complexes

For both the biphenyl and 1,10-phenanthroline series, more signals are observed than expected in both the <sup>1</sup>H and <sup>13</sup>C NMR spectra of the resulting Pt(II) complexes. It was initially thought that π-stacking<sup>242</sup> could be occurring in these complexes; consequently, <sup>1</sup>H NMR spectra of the complexes were recorded at 60°C, but no changes in the spectra were observed, suggesting the absence of π-stacking effects. The <sup>1</sup>H NMR spectrum of complex **149** (Figure 50) illustrates the multiplicity of signals seen in the spectra of the 1,10-phenanthroline platinum complexes - a feature which is particularly prominent in the aromatic region. The signal multiplicity may reflect either a certain asymmetry in the structures of the complexes or, possibly, the presence of isomeric systems in solution.

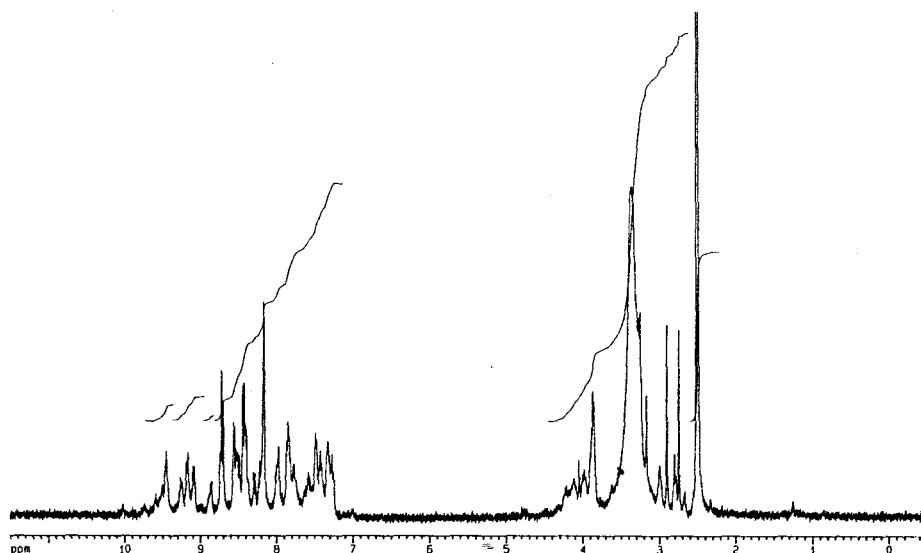


Figure 50: The 400 MHz <sup>1</sup>H NMR spectrum of complex 149 in DMSO-d<sub>6</sub>.

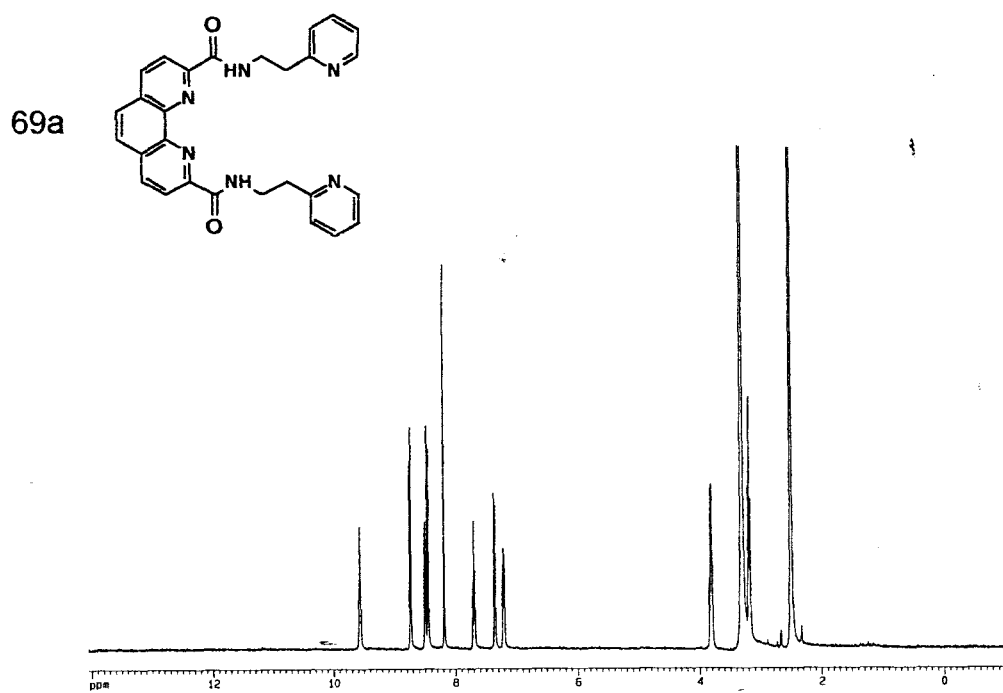


Figure 51: The 400 MHz <sup>1</sup>H NMR spectrum of ligand 69a in DMSO-d<sub>6</sub>.

### 2.3.4.3.3 IR studies of the platinum complexes

Platinum can coordinate to both nitrogen and oxygen and the IR studies were expected to reveal which donor atoms in the biphenyl and 1,10-phenanthroline amide complexes were involved in complexation. The IR data for relevant absorption bands are summarised in Table 19.

**Table 19:** Summary of the IR frequencies ( $\nu_{\text{M-Cl}}$ ) and the amide frequency shifts ( $\Delta\nu_{\text{NH}}$  and  $\Delta\nu_{\text{C=O}}$ )<sup>a</sup> for the biphenyl and 1,10-phenanthroline Pt(II) complexes.

Complex	$\Delta\nu_{\text{NH}}/\text{cm}^{-1}$	$\Delta\nu_{\text{C=O}}/\text{cm}^{-1}$	$\nu_{\text{M-Cl}}/\text{cm}^{-1}$
146	-69	4	315, 342 (cis)
148	31	4	335 (trans)
149	18	8	329 (trans)
151	-39	4	321 (trans)

<sup>a</sup> Frequency shift on complexation

From the data in Table 19 it appears that complexation does not involve deprotonation of the amide group since an amide NH band is observed in each case. It can also be seen that coordination through the amide nitrogen is preferred because positive shifts are observed for the amide carbonyl band in each case. These results also indicate, in most cases, that *trans* coordination of the chloride anion is favoured over *cis* coordination; in the case of complex **146**, however, the presence of weak Pt-Cl bands at 342 and 315  $\text{cm}^{-1}$  suggest a *cis*-geometry.<sup>243</sup>

The imidazole NH band is also present in the IR spectra of the biphenyl complex **148** (3120  $\text{cm}^{-1}$ ) and the 1,10-phenanthroline complex **151** (3135  $\text{cm}^{-1}$ ) - an observation in agreement with the microanalysis data which indicate four chloride anions in each complex. For the biphenyl complex **148** the polymeric structure in Scheme 26 has been tentatively suggested due to the *trans* coordination of the chloride anion in this complex.

The 1,10-phenanthroline complex **152** exhibits a strong NH band at  $3480\text{ cm}^{-1}$ , suggesting that the secondary amine is not deprotonated upon complexation - a conclusion which is consistent with the microanalysis data obtained for this complex.

The geometry of the platinum complexes could not be elucidated by UV-Vis spectroscopy due to masking of the absorption bands of interest by the solvent, DMF.

#### 2.3.4.3.4 Computer modelling of the platinum complexes

Since none of the dinuclear platinum complexes afforded crystals suitable for single crystal X-ray crystallography, computer modelling studies were undertaken to explore their possible 3-D arrangements. It was also hoped that the results of these modelling studies might explain the multiplicity of signals observed in the  $^1\text{H}$  and  $^{13}\text{C}$  NMR spectra of the 1,10-phenanthroline platinum complexes. The specimen complexes which were modelled are shown in Figure 52.

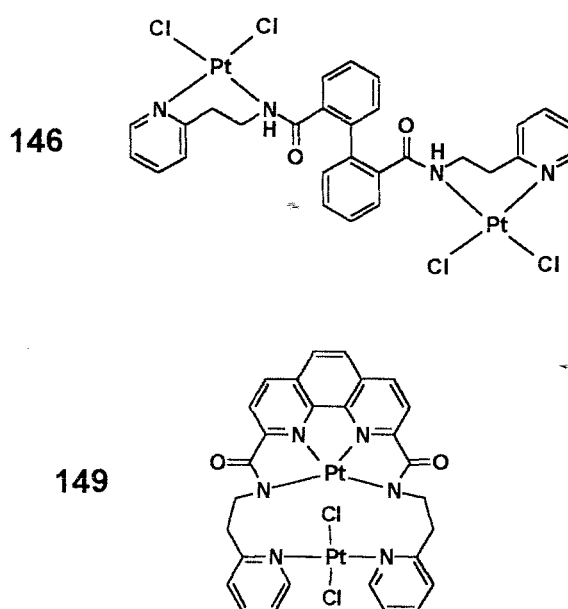


**Figure 52:** Proposed structures of the biphenyl and 1,10-phenanthroline platinum complexes investigated by computer modelling.

The energy-minimised structures for the two specimen systems are shown in Figure 53. The structure of complex **149** reveals a *trans* arrangement of the chlorine ligands in a square planar environment, while the biphenyl complex **146** exhibits a *cis*-arrangement of the chlorine ligands -- observations which are consistent with deductions based on the IR absorption data. The apparent symmetry in the model of the 1,10-phenanthroline complex **149**, however, is not consistent with the multiplicity of peaks observed in the aromatic region of the

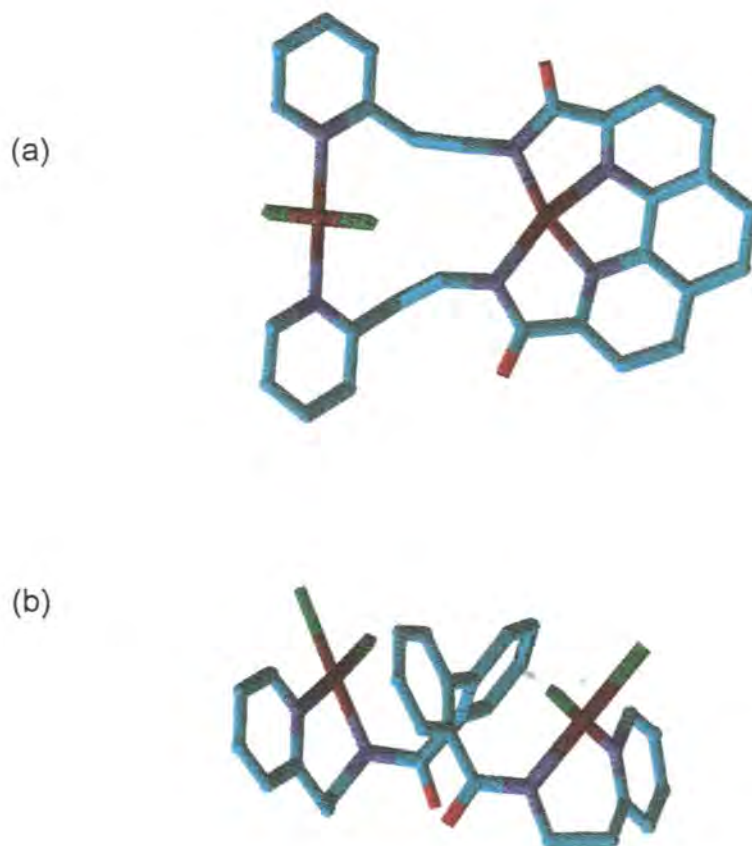


**Figure 53:** Computer modelled structures:- (a) complex **149**; (b) complex **146**.  
(Colours: Carbon: light-blue; nitrogen: dark-blue; oxygen: red;  
chlorine: green; platinum: lilac).

spectra of the 1,10-phenanthroline complexes. It is, of course, possible that the use of a universal force constant for platinum resulted in structures which reflect a degree of symmetry not present in the actual complexes.

## 2.4 ELECTROCHEMICAL STUDIES: CYCLIC VOLTAMMETRY

Electrochemical techniques can be used to study the redox properties of organometallic complexes. The synthetic dinuclear complexes were subjected to a particular electrochemical technique called cyclic voltammetry, to establish the oxidation state(s) and explore the electronic effects of the ligands. This technique also reveals the reversibility or irreversibility of a redox process when the redox potential of a redox couple is measured.

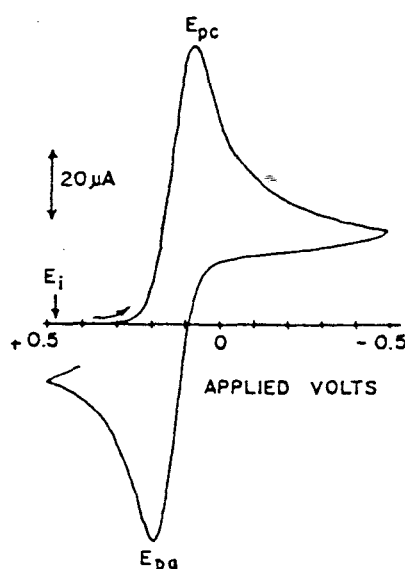


**Figure 54:** A cyclic voltammogram for a reversible redox process.

In cyclic voltammetry, the potential is scanned linearly from an initial value  $E_i$  to a second value  $E_j$  and then back to  $E_i$ , and the current monitored. The peaking in current occurs at the potential  $E_{pc}$  where the species of interest is reduced or oxidised. For reversible systems, the re-oxidation or re-reduction of the species in the vicinity of the electrode gives a current peak in the reverse scan, the potential corresponding to this peak is  $E_{pa}$  in Figure 54. For irreversible systems, no return peak is observed. The separation between the cathodic and anodic peak potentials,  $\Delta E$  ( $E_{pa} - E_{pc}$ ), is equal to  $59/n$ , where  $n$  is the number of electrons

required in the redox process for a reversible system. Disproportionation reactions cause irregularities in the shape of the curves in a cyclic voltammogram.<sup>244</sup> The redox potentials are, however, dependent upon various factors such as:

- solvent effects
- the electronic nature of the ligands and their substituents
- the steric demands of the ligand
- the flexibility of the ligand and the size of the chelate rings in the complex<sup>245</sup>

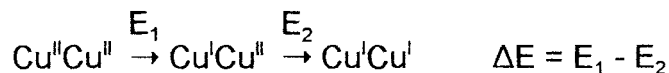
In the following discussion, an attempt has been made to explain the results of the cyclic voltammetric studies obtained for the copper, cobalt and nickel complexes of selected ligands.

#### 2.4.1 Copper Complexes

The analysis of the dinuclear copper complexes by cyclic voltammetry is important as the results may indicate the biomimetic potential of the synthetic models of the enzyme, tyrosinase. If reversibility is observed in the cyclic voltammogram of a synthetic model, then biomimetic activity may be expected; if no reversibility is observed, then the catalytic activity is likely to be poor or absent.

Since it is known that copper(I) is unstable and easily oxidised to copper(II) it is important to establish whether the synthetic models can maintain a copper(I) oxidation state and whether they permit the oxidation to copper(II). Dinuclear copper(II) complexes may be reduced in a single two-electron reduction, as observed for a triketonate complex,<sup>246</sup> or in a stepwise manner with a Cu(I)Cu(II) species being formed as an intermediate. Generally, it has been found that synthetic dinuclear copper complexes are reduced in a stepwise manner by two single-electron steps. "Type III" copper sites in proteins are, however, reduced in a single two-electron reduction at redox potentials that are higher than expected for their proposed coordination environment.<sup>246</sup> To quantify the redox processes,

the standard redox potentials are measured and the separation,  $\Delta E$ , between the consecutive reduction potentials, is determined, *i.e.*



where  $\Delta E$  is a measure of  $K_{\text{com}}$ , the comproportionation constant, which is the equilibrium constant for the reaction:



and  $K_{\text{com}}$  is related to  $\Delta E$  by the equation:<sup>247</sup>

$$\Delta E = E_1 - E_2 = 0.0591 \log K_{\text{com}}$$

For the dinuclear complexes examined here, the copper ions could, in principle, both be copper(I), both copper(II), or a combination of copper(I) and copper(II).

### ***The biphenyl and 1,10-phenanthroline complexes***

From the cyclic voltammograms, no reduction to  $\text{Cu}^0$  was evident during the analysis of the biphenyl and 1,10-phenanthroline copper complexes, except for complex **116**. Peaks that could not be assigned to either the ligand or the copper oxidation states, may be ascribed to ligand oxidation induced by the presence of copper. Such ligand oxidations have complicated the assignment of peaks in the cyclic voltammograms of the copper complexes and have also precluded the assignment of oxidation states for most of the copper complexes. Moreover, the polymeric nature of most of the copper complexes has resulted in complicated cyclic voltammograms. Nevertheless, an attempt has been made to assign some, but not all, of the peaks observed. The measured potentials of the copper complexes are summarised in Table 20.

**Table 20:** The measured potentials for the biphenyl and 1,10-phenanthroline copper complexes.

Complex	Potentials measured in cyclic voltammogram (V) vs Ag/AgCl
115	Oxidation side: 0.32 ( $E_a$ , $\text{Cu}^{2+}/\text{Cu}^{3+}$ ) Reduction side: -0.20 ( $E_a$ , ligand), -0.46 ( $E_a$ , $E_{1/2} = -0.51$ ) and -0.55 ( $E_c$ , $E_{1/2} = -0.51$ , $\text{Cu}^{\text{II}}\text{Cu}^{\text{II}} + 2e^- \rightarrow (\text{Cu}^{\text{I}}\text{Cu}^{\text{I}})$ ).
116	Reduction side: -0.29 ( $E_a$ ), -0.55 ( $E_c$ ) and -0.80 ( $E_c$ ).
118a	Oxidation side: 0.25 ( $E_a$ ). Reduction side: -0.46, -0.52 ( $E_c$ , ligand), -0.65 ( $E_c$ , ligand), -0.97 ( $E_a$ , $E_{1/2} = 1.1$ ), -1.13 ( $E_c$ , $E_{1/2} = 1.1$ , $\text{Cu}^{\text{II}}\text{Cu}^{\text{II}} + 2e^- \rightarrow (\text{Cu}^{\text{I}}\text{Cu}^{\text{I}})$ ).
118b	Oxidation side: 0.85 ( $E_a$ ), 0.48 ( $E_a$ ). Reduction side: -0.41 ( $E_c$ , ligand), -0.61 ( $E_c$ ), -1.17 ( $E_c$ ), -1.67 ( $E_c$ , ligand).
118c	Oxidation side: 0.86 ( $E_a$ ) Reduction side: -0.50 ( $E_c$ , $\text{Cu}^{\text{II}}\text{Cu}^{\text{II}} + 2e^- \rightarrow \text{Cu}^{\text{I}}\text{Cu}^{\text{I}}$ ), -1.57 ( $E_c$ , ligand).
119	Oxidation side: 0.75 ( $E_a$ , ligand), 0.34 ( $E_c$ , $\text{Cu}^{\text{II}}\text{Cu}^{\text{II}} \rightarrow \text{Cu}^{\text{III}}\text{Cu}^{\text{III}}$ ), 0.14 ( $E_c$ , ligand). Reduction side: -0.71 ( $E_a$ , $E_{1/2} = -0.77$ ) and -0.82 ( $E_c$ , $E_{1/2} = -0.77$ , $\text{Cu}^{\text{II}}\text{Cu}^{\text{II}} + 2e^- \rightarrow \text{Cu}^{\text{I}}\text{Cu}^{\text{I}}$ ).

For complex **115**, the reduction  $\text{Cu}^{\text{II}}\text{Cu}^{\text{II}} \rightarrow \text{Cu}^{\text{I}}\text{Cu}^{\text{I}}$  was assigned to the slightly reversible couple at -0.46 and -0.55 V, and the oxidation peak at 0.32 V to a  $\text{Cu}^{2+}/\text{Cu}^{3+}$  oxidation. For complex **116**, the sharp peak at -0.29 V has been assigned to copper deposition at the electrode [*i.e.* the formation<sup>245,248</sup> of copper(0)]; the sharp peak is typical for absorbed species. The peak observed at -0.80 V was assigned to a  $\text{Cu}^{\text{II}}\text{Cu}^{\text{II}} \rightarrow \text{Cu}^{\text{I}}\text{Cu}^{\text{I}}$  reduction and the one at -0.55 V to a  $\text{Cu}^{\text{I}}\text{Cu}^{\text{I}} \rightarrow \text{Cu}^0\text{Cu}^0$  reduction, which corresponds to a two-step, two-electron reduction process.

For complex **118a**, the peaks at -0.52 and -0.65 V have been ascribed to the ligand, while the couple at -0.97 and -1.13 V ( $E_{1/2} = -1.1$  V) has been assigned to a  $\text{Cu}^{\text{II}}\text{Cu}^{\text{II}} \rightarrow \text{Cu}^{\text{I}}\text{Cu}^{\text{I}}$  reduction.<sup>138</sup> For complex **118b**, it is not certain whether the peak at -1.67 V is due to  $\text{Cu}^{\text{II}} \rightarrow \text{Cu}^{\text{I}}$  reduction or whether it is due to ligand reduction. It is also not possible to tell whether the peaks at -0.61 V and -1.17 V are due to  $\text{Cu}^{\text{II}} \rightarrow \text{Cu}^{\text{I}}$  reduction, but they were not observed for the ligand. The peaks at 0.85 and 0.48 V are, however, attributed to ligand oxidation. For complex

**118c**, the peak at -0.50 V has been tentatively assigned to a  $\text{Cu}^{\text{II}} \rightarrow \text{Cu}^{\text{I}}$  reduction. The peak at -1.57 V cannot be assigned with certainty as a copper peak, and it may well be due to ligand reduction. For this complex, only one Cu(II) oxidation peak (0.86 V) is observed, which suggests that both copper atoms are in an irreversible Cu(II) oxidation state.

A peak at 0.34 V in the cyclic voltammogram of complex **119** may be due to a  $\text{Cu}^{\text{II}}\text{Cu}^{\text{II}} \rightarrow \text{Cu}^{\text{III}}\text{Cu}^{\text{III}}$  oxidation, and the couple at -0.71 and -0.82 V to a single two-electron  $\text{Cu}^{\text{II}}\text{Cu}^{\text{II}} \rightarrow \text{Cu}^{\text{I}}\text{Cu}^{\text{I}}$  reduction; the  $\Delta E$  of -0.11 V suggests a quasi-reversible one-electron system. The peaks observed at 0.75 and 0.14 V may be attributed to ligand oxidation, by comparison with the ligand cyclic voltammogram.

#### ***The Schiff base complexes and the macrocyclic complex***

The formation of copper(0) and its adsorption on the electrode is characterised by a sharp peak in the cyclic voltammogram.<sup>248</sup> The cyclic voltammogram of each of these copper complexes, but not their respective ligands, displayed this characteristically sharp peak. The measured potentials for these copper complexes are shown in Table 21.

**Table 21:** The measured potentials of the Schiff base and the macrocyclic copper complexes.

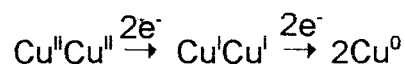
Complex	Potentials measured in cyclic voltammogram (V) vs Ag/AgCl
120	Reduction side: -0.26 ( $E_a$ ), -0.98 ( $E_c$ ) and -1.40 ( $E_c$ ), -1.75 ( $E_c$ ).
121	Oxidation side: 0.76 ( $E_a$ ). Reduction side: -0.22 ( $E_a$ ), -0.59, -0.75 ( $E_c$ ).
123	Oxidation side: 0.75 ( $E_a$ ). Reduction side: -0.13 ( $E_a$ ), -1.00 ( $E_c$ ), -1.75 ( $E_c$ ).
124	Reduction side: -0.28 ( $E_c$ ), -0.61 ( $E_c$ ).

\*Peaks assigned to  $\text{Cu}^{\text{I}}\text{Cu}^{\text{I}} \rightarrow \text{Cu}^0$  and copper deposition

Several peaks were observed for complex **120**. The strong, sharp peak at -0.26 V has been assigned to copper deposition at the electrode. The peak at -0.98 V is

attributed to a  $\text{Cu}^{\text{II}}\text{Cu}^{\text{II}} \rightarrow \text{Cu}^{\text{I}}\text{Cu}^{\text{I}}$  reduction and the peak at  $-1.40$  V to a  $\text{Cu}^{\text{I}}\text{Cu}^{\text{I}} \rightarrow \text{Cu}^0\text{Cu}^0$  reduction, thus representing a two-step, two-electron reduction process<sup>138</sup> to  $\text{Cu}^0$ . The peak at  $-1.75$  V is assigned to ligand reduction by comparison with the ligand cyclic voltammogram. For complex **121**, the cyclic voltammogram also exhibits a strong, sharp peak at  $-0.22$  V, and this is attributed to copper deposition. The peaks at  $-0.59$  and  $-0.75$  V have been assigned to a two-step, single-electron reduction process and the peak at  $0.76$  V to ligand oxidation. Complex **123** also exhibits similar peaks to those of complexes **120** and **121**. The strong, sharp peak at  $-0.13$  V has been assigned to copper deposition, and the peak at  $-1.75$  V to ligand reduction. Here, however, the two-step, single-electron reduction process was absent since only one peak was observed at  $-1.00$  V, and it is suggested that this peak may be due to a single, two-electron reduction process. The peak at  $0.75$  V has been ascribed to ligand oxidation. The macrocyclic complex **124** exhibits a strong peak at  $-0.28$  V, which is attributed to copper deposition, but the peak at  $-0.61$  V could not be assigned with certainty and it seems from a comparison with the ligand cyclic voltammogram, that this latter peak is due to ligand reduction.

A general mechanism reported in the literature for the reduction of copper(II) to copper(0) has been proposed<sup>138</sup> to follow the sequence:-



In this sequence, the two copper(II) ions are reduced to copper(I) by a potential of  $-0.98$  V, followed by a subsequent reduction to copper(0) by a potential of  $-1.40$  V. In turn, a potential of  $-0.26$  V results in the re-oxidation of copper(0).

### 2.4.2 Cobalt Complexes

In the case of the dinuclear cobalt complexes, cyclic voltammetry was used to establish whether the metal ions were cobalt(II) or (III) or a mixture of both. The measured potentials for the cobalt complexes are shown in Table 22. From the results it is apparent that cobalt(II) is oxidised to cobalt(III) on the cyclic voltammetric time scale. The observation of a strong peak at ca. 1 V, which was not observed for the ligand alone, indicates that the oxidation involves the cobalt ion. Since Co(III) cannot be oxidised any further, the results suggest that Co(II) is present and is oxidised to Co(III).

When comparing the oxidation potentials of the biphenyl diamide complexes (**133** and **134**) with those of the 1,10-phenanthroline diamide complexes (**137a**, **137b** and **137c**), it is apparent that the latter complexes have higher oxidation potentials. It was also observed that the 1,10-phenanthroline diamine complex **138** has a lower oxidation potential than the diamide complexes, and it is presumed that this is due to electron-withdrawal by the carbonyl oxygen of the amide group. Thus, complex **138** is more easily oxidised than the diamide complexes, complex **137a** proving to be the most difficult.

The higher oxidation potentials of the 1,10-phenanthroline-based complexes (compared to the biphenyl analogues) may be attributed to the presence of the additional, electronegative nitrogen atoms of the 1,10-phenanthroline nucleus, which increase the electron-withdrawing capacity of the ligands, thus increasing the oxidation potential of the resulting complexes. The rigidity of the 1,10-phenanthroline system and the smaller, less flexible 5-membered chelate rings which are formed upon complexation (in contrast to the flexibility of the biphenyl system and its formation of larger, more flexible 6-membered chelate rings) may also contribute to the higher oxidation potentials observed for the 1,10-phenanthroline complexes. Representative examples of the cyclic voltammograms obtained for the biphenyl and 1,10-phenanthroline cobalt complexes are illustrated

in Figures 55 and 56.

**Table 22:** Measured potentials for the biphenyl and 1,10-phenanthroline cobalt complexes.

Complex	Potentials measured in cyclic voltammogram (V) vs Ag <sup>+</sup> /AgCl
133	Oxidation side: 0.97 ( Co <sup>II</sup> Co <sup>II</sup> → Co <sup>III</sup> Co <sup>III</sup> )
134	Oxidation side: 0.99 ( Co <sup>II</sup> Co <sup>II</sup> → Co <sup>III</sup> Co <sup>III</sup> ).
137a	Oxidation side: 1.08 ( Co <sup>II</sup> Co <sup>II</sup> → Co <sup>III</sup> Co <sup>III</sup> ).
137b	Oxidation side: 1.06 ( Co <sup>II</sup> Co <sup>II</sup> → Co <sup>III</sup> Co <sup>III</sup> ).
137c	Oxidation side: 1.02 ( Co <sup>II</sup> Co <sup>II</sup> → Co <sup>III</sup> Co <sup>III</sup> ).
138	Oxidation side: 0.86 ( Co <sup>II</sup> Co <sup>II</sup> → Co <sup>III</sup> Co <sup>III</sup> ).

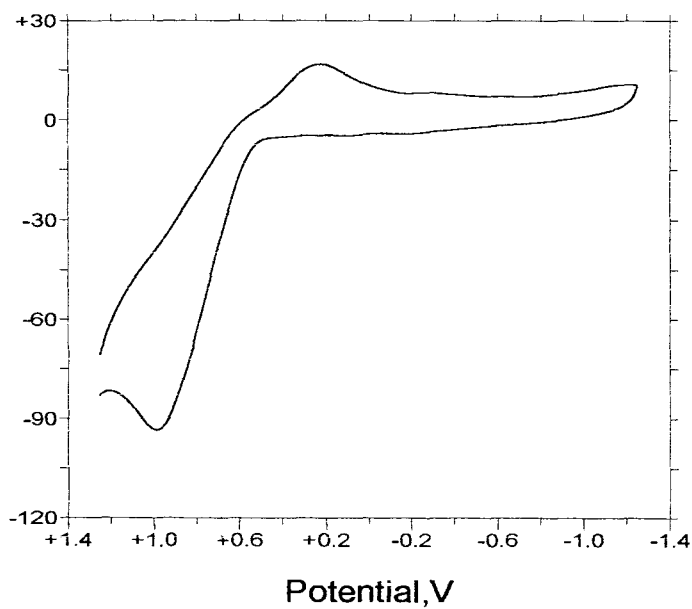


Figure 55: Cyclic voltammogram of biphenyl cobalt complex **134**.

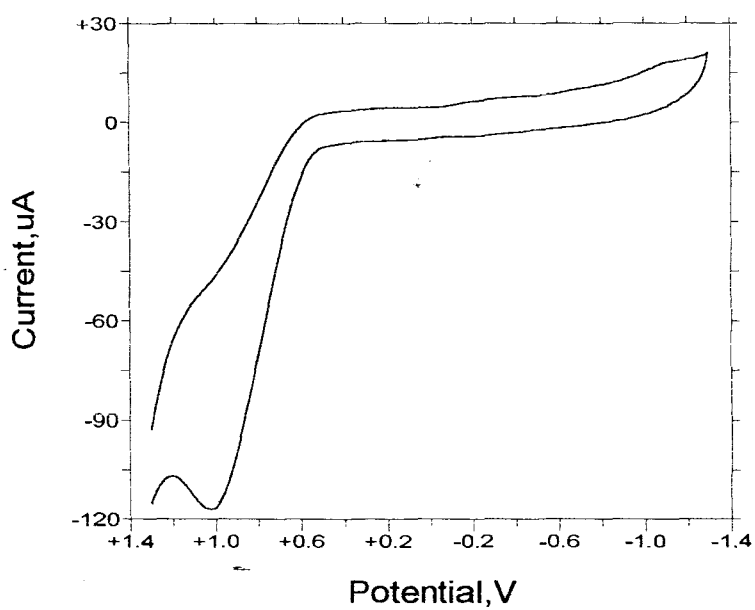


Figure 56: Cyclic voltammogram of 1,10-phenanthroline cobalt complex **137c**.

### 2.4.3 Nickel complexes

Cyclic voltammetry was also used to establish the oxidation state(s) of the metal ions in the dinuclear nickel complexes. Although the nickel(II) oxidation state is the most stable and most prevalent, the possibility of the Ni(III) and Ni(IV) oxidation states occurring within these complexes had to be considered. The cyclic voltammetry data for the complexes is summarised in Table 23.

From these results it can be seen that nickel(II) was oxidised to nickel(III) on the cyclic voltammetric time scale, since only one oxidation peak was observed in each case.<sup>249</sup> In certain complexes (**141**, **144a**, **144b** and **145**), ligand reduction is evidenced by the peaks between -1.13 and -1.25 V, the oxidation peak being clearly visible in the cyclic voltammogram of complex **142** (Figure 57); the cyclic voltammogram for the ligand **55c** is illustrated in Figure 58.

The 1,10-phenanthroline-cobalt complexes exhibit higher oxidation potentials than their biphenyl counterparts, this trend was not observed for the corresponding nickel complexes. It is also apparent that, of the biphenyl systems, complex **142** (Figure 57) has the highest oxidation potential and **141** the lowest.

Of the 1,10-phenanthroline nickel systems, complex **144b** has the highest oxidation potential and **144a** the lowest. Although the ligand **68a** has an oxidation potential at 0.86 V (see Figure 60) it was expected that the complex **145** would have a lower oxidation potential and, consequently, the peak at 0.85 V (Figure 59) has been tentatively assigned to the oxidation of Ni<sup>2+</sup>.

**Table 23:** Cyclic voltammetric data for the nickel complexes.

Complex	Potentials measured in cyclic voltammogram (V) vs Ag <sup>+</sup> /AgCl
140	oxidation side: 0.83 (Ni <sup>2+</sup> )
141	oxidation side: 0.80 (Ni <sup>2+</sup> /Ni <sup>3+</sup> ) reduction side: -1.25 (ligand reduction)
142	oxidation side: 0.84 (Ni <sup>2+</sup> /Ni <sup>3+</sup> )
144a	oxidation side: 0.79 (Ni <sup>2+</sup> /Ni <sup>3+</sup> ) reduction side: -1.13 (ligand reduction)
144b	oxidation side: 0.95 (Ni <sup>2+</sup> /Ni <sup>3+</sup> ) reduction side: -1.17 (ligand reduction)
144c	oxidation side: 0.82 (Ni <sup>2+</sup> )
145	oxidation side: 0.85 (Ni <sup>2+</sup> /Ni <sup>3+</sup> ) reduction side: -1.13 (ligand reduction)

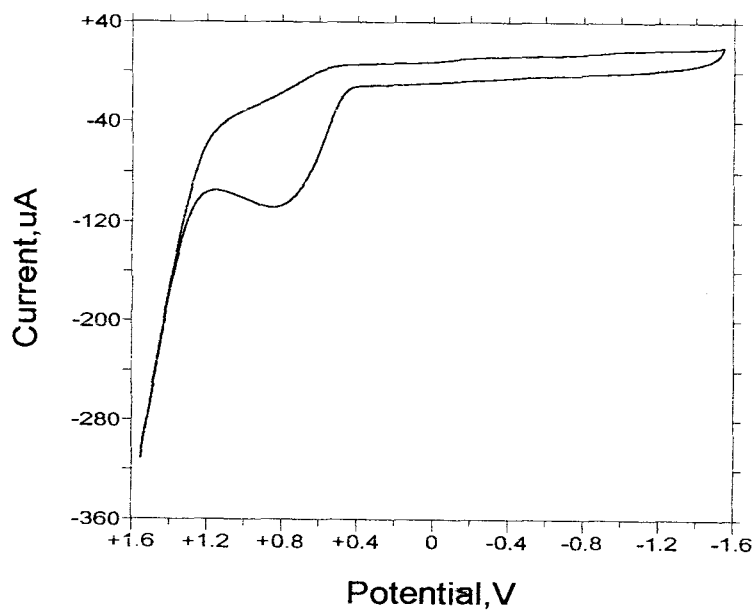


Figure 57: A cyclic voltammogram of biphenyl nickel complex **142**.

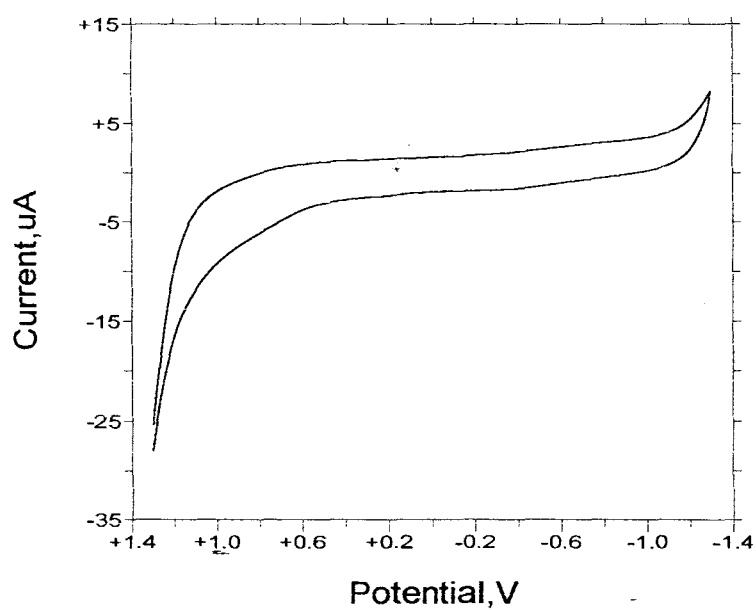


Figure 58: A cyclic voltammogram of ligand **55c**.

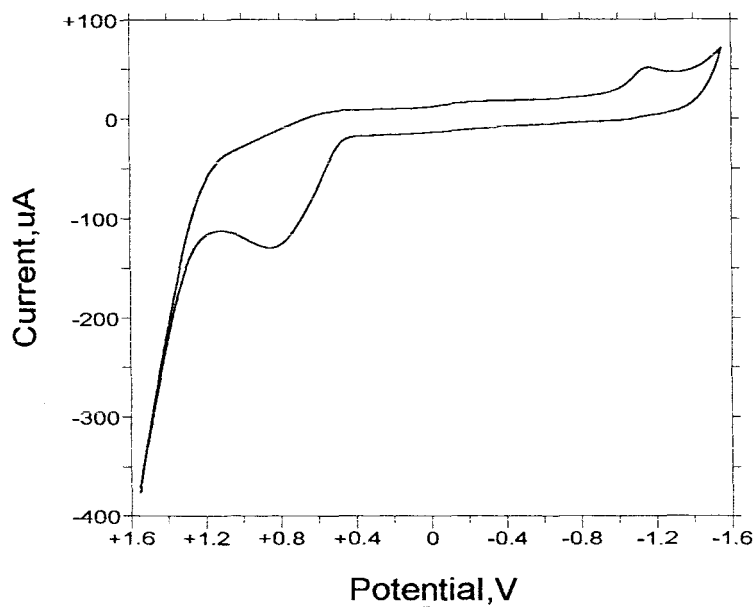


Figure 59: A cyclic voltammogram of the 1,10-phenanthroline nickel complex **145**.

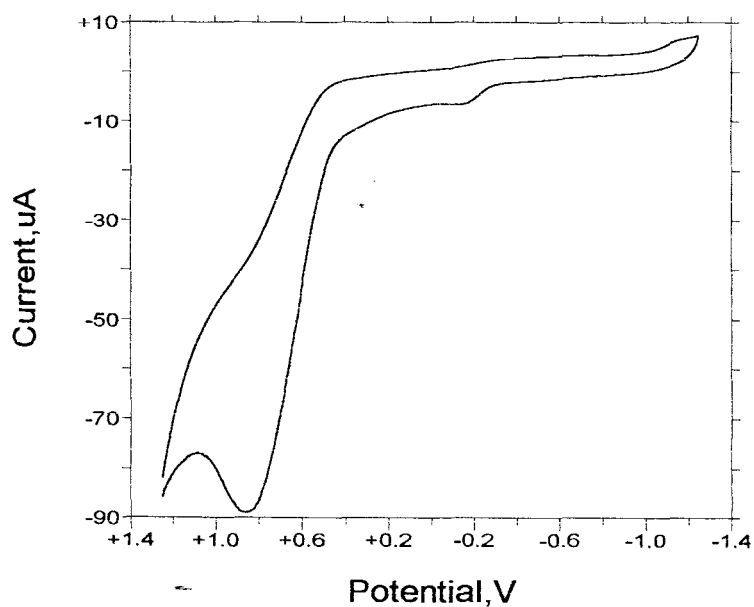


Figure 60: A cyclic voltammogram of the 1,10-phenanthroline ligand **68a** that has an oxidation potential at 0.86 V.

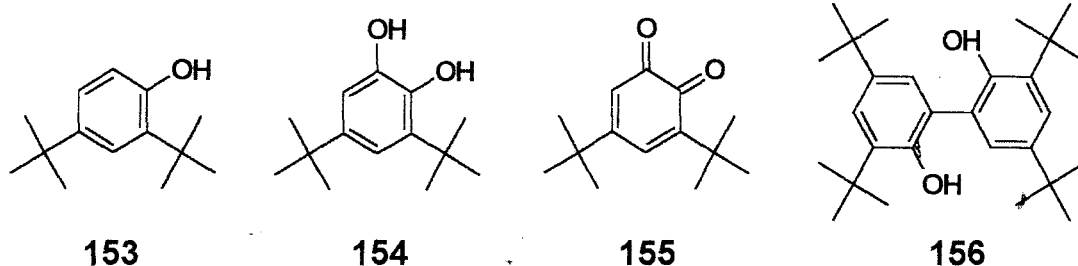
## Conclusion

The cyclic voltammetry studies of the copper complexes reveal that the 1,10-phenanthroline ligands are unstable once they are coordinated to copper, ligand oxidation being apparent in the cyclic voltammograms of the complexes. In the case of the biphenyl analogues, complex **115** exhibits a Cu(II) oxidation state, while in complex **116** the metal is reduced to Cu(0), resulting in copper deposition at one of the electrodes. In the Schiff base and macrocyclic complexes the copper is also reduced to Cu(0) with concomitant electrodeposition of Cu(0). As a result of the complexity of the cyclic voltammograms and the electrodeposition, it has been difficult to assess either the redox reversibility or the potential of the copper complexes as biomimetic catalysts.

In the cobalt complexes Co(II) is oxidised to Co(III) on the cyclic voltammetric time scale, indicating that cobalt is in the Co(II) oxidation state in the biphenyl- and 1,10-phenanthroline-based cobalt complexes. Similarly, the nickel complexes exhibit predominant oxidation of the metal to Ni(III) confirming the oxidation state of nickel in the biphenyl- and 1,10-phenanthroline-based complexes as Ni(II).

## 2.5 EVALUATION OF THE CATALYTIC ACTIVITY OF THE BIOMIMETIC COPPER COMPLEXES

In order to determine whether the copper complexes were suitable models of tyrosinase, their ability to oxidise a phenol and/or catechol was examined. For a model to be successful it should display either phenolase or catecholase activity using molecular oxygen. For this study, the substrate di-*t*-butylphenol (DTBP) **153** was used to evaluate the phenolase activity, and di-*t*-butylcatechol (DTBC) **154** the catecholase activity of these complexes.<sup>15,250</sup> These substrates were used because they are activated for electron-donation by their alkyl substituents,<sup>208</sup> and their oxidation products are somewhat resistant to polymerisation. DTBP is oxidised to DTBC which, in turn, is oxidised to 3,5-di-*t*-butyl-*o*-quinone (DTBQ) **155**. The *o*-quinone has a characteristic absorption band at 400 nm in the UV-visible spectrum and can therefore be detected spectroscopically ( $\epsilon = 1830 \text{ M}^{-1}\text{cm}^{-1}$ ). DTBP can also be oxidised to the coupled product **156**.



The reactions for evaluating biomimetic activity were conducted in DMF or in  $\text{CH}_2\text{Cl}_2$ . DMF was chosen because it is a highly polar solvent and was expected to dissolve, at least, some of the complex. Reactions were also attempted in  $\text{CH}_2\text{Cl}_2$  because of its capacity to dissolve dioxygen, which must be present in non-rate limiting concentrations. Tyrosinase can catalyse the oxidation of a variety of substrates in an aqueous medium, but the range of substrates is decreased when an organic medium is used.<sup>251</sup> In this study,  $^1\text{H}$  NMR spectroscopy was used to detect the product(s) of oxidation reactions catalysed by selected biphenyl and 1,10-phenanthroline copper complexes.

The  $^1\text{H}$  NMR data for the expected oxidation products DTBC **154** and DTBQ **155** and the coupled product **156** are detailed in Table 24, while the results of the biomimetic evaluation of the copper complexes are summarised in Table 25. At the conclusion of each reaction period, the reaction mixture was concentrated to dryness *in vacuo* and the residue analysed by  $^1\text{H}$  NMR spectroscopy to establish the substrate:product ratios.

**Table 24:**  $^1\text{H}$  NMR data for DTBC **154**, DTBQ **155** and the coupled product **156**.

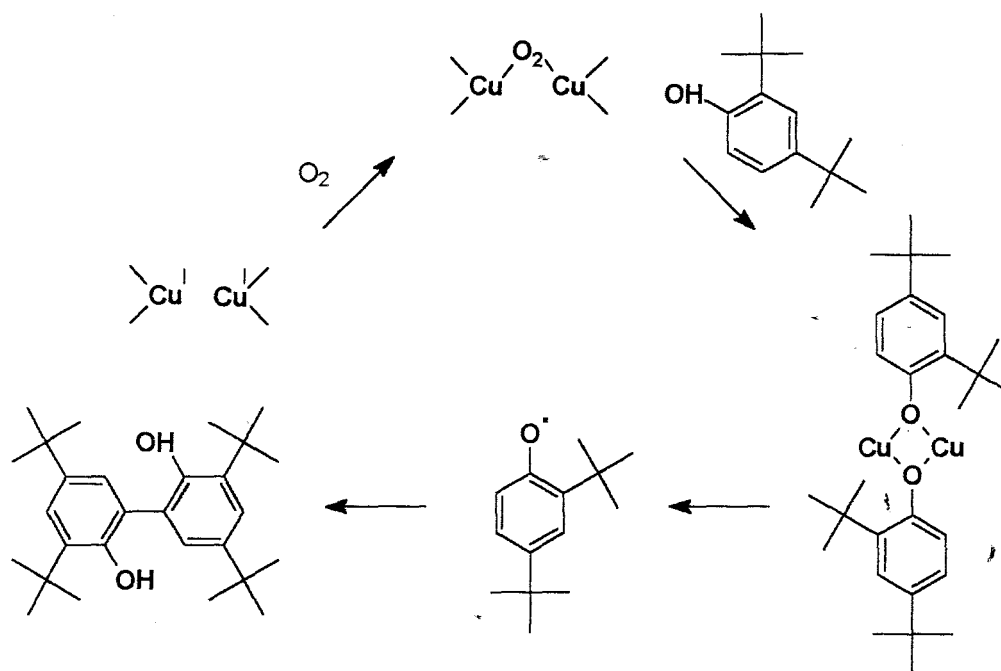
Compound	$\delta_{\text{H}}$ /ppm
DTBC <b>154</b>	1.27, s, 9H, Bu <sup>t</sup> 1.41, s, 9H, Bu <sup>t</sup> 6.76, d, 1H, H-4 6.89, d, 1H, H-6
DTBQ <b>155</b>	1.22, s, 9H, Bu <sup>t</sup> 1.26, s, 9H, Bu <sup>t</sup> 6.21, d, 1H, H-4 6.90, d, 1H, H-6
Coupled product <b>156</b>	1.31, s, 18H, Bu <sup>t</sup> 1.41, s, 18H, Bu <sup>t</sup> 7.10, d, 2H, H-4 and H-4' 7.38, d, 2H, H-6 and H-6'

**Table 25:** Results of the biomimetic evaluation of the copper complexes in DMF.

Entry	Complex	Solvent	Reaction time/h	Phenolase activity product	% Conversion	Catecholase activity product	% Conversion
1	115*	DMF	24 h	none	none	o-quinone	6.3
2	116	DMF	120 h	coupled product	8.8	o-quinone	13.3
3	118a*	DMF	24 h	coupled product	14.3	o-quinone	7.3
4	118b	DMF	120 h	coupled product	13.0	o-quinone	38.0
5	118c	DMF	120 h	none	none	o-quinone	54.3
6	119	DMF	120 h	none	none	none	none

\* Stirred for 24 h without Et<sub>3</sub>N

The catalytic oxidation reactions were first attempted in  $\text{CH}_2\text{Cl}_2$ , in the absence of  $\text{Et}_3\text{N}$ , but these were unsuccessful. The reactions were then repeated in DMF, but catalytic activity was only observed for certain complexes. The complexes which still failed to display any catalytic activity were then reacted, in DMF, in the presence of  $\text{Et}_3\text{N}$ .<sup>138</sup> Under these conditions, three more complexes exhibited biomimetic activity (Entries 2, 4 and 5; Table 25). From the tabulated results, it can be seen that some complexes displayed both phenolase and catecholase activity (Entries 2, 3 and 4), while all the complexes, with the exception of complex **119**, exhibited catecholase activity.



**Scheme 28** : Mechanism for the oxidative phenolic coupling proposed by Kitajima.<sup>20</sup>

Signals for the coupled product **156**, indicating phenolase activity, were thus observed in reactions with complexes **116**, **118a** and **118b**. The formation of the coupled product **156** has been observed by Reglier<sup>138</sup> and Karlin,<sup>253</sup> and other coupled biphenyl products from reactions of phenols and biomimetic-copper complexes have also been widely reported.<sup>254-257</sup> Kitajima has proposed a mechanism for the phenolic coupling, involving catalytic oxidation (Scheme 28).<sup>20</sup>

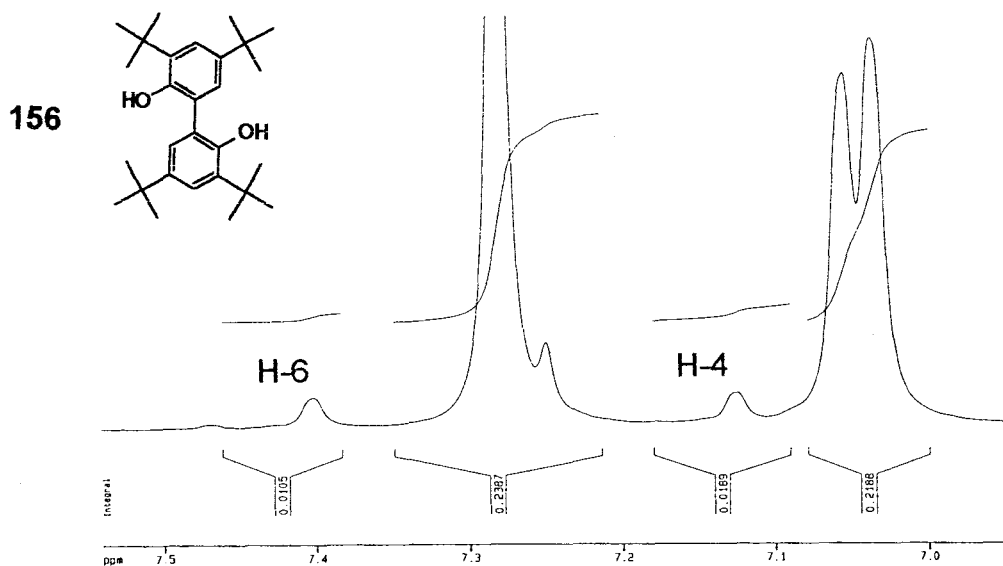


**Figure 61:** Partial  $^1\text{H}$  NMR spectrum, in  $\text{CDCl}_3$ , of the residue following reaction of complex **118a** and DTBP in DMF in the absence of  $\text{Et}_3\text{N}$ , showing the formation of the coupled product **156**, i.e. phenolase activity.

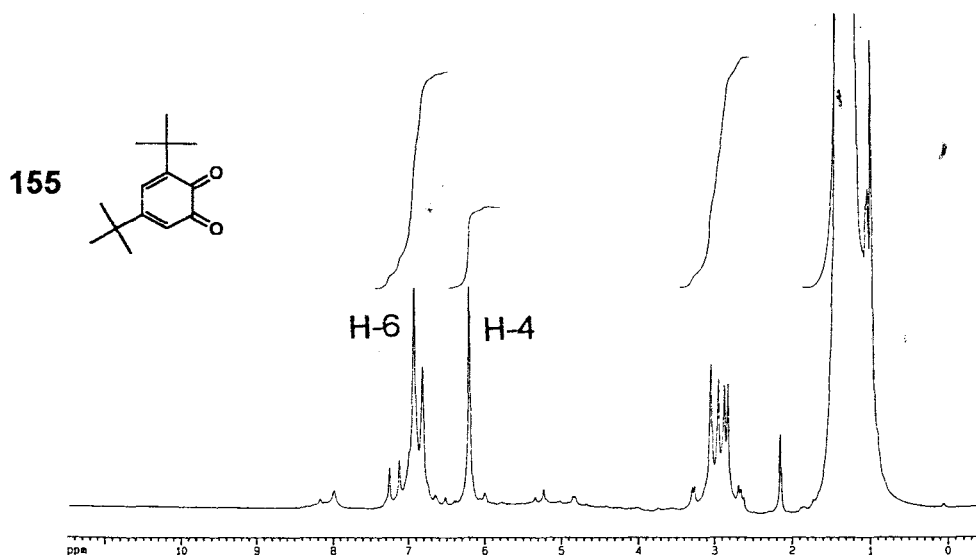


**Figure 62:** The 400 MHz  $^1\text{H}$  NMR spectrum, in  $\text{CDCl}_3$ , of the residue following reaction of complex **118c** and DTBC in DMF in the presence of  $\text{Et}_3\text{N}$ , showing formation of the *ortho*-quinone **155**, i.e. catecholase activity.

Catecholase activity was confirmed by the  $^1\text{H}$  NMR signals for the *o*-quinone at ca.  $\delta$ 6.2 and  $\delta$ 6.9 ppm observed in the spectra of residues from the reactions with complexes **115**, **116**, **118a**, **118b** and **118c** .

It is possible that the lack of phenolase activity exhibited by some of the complexes may be due to either the polymeric copper complexes being too flexible to bind DTBP **153**, or to coordination being limited to only one copper atom, thus making *o*-hydroxylation unlikely. The fact that both phenolase and catecholase activity is exhibited by some of the complexes suggests that, in these cases at least, the copper ions are sufficiently close (after binding dioxygen) to allow for the binding and bridging of DTBP **153** and DTBC **154**. While the copper complexes appear to be polymeric (see Section 2.3.1.1.), the formation of polymer-monomer equilibria in solution would afford some monomer molecules capable of acting as biomimetic catalysts. On the other hand, the macromolecular characteristics of tyrosinase may also have been simulated, to some extent, by the polymeric structure of the biomimetic complexes.

## 2.6 CONCLUSIONS

During the course of this research, several sets of ligands, designed to mimic the active site in tyrosinase, have been successfully prepared. The diimine ligands containing the biphenyl spacer have been shown to undergo intramolecular cyclisation during reduction with sodium borohydride, affording azepine derivatives; X-ray crystallographic analysis of cobalt and nickel complexes facilitated identification of the azepine systems, and a mechanism has been proposed to account for the observed cyclisation. In contrast, neither the 1,10-phenanthroline nor the Schiff base analogues undergo intramolecular cyclisation. However, Schiff base ligands, in which the imine functionalities are separated by one carbon atom, undergo significant tautomerism, forming six-membered H-bonded chelates.

Complexation of the biphenyl- and 1,10-phenanthroline-based amide ligands with copper appears to afford polymeric copper complexes, analysis of which reveals coordination through both the amide nitrogen and oxygen donor atoms, as well as through the tertiary and secondary nitrogen donors of the imidazole and benzimidazole moieties. In the case of the Schiff base copper complexes, unidentate and bidentate coordination of the nitrate anion has complicated elucidation of the structures.

Tetrahedral geometry appears to be dominant in the dinuclear cobalt complexes of the biphenyl- and 1,10-phenanthroline-based amide ligands. Coordination with nickel, results in the formation of complexes in which the metal exhibits tetrahedral, octahedral or square planar geometries, while the biphenyl and 1,10-phenanthroline platinum(II) complexes appear to favour a *trans* arrangement of the chlorine ligands in a square planar environment.

Unlike the polymeric copper complexes, the cobalt and nickel complexes afforded uncomplicated cyclic voltammograms, confirming the formation of cobalt(II) and

nickel(II) complexes with the biphenyl- and 1,10-phenanthroline-based ligands.

Despite the polymeric nature of the copper complexes, biomimetic activity for both biphenyl- and 1,10-phenanthroline-based polymeric complexes was observed. The presence of triethylamine appears to enhance the biomimetic activity, and it seems that the copper atoms in the complexes are close enough for dioxygen bridging to occur and that substrate binding is possible. Such evidence suggests the existence of polymer-monomer equilibria in solution, with the monomeric dicopper complexes capable of acting as biomimetic catalysts.

Future research in this area is expected to involve:-

- i) complexation of the biphenyl- and 1,10-phenanthroline-based amide ligands with copper in the presence of base;
- ii) complexation of the Schiff base and macrocyclic ligands with copper(I) to explore the potential of the resulting complexes as biomimetic catalysts;
- iii) an investigation of the potential of the biphenyl- and 1,10-phenanthroline-based cobalt(II) complexes to bind oxygen and thus catalyse the oxidation of 3,5-di-*t*-butylphenol and 3,5-di-*t*-butylcatechol; and
- iv) exploration of the potential of the nickel(II) complexes as catalysts for the hydrolysis of urea.

## 3 EXPERIMENTAL

### 3.1 GENERAL

Infrared spectra were recorded on Perkin Elmer 2000 and Perkin Elmer 180 spectrophotometers; the mid-infrared spectra ( $4000\text{--}300\text{ cm}^{-1}$ ) were recorded using potassium bromide discs and, nujol mulls and hexachlorobutadiene (HCBT). The far-infrared ( $500\text{--}50\text{ cm}^{-1}$ ) spectra were obtained using nujol mulls. NMR spectra were recorded on a Bruker AMX 400 spectrometer, and chemical shifts are reported relative to the solvent peaks. Low resolution mass spectra were obtained on a Hewlett-Packard 5988A mass spectrometer, and high resolution analyses on a Kratos MS80RF double focussing magnetic sector instrument (Cape Technikon Mass spectrometry unit); FAB mass spectra were obtained on a VG Micromass 70-70E spectrometer (Ion tech B11N FAB-gun), using Xe as bombarding gas (University of Potchefstroom). UV-Visible spectra were recorded on a Cary 1E UV-Visible spectrometer, and the resulting data for the cobalt and nickel complexes are summarised in Tables 14 and 17 respectively. Microanalysis (combustion analysis) was conducted at the University of Cape Town, and the data for the copper, cobalt, nickel and platinum complexes are reported in Tables 8, 12, 15 and 18 respectively. X-ray crystallographic data were collected on a Siemens SMART CCD diffractometer at the University of the Witwatersrand. Electrochemical data were recorded with a Bio Analytical Systems (BAS) CV-50 voltammograph. Melting points were obtained using a Kofler hot-stage microscope and are uncorrected.

### 3.2 PROCEDURES FOR LIGAND SYNTHESSES

#### 3.2.1 Biphenyl ligands

##### *Biphenyl-2,2'-dicarbaldehyde 48*<sup>140</sup>

A stirred suspension of phenanthrene **47** (2.5 g, 14 mmol) in dry methanol (50 mL) was cooled to -30°C in an ozonolysis vessel. O<sub>3</sub> was gently bubbled through the mixture until all of the substrate had dissolved. KI (8.5 g) and glacial AcOH (7.5 mL) were added to the mixture at 0°C. The mixture was then allowed to stand at room temperature for 1 h, after which, an aqueous solution of Na<sub>2</sub>S<sub>2</sub>O<sub>3</sub> (10%) was added. A stream of air was passed through the mixture for 2 h. Cold H<sub>2</sub>O (0°C; 50 mL) was added, and the solid product was filtered off and recrystallised from Et<sub>2</sub>O-hexane to give, as a pale yellow solid, biphenyl-2,2'-dicarbaldehyde **48** (2.74 g, 93%), mp 61-62°C [lit.<sup>140</sup> 62-63°C];  $\nu_{\max}(\text{KBr}/\text{cm}^{-1})$  1700 (CO);  $\delta_{\text{H}}(400\text{MHz}; \text{CDCl}_3)$  7.35 (2H, d, ArH) 7.59 (2H, t, ArH), 7.64 (2H, t, ArH), 8.05 (2H, d, ArH) and 9.83 (2H, s, CHO).

##### *Diphenic Acid 49*<sup>141</sup>

Phenanthrene **47** (10 g, 56 mmol) was dissolved in glacial AcOH (113 mL) and the solution warmed to 85°C on a water bath. An aqueous solution of H<sub>2</sub>O<sub>2</sub> (30%; 39 mL, 0.45 mmol) was added dropwise during a period of 40 minutes after which the mixture was heated for a further 3-4 h. The volume of the mixture was then reduced to half by distillation under reduced pressure, and the diphenic acid, which precipitated out, was filtered off. The filtrate was evaporated almost to dryness under reduced pressure and then extracted through warming with an aqueous solution of Na<sub>2</sub>CO<sub>3</sub> (10%; 42 mL). This extract was boiled with a little decolourising carbon and then filtered. To the filtrate, dilute HCl was added until a pH of 4.5 was reached (using narrow range indicator paper). The solution was further stirred with a small amount of activated charcoal and the tarry material was filtered off. The clear solution was then acidified with dilute HCl at 0°C. The crude diphenic acid was collected by filtration, washed with H<sub>2</sub>O, dried at 110°C and then

recrystallised from glacial AcOH. The total yield of diphenic acid **49** was 9.1 g (67%), mp 228-229°C [lit.<sup>141</sup> 230°C];  $\nu_{\max}$ (KBr/cm<sup>-1</sup>) 2500-3500 (OH stretch), 1700 (CO);  $\delta_{\text{H}}$ (400 MHz; DMSO-*d*<sub>6</sub>) 7.18 (2H, d, ArH) 7.43 (2H, t, ArH), 7.53 (2H, t, ArH), 7.93 (2H, d, ArH) and 12.44 (2H, s, CO<sub>2</sub>H).

### 2-(2-Aminoethyl)benzimidazole **52**<sup>138</sup>

A stirred mixture of 1,2-diaminobenzene **57** (8.33 g, 77 mmol) and  $\beta$ -alanine **58** (10.2 g, 115 mmol in HCl (6M; 90 mL) was boiled under reflux for 48 h, and then allowed to stand for 48 h at room temperature. The completion of the reaction was confirmed by TLC. The solvent was removed under reduced pressure at 90°C, and the residual solid was dissolved in H<sub>2</sub>O (50 mL). EtOH (100 mL) was then added, and the dihydrochloride salt crystallised out as blue needles on cooling. Recrystallisation from 95% EtOH gave the dihydrochloride (4.0 g, 32%). A methanolic solution of NaOMe (0.1 M; 171 mL, 17.1 mmol) was then added to the salt (2.0 g), and the mixture stirred for 1.5 h. The solvent was removed under reduced pressure before adding CHCl<sub>3</sub> (50 mL) to dissolve the amine. The solution was filtered, and a pale pink product was obtained after removing the CHCl<sub>3</sub> under reduced pressure. Recrystallisation from THF gave 2-(2-aminoethyl)benzimidazole **52** (1.1 g, 80%), mp 134 - 135°C (lit.<sup>138</sup> 134 - 136°C);  $\nu_{\max}$  (KBr/cm<sup>-1</sup>) 3350 (NH) and 1540 (C=N);  $\delta_{\text{H}}$ (400 MHz; D<sub>2</sub>O) 2.91 (2H, t, CH<sub>2</sub>), 2.99 (2H, t, CH<sub>2</sub>), 7.21 (2H, m, ArH), 7.49 (2H, m, ArH).

### Histamine **53**

Histamine dihydrochloride (2.0 g, 11mmol) was added to a methanolic solution of NaOMe (0.1M; 220 mL, 22 mmol) and the resulting mixture stirred for 1.5 h at room temperature. The solvent was then removed under reduced pressure, and CHCl<sub>3</sub> was added to the residue. The flask was warmed to aid the dissolution of the liberated amine; the solution was filtered, and evaporation of the solvent gave, as a light yellow oil, histamine **53** (1.20 g, 98%);  $\nu_{\max}$ (thin film/cm<sup>-1</sup>) 3481 and 3250 (NH);  $\delta_{\text{H}}$ (400MHz; CDCl<sub>3</sub>) 2.72 (2H, t, CH<sub>2</sub>), 2.99 (2H, t, CH<sub>2</sub>), 4.5 (2H, br s, NH<sub>2</sub>), 6.79 (1H, s, ArH) and 7.53 (1H, s, ArH).

**2,2'-Bis[4-(2-pyridyl)-2-azabut-1-enyl]biphenyl 54a**<sup>103</sup>

2-(2-Aminoethyl)pyridine **51** (1.1 mL, 9.0 mmol) was added to a solution of 1,1'-biphenyl-2,2'-dicarbaldehyde **48** (1.00 g, 4.76 mmol) in  $\text{CHCl}_3$  (50 mL) in a 2-necked flask fitted with a condenser and a modified Dean-Stark apparatus. The mixture was boiled under reflux for 16 h, and completion of the reaction was confirmed by IR spectroscopy. The  $\text{CHCl}_3$  was removed under reduced pressure to afford, as a pure brown oil, 2,2'-bis[4-(2-pyridyl)-2-azabut-1-enyl]biphenyl **54a** [(1.88 g, 97%);  $\nu_{\text{max}}$  ( $\text{NaCl}/\text{cm}^{-1}$ ) 1650 (C=N);  $\delta_{\text{H}}$  (400 MHz;  $\text{CDCl}_3$ ) 3.03 (4H, t,  $\text{NCH}_2\text{CH}_2$ ), 3.76 (4H, m,  $\text{NCH}_2\text{CH}_2$ ), 7.00 (4H, t, ArH), 7.06 (2H, d, ArH), 7.34 (4H, m, ArH), 7.47 (2H, t, ArH), 7.85 (2H, s, CH=N), 8.04 (2H, d, ArH), 8.40 (2H, d, ArH)], which was used without further purification.

**2,2'-Bis[[2-(2-pyridyl)ethylamino]carbonyl]biphenyl 55a**

Diphenic acid **49** (1.00 g, 4.1 mmol) was dissolved in dry DMF (10 mL) in a round-bottomed flask fitted with a reflux condenser and drying tube. The solution was warmed to 40°C, and CDI (2.13 g, 13.1 mmol) was added with stirring. The mixture was stirred for 5 min at 40°C, after which time, gas evolution ceased. After cooling to room temperature, 2-(2-aminoethyl)pyridine **51** (1.1 mL, 9.0 mmol) was added. The resulting solution was stirred for 1 h at room temperature, and the reaction was quenched with  $\text{H}_2\text{O}$  (7 mL). Volatiles were removed under reduced pressure, and aqueous 1M  $\text{Na}_2\text{CO}_3$  (50 mL) was added to the residual oil. The mixture was extracted with EtOAc (2 x 80 mL), and the combined extracts were washed with  $\text{H}_2\text{O}$  (80 mL) and brine (80 mL), and dried ( $\text{MgSO}_4$ ). The solvent was evaporated and the residue chromatographed [flash chromatography on silica gel; elution with  $\text{CHCl}_3$ -hexane-MeOH (3:3:1)] to afford, as a brown oil, 2,2'-bis[[2-(2-pyridyl)ethylamino]carbonyl]biphenyl **55a** (1.00 g, 54%) (Found:  $\text{M}^+$ , 450.2044).

$C_{28}H_{26}O_2N_4$  requires,  $M$  450.2054);  $\nu_{\max}$ (thin film/ $cm^{-1}$ ) 3321 (amide NH), 1634 (CO);  $\delta_H$ (400 MHz;  $CDCl_3$ ) 2.68 (4H, quintet,  $NHCH_2CH_2$ ), 3.42-3.67 (4H, m,  $NHCH_2CH_2$ ), 7.02-7.12 (6H, m, ArH), 7.25-7.35 (4H, m, ArH), 7.48 (2H, m, ArH), 7.52-7.58 (2H, m, ArH), 7.74 (2H, t, NH), 8.45 (2H, d, ArH);  $\delta_C$ (100 MHz;  $CDCl_3$ ) 37.1 ( $NHCH_2CH_2$ ), 39.1 ( $NHCH_2CH_2$ ), 121.7, 123.6, 127.4, 128.0, 129.6, 129.7, 136.6, 136.8, 139.4, 149.4 and 159.6 (ArC) and 170.1 (CO).

### 2,2'-Bis[[2-(2-benzimidazolyl)ethylamino]carbonyl]biphenyl **55b**

Following the procedure used for synthesising 2,2'-bis[[2-(2-pyridyl)ethylamino]carbonyl]biphenyl **55a**, a solution of diphenic acid **49** (1.00 g, 4.1 mmol), 2-(2-aminoethyl)benzimidazole **52** (1.46 g, 9.0 mmol) and CDI (2.13 g, 13.1 mmol) in dry DMF (10 mL) was stirred for 64 h at room temperature. The reaction was quenched with  $H_2O$  (7 mL), and the solvent was removed under reduced pressure. Addition of aqueous  $Na_2CO_3$  (1M; 50 mL) to the residual oil precipitated the crude product, which was recrystallised from DMF- $H_2O$  to afford, as a pale pink powder, 2,2'-bis[[2-(2-benzimidazolyl)ethylamino]carbonyl]biphenyl **55b** (1.21 g, 56%) mp > 250°C (Found:  $M^+$ , 528.2261.  $C_{32}H_{28}N_6O_2$  requires,  $M$  528.2272;  $\nu_{\max}$ (KBr/ $cm^{-1}$ ) 3172 (amide NH), 1656 (CO);  $\delta_H$ (400 MHz;  $DMSO-d_6$ ) 2.62 (4H, s,  $NHCH_2CH_2$ ), 3.43 (4H, s,  $NHCH_2CH_2$ ), 6.99 (2H, d, ArH), 7.05-7.16 (4H, m, ArH), 7.28-7.37 (4H, m, ArH), 7.38-7.42 (4H, m, ArH), 7.49 (2H, d, ArH), 8.64 (2H, m, amide NH), 12.14 (2H, s, NH);  $\delta_C$ (100 MHz;  $DMSO-d_6$ )<sup>†</sup> 28.2 ( $NHCH_2CH_2$ ), 37.2, ( $NHCH_2CH_2$ ), 110.7, 118.0, 120.7, 121.4, 126.9, 127.2, 128.9, 134.2, 136.2, 138.5, 143.2 and 152.1 (ArC) and 169.0 (CO).

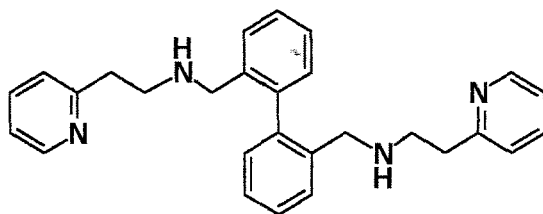
### 2,2'-Bis[[2-(4-imidazolyl)ethylamino]carbonyl]biphenyl **55c**

The procedure described for the synthesis of 2,2'-bis[[2-(2-pyridyl)ethylamino]carbonyl]biphenyl **55a** was followed, using histamine **53** (1.00 g, 9.0 mmol), CDI (2.13 g, 13.1 mmol) and diphenic acid **49** (1.0 g, 4.1 mmol). After stirring for 94 h at room temperature in dry DMF (10 mL), the reaction was quenched with  $H_2O$  (7 mL) and the volatiles were removed under reduced pressure. The addition of

<sup>†</sup> The coincidence of some  $^{13}C$  signals is presumed.

aqueous 1M Na<sub>2</sub>CO<sub>3</sub> (50 mL) to the residual oil precipitated the crude product, which was recrystallised from DMF-H<sub>2</sub>O to afford, as an off-white powder, 2,2'-bis[[2-(4-imidazolyl)ethylamino]carbonyl]biphenyl **55c** (1.44 g, 82%), mp 232-234°C (from DMF-H<sub>2</sub>O) (Found: **M**<sup>+</sup>, 428.1955. C<sub>24</sub>H<sub>24</sub>O<sub>2</sub>N<sub>6</sub> requires, *M* 428.1961);  $\nu_{\max}$ (KBr/cm<sup>-1</sup>) 3187 (amide NH), 1640 (CO);  $\delta_{\text{H}}$ (400 MHz; MeOH-*d*<sub>4</sub>) 2.51 (4H, s, NHCH<sub>2</sub>CH<sub>2</sub>), 3.34 (4H, s, NHCH<sub>2</sub>CH<sub>2</sub>), 6.73 (2H, s, ArH), 7.08 (2H, m, ArH), 7.40 (4H, m, ArH), 7.48 (2H, m, ArH), 7.53 (2H, s, ArH);  $\delta_{\text{C}}$ (100 MHz; MeOH-*d*<sub>4</sub>) 27.5 (NHCH<sub>2</sub>CH<sub>2</sub>), 40.5 (NHCH<sub>2</sub>CH<sub>2</sub>), 117.9, 128.4, 128.9, 130.6, 130.7, 135.7, 136.1, 137.4 and 140.4 (ArC) and 172.5 (CO).

*2,2'-Bis[[2-(2-pyridyl)ethylamino]methyl]biphenyl 56a*



*Attempted method 1.*

2,2'-Bis[4-(2-pyridyl)-2-azabut-1-enyl]biphenyl **54a** (1.00 g, 2.39 mmol) was added to methanol (10 mL) in a 2-necked flask fitted with a reflux condenser. To the heated mixture, NaBH<sub>4</sub> (0.18 g, 4.8 mmol) was added in portions while stirring. Once the addition was complete, the reaction mixture was boiled under reflux for 0.5 h and then quenched with ice. The product was extracted with CHCl<sub>3</sub> (3 x 40 mL) and the combined extracts were dried over anhydrous MgSO<sub>4</sub>. The CHCl<sub>3</sub> was removed under reduced pressure. A sample of the crude product was purified by preparative thin layer chromatography [on silica; elution with MeOH-CHCl<sub>3</sub>-hexane (1:4:1)] to afford 1-[2-(2-pyridyl)ethyl]dibenz[*c,e*]perhydroazepine **61a** as a brown oil;  $\delta_{\text{H}}$ (400 MHz; CDCl<sub>3</sub>) 2.97-3.01 (2H, m, NCH<sub>2</sub>CH<sub>2</sub>), 3.11-3.14 (2H, m, NCH<sub>2</sub>CH<sub>2</sub>), 3.48 (4H, s, 2-x CH<sub>2</sub>), 7.10-7.13 (1H, m, ArH), 7.23 (1H, d, ArH), 7.33-7.36 (4H, m, ArH), 7.40-7.44 (2H, m, ArH), 7.49 (2H, d, ArH), 7.60 (1H, td, ArH), 8.54 (1H, d, ArH);  $\delta_{\text{C}}$ (100 MHz; CDCl<sub>3</sub>) 37.2 (NCH<sub>2</sub>CH<sub>2</sub>), 55.43 (NCH<sub>2</sub>CH<sub>2</sub>), 55.51 (ArCH<sub>2</sub>N), 121.2, 123.2, 127.5, 127.6, 128.0, 129.7, 134.7, 136.3, 141.1, 149.3 and

160.3 (ArC).

*Attempted method 2.*

NaBH<sub>4</sub> (0.18 g, 4.8 mmol) was added in portions to a stirred solution of 2,2'-bis[4-(2-pyridyl)-2-azabut-1-enyl]biphenyl **54a** (0.46 g, 1.1 mmol) in EtOH (20 mL), effervescence occurring during the addition of the NaBH<sub>4</sub>. The solution was stirred for 67 h, at room temperature, before evaporating the EtOH under reduced pressure to yield a yellow powder. This residue was dried under high vacuum to remove remaining EtOH. CHCl<sub>3</sub> was added to the residue to dissolve the product, and the mixture was then filtered to remove unreacted NaBH<sub>4</sub>. The CHCl<sub>3</sub> was removed under reduced pressure to afford, as a pale brown oil, 1-[2-(2-pyridyl)ethyl]dibenz[*c,e*]perhydro-azepine **61a** (0.46 g, 100%).

*2,2'-Bis{[2-(2-benzimidazolyl)ethylamino]methyl}biphenyl 56b*

*Attempted method 1.*

A solution of biphenyl-2,2'-dicarbaldehyde **48** (0.49 g, 2.3 mmol) and 2-(2-aminoethyl)benzimidazole **52** (0.74 g, 4.6 mmol) in CHCl<sub>3</sub> (100 mL) was boiled under reflux for 59 h. The completion of the reaction was confirmed by TLC. The solvent was removed under reduced pressure, and the residue recrystallised from MeCN to afford the diimine **54b** as a yellow powder (0.9 g, 80%). NaBH<sub>4</sub> (0.27 g, 7.1 mmol) was then added to a solution of the diimine **54b** in MeOH (10 mL), and the mixture was boiled under reflux for 30-40 min. Ice was then added to the reaction mixture to quench the reaction, precipitating, as a pale yellow powder, 1-[2-(2-benzimidazolyl)ethyl]dibenz[*c,e*]perhydroazepine **61b** (0.49 g, 65%) (Found: MH<sup>+</sup>, 340.1814. C<sub>23</sub>H<sub>21</sub>N<sub>3</sub> requires MH, 340.1814), mp 184-186 °C;  $\nu_{\max}$ (KBr/cm<sup>-1</sup>) 3174 (NH);  $\delta_{\text{H}}$ (400 MHz; MeOH-*d*<sub>4</sub>) 3.10 (2H, m, NHCH<sub>2</sub>CH<sub>2</sub>), 3.23 (2H, t, NHCH<sub>2</sub>CH<sub>2</sub>), 3.50 (4H, s, CH<sub>2</sub>NHCH<sub>2</sub>CH<sub>2</sub>), 7.17-7.21 (2H, m, ArH), 7.34-7.41 (4H, m, ArH), 7.44-7.48 (2H, m, ArH), 7.49-7.52 (4H, m, ArH);  $\delta_{\text{C}}$ (100 MHz; MeOH-*d*<sub>4</sub>)<sup>†</sup> 28.2 (NHCH<sub>2</sub>CH<sub>2</sub>), 54.4 (NHCH<sub>2</sub>CH<sub>2</sub>), 56.0 (CH<sub>2</sub>NHCH<sub>2</sub>CH<sub>2</sub>), 115.5, 123.4, 128.8, 129.1, 129.8, 131.2, 134.7, 139.4, 142.5 and 154.7 (ArC).

*Attempted method 2.*

Following the procedure described for the attempted preparation of 2,2'-bis[[2-(4-imidazolyl)ethylamino]methyl]biphenyl **55c** (method 2), a stirred mixture of 2,2'-bis-[[2-(2-benzimidazolyl)ethylamino]carbonyl]biphenyl **55b** (0.50 g, 0.95 mmol) and LiAlH<sub>4</sub> (0.72 g, 19 mmol) was boiled under reflux in dry THF (50 mL) for 55 h under N<sub>2</sub>. <sup>1</sup>H NMR and IR spectroscopy of the material obtained after work-up indicated that the desired product had not been obtained.

*Attempted method 3.*

A mixture of 2,2'-bis[[2-(2-benzimidazolyl)ethylamino]carbonyl]biphenyl **55b** (1.0 g, 1.9 mmol) and Raney nickel (0.33 g) in absolute EtOH (60 mL) was stirred under H<sub>2</sub> for 48 h at room temperature. The reaction mixture was filtered through a celite pad to remove the Raney nickel, which was quenched with HCl. The filtrate was evaporated to dryness under reduced pressure. The residue was vacuum dried, and analysis by <sup>1</sup>H NMR and IR spectroscopy indicated that this reaction was also unsuccessful.

*Attempted method 4.*

A solution of 2,2'-bis{N-[2-(2-benzimidazolyl)ethyl]-N-benzamidomethyl}biphenyl **63** (0.80 g, 1.1 mmol) in HCl (6N; 15 mL) was boiled under reflux for 12 h. The reaction mixture was washed with Et<sub>2</sub>O, basified with NaOH (10N) and then extracted with CHCl<sub>3</sub>. The CHCl<sub>3</sub> extracts were combined and then dried with anhydrous MgSO<sub>4</sub>. The CHCl<sub>3</sub> was removed under reduced pressure to yield an off-white powder, <sup>1</sup>H NMR spectroscopy of which, showed that the reaction had been unsuccessful.

*2,2'-Bis-[[2-(4-imidazolyl)ethylamino]methyl]biphenyl 56c**Attempted method 1.*

Biphenyl-2,2'-dicarbaldehyde **48** (0.72 g, 3.4 mmol) was added to a solution of histamine **53** (0.75 g, 6.8 mmol) in CHCl<sub>3</sub> (100 mL), and the resulting solution

boiled under reflux for 6 h, using a modified Dean-Stark apparatus to remove H<sub>2</sub>O. The solvent was removed under reduced pressure to yield a glassy yellow solid shown, by <sup>1</sup>H NMR spectroscopy, to be the impure diimine **54c** (1.34 g, 99%) [ $\nu_{\max}$ (KBr/cm<sup>-1</sup>) 1650 (C=N)]. The crude product (1.00 g, 1.2 mmol) was then dissolved in methanol (10 mL), and NaBH<sub>4</sub> was added in portions. The resulting mixture was boiled under reflux for 40 min. before adding ice to quench the reaction. The precipitated product was washed with Et<sub>2</sub>O to afford, as a white powder, 1-[2-(4-imidazolyl)ethyl]dibenz[c,e]perhydroazepine **61c** (0.32 g, 33%), mp 149-151°C (Found: MH<sup>+</sup>, 290.165729. C<sub>19</sub>H<sub>19</sub>N<sub>3</sub> requires, MH 290.1657;  $\nu_{\max}$ (KBr/cm<sup>-1</sup>) 3413 (NH);  $\delta_{\text{H}}$ (400 MHz; MeOH-*d*<sub>4</sub>) 2.89 (2H, m, NCH<sub>2</sub>CH<sub>2</sub>), 2.95 (2H, m, NCH<sub>2</sub>CH<sub>2</sub>), 3.46 (4H, s, 2 x CH<sub>2</sub>), 6.83-6.87 (1H, m, ArH), 7.37-7.44 (4H, m, ArH), 7.45-7.58 (4H, m, ArH), 7.59-7.63 (1H, m, ArH);  $\delta_{\text{C}}$ (100 MHz; MeOH-*d*<sub>4</sub>)<sup>†</sup> 56.08 (2 x CH<sub>2</sub>), 56.35 (NCH<sub>2</sub>CH<sub>2</sub>), 128.7, 129.0, 129.6, 131.1, 135.2, 136.0 and 142.5 (ArC).

#### Attempted method 2.

2,2'-Bis[[2-(4-imidazolyl)ethylamino]carbonyl]biphenyl **55c** (0.80 g, 1.8 mmol) was added in portions to a suspension of LiAlH<sub>4</sub> (0.35 g, 9.2 mmol) in dry THF (40 mL), and the stirred mixture was boiled under reflux for 8 h under N<sub>2</sub>. Aqueous NaOH (4M, 25 mL) was added to the reaction mixture, which was then stirred overnight to ensure quenching of the excess LiAlH<sub>4</sub>. The precipitated solid was filtered off and washed with THF.<sup>¶</sup> The filtrate and the washings were combined and evaporated to dryness under reduced pressure. <sup>1</sup>H NMR and IR analysis of the vacuum-dried residue indicated that the reaction was unsuccessful.

#### *N*-[(2-Benzimidazolyl)ethyl]benzamide **62**

A mixture of benzoic acid (1.00 g, 8.19 mmol), CDI (2.16 g, 13.3 mmol) and 2-(2-aminoethyl)benzimidazole (1.32 g, 8.19 mmol) in DMF (20 mL) was stirred for 2.5 d following the procedure used for the preparation of 2,2'-bis[[2-(2-pyridyl)ethylamino]carbonyl]biphenyl **55a**. The pale pink powder, which

precipitated out, was filtered off and washed with aqueous  $\text{Na}_2\text{CO}_3$  (1M; 50 mL) to give *N*-[2-(2-benzimidazolyl)ethyl]benzamide **62** (1.58 g, 73%), mp  $>250^\circ\text{C}$  (from DMF- $\text{H}_2\text{O}$ ) (Found:  $\text{MH}^+$ , 266.1294.  $\text{C}_{16}\text{H}_{15}\text{N}_3\text{O}$  requires, *MH* 266.1293);  $\nu_{\text{max}}$ (KBr/ $\text{cm}^{-1}$ ), 3305 (NH), 3176 (amide NH), 1638 (CO);  $\delta_{\text{H}}$ (400 MHz; DMSO- $d_6$ ) 3.09 (2H, t,  $\text{NHCH}_2\text{CH}_2$ ), 3.73 (2H, m,  $\text{NHCH}_2\text{CH}_2$ ), 7.12 (2H, m, ArH), 7.49 (5H, m, ArH), 7.84 (2H, d, ArH), 8.63 (1H, m, amide NH), 12.50 (1H, s, NH);  $\delta_{\text{C}}$ (100 MHz; DMSO- $d_6$ )<sup>†</sup> 28.7 ( $\text{NHCH}_2\text{CH}_2$ ), 37.9 ( $\text{NHCH}_2\text{CH}_2$ ), 121.0, 127.0, 128.1, 131.0, 134.4 and 152.7 (ArC) and 166.2 (CO).

### 2,2'-Bis-{*N*-[2-(2-benzimidazolyl)ethyl]benzamidomethyl}biphenyl **63**

To a stirred suspension of NaH (50% dispersion in oil, pre-washed with dry DMF under  $\text{N}_2$ ; 0.19 g, 3.2 mmol) in dry DMF (10 mL), was added *N*-[2-(2-benzimidazolyl)ethyl]benzamide **62** (0.78 g, 2.9 mmol), and the resulting mixture was boiled under reflux for 1.5 h under  $\text{N}_2$ . 2,2'-Bis-(bromomethyl)biphenyl (0.50 g, 1.5 mmol) was then added and stirring was continued at room temperature under  $\text{N}_2$  for 2.5 d. The reaction mixture was heated for 2 h before working up. The DMF was removed under reduced pressure before adding  $\text{H}_2\text{O}$  to the residue. The precipitated solid was filtered off, washed with  $\text{H}_2\text{O}$  and recrystallised from DMF- $\text{H}_2\text{O}$  to give, as an off-white solid, 2,2'-bis-{*N*-[2-(2-benzimidazolyl)ethyl]benzamidomethyl}biphenyl **63** (1.01 g, 97%), mp  $>250^\circ\text{C}$  (Found:  $\text{MH}^+$ , 709.329087.  $\text{C}_{46}\text{H}_{40}\text{N}_6\text{O}_2$  requires, *MH* 709.329099);  $\nu_{\text{max}}$ (KBr/ $\text{cm}^{-1}$ ) 1638 (CO);  $\delta_{\text{H}}$ (400 MHz; DMSO- $d_6$ ) 2.89 (4H, s,  $\text{CH}_2\text{CH}_2\text{NCH}_2$ ), 3.64 (4H, m,  $\text{CH}_2\text{CH}_2\text{NCH}_2$ ), 5.10-5.24 (4H, m,  $\text{CH}_2\text{CH}_2\text{NCH}_2$ ), 6.67 (2H, d, ArH), 7.12 (4H, t, ArH), 7.06-7.17 (4H, m, ArH), 7.20-7.27 (4H, m, ArH), 7.27-7.34 (2H, m, ArH), 7.34-7.43 (6H, m, ArH), 7.45-7.50 (2H, m, ArH), 7.61 (2H, d, ArH), 7.71 (4H, d, ArH), 8.59 (2H, s, NH);  $\delta_{\text{C}}$ (100 MHz; DMSO- $d_6$ ) 26.7 ( $\text{CH}_2\text{CH}_2\text{NCH}_2$ ), 37.3 ( $\text{CH}_2\text{CH}_2\text{NCH}_2$ ), 44.6 ( $\text{CH}_2\text{CH}_2\text{NCH}_2$ ), 110.0, 118.5, 121.3, 121.8, 126.2, 126.9, 127.6, 128.0, 128.3, 129.7, 130.9, 134.17, 134.2, 135.1, 138.0, 142.2 and 153.1 (ArC) and 166.2 (CO).

### 3.2.2 1,10-Phenanthroline-based ligands

#### *1,10-Phenanthroline-2,9-dicarbaldehyde 65*<sup>145</sup>

A mixture of neocuproine **64** (3.0 g, 14 mmol) and SeO<sub>2</sub> (7.5 g) in dioxan (200 mL) was boiled under reflux for 2 h, and then filtered through celite while hot. The filtrate was cooled on ice, and the crude dialdehyde (2.5 g, 73%) separated from the cold filtrate as a yellow powder. Recrystallisation from THF gave, as yellow crystals, 1,10-phenanthroline-2,9-dicarbaldehyde **65**, mp 231-232°C (lit.<sup>145</sup> 231-232°C);  $\nu_{\max}$ (KBr/cm<sup>-1</sup>) 1720 (CO);  $\delta_{\text{H}}$  (DMSO-*d*<sub>6</sub>) 8.28 (2H, s, Ar-H), 8.31 (2H, d, Ar-H), 8.79 (2H, d, Ar-H), 10.36 (CHO).

#### *1,10-Phenanthroline-2,9-dicarboxylic acid 66*<sup>145</sup>

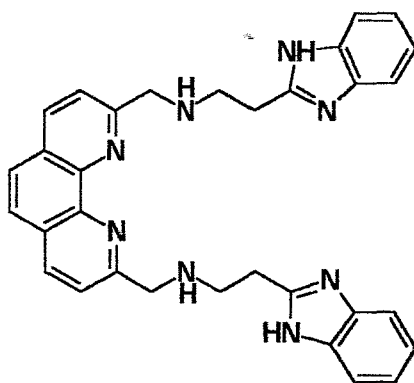
A solution of 1,10-phenanthroline-2,9-dicarbaldehyde **65** (0.5 g, 2.1 mmol) and 80% HNO<sub>3</sub> (10 mL) was boiled under reflux for 3 h. After cooling, the solution was poured onto ice and the precipitated solid recrystallised from MeOH to give, as a yellow solid, 1,10-phenanthroline-2,9-dicarboxylic acid **66** (0.40 g, 65%), mp 238°C (lit.<sup>145</sup> 238°C);  $\nu_{\max}$ (KBr/cm<sup>-1</sup>) 1724 (CO), 2800-3700 (COOH).

#### *2,9-Bis{[2-(2-pyridyl)ethyl]aminomethyl}-1,10-phenanthroline 68a*

To a suspension of 1,10-phenanthroline-2,9-dicarbaldehyde **65** (1.12 g, 4.7 mmol) in CHCl<sub>3</sub> (50 mL), was added 2-(2-aminoethyl)pyridine **51** (1.0 mL, 8.2 mmol), and the resulting mixture boiled under reflux for 2 h. The completion of the reaction was confirmed by IR spectroscopy. The CHCl<sub>3</sub> was removed under reduced pressure to yield the crude diimine **67a** as a dark-brown oil (2.11 g, 95%), which became semi-solid upon standing at room temperature. <sup>1</sup>H NMR and IR analysis confirmed that the reaction had been successful. The semi-solid diimine **67a** (1.0 g, 2.3 mmol) was dissolved in dry MeOH (10 mL), and NaBH<sub>4</sub> (0.17 g, 4.51 mmol) was added to the solution in portions. The resulting mixture was then refluxed for 2.5 h, after which the reaction was quenched with ice. The product was extracted with CHCl<sub>3</sub> (4 x 40 mL) and the combined extracts were dried over anhydrous MgSO<sub>4</sub>. The CHCl<sub>3</sub> was removed under reduced pressure to yield, as a brown oil,

which became a semi-solid upon standing at room temperature, 2,9-bis[[2-(2-pyridyl)ethyl]aminomethyl]-1,10-phenanthroline **68a** (0.71 g, 71%) (Found:  $M^+$ , 448.2371.  $C_{28}H_{28}N_6$  requires  $M$ , 448.2375;  $\nu_{max}$  (thin film/ $cm^{-1}$ ) 3300 (NH) and 1590 (C=N);  $\delta_H$ (400 MHz;  $CDCl_3$ ) 3.08 (4H, t,  $CH_2NHCH_2CH_2$ ), 3.17 (4H, t,  $CH_2NHCH_2CH_2$ ), 4.32 (4H, s,  $CH_2NHCH_2CH_2$ ), 7.06 (2H, t, ArH), 7.19 (2H, t, ArH), 7.54 (2H, td, ArH), 7.72 (2H, d, ArH), 8.14 (2H, d, ArH), 8.49 (2H, t, ArH);  $\delta_C$ (100 MHz;  $CDCl_3$ ) 38.5 ( $CH_2CH_2NHCH_2$ ), 49.3 ( $CH_2CH_2NHCH_2$ ), 56.0 ( $CH_2CH_2NHCH_2$ ), 121.2, 122.0, 123.3, 125.8, 127.7, 136.3, 136.5, 145.2, 149.3, 160.3 and 160.8 (ArC).

2,9-Bis-[[2-(2-benzimidazolyl)ethyl]aminomethyl]-1,10-phenanthroline **68b**



A solution of 2-(2-aminoethyl)benzimidazole **52** (0.74 g, 4.7 mmol) in MeOH (10 mL) was added dropwise to a hot solution of 1,10-phenanthroline-2,9-dicarbaldehyde **65** (0.54 g, 2.3 mmol) in MeOH (30 mL). The resulting solution was boiled under reflux for 1.5 h, completion of the reaction being confirmed by IR spectroscopy. After removing the solvent under reduced pressure, the crude diimine **67b** was obtained as a glassy orange-brown solid.  $NaBH_4$  (0.29 g, 7.6 mmol) was then added in portions to a solution of the crude diimine **67b** (1.0 g, 1.9 mmol) in MeOH (20 mL). After boiling the mixture under reflux for 45 min., the reaction was quenched with ice precipitating, as an orange-yellow powder, 2,9-bis[[2-(2-benzimidazolyl)ethylamino]methyl]-1,10-phenanthroline **68b**, (0.40 g, 40%), mp  $>250^\circ C$  (Found:  $MH^+$ , 527.2672.  $C_{32}H_{30}N_8$  requires  $MH$ , 527.2672);  $\delta_H$ (400 MHz;  $DMSO-d_6$ ) 3.0-3.12 (8H, m,  $CH_2NHCH_2CH_2$ ), 4.16 (4H, s,

$\text{CH}_2\text{NHCH}_2\text{CH}_2$ ), 6.9-7.3 (4H, m, ArH), 7.30-7.60 (4H, br s, ArH), 7.87 (2H, d, ArH), 7.91 (2H, s, ArH), 8.41 (2H, d, ArH), 12.31 (2H, br s, NH);  $\delta_{\text{C}}$ (100 MHz; DMSO- $d_6$ )<sup>†</sup> 29.3 ( $\text{CH}_2\text{NHCH}_2\text{CH}_2$ ), 47.2 ( $\text{CH}_2\text{NHCH}_2\text{CH}_2$ ), 55.0 ( $\text{CH}_2\text{NHCH}_2\text{CH}_2$ ), 120.9, 121.6, 125.7, 127.3, 136.4, 144.4, 153.8 and 160.8 (ArC).

#### Attempted Method

A stirred mixture of 2,9-bis[[2-(2-benzimidazolyl)ethylamino]carbonyl]-1,10-phenanthroline **69b** (1.0 g, 1.7 mmol) and  $\text{LiAlH}_4$  (0.66 g, 17 mmol) in dry THF (40 mL) was boiled under reflux for 8 h under  $\text{N}_2$ , and worked-up following the procedure described for the attempted preparation of 2,2'-bis[[2-(4-imidazolyl)ethylamino]carbonyl]biphenyl **55c** (Method 2).  $^1\text{H}$  NMR and IR analysis of the isolated material revealed that the reaction had been unsuccessful.

#### 2,9-Bis[[2-(4-imidazolyl)ethyl]aminomethyl]-1,10-phenanthroline **68c**

##### Attempted Method

To a suspension of  $\text{LiAlH}_4$  (0.36 g, 9.6 mmol) in THF (20 mL), 2,9-bis[[2-(4-imidazolyl)ethylamino]carbonyl]-1,10-phenanthroline **69c** (0.80 g, 1.9 mmol) was added in portions. The resulting mixture was boiled under reflux for 9 h, and worked-up following the procedure described for the attempted preparation of 2,2'-bis[[2-(2-imidazolyl)ethylamino]carbonyl]biphenyl **55c** (Method 2). IR and  $^1\text{H}$  NMR spectra of the isolated material indicated that the reaction had not been successful.

#### 2,9-Bis[[2-(2-pyridyl)ethylamino]carbonyl]-1,10-phenanthroline **69a**

A solution of 1,10-phenanthroline-2,9-dicarboxylic acid **66** (0.48 g, 2.05 mmol) in dry DMF (10 mL) was heated to 40-50°C. CDI (1.07 g, 13.1 mmol) was added in portions and the resulting mixture stirred until effervescence ceased. 2-(2-Aminoethyl)pyridine **51** (0.55 mL, 4.5 mmol) was then added at room temperature, and the reaction mixture was stirred for 4.5 days. The reaction was quenched with  $\text{H}_2\text{O}$  (7 mL), and the solvents were removed under reduced pressure at 90°C. Aqueous

$\text{Na}_2\text{CO}_3$  (1 M, 50 mL) was added to the residue, and the resulting precipitate was filtered off to give, as a light-brown powder, 2,9-bis[[2-(2-pyridyl)ethylamino]carbonyl]-1,10-phenanthroline **69a** (0.78 g, 73%), mp 55-57°C (from DMF- $\text{H}_2\text{O}$ ) (Found:  $\text{M}^+$ , 476.1960.  $\text{C}_{28}\text{H}_{24}\text{N}_6\text{O}_2$  requires  $M$ , 476.1961);  $\nu_{\text{max}}$  (KBr/ $\text{cm}^{-1}$ ) 3256 (NH) and 1651 (CO);  $\delta_{\text{H}}$  (400 MHz; DMSO- $d_6$ ) 3.18 (4H, t,  $\text{NHCH}_2\text{CH}_2$ ), 3.75-3.85 (4H, m,  $\text{NHCH}_2\text{CH}_2$ ), 7.20 (2H, dd, ArH), 7.35 (2H, d, ArH), 7.69 (2H, t, ArH), 8.18 (2H, s, ArH), 8.44 (2H, d, ArH), 8.49 (2H, d, ArH), 8.73 (2H, d, ArH), 9.56 (2H, br s, NH);  $\delta_{\text{C}}$  (100 MHz; DMSO- $d_6$ ) 36.9 ( $\text{NHCH}_2\text{CH}_2$ ), 39.0 ( $\text{NHCH}_2\text{CH}_2$ ), 120.8, 121.6, 123.0, 127.7, 130.1, 136.7, 138.1, 143.6, 148.8, 149.4 and 159.0 (ArC) and 163.7 (CO).

**2,9-Bis[[2-(2-benzimidazolyl)ethylamino]carbonyl]-1,10-phenanthroline 69b**

A mixture of 2-(2-aminoethyl)benzimidazole **52** (1.46 g, 9.0 mmol), 1,10-phenanthroline-2,9-dicarboxylic acid **66** (0.96 g, 4.1 mmol) and CDI (2.13 g, 13.1 mmol) in dry DMF (20 mL) was stirred for 26 h, using the procedure described for the synthesis of 2,9-bis-[[2-(2-pyridyl)ethylamino]carbonyl]-1,10-phenanthroline **69a**. Work-up afforded as a light-brown solid, 2,9-bis[[2-(2-benzimidazolyl)ethylamino]carbonyl]-1,10-phenanthroline **69b** (1.53 g, 61%), mp >250°C (from DMF- $\text{H}_2\text{O}$ ) (Found:  $\text{M}^+$ , 554.2179.  $\text{C}_{32}\text{H}_{26}\text{N}_8\text{O}_2$  requires  $M$ , 554.2179);  $\nu_{\text{max}}$  (KBr/ $\text{cm}^{-1}$ ) 3145 and 3323 (NH) and 1630 (CO);  $\delta_{\text{H}}$  (400 MHz, DMSO- $d_6$ ) 3.29 (4H, t,  $\text{NHCH}_2\text{CH}_2$ ), 3.90 (4H, dd,  $\text{NHCH}_2\text{CH}_2$ ), 7.06-7.12 (4H, m, ArH), 7.41-7.49 (4H, m, ArH), 8.15 (2H, s, ArH), 8.45 (2H, d, ArH), 8.71 (2H, d, ArH), 9.71 (2H, br s, amide NH);  $\delta_{\text{C}}$  (100 MHz, DMSO- $d_6$ )<sup>†</sup> 28.2 ( $\text{NHCH}_2\text{CH}_2$ ), 37.8 ( $\text{NHCH}_2\text{CH}_2$ ), 120.8, 121.2, 127.8, 130.1, 138.1, 143.5, 149.4 and 152.8 (ArC) and 163.6 (CO).

**2,9-Bis-[[2-(4-imidazolyl)ethylamino]carbonyl]-1,10-phenanthroline 69c**

Following the procedure described for the preparation of 2,9-bis[[2-(2-pyridyl)ethylamino]carbonyl]-1,10-phenanthroline **69a**, a mixture of histamine **53** (1.00 g, 9.0 mmol), 1,10-phenanthroline-2,9-dicarboxylic acid **66** (0.96 g, 4.1 mmol) and CDI (2.13 g, 13.1 mmol) in dry DMF (15 mL) was stirred for 55 h. Work-up afforded, as a light-brown solid, 2,9-bis[[2-(4-imidazolyl)ethylamino]carbonyl]-1,10-

*phenanthroline 69c* (1.18 g, 63%), mp 122-124°C (from DMF-H<sub>2</sub>O) (Found  $M^+$ , 454.1851.  $C_{24}H_{22}N_8O_2$  requires  $M$ , 454.1866);  $\nu_{\max}$ (KBr/cm<sup>-1</sup>) 3130 and 3297 (NH) and 1649 (CO);  $\delta_H$ (400 MHz, DMSO-*d*<sub>6</sub>) 2.93 (4H, t, NHCH<sub>2</sub>CH<sub>2</sub>), 3.68 (4H, dd, NHCH<sub>2</sub>CH<sub>2</sub>), 6.91 (2H, s, ArH), 7.57 (2H, s, ArH), 8.17 (2H, s, ArH), 8.45 (2H, d, ArH), 8.68 (2H, d, ArH), 9.55 (2H, t, amide NH);  $\delta_C$ (100 MHz, DMSO-*d*<sub>6</sub>)<sup>†</sup> 26.8 (NHCH<sub>2</sub>CH<sub>2</sub>), 39.3 (NHCH<sub>2</sub>CH<sub>2</sub>), 120.8, 127.7, 130.1, 134.7, 138.0, 143.6 and 149.5 (ArC) and 163.7 (CO).

### 3.2.3 Schiff base ligands prepared from diketones and 2-(2-aminoethyl)-pyridine

#### *N,N'*-Bis[2-(2-pyridyl)ethyl]pentane-2,4-diimine **76**<sup>§</sup>

Acetylacetone **70** (0.41 mL, 4.0 mmol) was dissolved in CHCl<sub>3</sub> (5 mL). To this solution, 2-(2-aminoethyl)pyridine **51** (0.95 mL, 7.9 mmol) was added and the resulting mixture was boiled under reflux for 2 h and then stirred at room temperature for 48 h. The completion of the reaction was confirmed by TLC. The solvent was removed under reduced pressure and the residue was purified by chromatography [flash chromatography on silica; elution with MeOH-benzene-EtOAc (1:4:4)] to afford, as a brown oil, *N,N'*-bis[2-(2-pyridyl)ethyl]pentane-2,4-diimine **76** (0.70 g, 57%) (Found: **MH**<sup>+</sup>, 309.2079. C<sub>19</sub>H<sub>24</sub>N<sub>4</sub> requires *MH*, 309.2079); δ<sub>H</sub>(400 MHz; CDCl<sub>3</sub>) 1.82 (3H, s, CH<sub>3</sub>), 1.95 (3H, s, CH<sub>3</sub>), 3.01 (4H, t, NHCH<sub>2</sub>CH<sub>2</sub>), 3.65 (4H, q, NHCH<sub>2</sub>CH<sub>2</sub>), 4.89 (1H, s, NHC=CH), 7.09-7.14 (2H, m, ArH), 7.16 (2H, d, ArH), 7.58 (2H, t, ArH), 8.52 (2H, d, ArH), 10.85 (1H, br s, D<sub>2</sub>O exchangeable, NH); δ<sub>C</sub>(100 MHz; CDCl<sub>3</sub>) 18.6 (CH<sub>3</sub>), 28.7 (CH<sub>3</sub>), 38.8 (NHCH<sub>2</sub>CH<sub>2</sub>), 42.6 (NHCH<sub>2</sub>CH<sub>2</sub>), 95.2 (NHC=CH), 121.7, 123.6, 136.5, 149.5, 158.2, 162.8 and 194.7 (ArC, NHC=C and C=N).

#### *3-methyl-N,N'*-bis[2-(2-pyridyl)ethyl]pentane-2,4-diimine **77**<sup>§</sup>

To a solution of 3-methyl-2,4-pentanedione **71** (0.41 mL, 3.5 mmol) in CHCl<sub>3</sub> (5 mL), 2-(2-aminoethyl)pyridine **51** (0.87 mL, 7.0 mmol) was added, and the reaction mixture was boiled under reflux for 2 h and then stirred at room temperature for 3 h. Completion of the reaction was confirmed by TLC. The CHCl<sub>3</sub> was evaporated off under reduced pressure. Purification of the residue by chromatography [(flash chromatography on silica gel; elution with MeOH-benzene-EtOAc (1:4:4)] yielded, as a brown oil, *3-methyl-N,N'*-bis[2-(2-pyridyl)ethyl]pentane-2,4-diimine **77** (0.48 g, 43%); (Found: **MH**<sup>+</sup>, 323.2235. C<sub>20</sub>H<sub>26</sub>N<sub>4</sub> requires *MH*, 323.2236); δ<sub>H</sub>(400 MHz; CDCl<sub>3</sub>) 1.78 (3H, s, CH<sub>3</sub>), 1.90 (3H, s, CH<sub>3</sub>), 2.08 (3H, s, CH<sub>3</sub>), 3.01 (4H, t, NHCH<sub>2</sub>CH<sub>2</sub>), 3.66 (4H, q, NHCH<sub>2</sub>CH<sub>2</sub>), 7.11 (2H, m, ArH), 7.18 (2H, d, ArH), 7.58

§ In CDCl<sub>3</sub>, the compound exists as a monoimino tautomer.

(2H, td, ArH), 8.52 (2H, d, ArH), 12.00 (1H, br s, NH);  $\delta_{\text{C}}$ (100 MHz;  $\text{CDCl}_3$ ) 14.7 ( $\text{CH}_3$ ), 15.0 ( $\text{CH}_3$ ), 28.4 ( $\text{CH}_3$ ), 39.0 ( $\text{NHCH}_2\text{CH}_2$ ), 43.1 ( $\text{NHCH}_2\text{CH}_2$ ), 98.1 ( $\text{NHC}=\text{C}$ ), 121.6, 123.6, 136.5, 149.5, 158.5, 161.9 and 194.6 (ArC,  $\text{NHC}=\text{C}$  and  $\text{C}=\text{N}$ ).

### *3-Ethyl-N,N'-bis[2-(2-pyridyl)ethyl]pentane-2,4-diimine 78<sup>s</sup>*

A solution of 2-(2-aminoethyl)pyridine **51** (1.50 mL, 12.5 mmol) and 3-ethyl-2,4-pentanedione **72** (0.84 mL, 6.2 mmol) in  $\text{CHCl}_3$  (5 mL) was boiled under reflux for 1 h. The reaction was shown to be complete by TLC. After removal of the solvent under reduced pressure, the residue was chromatographed [flash chromatography on silica; elution with MeOH-benzene-EtOAc (1:4:4)] to give, as a brown oil, 3-ethyl-N,N'-bis[2-(2-pyridyl)ethyl]pentane-2,4-diimine **78** (0.73 g, 35%) (Found:  $\text{MH}^+$ , 337.2392.  $\text{C}_{21}\text{H}_{28}\text{N}_4$  requires  $\text{MH}$ , 337.2392);  $\delta_{\text{H}}$ (400 MHz;  $\text{CDCl}_3$ ) 0.94 (3H, t,  $\text{CH}_2\text{CH}_3$ ), 1.90 (3H, s,  $\text{CH}_3$ ), 2.10 (3H, s,  $\text{CH}_3$ ), 2.20 (2H, q,  $\text{CH}_2\text{CH}_3$ ), 3.01 (4H,  $\text{NHCH}_2\text{CH}_2$ ), 3.65 (4H, q,  $\text{NHCH}_2\text{CH}_2$ ), 7.10 (2H, t, ArH), 7.17 (2H, d, ArH), 7.57 (2H, t, ArH), 8.52 (2H, d, ArH), 12.14 (1H, br s, NH);  $\delta_{\text{C}}$ (100 MHz;  $\text{CDCl}_3$ ) 14.3 ( $\text{CH}_2\text{CH}_3$ ), 15.5 ( $\text{CH}_2\text{CH}_3$ ), 22.0 ( $\text{CH}_3$ ), 27.3 ( $\text{CH}_3$ ), 38.9 ( $\text{NHCH}_2\text{CH}_2$ ), 43.1 ( $\text{NHCH}_2\text{CH}_2$ ), 105.5 ( $\text{NHC}=\text{CH}$ ), 121.6, 123.6, 136.5, 149.47, 149.49, 158.5, 162.2 and 194.6 (ArC,  $\text{NHC}=\text{C}$  and  $\text{C}=\text{N}$ ).

### *3-benzyl-2,4-pentanedione 73*

A stirred solution of acetylacetone **70** (0.82 mL, 8.0 mmol) in methanolic NaOMe (79.9 mL, 8.0 mmol) was boiled under reflux for 1.5 h. Benzyl bromide (0.95 mL, 8.0 mmol) was then added to the mixture, and stirring continued at room temperature for 2.5 d. The solvent was evaporated off under reduced pressure and the residue extracted with EtOAc. This mixture was then gently heated and filtered. Evaporation of the solvent under reduced pressure gave, as a pale yellow oil, 3-benzyl-2,4-pentanedione **73** (0.92 g, 61%) [ $\delta_{\text{C}}$ (100 MHz;  $\text{CDCl}_3$ ) 29.7 ( $\text{CH}_2$ ), 30.0 ( $\text{CH}_3$ ), 72.1 (CH), 126.0, 128.21, 128.42, 140.9 (ArC) and 207.8 (CO)], which was used without further purification.

**3-Benzyl-N,N'-bis[2-(2-pyridyl)ethyl]pentane-2,4-diimine 79<sup>s</sup>**

To a solution of crude 3-benzyl-2,4-pentanedione **73** (0.59 g, 3.1 mmol) in  $\text{CHCl}_3$  (5 mL) was added 2-(2-aminoethyl)pyridine **51** (0.75 mL, 6.3 mmol), and the resulting mixture was boiled under reflux for 2.5 h. After removal of the solvent under reduced pressure, the residue was chromatographed [flash chromatography on silica; elution with MeOH-EtOAc (1:8)] to give, as a brown oil, 3-benzyl-N,N'-bis[2-(2-pyridyl)ethyl]pentane-2,4-diimine **79** (0.35 g, 25%) (Found:  $\text{MH}^+$ , 399.2548.  $\text{C}_{26}\text{H}_{30}\text{N}_4$  requires  $MH$ , 399.2549);  $\delta_{\text{H}}$  (400 MHz;  $\text{CDCl}_3$ ) 1.80 (3H, s,  $\text{CH}_3$ ), 2.03 (3H, s,  $\text{CH}_3$ ), 3.07 (4H, t,  $\text{NHCH}_2\text{CH}_2$ ), 3.63 (2H, s,  $\text{CH}_2\text{Ph}$ ), 3.71 (4H, q,  $\text{NHCH}_2\text{CH}_2$ ), 7.10 (2H, d, ArH), 7.11-7.18 (2H, m, ArH), 7.19-7.26 (4H, m, Ar-H), 7.61 (2H, td, ArH), 8.54 (2H, d, ArH), 12.36 (1H, br s, NH);  $\delta_{\text{C}}$  (100 MHz;  $\text{CDCl}_3$ ) 15.0 ( $\text{CH}_3$ ), 27.9 ( $\text{CH}_3$ ), 34.6 ( $\text{CH}_2\text{Ph}$ ), 39.0 ( $\text{NHCH}_2\text{CH}_2$ ), 43.2 ( $\text{NHCH}_2\text{CH}_2$ ), 101.4 ( $\text{CCH}_2\text{Ph}$ ), 121.7, 123.8, 125.7, 127.5, 128.4, 136.5, 141.7, 149.6, 158.4, 163.7 and 195.4 (ArC,  $\text{NHC}=\text{C}$  and  $\text{C}=\text{N}$ ).

**1,3-Diphenyl-N,N'-bis[2-(2-pyridyl)ethyl]propane-1,3-diimine 80<sup>s</sup>**

2-(2-Aminoethyl)pyridine **51** (0.85 mL, 7.1 mmol) was added to a solution of dibenzoylmethane **74** (0.80 g, 3.6 mmol) in  $\text{CHCl}_3$  (10 mL), and the reaction mixture was boiled under reflux for 6 d. Completion of the reaction was confirmed by TLC. After removing the solvent under reduced pressure, the residual material was chromatographed (flash chromatography on silica gel; elution with EtOAc) to afford, as a yellow-green oil, 1,3-diphenyl-N,N'-bis[2-(2-pyridyl)ethyl]propane-1,3-diimine **80** (0.90 g, 58%) (Found:  $\text{MH}^+$ , 433.2392.  $\text{C}_{29}\text{H}_{28}\text{N}_4$  requires  $MH$ , 433.2392);  $\delta_{\text{H}}$  (400 MHz;  $\text{CDCl}_3$ ) 3.02 (4H, t,  $\text{NHCH}_2\text{CH}_2$ ), 3.64 (4H, q,  $\text{NHCH}_2\text{CH}_2$ ), 5.69 (1H, s,  $\text{NHC}=\text{CH}$ ), 7.09-7.17 (4H, m, ArH), 7.26-7.28 (4H, m, ArH), 7.33-7.43 (12H, m, ArH), 7.53-7.60 (2H, m, ArH), 7.30-7.87 (4H, m, ArH), 8.49 (2H, d, ArH), 11.41 (1H, br s, NH);  $\delta_{\text{C}}$  (100 MHz;  $\text{CDCl}_3$ ) 39.4 ( $\text{NHCH}_2\text{CH}_2$ ), 44.4 ( $\text{NHCH}_2\text{CH}_2$ ), 93.6 ( $\text{NHC}=\text{CH}$ ), 121.6, 123.6, 127.0, 127.6, 128.1, 128.5, 129.4, 130.6, 135.6, 136.4, 140.35, 149.5, 158.2, 166.7 and 188.4 (ArC,  $\text{NHC}=\text{C}$  and  $\text{C}=\text{N}$ ).

*1-Phenyl-N,N'-bis[2-(2-pyridyl)ethyl]butane-1,3-diimine 81<sup>s</sup>*

To a solution of benzoylacetone **75** (0.80 g, 4.9 mmol) in CHCl<sub>3</sub> (10 mL) was added 2-(2-aminoethyl)pyridine **51** (1.2 mL, 9.9 mmol), and the reaction mixture was boiled under reflux for 76 h. The reaction was monitored by TLC and completion was confirmed. The CHCl<sub>3</sub> was removed under reduced pressure, and the residue was chromatographed [flash chromatography on silica; elution with MeOH-CHCl<sub>3</sub>-hexane (1:4:1)] to afford, as a light-brown oil, *1-phenyl-N,N'-bis[2-(2-pyridyl)ethyl]butane-1,3-diimine 81* (0.77 g, 43%) (Found: **MH**<sup>+</sup>, 371.2235. C<sub>24</sub>H<sub>26</sub>N<sub>4</sub> requires *MH*, 371.2236); δ<sub>H</sub>(400 MHz; CDCl<sub>3</sub>) 1.97 (3H, s, CH<sub>3</sub>), 3.09 (4H, t, NHCH<sub>2</sub>CH<sub>2</sub>), 3.76 (4H, q, NHCH<sub>2</sub>CH<sub>2</sub>), 5.60 (1H, s, NHC=CH), 7.14 (2H, m, ArH), 7.20 (2H, d, ArH), 7.33-7.43 (3H, m, ArH), 7.59 (2H, td, ArH), 7.82 (2H, m, ArH), 8.56 (2H, d, ArH), 11.49 (1H, br s, NH); δ<sub>C</sub>(100 MHz; CDCl<sub>3</sub>) 19.2 (CH<sub>3</sub>), 38.8 (NHCH<sub>2</sub>CH<sub>2</sub>), 42.9 (NHCH<sub>2</sub>CH<sub>2</sub>), 92.1 (NHC=CH), 121.7, 123.7, 126.8, 128.0, 130.3, 136.5, 140.4, 149.6, 158.2, 164.7 and 187.7 (ArC, NHC=C and C=N).

*N,N'-Bis[2-(2-pyridyl)ethyl]hexane-2,5-diimine 84*

2-(2-Aminoethyl)pyridine **51** (0.84 mL, 7.0 mmol) was added to a solution of acetonylacetone **82** (0.41 mL, 3.5 mmol) in CHCl<sub>3</sub> (5 mL), and the resulting mixture was boiled under reflux for 2.5 d, completion of the reaction being confirmed by TLC. The solvent was removed under reduced pressure, and the residual material was chromatographed [flash chromatography on silica gel; elution with MeOH-EtOAc(1:8)] to give, as a brown oil, *N,N'-bis[2-(2-pyridyl)ethyl]hexane-2,5-diimine 84* (0.68 g, 60%) (Found: **MH**<sup>+</sup>, 323.2236. C<sub>20</sub>H<sub>26</sub>N<sub>4</sub> *MH*, requires 323.2236); ν<sub>max</sub>(NaCl/cm<sup>-1</sup>) 1652 (C=N); δ<sub>H</sub>(400 MHz; 2.13 (6H, s, CH<sub>3</sub>), 3.06 (4H, t, CH<sub>2</sub>CH<sub>2</sub>N), 4.13 (4H, t, CH<sub>2</sub>CH<sub>2</sub>N), 5.74 (4H, s, N=CCH<sub>2</sub>), 6.92 (2H, d, ArH), 7.12-7.18 (2H, m, ArH), 7.55 (2H, td, ArH), 8.57 (2H, d, ArH); δ<sub>C</sub>(100 MHz; CDCl<sub>3</sub>) 12.3 (CH<sub>3</sub>), 39.6 (CH<sub>2</sub>CH<sub>2</sub>C=N), 43.4 (CH<sub>2</sub>CH<sub>2</sub>C=N), 105.2 (NCH<sub>2</sub>CH<sub>2</sub>), 121.7, 123.6, 127.4, 136.5 (ArC), 149.5 and 158.6 (ArC and C=N).

---

**1,5-Diphenyl-N,N'-bis[2-(2-pyridyl)ethyl]pentane-1,5-diimine **85******Attempted preparation**

1,3-Dibenzoylpropane **83** (0.8 g, 3 mmol) and 2-(2-aminoethyl)pyridine **51** (0.76 mL, 6.3 mmol) were added to  $\text{CHCl}_3$  (10 mL), and the resulting mixture was boiled under reflux for ca. 3.5 d. Completion of the reaction was confirmed by TLC. The solvent was evaporated under reduced pressure, and the residual material was chromatographed [flash chromatography on silica gel; elution with MeOH-benzene-hexane (1:4:1)] to yield a red-brown oil,  $^1\text{H}$  NMR analysis of which indicated the absence of the required product.

### 3.2.4 The Baylis-Hillman approach to ligand synthesis

#### *3-Hydroxy-2-methylene-3-(2-pyridyl)propanenitrile 92*<sup>149</sup>

A mixture of pyridine-2-carbaldehyde **91** (2.95 g, 28 mmol), acrylonitrile (1.54 g, 29 mmol) and DABCO (0.15 g, 1.3 mmol) in  $\text{CHCl}_3$  (2 mL) was allowed to stand at room temperature for 4 d. The solvent was evaporated, and the residue chromatographed (flash chromatography on silica gel; elution with EtOAc) to afford, as colourless crystals, 3-hydroxy-2-methylene-3-(2-pyridyl)propanenitrile **92** (4.09 g, 91%), mp 65–66°C (from hexane) (lit.<sup>149</sup> 66–67°C);  $\nu_{\text{max}}$ (thin film/ $\text{cm}^{-1}$ ) 3220 (OH) 2227 (CN) and 1600 (C=N);  $\delta_{\text{H}}$ ( $\text{CDCl}_3$ ) 5.28 (2H, 2 x overlapping s, CHOH and OH), 5.99 and 6.15 (2H, 2 x s, C=CH<sub>2</sub>), 7.23 (1H, m, 5'-H), 7.38 (1H, d, 3'-H), 7.71 (1H, m, 4'-H) and 8.49 (1H, m, 6'-H).

#### *3-Acetoxy-2-methylene-3-(2-pyridyl)propanenitrile 93*<sup>149</sup>

A mixture of  $\text{Ac}_2\text{O}$  (5 mL) and 3-hydroxy-2-methylene-3-(2-pyridyl)propanenitrile **92** (1.0 g, 6.2 mmol) was heated at 100°C for 30 min. in a flask fitted with a reflux condenser and drying tube. After cooling, the mixture was poured on to  $\text{NaHCO}_3$ -ice and, after stirring for 30 min., extracted with  $\text{Et}_2\text{O}$  (2 x 100 mL). The combined extracts were washed with aqueous  $\text{NaHCO}_3$  (100 mL) and dried over anhydrous  $\text{MgSO}_4$ . The solvent was removed under reduced pressure, and the residue was chromatographed [flash chromatography on silica gel; elution with EtOAc-hexane (5:5)] to give, as a yellow oil, 3-acetoxy-2-methylene-3-(2-pyridyl)propanenitrile **93** (0.75 g, 60%);  $\nu_{\text{max}}$ (thin film  $\text{cm}^{-1}$ ) 2226 (CN) and 1748 (CO);  $\delta_{\text{H}}$ (400 MHz;  $\text{CDCl}_3$ ) 2.21 (3H, s,  $\text{CH}_3\text{CO}$ ), 6.14 and 6.17 (2H, 2 x s, C=CH<sub>2</sub>), 6.38 (1H, s, CHOAc), 7.28 (1H, m, 5'-H), 7.48 (1H, d, 3'-H), 7.76 (1H, m, 4'-H), 8.60 (1H, m, 6'-H).

#### *2-[(1-Piperidiny)methyl]-3-(2-pyridyl)prop-2-enenitrile 96*

Piperidine (0.64 g, 7.6 mmol) was added to a solution of 3-acetoxy-2-methylene-3-(2-pyridyl)propanenitrile **93** (1.5 g, 6.9 mmol) in THF (5 mL), and the resulting mixture was allowed to stand for 4 d at room temperature. Work-up, following the procedure described for preparing 3-(2-pyridyl)-1-[1-pyrrolidinyl)methyl]prop-2-enenitrile **97**, gave, as a brown oil, 2-[(1-piperidiny)methyl]-3-(2-pyridyl)-prop-2-

*enenitrile 96* (1.08 g, 69%) (Found:  $MH^+$ , 228.1500.  $C_{14}H_{17}N_3$  requires  $MH$ , 228.1500);  $\nu_{max}$ (thin film/ $cm^{-1}$ ) 2217 (CN);  $\delta_H$ (400 MHz;  $CDCl_3$ ) 1.40-1.47 (2H, m,  $CH_2$ ), 1.55-1.65 (4H, m, 2 x  $CH_2$ ), 2.49 (4H, m, 2 x  $CH_2$ ), 3.29 (2H, d,  $CH_2$ ), 7.23 (1H, CH=C), 7.28 (1H, m, ArH), 7.73 (1H, td, ArH), 7.86 (1H, d, ArH), 8.65 (1H, d, ArH);  $\delta_C$ (400 MHz;  $CDCl_3$ ) 24.1 ( $CH_2$ ), 25.9 ( $CH_2$ ), 54.2 ( $CH_2$ ), 62.9 ( $CH_2$ ), 112.9 (CH=C), 118.2 (CN), 123.5 (ArC), 124.1 (ArC), 136.7 (ArC), 144.0 (CH=C), 149.9 (ArC) and 152.1 (ArC).

*3-(2-Pyridyl)-2-[1-pyrrolidiny]methyl]prop-2-enitrile 97*

A mixture of pyrrolidine (0.18 g, 2.5 mmol) and 3-acetoxy-2-methylene-3-(2-pyridyl)propanenitrile **93** (0.50 g, 2.3 mmol) in THF (2mL) was allowed to stand at room temperature for 4 d. The solvent was removed under reduced pressure, and the residue was washed with NaOH (50 mL) and extracted with  $CHCl_3$  (3 x 40 mL). The combined extracts were dried with anhydrous  $MgSO_4$ , and the solvent was evaporated under reduced pressure to give, as a brown oil, *3-(2-pyridyl)-2-[1-pyrrolidiny]methyl]prop-2-enitrile 94* (0.39 g, 80%) (Found:  $MH^+$ , 214.1344.  $C_{13}H_{15}N_3$  requires  $MH$ , 214.1344);  $\nu_{max}$ (thin film/ $cm^{-1}$ ) 2217 (CN);  $\delta_H$ (400 MHz;  $CDCl_3$ ) 1.81 (4H, s, 2 x  $CH_2$ ), 2.62 (4H, s, 2 x  $CH_2$ ), 3.44 (2H, s,  $CH_2$ ), 7.25-7.40 (2H, m, ArH and CH=C), 7.73 (1H, t, ArH), 7.82 (1H, d, ArH), 8.68 (1H, d, ArH);  $\delta_C$ (400 MHz;  $CDCl_3$ ) 23.7 ( $CH_2$ ), 53.8 ( $CH_2$ ), 59.8 ( $CH_2$ ), 113.4 (CH=C), 118.2 (CN), 123.5 (ArC), 124.1 (ArC), 136.7 (ArC), 143.6 (CH=C), 149.8 (ArC) and 152.0 (ArC).

*2,10-Dicyano-1,11-bis(2-pyridyl)-5,8-diazaundeca-1,11-diene 98*

Attempted preparation

A mixture of 3-acetoxy-2-methylene-3-(2-pyridyl)propanenitrile **93** (0.48 g, 7.3 mmol) and 1,3-diaminopropane (0.26 g, 3.7 mmol) in THF (6 mL) was allowed to stand at room temperature for 4 d. Completion of the reaction was confirmed by TLC, and the THF was removed under reduced pressure. The residual dark-brown oil was washed with aqueous  $NaHCO_3$  (70 mL) and brine (60 mL).  $^1H$  NMR

analysis of the fractions obtained by flash chromatography of the residue failed to indicate the presence of the required product.

### *2,9-Bis(2-cyano-1-hydroxy-2-propenyl)-1,10-phenanthroline 87*

#### Attempted preparations

##### Method 1

A mixture of 1,10-phenanthroline-2,9-dicarbaldehyde **66** (1.0 g, 4.2 mmol), acrylonitrile (0.46 g, 8.6 mmol) and DABCO (0.02 g, 0.4 mmol) in CHCl<sub>3</sub> (8 mL) was stirred at room temperature for 10 d. The CHCl<sub>3</sub> was removed *in vacuo* and the residue analysed by <sup>1</sup>H NMR spectroscopy. The characteristic peaks for the Baylis-Hillman product between δ5.0-6.5 ppm were not observed in the spectrum.

##### Method 2

A mixture of acrylonitrile (0.94 g, 18 mmol), 1,10-phenanthroline-2,9-dicarbaldehyde **66** (0.5 g, 2 mmol) and DABCO (0.02 g, 0.4 mmol) in CHCl<sub>3</sub> (22 mL) was boiled under reflux for 40 min., followed by stirring at room temperature for 7 d. After evaporating off the CHCl<sub>3</sub>, the residue was analysed by <sup>1</sup>H-NMR spectroscopy, but the characteristic peaks for the Baylis-Hillman product were not observed.

##### Method 3

A mixture of acrylonitrile (0.94 g, 18 mmol), 1,10-phenanthroline-2,9-dicarbaldehyde **66** (0.5 g, 2 mmol) and DABCO (0.02 g, 0.4 mmol) in CHCl<sub>3</sub> (22 mL) was stirred at room temperature for 7 d. After evaporating off the CHCl<sub>3</sub>, the residue was analysed by <sup>1</sup>H NMR spectroscopy, but the characteristic peaks for the Baylis-Hillman product were not observed.

##### Method 4

1,10-Phenanthroline-2,9-dicarbaldehyde **66** (1.0 g, 4.2 mmol) was dissolved in hot MeOH (110 mL) to give a clear yellow solution. DABCO (0.45 g, 9 mmol) and

---

acrylonitrile (0.94 g, 18 mmol) were added to the hot solution, and the resulting mixture was boiled under reflux for *ca.* 3.5 h. The MeOH was evaporated off under reduced pressure and the residue analysed by  $^1\text{H}$  NMR spectroscopy, which indicated that the reaction had been unsuccessful.

### 3.2.5 Macrocycle syntheses

#### *The dibenzo macrocycle 99*

A stirred mixture of 1,10-phenanthroline-2,9-dicarbaldehyde **66** (0.70 g, 3.0 mmol) and 1,2-diaminobenzene (0.35 g, 3.0 mmol) in MeOH (85 mL) was boiled under reflux for 5 min. The mixture was then stirred at room temperature for 12 h, during which time, a yellow solid precipitated, which was filtered off to give, as a cream powder, *the dibenzo macrocycle 99* (0.56 g, 30%) mp 239-241°C (Found:  $\text{MH}^+$  616.2122.  $\text{C}_{40}\text{H}_{24}\text{N}_8$  requires  $\text{MH}$ , 616.2124);  $\nu_{\text{max}}$  (KBr/ $\text{cm}^{-1}$ ) 1619 (C=N).

#### *The macrocycle 100*

##### Attempted preparations

##### Method 1<sup>162</sup>

1,10-Phenanthroline-2,9-dicarbaldehyde **66** (0.70 g, 3.0 mmol) was dissolved in MeOH (80 mL) by heating and stirring. The yellow solution was allowed to cool to room temperature and was then added dropwise, during 40 min., to a solution of 1,2-diaminoethane MeOH (50 mL). The mixture was then stirred for 12 h at room temperature. The MeOH was evaporated off *in vacuo* to afford a brown powder, which was insoluble in DMSO, and clearly not the expected product.

##### Method 2

1,2-Diaminoethane (0.18 g, 3.0 mmol) was added to a hot solution of 1,10-phenanthroline-2,9-dicarbaldehyde **66** (0.7 g, 3.0 mmol) in MeOH (70 ml), and the resulting mixture was boiled under reflux for 2.5 h. The MeOH was removed under reduced pressure to yield a brown powder, which was insoluble in DMSO, and was not the expected product.

### 3.2.6 Dendrimer-based ligands

#### *Tris(2-cyanoethyl)nitromethane 102*<sup>172</sup>

Acrylonitrile (3.98 g, 75 mmol) was added dropwise to a stirred solution of nitromethane **101** (1.52 g, 24.9 mmol) and 40% aqueous Triton B (trimethylbenzylammonium hydroxide) (0.25 g) in dioxan (2.50 g, 62.5 mmol) over a period of ca. 25 min. while maintaining the temperature of the exothermic reaction at 25-30°C by external cooling. The reaction mixture was then allowed to stand at room temperature for 18 h. Dilute HCl was used to neutralise (pH 7) the reaction mixture, which was then extracted with an equal volume of dichloroethane. The extract was washed with H<sub>2</sub>O (2.5 mL), and the dichloroethane evaporated off under reduced pressure. The crystalline product (2.15 g, 39%) was recrystallised from EtOH to give, as colourless prisms, tris(2-cyanoethyl)nitromethane **102**, mp 107-109°C (lit.<sup>172</sup> mp 114°C);  $\delta_c$ (100 MHz; MeOH-*d*<sub>4</sub>) 12.7 (CH<sub>2</sub>CH<sub>2</sub>CN), 31.4 (CH<sub>2</sub>CN), 92.3 (CNO<sub>2</sub>) and 119.7 (CN).

#### *4-[2-Carboxyethyl]-4-nitroheptanedioic acid 103*<sup>172</sup>

Tris(2-cyanoethyl)nitromethane **102** (1.5 g, 6.8 mmol) was dissolved in concentrated HCl (6.5 mL), and the resulting solution boiled under reflux for 45 min., and then cooled to 5°C. The white solid which precipitated out was filtered off, washed with cold H<sub>2</sub>O (4 x 15 mL) and dried *in vacuo* to yield 4-[2-carboxyethyl]-4-nitroheptanedioic acid **103** (1.25 g, 66%), mp 186-187°C (lit.<sup>172</sup> mp 186°C);  $\nu_{\max}$ (KBr/cm<sup>-1</sup>) 1721 (C=O), 2500-3500 (OH);  $\delta_c$ (100 MHz; MeOH-*d*<sub>4</sub>) 29.4 (CH<sub>2</sub>CH<sub>2</sub>CO<sub>2</sub>H), 31.5 (CH<sub>2</sub>CO<sub>2</sub>H), 93.9 (CNO<sub>2</sub>) and 175.6 (C=O).

#### *4-Nitro-4-(3-hydroxypropyl)-1,7-heptanediol 104*<sup>172</sup>

To a stirred solution of the triacid, 4-[2-carboxyethyl]-4-nitroheptanedioic acid **103** (1.0 g, 3.6 mmol) in dry THF (50 mL) at 0°C, a BH<sub>3</sub>-THF solution (1.0 M; 11.9 mL, 11.9 mmol) was added dropwise. The temperature was allowed to rise to 25°C once the white precipitate had formed. After stirring for another 30 min., H<sub>2</sub>O was slowly added until the solid had dissolved. Saturated NaHCO<sub>3</sub> was then added and

the solvent was removed under reduced pressure. The residual oil was dried *in vacuo*, and the resultant solid triturated with hot EtOH (3 x 60 mL), the ethanolic solution being filtered in each case. The combined extracts were concentrated under reduced pressure to give 4-nitro-4-(3-hydroxypropyl)-1,7-heptanediol **104** (0.78 g, 93%);  $\nu_{\max}(\text{KBr}/\text{cm}^{-1})$  3040-3575 (OH);  $\delta_{\text{c}}(100 \text{ MHz}; \text{MeOH}-d_4)$  26.6 ( $\text{CH}_2\text{CH}_2\text{OH}$ ), 31.7 ( $\text{CH}_2\text{CH}_2\text{CH}_2\text{OH}$ ), 60.3 ( $\text{CH}_2\text{OH}$ ) and 94.5 ( $\text{CNO}_2$ ).

#### *4-Amino-4-(3-hydroxypropyl)-1,7-heptanediol 105*<sup>172</sup>

A mixture of T-1 Raney Ni (ca. 3.0 g), nitro triol **104** (2.5 g, 10.6 mmol) and absolute EtOH (100 mL) was shaken under  $\text{H}_2$  in a Parr hydrogenator at 3 atm for 3 d. The catalyst was cautiously removed by filtering the mixture through celite. The solvent was then removed under reduced pressure, and the residual oil was dried *in vacuo* to yield, as a semi-solid, 4-amino-4-(3-hydroxypropyl)-1,7-heptanediol **105**, shown by  $^1\text{H}$  NMR spectroscopy to be eventually pure, (1.67 g, 77%);  $\delta_{\text{H}}(400 \text{ MHz}; \text{DMSO}-d_6)$  1.20-1.26 (6H, m,  $\text{CH}_2\text{CH}_2\text{OH}$ ), 1.32-1.42 (6H, m,  $\text{CH}_2\text{CH}_2\text{CH}_2\text{OH}$ ), 3.35 (6H, t,  $\text{CH}_2\text{OH}$ ), 4.61 (3H, br s, OH);  $\delta_{\text{c}}(100 \text{ MHz}; \text{DMSO}-d_6)$  26.7 ( $\text{CH}_2\text{CH}_2\text{OH}$ ), 36.2 ( $\text{CH}_2\text{CH}_2\text{CH}_2\text{OH}$ ), 52.1 ( $\text{CNH}_2$ ) and 61.6 ( $\text{CH}_2\text{OH}$ ).

#### *Preparation of the T-1 Raney nickel catalyst*<sup>173</sup>

Raney nickel-aluminium alloy (50%; 20 g) was added in small portions during ca. 25 min. to a stirred aqueous NaOH solution (10%, 300 mL). The temperature was maintained at 90-95°C during the addition. Once the addition was complete, the mixture was stirred for 1 h, after which the nickel was allowed to settle, and the supernatant solution was decanted. The residue was washed with water (5 x 100 mL) and then with EtOH (5 x 25 mL). The washing was done in such a way that the catalyst was always covered with liquid. The catalyst was then kept under EtOH and stored under refrigeration.

#### *The dendrimer-based ligand 112*

To a hot solution of 1,10-phenanthroline-2,9-dicarbaldehyde **66** (0.57 g, 2.4 mmol) in absolute EtOH (60 mL) was added a solution of 4-amino-4-(3-hydroxypropyl)-

1,7-heptanediol **105** (1.0 g, 4.9 mmol) in EtOH (30 mL), and the resulting mixture was boiled under reflux for ca. 20 min. The completion of the reaction was confirmed by IR spectroscopy. The solvent was removed under reduced pressure to yield, as a brown oil, the *dendrimer-based ligand* **112** (1.4 g, 96%) (Found:  $MNa^+$ , 633.3627.  $C_{34}H_{50}N_4O_6$  requires  $MNa$ , 633.3628);  $\nu_{max}$  (KBr/cm<sup>1</sup>) 1647 (C=N);  $\delta_H$  (400 MHz; DMSO-*d*<sub>6</sub>) 1.37 (24H, s, CH<sub>2</sub>CH<sub>2</sub>CH<sub>2</sub>OH), 1.64 (12H, s, CH<sub>2</sub>OH), 4.44 (6H, br s, OH), 8.09 (2H, s, CH=N), 8.36 (2H, d, ArH), 8.53 (2H, d, ArH) and 8.62 (2H, s, ArH);  $\delta_C$  (100 MHz; DMSO-*d*<sub>6</sub>) 29.1 (CH<sub>2</sub>CH<sub>2</sub>OH), 33.2 (CH<sub>2</sub>CH<sub>2</sub>CH<sub>2</sub>OH), 63.5 (CH<sub>2</sub>OH), 94.5, 119.6 (ArC), 127.3 (ArC), 129.34 (ArC), 137.1 (ArC), 144.8 (ArC) and 154.8 (ArC) and 157.5 (C=N).

*2,9-Dimethyl-1,10-phenanthroline-5,6-dione* **109**<sup>175,176</sup> - attempted synthesis

To a mixture of neocuproine **64** (2.5 g, 12 mmol) and NaBr (2.5 g), was added an ice cold mixture of H<sub>2</sub>SO<sub>4</sub> (30 mL) and HNO<sub>3</sub> (15 mL). The resulting mixture was then boiled under reflux for 3 h. The hot solution was added to 400 mL of ice and neutralised very cautiously with NaOH until neutral or slightly acidic. The resulting mixture was extracted with CHCl<sub>3</sub> and the extract dried with anhydrous MgSO<sub>4</sub>. The solvent was removed under reduced pressure, and analysis of the residue revealed that the central ring in neocuproine was still intact.

*The monoketone* **111**<sup>174</sup> - attempted synthesis

To a boiling solution of neocuproine **64** (2.0 g) and KOH (1.0 g) in H<sub>2</sub>O (150 mL) was added, in portions with stirring, a hot solution of KMnO<sub>4</sub> (5.0 g) in H<sub>2</sub>O (80 mL). The reaction mixture was then boiled under reflux for 1.5 h and filtered while hot; the brown cake was washed with H<sub>2</sub>O (120 mL). The orange filtrate and washings were extracted with CHCl<sub>3</sub> (3 x 60 mL), and the combined extracts dried with anhydrous MgSO<sub>4</sub>. The CHCl<sub>3</sub> was evaporated off under reduced pressure. The residue was analysed by <sup>1</sup>H NMR spectroscopy, which indicated that oxidation of the central ring of neocuproine had not occurred.

### 3.3 SYNTHETIC PROCEDURES FOR THE PREPARATION OF COMPLEXES

#### 3.3.1 Copper Complexes<sup>‡</sup>

##### Preparation of tetrakis(acetonitrile)copper(I) hexafluorophosphate

Copper (I) oxide (4.0 g, 28 mmol) was dissolved in MeCN (80 mL) and stirred under N<sub>2</sub> in a closed flask fitted with a pressure-compensating dropping funnel. An aqueous solution of HPF<sub>6</sub> (60-65%; 10 mL, 113 mL) was added from the funnel, and the mixture was stirred for at least 5 min. The mixture was then filtered and cooled to -20°C to precipitate the crude product, which was recrystallised by redissolving in MeCN (100 mL) and adding Et<sub>2</sub>O (100 mL), followed by cooling for approximately 6 h. The white crystalline complex [Cu(MeCN)<sub>4</sub>][PF<sub>6</sub>] (9.1 g, 44%) was filtered off, dried under reduced pressure and stored at 4°C under N<sub>2</sub> in a sealed container placed in a desiccator.

##### *Biphenyl and 1,10-phenanthroline complexes*

###### *The copper complex 115*

A clear, pink solution of 2,2'-bis[[2-(2-benzimidazolyl)ethylamino]carbonyl]biphenyl **55b** (0.23 g, 0.44 mmol) in hot, dry, degassed DMF (20 mL) was added dropwise to a stirred solution of [Cu(MeCN)<sub>4</sub>][PF<sub>6</sub>] (0.34 g, 0.92 mmol) in dry, degassed MeCN (10 mL). The resulting pale yellow-green solution gradually changed to a clear green colour as the reaction mixture was stirred under N<sub>2</sub> for 3.5 h. The addition of Et<sub>2</sub>O resulted in the precipitation of *the copper complex 115* as a light-green, polymeric solid (0.30 g), mp 198-202°C;  $\nu_{\max}$  (HCBd/cm<sup>-1</sup>) 3237 (amide NH);  $\nu_{\max}$  (nujol/cm<sup>-1</sup>) 1651 (CO) and 845 (PF<sub>6</sub>).

<sup>‡</sup> See Table 8 (p.84) for microanalysis data.

*The copper complex 116*

A solution of  $[\text{Cu}(\text{MeCN})_4][\text{PF}_6]$  (0.34 g, 0.92 mmol) in dry, degassed MeCN (10 mL) was added to a hot solution of 2,2'-bis[[2-(4-imidazolyl)ethylamino]carbonyl]biphenyl **55c** (0.19 g, 0.44 mmol) in a mixture of dry, degassed DMF (10 mL) and dry, degassed MeCN (20 mL). The reaction mixture turned blue and, upon addition of  $\text{Et}_2\text{O}$ , *the copper complex 116* precipitated out as a light-green solid (0.17g), mp 212-214°C;  $\nu_{\text{max}}(\text{HCBBD}/\text{cm}^{-1})$  3242 (amide NH) and 3156 (imidazole NH);  $\nu_{\text{max}}(\text{nujol}/\text{cm}^{-1})$  1652 (CO) and 846 ( $\text{PF}_6$ ).

*Attempted preparation of the biphenyl dicopper complex 117*

A colourless solution of  $[\text{Cu}(\text{MeCN})_4][\text{PF}_6]$  (0.34 g, 0.92 mmol) in dry, degassed MeCN (10 mL) was added to an almost colourless solution of 2,2'-bis[[2-(2-pyridyl)ethylamino]carbonyl]biphenyl **55a** (0.20 g, 0.44 mmol) in dry, degassed MeCN (4 mL). No colour change was observed when the ligand solution was added dropwise to the solution of the Cu(I) reagent, but a solid precipitated out of the reaction mixture during stirring under  $\text{N}_2$  for 3.5 h. The solid was filtered off and  $\text{Et}_2\text{O}$  was added to the filtrate to precipitate out more of the product. The microanalysis results were not consistent with formation of the expected product.

*The copper complex 118a*

2,9-Bis[[2-(2-pyridyl)ethylamino]carbonyl]-1,10-phenanthroline **69a** (0.20 g, 0.44 mmol) was dissolved in a mixture of hot, dry, degassed DMF (10 mL) and MeCN (15 mL). Dropwise addition of this solution to a colourless solution of  $[\text{Cu}(\text{MeCN})_4][\text{PF}_6]$  (0.34 g, 0.92 mmol) in dry, degassed MeCN (10 mL) gave a dark-red mixture, the colour of which changed to dirty green upon stirring under  $\text{N}_2$  for 6 h. The precipitated solid was filtered off and  $\text{Et}_2\text{O}$  was added to the filtrate to precipitate out the remainder of *the copper complex 118a*, which was filtered off as a green powder (0.27 g), mp >230°C;  $\nu_{\text{max}}(\text{nujol}/\text{cm}^{-1})$  1630 (CO) and 842 ( $\text{PF}_6$ ).

*The copper complex 118b*

A brown solution of 2,9-bis[[2-(2-benzimidazolyl)ethylamino]carbonyl]-1,10-phenanthroline **69b** (0.25 g, 0.44 mmol) in hot, dry, degassed DMF (20 mL) was added to a colourless solution of  $[\text{Cu}(\text{MeCN})_4][\text{PF}_6]$  (0.34 g, 0.92 mmol) in dry, degassed MeCN (10 mL). The initially dark-red colour changed to green-brown and later to light-green during stirring under  $\text{N}_2$  for 4.5 h.  $\text{Et}_2\text{O}$  was added to precipitate *the copper complex 118b* as a green-brown solid (0.29 g), mp  $>230^\circ\text{C}$ ;  $\nu_{\text{max}}(\text{HCBD}/\text{cm}^{-1})$  3227 (NH);  $\nu_{\text{max}}(\text{nujol}/\text{cm}^{-1})$  1645 (CO) and 846 ( $\text{PF}_6$ ).

*The copper complex 118c*

A hot, dark-brown solution of 2,9-bis[[2-(4-imidazolyl)ethylamino]carbonyl]-1,10-phenanthroline **69c** (0.19 g, 0.44 mmol) in dry, degassed DMF (20 mL) was added dropwise to a colourless solution of  $[\text{Cu}(\text{MeCN})_4][\text{PF}_6]$  (0.34 g, 0.92 mmol) in dry, degassed MeCN (10 mL). The solution became dark red-brown in colour when stirred under  $\text{N}_2$  for 5.5 h. Addition of  $\text{Et}_2\text{O}$  precipitated *the copper complex 118c* as a brown solid (0.15 g), mp  $>230^\circ\text{C}$ ;  $\nu_{\text{max}}(\text{HCBD}/\text{cm}^{-1})$  3157;  $\nu_{\text{max}}(\text{nujol}/\text{cm}^{-1})$  1651 (CO) and 845 ( $\text{PF}_6$ ).

*The copper complex 119*

A solution of 2,9-bis[[2-(2-pyridylethylamino)methyl]-1,10-phenanthroline] **68a** (0.20 g, 0.44 mmol) in dry, degassed MeCN (50 mL) was added dropwise to a solution of  $[\text{Cu}(\text{MeCN})_4]\text{PF}_6$  (0.34 g, 0.44 mmol) in dry, degassed MeCN (10 mL). The reaction mixture was stirred for 1.5 h under  $\text{N}_2$  before adding  $\text{Et}_2\text{O}$  to precipitate, as a brown solid, *the copper complex 119* (0.38 g, 78%), mp  $>230^\circ\text{C}$ ;  $\nu_{\text{max}}(\text{HCBD}/\text{cm}^{-1})$  3273 (NH);  $\nu_{\text{max}}(\text{nujol}/\text{cm}^{-1})$  842 ( $\text{PF}_6$ ).

**Schiff base complexes and the macrocyclic complex*****The copper complex 120***

To a stirred solution of  $\text{Cu(II)(NO}_3)_2 \cdot 3\text{H}_2\text{O}$  (0.47 g, 1.95 mmol) in MeCN (3.5 mL), *N,N'*-bis[2-(2-pyridyl)ethyl]pentane-2,4-diimine **76** (0.30 g, 0.97 mmol) in MeCN (3.5 mL) was added dropwise. The colour of the reaction mixture changed from turquoise to dark green during the addition. The reaction mixture was stirred for 3 d before  $\text{Et}_2\text{O}$  was added and *the copper complex 120* separated out as a green, hygroscopic oil (0.68 g, 87%);  $\nu_{\text{max}}$ (KBr/ $\text{cm}^{-1}$ ) 1638 (C=N) and 1383 ( $\text{NO}_3$ ).

***The copper complex 121***

A solution of 3-methyl-*N,N'*-bis[2-(2-pyridyl)ethyl]pentane-2,4-diimine **77** (0.20 g, 0.62 mmol) in MeCN (2 mL) was added dropwise to a stirred solution of  $\text{Cu(II)(NO}_3)_2 \cdot 3\text{H}_2\text{O}$  (0.30 g, 1.2 mmol) in MeCN (2.5 mL). The reaction mixture changed from turquoise to dark green in colour during the addition. After stirring for 3 d,  $\text{Et}_2\text{O}$  was added to precipitate the crude complex, which was redissolved in MeCN. Evaporation of the solvent under reduced pressure yielded, as a green, hygroscopic semi-solid, *the copper complex 121* (0.36 g, 58%);  $\nu_{\text{max}}$ (KBr/ $\text{cm}^{-1}$ ) 1637 (C=N), 1480, 1445, 1315, 1283 and 1013 ( $\text{NO}_3$ ).

***The copper complex 122 - attempted synthesis***

A solution of 3-ethyl-*N,N'*-bis[2-(2-pyridyl)ethyl]pentane-2,4-diimine **78** (0.30 g, 0.89 mmol) in MeCN (3 mL) was added dropwise to a stirred solution of  $\text{Cu(II)(NO}_3)_2 \cdot 3\text{H}_2\text{O}$  (0.43 g, 1.78 mmol) in MeCN (2 mL). The colour changed from turquoise to dark blue and, after 3 d,  $\text{Et}_2\text{O}$  was added to affect separation of the copper complex. Microanalysis of the resulting green hygroscopic semi-solid indicated that the expected complex had not been obtained.

*The copper complex 123*

A solution of 3-benzyl-*N,N'*-bis[2-(2-pyridyl)ethyl]pentane-2,4-diimine **79** (0.30 g, 0.75 mmol) in MeCN (3 mL) was added dropwise to a stirred solution of Cu(II)(NO<sub>3</sub>)<sub>2</sub>·3H<sub>2</sub>O (0.36 g, 1.5 mmol) in MeCN (3 mL). The colour of the reaction mixture changed from turquoise to dark-green, and stirring was continued for 3 d before Et<sub>2</sub>O was added to effect separation of *the copper complex 123* as a green, hygroscopic, semi-solid (0.41 g, 58%);  $\nu_{\max}$ (KBr/cm<sup>-1</sup>) 1638 (C=N), 1483, 1383 and 1288 (NO<sub>3</sub>).

*The macrocyclic copper complex 124*

A solution of macrocycle **99** (0.35 g, 1.1 mmol) in DMF (8 mL) was added to a stirred solution of Cu(II)(NO<sub>3</sub>)<sub>2</sub>·3H<sub>2</sub>O (0.52 g, 2.17 mmol) in DMF (4 mL). The colour changed from turquoise to red-brown and, after stirring for 2.5 d, Et<sub>2</sub>O was added to precipitate, as a dark-brown solid, *the macrocyclic copper complex 124* (0.38 g, 35%), mp >250°C;  $\nu_{\max}$ (KBr/cm<sup>-1</sup>) 1653 (C=N) and 1383 (NO<sub>3</sub>).

*Attempted preparation of the copper complex 125*

A solution of 1-phenyl-*N,N'*-bis[2-(2-pyridyl)ethyl]butane-1,3-diimine **81** (0.20 g, 0.54 mmol) in MeCN (3 mL) was added dropwise with stirring to a solution of Cu(II)(NO<sub>3</sub>)<sub>2</sub>·3H<sub>2</sub>O (0.26 g, 1.1 mmol) in MeCN (2 mL). A colour change from turquoise to dark-green was observed during the addition and, after stirring for 3 d, Et<sub>2</sub>O was added to precipitate the crude product which was redissolved in MeCN. Evaporation of the solvent under reduced pressure gave a green, crystalline material, microanalysis of which indicated that the desired complex had not been formed.

*Attempted preparation of the copper complex 126*

A solution of 1,3-diphenyl-*N,N'*-bis[2-(2-pyridyl)ethyl]propane-1,3-diimine **80** (0.40 g, 0.93 mmol) in MeCN (5 mL), was added dropwise to a stirred solution of Cu(II)(NO<sub>3</sub>)<sub>2</sub>·3H<sub>2</sub>O (0.45 g, 1.9 mmol) in MeCN (3 mL). The reaction mixture was

stirred for 1 d before adding Et<sub>2</sub>O to precipitate out the product, microanalysis of which indicated that the expected complex had not been formed.

#### *Attempted preparation of the dicopper complex 127*

A solution of *N,N'*-bis[2-(2-pyridyl)ethyl]hexane-2,5-diimine **84** (0.30 g, 0.93 mmol) in MeCN (5 mL) was added dropwise to a stirred solution of Cu(II)(NO<sub>3</sub>)<sub>2</sub>·3H<sub>2</sub>O (0.45 g, 1.9 mmol) in MeCN (3 mL). After stirring the reaction mixture for 2 d, Et<sub>2</sub>O was added to precipitate out the product, microanalysis of which indicated that the expected complex had not been formed.

### 3.3.2 Cobalt Complexes<sup>§</sup>

#### *The cobalt complex 133*

To a stirred solution of CoCl<sub>2</sub>·6H<sub>2</sub>O (0.22 g, 0.92 mmol) in MeOH (5 mL), a solution of 2,2'-bis[[2-(2-pyridyl)ethylamino]carbonyl]biphenyl **56a** (0.20 g, 0.44 mmol) in MeCN (5 mL) was added dropwise, and the resulting mixture was stirred for 48 h. Et<sub>2</sub>O was then added to precipitate *the cobalt complex 133* as a blue solid (0.21 g, 66%), mp 198-200°C;  $\nu_{\max}$ (KBr/cm<sup>-1</sup>) 1622 (CO);  $\nu_{\max}$ (nujol/cm<sup>-1</sup>) 306 (Co-Cl).

#### *The cobalt complex 134*

A clear, colourless solution of 2,2'-bis[[2-(2-benzimidazolyl)ethylamino]carbonyl]biphenyl **55b** (0.23 g, 0.44 mmol) in hot DMF (20 mL) was added to a stirred, blue solution of CoCl<sub>2</sub>·6H<sub>2</sub>O (0.22 g, 0.92 mmol) in MeOH (5 mL) and stirred for 25 h. The volume of the reaction mixture was reduced to less than half the original volume by evaporating off the solvents under reduced pressure, and Et<sub>2</sub>O was added to precipitate, as a blue solid, *the cobalt complex 134* (0.24 g, 59%), mp >230°C;

<sup>§</sup> See Table 12 (p.102) for microanalysis data.

$\nu_{\max}$ (KBr/cm<sup>-1</sup>) 3185 (amide NH) and 1633 (CO);  $\nu_{\max}$ (nujol/cm<sup>-1</sup>) 295 (Co-Cl).

*The cobalt complex 135* - attempted preparation

A solution of 2,2'-[[2-(4-imidazolyl)ethylamino]carbonyl]biphenyl **55c** (0.20 g, 0.46 mmol) in MeOH (10 mL) was added to a stirred solution of CoCl<sub>2</sub>·6H<sub>2</sub>O (0.23 g, 0.96 mmol) in MeOH (5 mL). After stirring for 48 h, during which time the colour changed from light-blue to dark-blue, Et<sub>2</sub>O was added to precipitate the product. Microanalysis of the resulting dark-blue hygroscopic semi-solid indicated that the desired complex had not been obtained.

*The cobalt complex 136*

A solution of 1-[2-(2-pyridyl)ethyl]dibenzo[*c,e*]perhydroazepine **61a** (0.19 g, 0.44 mmol) in MeCN (5 mL) was added dropwise to a solution of CoCl<sub>2</sub>·6H<sub>2</sub>O (0.22 g, 0.92 mmol) in MeCN (10 mL), and the resulting mixture was stirred for 48 h. The MeCN was allowed to evaporate off at room temperature, during which time, blue crystals of *the cobalt complex 136* precipitated and were filtered off (0.17 g, 89%), mp >250°C;  $\nu_{\max}$ (nujol/cm<sup>-1</sup>) 298 (Co-Cl).

*The cobalt complex 137a*

A solution of 2,9-bis[[2-(2-pyridyl)ethylamino]carbonyl]-1,10-phenanthroline **69a** (0.20 g, 0.44 mmol) in a mixture of hot MeOH (10 mL) and MeCN (5 mL) was added dropwise to a purple solution of CoCl<sub>2</sub>·6H<sub>2</sub>O (0.22 g, 0.92 mmol) in MeOH (4 mL). The colour of the reaction mixture changed to dark-green during stirring for 22.5 h. The reaction mixture was concentrated *in vacuo* to half the original volume. Et<sub>2</sub>O was added to precipitate, as a green solid, *the cobalt complex 137a* (0.26 g, 100%), mp 78°C;  $\nu_{\max}$ (KBr/cm<sup>-1</sup>) 3274 (NH) and 1645 (CO);  $\nu_{\max}$ (nujol/cm<sup>-1</sup>) 303 (Co-Cl).

*The cobalt complex 137b*

A solution of 2,9-bis[[2-(2-benzimidazolyl)ethylamino]carbonyl]-1,10-phenanthroline

**69b** (0.23 g, 0.40 mmol) in DMF (10mL) was added dropwise to a solution of  $\text{CoCl}_2 \cdot 6\text{H}_2\text{O}$  (0.20 g, 0.84 mmol) in DMF (5mL). The resulting mixture was stirred for 52 h, during which time, the colour changed from purple-blue to dark-green. The volume of the reaction mixture was reduced to less than half by evaporating off the solvent under reduced pressure. The subsequent addition of  $\text{Et}_2\text{O}$  resulted in the precipitation of *the cobalt complex 137b* as a green powder (0.32 g, 57%), mp  $>230^\circ\text{C}$ ;  $\nu_{\text{max}}(\text{KBr}/\text{cm}^{-1})$  3251 (amide NH) and 1651 (CO);  $\nu_{\text{max}}(\text{nujol}/\text{cm}^{-1})$  311 (Co-Cl).

#### *The cobalt complex 137c*

A solution of 2,9-bis{[2-(4-imidazolyl)ethylamino]carbonyl}-1,10-phenanthroline **69c** (0.19 g, 0.44 mmol) in hot DMF (15 mL) was added to a stirred solution of  $\text{CoCl}_2 \cdot 6\text{H}_2\text{O}$  (0.22 g, 0.92 mmol) in DMF (10 mL), resulting in a dark-green mixture. After stirring for 41 h, the volume of the reaction mixture was reduced to less than half by evaporating off the DMF under reduced pressure. This was followed by the addition of  $\text{Et}_2\text{O}$  which precipitated, as a dark-green solid, *the cobalt complex 137c* (0.31 g, 94%), mp  $206\text{-}210^\circ\text{C}$ ;  $\nu_{\text{max}}(\text{KBr}/\text{cm}^{-1})$  3259 (amide NH) and 3121 (imidazole NH);  $\nu_{\text{max}}(\text{nujol}/\text{cm}^{-1})$  299 (Co-Cl).

#### *The cobalt complex 138*

A solution of 2,9-bis{[2-(2-pyridylethylamino)methyl]-1,10-phenanthroline} **68a** (0.20 g, 0.44 mmol) in MeCN (10 mL) was added dropwise to a solution of  $\text{CoCl}_2 \cdot 6\text{H}_2\text{O}$  (0.22 g, 0.92 mmol) in MeCN (10 mL). The colour changed from bright blue to green, and, after stirring for 18 h *the cobalt complex 138*, precipitated out as a green powder (0.19 g, 49%), mp  $>230^\circ\text{C}$ ;  $\nu_{\text{max}}(\text{KBr}/\text{cm}^{-1})$  3398 (NH);  $\nu_{\text{max}}(\text{nujol}/\text{cm}^{-1})$  311 (Co-Cl).

### 3.3.3 Nickel Complexes<sup>†, ††</sup>

#### *The nickel complex 140*

A solution of 2,2'-bis[[2-(2-pyridyl)ethylamino]carbonyl]biphenyl **55a** (0.20 g, 0.44 mmol) in MeOH (5 mL) was added to a stirred solution of NiCl<sub>2</sub>·6H<sub>2</sub>O (0.22 g, 0.92 mmol) in MeCN (5 mL). After stirring for 2.5 d, Et<sub>2</sub>O was added to precipitate, as a light-green, hygroscopic solid, *the nickel complex 140* (0.26 g, 72%), mp 48-49°C;  $\nu_{\max}(\text{KBr}/\text{cm}^{-1})$  3336 (amide NH) and 1619 (CO);  $\nu_{\max}(\text{nujol}/\text{cm}^{-1})$  325 and 276 (Ni-Cl).

#### *The nickel complex 141*

A hot solution of 2,2'-bis[[2-(2-benzimidazolyl)ethylamino]carbonyl]biphenyl **55b** (0.23 g, 0.44 mmol) was added dropwise to a stirred solution of NiCl<sub>2</sub>·6H<sub>2</sub>O (0.22 g, 0.92 mmol) in DMF (7 mL). The reaction mixture was stirred for 57 h before Et<sub>2</sub>O was added to precipitate, as a light-green solid, *the nickel complex 141* (0.29 g, 53%), mp >250°C;  $\nu_{\max}(\text{KBr}/\text{cm}^{-1})$  3183 (amide NH) and 1650 (CO);  $\nu_{\max}(\text{nujol}/\text{cm}^{-1})$  387 (Ni-Cl)

#### *The nickel complex 142*

A solution of 2,2'-bis[[2-(4-imidazolyl)ethylamino]carbonyl]biphenyl **55c** (0.15 g, 0.35 mmol) in DMF (10 mL) was added dropwise to a stirred solution of NiCl<sub>2</sub>·6H<sub>2</sub>O (0.17 g, 0.72 mmol) in MeOH (5 mL). Stirring was continued for 55 h before adding Et<sub>2</sub>O to precipitate, as a hygroscopic dark blue-green solid, *the nickel complex 142*, (0.10 g, 27%), mp 204-205°C;  $\nu_{\max}(\text{KBr}/\text{cm}^{-1})$  3248 (amide NH), 3143 (imidazole NH) and 1653 (CO);  $\nu_{\max}(\text{nujol}/\text{cm}^{-1})$  378 (Ni-Cl).

#### *The nickel complex 143*

To a stirred solution of NiCl<sub>2</sub>·6H<sub>2</sub>O (0.22 g, 0.92 mmol) in MeOH (4 mL), a solution of 1-[2-(2-pyridyl)ethyl]dibenz[c,e]perhydroazepine **61a** (0.19 g, 0.44 mmol) in MeCN

<sup>†</sup> While <sup>1</sup>H and <sup>13</sup>C NMR spectra were obtained for each of these complexes, the complexity of their spectra (see Discussion 2.3.4.2.2 p.118) precludes systematic peak assignment.

<sup>††</sup> See Table 15 (p.115) for microanalysis data.

(10 mL) was added dropwise, and stirring was continued for 19 h. The solvent was allowed to evaporate off at room temperature, during which time, purple crystals precipitated from the reaction mixture and were filtered off to give *the nickel complex 143* (0.13 g, 65%), mp >250°C;  $\nu_{\max}$ (nujol/cm<sup>-1</sup>) 329 and 289 (Ni-Cl).

#### *The nickel complex 144a*

To a stirred solution of NiCl<sub>2</sub>·6H<sub>2</sub>O (0.20 g, 0.92 mmol) in MeOH (5 mL), a solution of 2,9-bis[[2-(2-pyridyl)ethylamino]carbonyl]-1,10-phenanthroline **69a** (0.20 g, 0.44 mmol) in DMF (5 mL) was added dropwise. Although no immediate colour change was observed, a suspension formed during stirring for 48 h. Et<sub>2</sub>O was then added to the reaction mixture to precipitate, as a light green solid, *the nickel complex 144a* (0.24 g, 71%), mp 249-252°C;  $\nu_{\max}$  (KBr/cm<sup>-1</sup>) 3223 (amide NH) and 1653 (CO);  $\nu_{\max}$  (nujol/cm<sup>-1</sup>) 378 and 253 (Ni-Cl).

#### *The nickel complex 144b*

A solution of 2,9-bis[[2-(2-benzimidazolyl)ethylamino]carbonyl]-1,10-phenanthroline **69b** (0.22 g, 0.44 mmol) in DMF (15 mL) was added dropwise to a solution of NiCl<sub>2</sub>·6H<sub>2</sub>O (0.20 g, 0.92 mmol) in DMF (7 mL). After stirring for 52 h Et<sub>2</sub>O was added to precipitate, as a brown, hygroscopic solid, *the nickel complex 144b* (0.31 g, 66%), mp >250°C;  $\nu_{\max}$  (KBr/cm<sup>-1</sup>) 3245 (amide NH) and 1653 (CO);  $\nu_{\max}$  (nujol/cm<sup>-1</sup>) 384 and 283 (Ni-Cl).

#### *The nickel complex 144c*

A solution of 2,9-bis[[2-(4-imidazolyl)ethylamino]carbonyl]-1,10-phenanthroline **69c** (0.20 g, 0.44 mmol) in DMF (6.5 mL) was added dropwise to a stirred solution of NiCl<sub>2</sub>·6H<sub>2</sub>O (0.21 g, 0.88 mmol) in DMF (5 mL). The resulting suspension was stirred for 20.5 h before adding Et<sub>2</sub>O to precipitate, as a light-green solid, *the nickel complex 144c* (0.31 g, 94%), mp >250°C;  $\nu_{\max}$  (KBr/cm<sup>-1</sup>) 3236 (amide NH) and 1649 (CO);  $\nu_{\max}$  (nujol/cm<sup>-1</sup>) 373 and 310 (Ni-Cl).

*The nickel complex 145*

A solution of 2,9-bis{[2-(2-pyridylethylamino)methyl]-1,10-phenanthroline **68a** (0.25 g, 0.56 mmol) in MeOH (5 mL) was added dropwise to a solution of NiCl<sub>2</sub>·6H<sub>2</sub>O (0.26 g, 1.11 mmol) in MeOH (5 mL). The colour changed from light-green to dark-green and, after stirring for 48 h, Et<sub>2</sub>O was added to precipitate, as a light-green solid, *the nickel complex 145* (0.30 g, 70%), mp 244-246°C;  $\nu_{\max}$ (KBr/cm<sup>-1</sup>) 3367 (NH);  $\nu_{\max}$ (nujol/cm<sup>-1</sup>) 352 and 278 (Ni-Cl).

**3.3.4 Platinum Complexes<sup>††, †</sup>***The platinum complex 146*

A solution of 2,2'-bis{[2-(2-pyridyl)ethylamino]carbonyl}biphenyl **56a** (0.12 g, 0.26 mmol) in MeCN (5 mL) was added dropwise to a stirred solution of K<sub>2</sub>[PtCl<sub>4</sub>] (0.24 g, 0.57 mmol) in H<sub>2</sub>O (3 mL). After stirring for 51 h, the solvents MeCN and H<sub>2</sub>O were evaporated, almost to dryness, under reduced pressure, before adding H<sub>2</sub>O to precipitate out, as a yellow solid, *the platinum complex 146* (0.16 g, 55%), mp 209-214°C;  $\nu_{\max}$ (HCBD/cm<sup>-1</sup>) 3252 (amide NH);  $\nu_{\max}$ (nujol/cm<sup>-1</sup>) 1634 (CO) and, 342 and 315 (Pt-Cl).

*The platinum complex 147 - Attempted synthesis*

To a solution of K<sub>2</sub>[PtCl<sub>4</sub>] (0.40 g, 0.76 mmol) in DMF (84 mL), a solution of 2,2'-bis{[2-(2-benzimidazolyl)ethylamino]carbonyl}biphenyl **56b** (0.20 g, 0.38 mmol) in DMF (6 mL) was added dropwise while stirring. After stirring for 7 d, the volume of DMF was evaporated to less than half the original volume before adding Et<sub>2</sub>O to precipitate out a cream powder, microanalysis of which indicated that the desired complex **147** had not been obtained.

†† While the <sup>1</sup>H and <sup>13</sup>C NMR spectra were obtained for each of these complexes, the complexity of their spectra (see Discussion 2.3.4.2.2 p.130) precludes systematic peak assignment.

† See Table 18 (p.122) for microanalysis data.

*The platinum complex 148*

A solution of 2,2'-bis[[2-(4-imidazolyl)ethylamino]carbonyl]biphenyl **56c** (0.11 g, 0.26 mmol) in DMF (6 mL) was added dropwise to a stirred solution of  $K_2[PtCl_4]$  (0.24 g, 0.57 mmol) in  $H_2O$  (3 mL). After stirring for 52.5 h, the solvents were evaporated under reduced pressure to afford, as a light-brown solid, *the platinum complex 148* (0.16 g, 62%), mp  $>230^\circ C$ ;  $\nu_{max}(\text{nujol}/\text{cm}^{-1})$  3218 (amide NH), 3120 (imidazole NH) and 1627 (CO);  $\nu_{max}(\text{nujol}/\text{cm}^{-1})$  335 (Pt-Cl).

*The platinum complex 149*

The dropwise addition of a solution of 2,9-bis[[2-(2-pyridyl)ethylamino]carbonyl]-1,10-phenanthroline **69a** (0.11 g, 0.23 mmol) in DMF (4 mL) to a stirred solution of  $K_2[PtCl_4]$  (0.21 g, 0.50 mmol) in  $H_2O$  (4 mL) was accompanied by the formation of a suspension. After stirring for 65 h, the precipitate was filtered off to afford, as an orange-brown powder, *the platinum complex 149* (0.22 g, 100%), mp  $>230^\circ C$ ;  $\nu_{max}(\text{nujol}/\text{cm}^{-1})$  1660 (CO);  $\nu_{max}(\text{nujol}/\text{cm}^{-1})$  329 (Pt-Cl).

*The platinum complex 150 - Attempted synthesis*

A solution of 2,9-bis[[2-(2-benzimidazolyl)ethylamino]carbonyl]-1,10-phenanthroline **69b** (0.15 g, 0.27 mmol) in DMF (10 mL) was added dropwise to a stirred solution of  $K_2[PtCl_4]$  (0.23 g, 0.54 mmol) in DMF (20 mL) and  $H_2O$  (8 mL). The resulting mixture was stirred for 6 d before concentrating the mixture *in vacuo* to less than half the original volume.  $Et_2O$  was then added to precipitate a peach-coloured solid, microanalysis of which indicated that the expected complex **150** had not been obtained.

*The platinum complex 151*

A solution of 2,9-bis[[2-(4-imidazolyl)ethylamino]carbonyl]-1,10-phenanthroline **69c** (0.20 g, 0.44 mmol) in DMF (5 mL) was added dropwise to a stirred solution of  $K_2[PtCl_2]$  (0.21 g, 0.50 mmol) in DMF (20 mL) and  $H_2O$  (9 mL). After stirring for 6 d,

the mixture was concentrated to less than half the original volume under reduced pressure. The addition of Et<sub>2</sub>O resulted in precipitation of *the platinum complex 151* as an orange-yellow solid (0.43 g, 100%), mp >250°C;  $\nu_{\max}(\text{KBr}/\text{cm}^{-1})$  3259 (amide NH), 3135 (imidazole NH) and 1653 (CO);  $\nu_{\max}(\text{nujol}/\text{cm}^{-1})$  321 (Pt-Cl).

*The platinum complex 152*

To a solution of K<sub>2</sub>[PtCl<sub>4</sub>] (0.21 g, 0.50 mmol) in H<sub>2</sub>O (3 mL) and HCl (2.5 mL, 2M) was added dropwise 2,9-bis[[2-(2-pyridylethylamino)methyl]-1,10-phenanthroline **68a** (0.11 g, 0.23 mmol) in a mixture of DMF (4 mL) and MeCN (26 mL). The colour changed from orange-red to dark-brown and a suspension formed during stirring for 5 d. After this time, the mixture was filtered and the filtrate evaporated, almost to dryness, under reduced pressure. Addition of H<sub>2</sub>O to the residue afforded, as a brown solid, *the platinum complex 152* (0.25 g, 100%), mp >230°C;  $\nu_{\max}(\text{nujol}/\text{cm}^{-1})$  3480 (NH) and 318 (Pt-Cl).

### 3.4 PROCEDURE FOR COMPUTER MODELLING OF COMPLEXES

Computer modelling was conducted using the MSI Cerius<sup>2</sup> version 3.2 modelling package on a Silicon Graphics O<sup>2</sup> platform. The sequence followed for the computer modelling runs for both ligands and complexes is outlined in Figure 63, and was aimed at establishing the global minimum in each case.

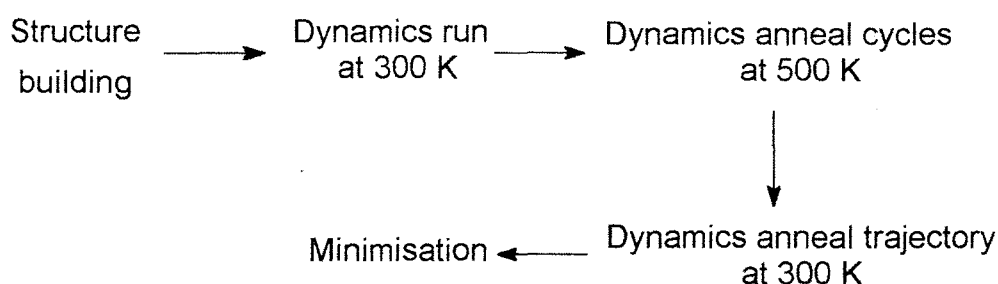


**Figure 63:** The procedure followed for the modelling of the ligands and complexes.

This sequence involved starting with structure building followed by a dynamics run of 5000 steps at 300 K. This was then followed by 250 dynamics anneal cycles during which the temperature was raised to 500 K followed by a dynamics anneal trajectory involving cooling to 300 K. The lowest energy structure was then energy-minimised. Minimisations were considered to converge when the energy gradient was less than 0.01 kcalmol<sup>-1</sup>. The ligands were first modelled and then the metals were inserted and the modelling process repeated for the complex. Dioxygen was inserted once the minimised model of the complex was obtained, and the modelling process once again repeated for the copper-dioxygen complex. The potential energies and the Cu-Cu distances of these minimised models were then recorded for selected complexes. A universal force field was used for modelling all the complexes except copper.

### 3.5 ELECTROCHEMICAL STUDIES: CYCLIC VOLTAMMETRY

Electrochemical data were collected with a Bio Analytical Systems (BAS) CV-50 voltammograph. The measurements were carried out under a nitrogen atmosphere using freshly distilled, dried, degassed solvents. A glass carbon electrode (diameter = 3.0 mm) was used as the working electrode and a platinum wire as the counter electrode. A non-aqueous reference electrode was employed. The electrode solution for the non-aqueous reference electrode was prepared by dissolving 0.01 M  $\text{AgNO}_3$  in 0.1 M TEAP (tetraethylammonium perchlorate) in MeCN or DMF, resulting in a  $\text{Ag}/\text{Ag}^+$  (TEAP/MeCN or TEAP/DMF) electrode. TEAP was employed as an electrolyte. The same reference electrode was used for both MeCN and DMF.

#### 3.4.1 Copper complexes

The conditions used for the analysis of the copper complexes are summarised in Table 26. The resulting cyclic voltammograms are illustrated in Figures 65-67. Cyclic voltammograms were also obtained for the ligands **55b** and **69b** (Figure 64).

**Table 26:** Conditions used to measure the cyclic voltammograms of the copper complexes.

Complex	Solvent	Scanning range (mV)	Scanning speed ( $\text{mV}\cdot\text{s}^{-1}$ )
115	DMF	1300 to -1300	1000
116	DMF	1550 to -1550	500
118a	DMF	1580 to -1580	200
118b	DMF	2200 to -2200	1000
118c	DMF	2000 to -2050	500
119	DMF	1200 to -1200	200
120	MeCN	2200 to -2200	300
121	MeCN	2200 to -2200	500
123	MeCN	2250 to -2250	100
127	DMF	1650 to -1650	500

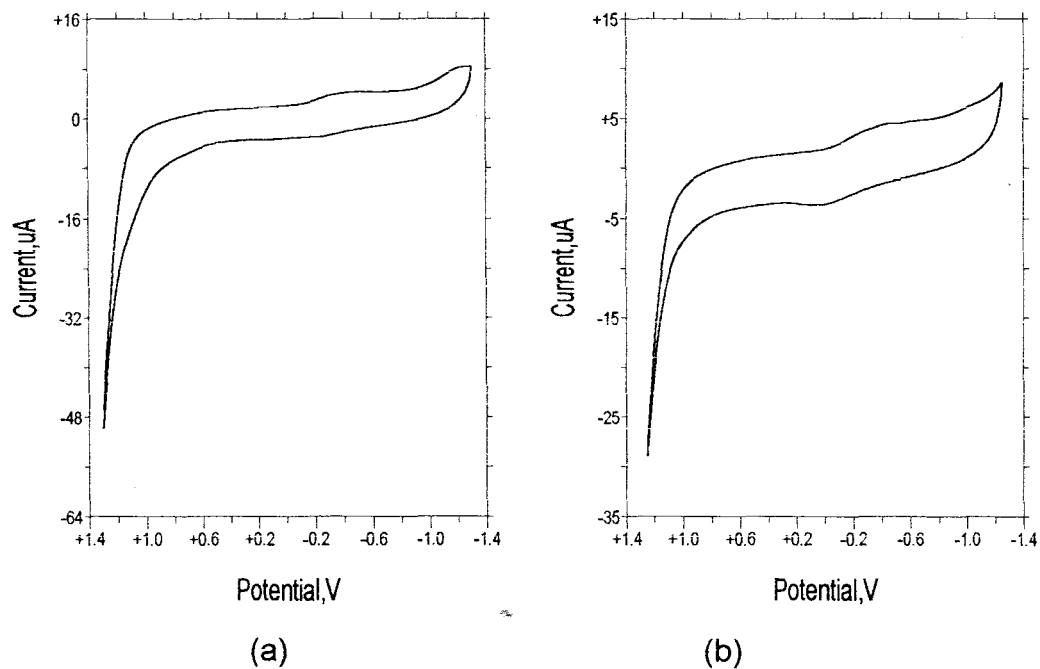


**Figure 64:** Cyclic voltammograms of: (a) the biphenyl ligand **55b** and (b) the 1,10-phenanthroline ligand **69b**.

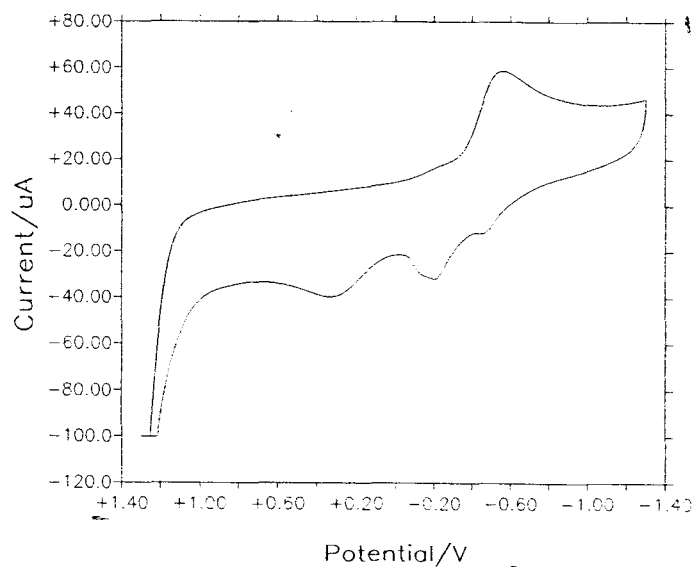


**Figure 65:** Cyclic voltammogram of the biphenyl copper complex **115**.

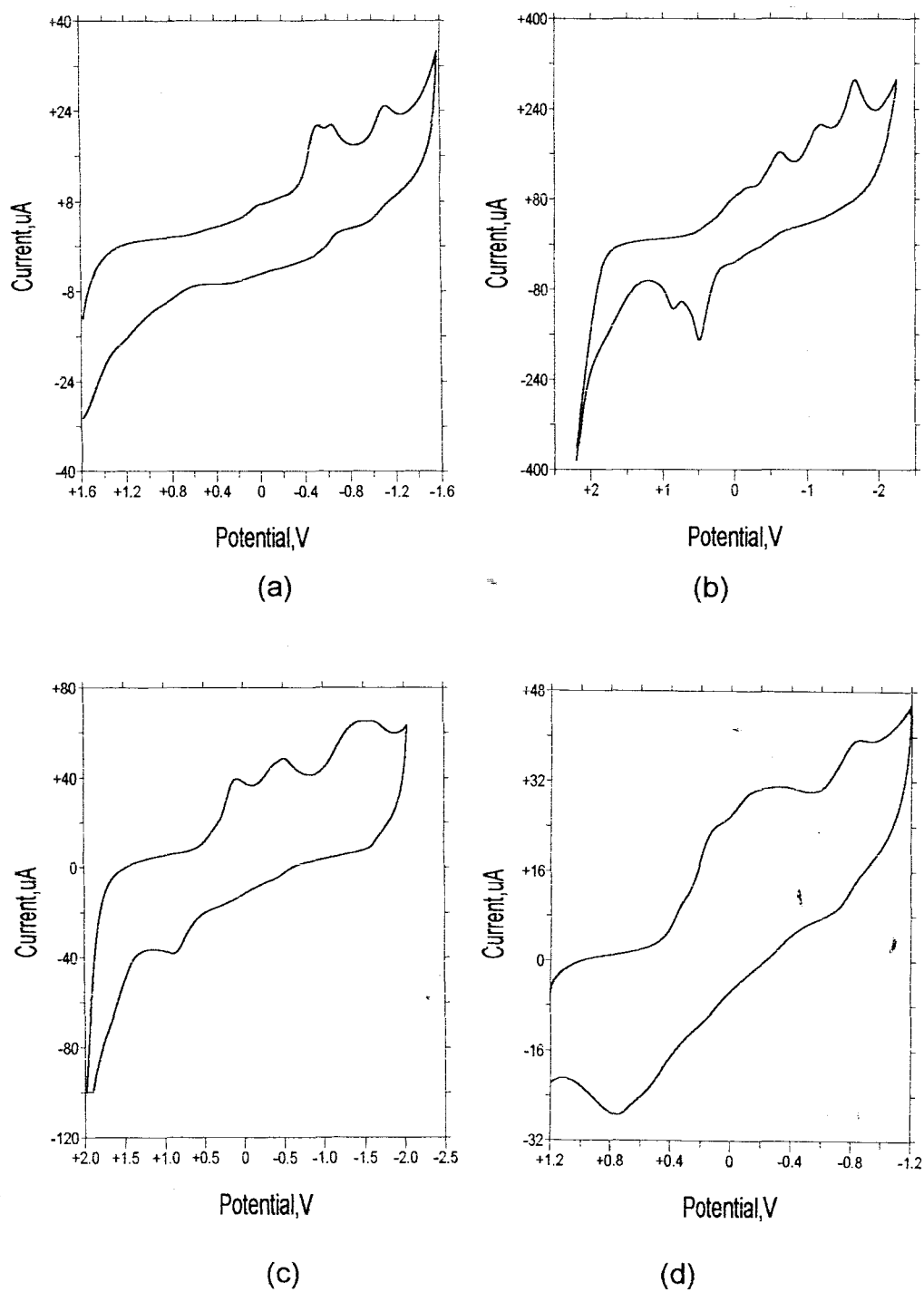


**Figure 66:** Cyclic voltammograms of the 1,10-phenanthroline complexes: (a) 118a; (b) 118b; (c) 118c; and (d) 119.

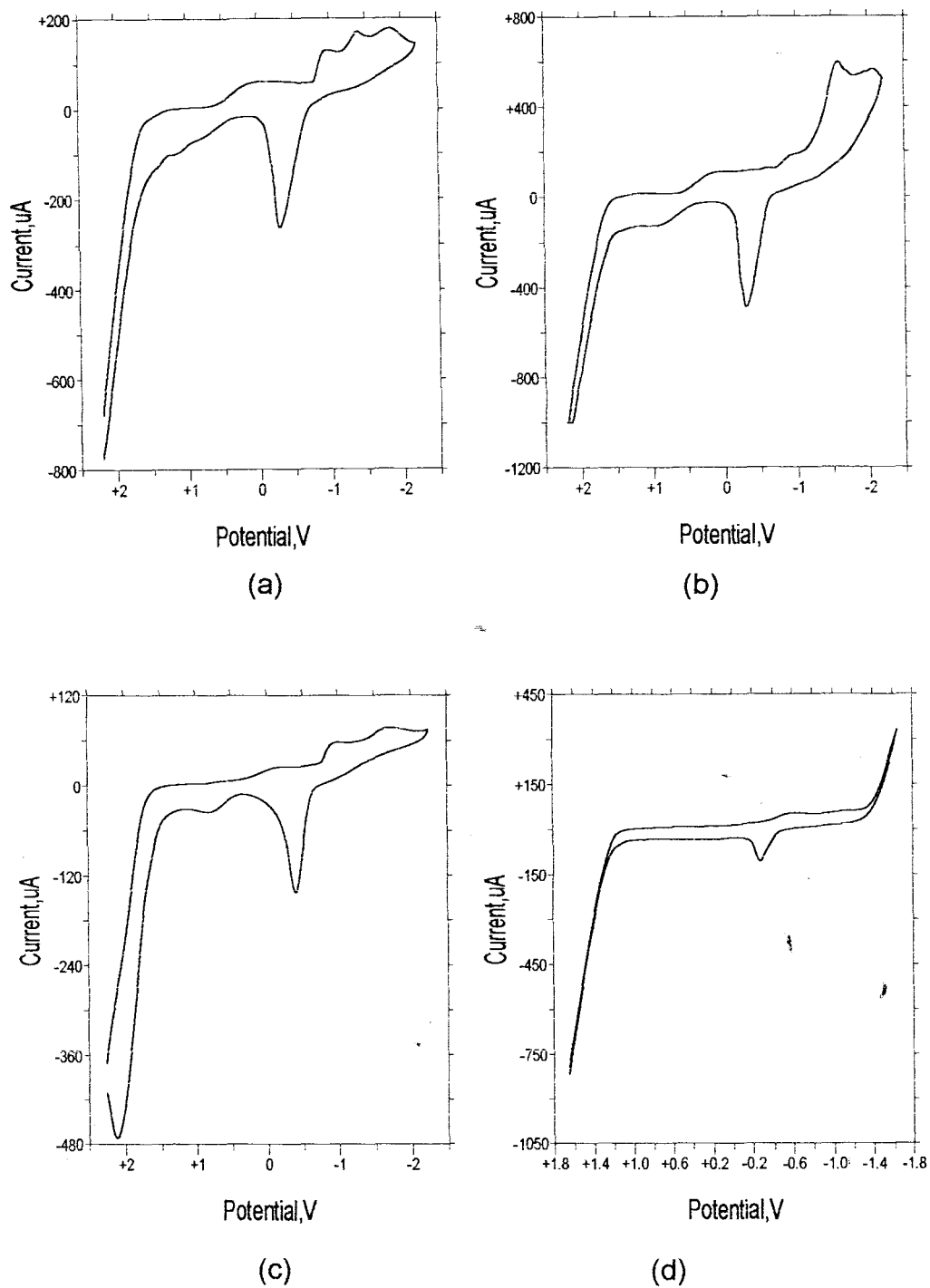


**Figure 67:** Cyclic voltammograms obtained for the Schiff base complexes and the macrocycle complex: (a) 120; (b) 121; (c) 123; and (d) 124.

### 3.4.2 Cobalt Complexes

The conditions used for the analysis of the cobalt complexes are summarised in Table 27.

**Table 27:** Conditions used to measure the cyclic voltammograms of the cobalt complexes.

Complex	Solvent	Scanning range (mV)	Scanning speed (mV.s <sup>-1</sup> )
133	DMF	1600 to -1600	500
134	DMF	1250 to -1250	300
137a	DMF	1600 to -1600	400
137b	DMF	1250 to -1250	300
137c	DMF	1300 to -1300	400
138	DMF	1250 to -1250	300

### 3.4.3 Nickel Complexes

The conditions used for the analysis of the nickel complexes are summarised in Table 28.

**Table 28:** Conditions used to measure the cyclic voltammograms of the nickel complexes.

Complex	Solvent	Scanning range (mV)	Scanning speed (mV.s <sup>-1</sup> )
140	DMF	1550 to -1550	300
141	DMF	1550 to -1550	500
142	DMF	1550 to -1550	300
144a	DMF	1550 to -1550	300
144b	DMF	1550 to -1550	700
144c	DMF	1550 to -1550	500
145	DMF	1550 to -1550	500

### 3.6 METHOD FOR THE EVALUATION OF THE CATALYTIC ACTIVITY OF THE COPPER COMPLEXES

The substrates DTBP **153** and DTBC **154** were added to separate suspensions of the complexes in dry DMF (3 mL) or CH<sub>2</sub>Cl<sub>2</sub> (3 mL) in molar ratios of 100:1 (substrate: complex). The resulting mixtures were aerated by vigorously stirring at room temperature to provide the oxygen necessary for reaction. Generally the reactions conducted in CH<sub>2</sub>Cl<sub>2</sub> were stirred for ca. 3–4 d, reactions in DMF for ca. 5 d; the reactions with complexes **115** and **118a**, however, showed biomimetic activity after stirring for 24 h. The reactions in DMF, which displayed no catalytic activity, were repeated in the presence of triethylamine (30 μL per reaction) to inhibit decomposition of the complex.<sup>138</sup> After stirring, the reaction mixtures were concentrated to dryness *in vacuo*, and the solid residues analysed by <sup>1</sup>H NMR spectroscopy. The extent of conversion to the products was determined by comparing the integrals of signals corresponding to the individual products and unreacted substrate (see Tables 29 and 30).

**Table 29:** Data for the catalytic oxidation of DTBP **153** to the coupled product **156**.

Complex	Integral ratio	% conversion
116	10.33:1	8.8
118a	6:1	14.3
118b	6.67:1	13.0

**Table 30:** Data for the catalytic oxidation of DTBC **101** to DTBQ **102**.

Complex	Integral ratio	% conversion
115	15:1	6.3
116	13:2	13.3
118a	12.7:1	7.3
118b	5:3	38.0
118c	1:1.19	54.3

#### 4 REFERENCES

1. R. J. P. Williams, *Endeavour*, 1967, **26**, 96.
2. A. S. Milvan and M. Cohn, *Adv. Enzymol.*, 1970, **33**, 1.
3. W. N. Lipscomb and N. Strater, *Chem. Rev.*, 1996, **96**, 2375
4. G. C. Dismukes, *Chem. Reviews*, 1996, **96**, 2909.
5. R. W. Hay, *Bio-inorganic Chemistry*, Ellis Horwood Ltd., Chichester, 1987, p.102.
6. D. E. Wilcox, *Chem. Rev.*, 1996, **96**, 2435.
7. S.J. Lippard and J. M. Berg, *Principles of Bioinorganic Chemistry*, University Science Books, Mill Valley, California, 1994, p.31.
8. D. W. Christianson, *Acc. Chem. Res.*, 1989, **22**, 62..
9. K.D. Karlin, *Science*, 1993, **261**, 701.
10. C. A. McAuliffe, *Techniques and Topics in Bioinorganic Chemistry*, The McMillan Press Ltd, London, 1975, Pp.3-5.
11. H. S. Mason, W. B. Fowlks and E. W. Peterson, *J. Am. Chem. Soc.*, 1955, **77**, 2914; E. Bourquelot and G. Bertrand, *Compt. Rend. Soc. Biol.*, 1895, **47**, 582.
12. J. N. Rodriguez-Lopez, J. Tudela, R. Varon, F. Garcia-Carmona, F. Garcia-Carnovas, *J. Biol. Chem.*, 1992, **267**, 3801.
13. T. Tsukihara, H. Aoyama, E. Yamashita, T. Tomizaki, K. Shinwaza-Itoh, R. Nakashima, R. Yaono, S. Yoshika-wa, *Science*, 1995, **269**, 1069.
14. K. D. Karlin and Y. Gultneh, *J. Chem. Ed.*, 185, **62**, 983.
15. P. A. Vigato, S. Tamburini and D. E. Fenton, *Coord. Chem. Rev.*, 1990, **106**, 25.
16. G. L. Woolery, L. Powers, M. Winkler, E. I. Solomon, K. Lerch and T. G. Spiro, *Biochim. Biophys. Acta*, 1984, **788**, 155.
17. N. Makino and H. S. Mason, *Biol. Chem.*, 1973, **248**, 5731.
18. D. E. Wilcox, A. G. Porras, Y. T. Hwang, K. Lerch, M. Winkler and E. I. Solomon, *J. Am. Chem. Soc.*, 1985, **107**, 4015.
19. T. B. Freedman, J. S. Loehr and T. M. Loehr, *J. Am. Chem. Soc.*, 1986, **98**, 2809.

20. N. Kitajima, *Adv. Inorganic Chem.*, 1992, **39**, 1.
21. P. K. Ross and E. I. Solomon, *J. Am. Chem. Soc.*, 1990, **112**, 5871.
22. P. K. Ross and E. I. Solomon, *J. Am. Chem. Soc.*, 1991, **113**, 3246.
23. M. J. Baldwin, D. E. Root, J. E. Pate, K. Fujisawa, N. Kitajima and E. I. Solomon, *J. Am. Chem. Soc.*, 1992, **114**, 10421.
24. S. Mahapatra, J. A. Halfen, E. C. Wilkinson, G. Pan, C. J. Cramer, L. Que and W. B. Tolman, *J. Am. Chem. Soc.*, 1995, **117**, 8865.
25. J. A. Halfen, S. Mahapatra, E. C. Wilkinson, S. Kaderli, V. G. Y. L. Que, A. D. Zuberbuhler and W. B. Tolman, *Science*, 1996, **271**, 1397.
26. C. H. Langford and H. B. Gray, *Ligand Substitution Processes*, Benjamin, Reading MA, 1966.
27. K. Lerch and M. Huber, *J. Inorg. Biochem.*, 1986, **26**, 213.
28. K. Lerch in *Enzymatic Browning and Its Prevention*, eds. C. Y. Lee and J. R. Whitaker, ACS, Washington, DC, 1995.
29. W. H. Lang and K. E. Holde, *Proc. Natl. Acad. Sci. U.S.A.*, 1991, **88**, 244.
30. E. Pfiffner and K. Lerch, *Biochemistry*, 1981, **20**, 6029.
31. M. P. Jackman, A. Hajnal and K. Lerch, *Biochem. J.*, 1991, **274**, 707.
32. C. Gielens, N. D. Geest, X. -Q. Xin and G. Préaux, *Arch. Int. Physiol. Biochim. Biophys.*, 1991, **102**, B11.
33. N. Ito, S. E. V. Phillips, C. Stevens, Z. B. Ogel, M. J. McPherson, J. N. Keen and P. F. Knowles, *Nature*, 1991, **350**, 87.
34. A. J. M. S. Uiterkamp, *FEBS Lett.*, 1972, **20**, 93.
35. A. J. M. S. Uiterkamp, H. v. d. Deen, J. Berendsen and J. F. Boas, *Biochem. Biophys. Res. Commun.*, 1974, **372**, 407.
36. N. C. Eickman, R. S. Himmelwright and E. I. Solomon, *Proc. Natl. Acad. Sci. U.S.A.*, 1979, **76**, 2094.
37. A. F. Hepp, R. S. Himmelwright, N. C. Eickman and E. I. Solomon, *Biochem. Biophys. Res. Commun.*, 1979, **89**, 1050.
38. R. S. Himmelwright, N. C. Eickman and E. I. Solomon, *Biochem. Biophys. Res. Commun.*, 1978, **81**, 237.
39. R. S. Himmelwright, N. C. Eickman and E. I. Solomon, *Biochem. Biophys.*

- Res. Commun.*, 1978, **84**, 300.
40. R. S. Himmelwright, N. C. Eickman and E. I. Solomon, *Biochem. Biophys. Res. Commun.*, 1979, **86**, 628.
41. R. S. Himmelwright, N. C. Eickman, C. D. Lubien and E. I. Solomon, *Biochem. Biophys. Res. Commun.*, 1980, **102**, 5378.
42. R. S. Himmelwright, N. C. Eickman, C. D. Lubien, K. Lerch and E. I. Solomon, *J. Am. Chem. Soc.*, 1980, **102**, 7339.
43. R. L. Jolley, L. H. Evans and H. S. Mason, *Biochem. Biophys. Res. Commun.*, 1972, **46**, 878.
44. R. L. Jolley, L. H. Evans, N. Makino and H. S. Mason, *J. Biol. Chem.*, 1974, **249**, 335.
45. A. J. M. S. Uiterkamp and H. S. Mason, *Proc. Natl. Acad. Sci. U.S.A.*, 1973, **70**, 993.
46. N. C. Eickman, E. I. Solomon, J. A. Larrabee, T. G. Spiro and K. Lerch, *J. Am. Chem. Soc.*, 1978, **100**, 6529
47. K. A. Magnus, B. Hazes, H. Ton-That, C. Bonaventura, J. Bonaventura and W. G. J. Hol, *Proteins*, 1994, **19**, 302.
48. S. H. Pomerantz, *J. Biol. Chem.*, 1960, **241**, 161.
49. H. W. Duckworth and J. Coleman, *J. Biol. Chem.*, 1970, **245**, 1613.
50. E. I. Solomon, U. M. Sundaram and T. E. Machonkin, *Chem. Rev.*, 1996, **96**, 2563.
51. S. C. Atlow, L. Bonadonna-Aparo and A. M. Klibanov, *Biotech. Bioeng.*, 1984, **26**, 599.
52. S. Wada, H. Ichikawa and K. Tatsumi, *Biotech. Bioeng.*, 1995, **45**, 304.
53. S. Wada, H. Ichikawa and K. Tatsumi, *Biotech. Bioeng.*, 1993, **42**, 854.
54. J. G. Schiller and C. C. Liu, *Biotech. Bioeng.*, 1993, **118**, 979.
55. J. G. Schiller, A. K. Chen and C. C. Liu, *Anal. Biochem.*, 1978, **85**, 25.
56. K. G. Kjellen and H. Y. Neujahr, *Biotech. Bioeng.*, 1980, **22**, 299.
57. Z. Tyeklar and K. D. Karlin, *Acc. Chem. Res.*, 1989, **22**, 241.
58. T. N. Sorrell, *Tetrahedron*, 1989, **45**, 3.
59. K. D. Karlin, *Science*, 1993, **261**, 701.

60. K. D. Karlin and Y. Gultneh, *Prog. Inorg. Chem.*, 1987, **35**, 219.
61. L. Casella, O. Carugo, M. Gullotti, S. Garfani and P. Zanello, *Inorg. Chem.*, 1993, **32**, 2056.
62. P. V. Bernhart and P. Comba, *Inorg. Chem.*, 1992, **31**, 2638.
63. T. Pandiyan, M. Palandiandavar, M. Lakshminarayanan and H. Manohar, *J. Chem. Soc. Dalton Trans.*, 1992, 3377.
64. M. R. Malchowski, L. J. Tomlinson, M. G. Davidson and M. J. Hall, *J. Coord. Chem.*, 1992, **25**, 171.
65. K. D. Karlin, P. L. Dahlstrom, S. N. Cozzette, P. M. Scensny and J. Zubieta, *J. Chem. Soc., Chem. Commun.*, 1981, 881.
66. G. S. Patterson and R. H. Holm, *Bioinorg. Chem.*, 1975, **257**, 4.
67. K. D. Karlin and J. K. Yandell, *Inorg. Chem.*, 1984, **23**, 1184.
68. A. W. Addison in *Copper Coordination Chemistry: Biochemical and Inorganic Perspectives*, eds. K. D. Karlin and J. Zubieta, Adenine, Guilderland, New York, 1983, p. 109-128.
69. R. J. Kassner, *Proc. Natl. Acad. Sci.*, 1972, **69**, 2263.
70. K. D. Karlin, *Prog. Inorg. Chem.*, 1987, **35**, 219.
71. G. L. Woolery, L. Powers, M. Winkler, E. I. Solomon and T. G. Spiro, *J. Am. Chem. Soc.*, 1984, **106**, 86.
72. T. B. Freedman, J. S. Loehr and T. M. Loehr, *J. Am. Chem. Soc.*, 1976, **98**, 2809.
73. J. A. Larrabee and T. G. Spiro, *J. Am. Chem. Soc.*, 1980, **102**, 4217.
74. J. A. Larrabee and T. G. Spiro, *J. Am. Chem. Soc.*, 1980, **102**, 4217.
75. M. K. Jacobsohn, V. C. Dobre, C. Branam and G. M. Jacobsohn, *J. Steroid Biochem.*, 1988, **31**, 377.
76. E. I. Solomon, *Pure Applied Chem.*, 1983, **55**, 1069.
77. W. P. Gaykema, A. Volbeda and W. G. J. Hol, *J. Mol. Biol.*, 1985, **187**, 255.
78. D. E. Fenton in *Biocoordination Chemistry*, Oxford-University Press, New York, 1995, p.29.
79. N. Kitajima in *Bioinorganic Chemistry of Copper*, eds K. D. Karlin and Z. Tyeklár, Chapman and Hall, New York, 1993, p.251.

80. K. A. Magnus, H. Ton-That and J. E. Carpenter, *Chem. Rev.*, 1994, **94**, 727.
81. E. Spodine and J. Manzur, *Coord. Chem. Rev.*, 1992, **119**, 171.
82. M. G. Simmons and L. G. Wilson, *J. Chem. Soc., Chem. Commun.*, 1988, 151.
83. M. G. Simmons, C. L. Merrill, L. G. Wilson, L. A. Bottomley and K. M. Kadish, *J. Chem. Soc., Dalton Trans.*, 1980, 1827.
84. J. D. Korp, I. Bernal, C. L. Merrill and L. J. Wilson, *J. Chem. Soc., Dalton Trans.*, 1981, 1951.
85. C. L. Merrill, L. J. Wilson, T. J. Thamann, T. M. Loehr, N. S. Ferris and W. H. Woodruff, *J. Chem. Soc., Dalton Trans.*, 1984, 2207.
86. L. Casella, M. E. Silver and J. A. Ibers, *Inorg. Chem.*, 1984, **23**, 1409.
87. R. R. Jacobson, Z. Tyeklár, A. Farooq, K. D. Karlin, S. Liu and J. Zubieta, *J. Am. Chem. Soc.*, 1988, **110**, 3690.
88. N. Wei, N. N. Murthy, Z. Tyeklár and K. D. Karlin, *Inorg. Chem.*, 1994, **33**, 1177.
89. R. H. Holm, *Chem. Rev.*, 1987, **87**, 1401.
90. K. D. Karlin and Y. Gultneh, *Prog. Inorg. Chem.*, 1987, **35**, 219.
91. K. D. Karlin, M. S. Haka, R. W. Cruse and Y. Gultneh, *J. Am. Chem. Soc.*, 1985, **107**, 5828.
92. K. D. Karlin, M. S. Haka, R. W. Cruse, G. J. Meyer, A. Farooq, Y. Gultneh, J. C. Hayes and J. Zubieta, *J. Am. Chem. Soc.*, 1988, **110**, 1196.
93. N. J. Blackburn, R. W. Strange, A. Farooq, M. S. Haka and K. D. Karlin, *J. Am. Chem. Soc.*, 1985, **110**, 4263.
94. K. D. Karlin, Z. Tyeklár, A. Farooq, R. R. Jacobson, E. Sinn, D. W. Lee, J. E. Bradshaw and L. J. Wilson, *Inorg. Chem. Acta*, 1991, **182**, 1.
95. F. Zippel, F. Ahlers, R. Werner, W. Haase, H-F. Nolting and B. Krebs, *Inorg. Chem.*, 1996, **35**, 3409.
96. E. Müller, G. Bernardinelli and J. Reedjik, *Inorg. Chem.*, 1995, **34**, 5979.
97. N. Kitajima and Y. Moro-oka, *Chem. Rev.*, 1994, **94**, 737.
98. Y. Nishida, H. Shimo, J. Maehara and S. Kida, *J. Chem. Soc., Dalton*

*Trans.*, 1985, 1945

99. S. K. Mandal, L. K. Thompson, M. J. Newlands, A. K. Biswas, B. Adhikary, K. Nag, E. J. Gabe and F. L. Lee, *Can. J. Chem.*, 1989, **67**, 662.
100. S. S. Tandon, L. K. Thompson, J. N. Bridgson, V. McKee and A. J. Downward, *Inorg. Chem.*, 1992, **31**, 4635.
101. S. M. Nelson, F. Esho, A. Lavery and M. G. B. Drew, *J. Am. Chem. Soc.*, 1983, **105**, 5693.
102. B. L. Feringa in *Bioinorganic Chemistry of Copper*, eds K. D. Karlin and Z. Tyeklár, Chapman and Hall, New York, 1993, p.306.
103. M. Reglier, C. Jorand and B. Waegell, *J. Chem. Soc., Chem. Commun.*, 1990, 1752.
104. L. Casella, M. Gullotti, R. Radaelli, P. Di Gennaro, *J. Am. Chem. Soc., Chem. Commun.*, 1991, 1611.
105. J. Reim and B. Krebs, *J. Chem. Soc., Dalton Trans.*, 1997, 3793.
106. L. Casella, M. Gullotti, M. Bartosek, G. Pallanza and E. Laurenti, *J. Chem. Soc., Chem. Commun.*, 1991, 1235.
107. L. Casella and M. Gullotti in *Bioinorganic Chemistry of Copper*, eds K. D. Karlin and Z. Tyeklár, Chapman and Hall, New York, 1993, p.292.
108. G. Alzuet, L. Casella, M. L. Villa, O. Carugo and M. Gullotti, *J. Chem. Soc., Dalton Trans.*, 1997, 4789.
109. D. E. Fenton in *Advances in Inorganic and Bioinorganic Mechanisms*, Vol. 2, ed. A. G. Sykes, Academic press, London, 1983, p.187.
110. K. D. Karlin and J. Zubieta, *Biological and Inorganic Copper Chemistry*, Vols. 1 and 2, Adenine Press, 1983.
111. D. E. Fenton, U. Casellato, P. A. Vigato and M. Vidali, *Inorg. Chim. Acta*, 1984, **95**, 187.
112. D. E. Fenton, U. Casellato, P. A. Vigato and M. Vidali, *Inorg. Chim. Acta*, 1982, **62** 57.
113. U. Casellato, P. A. Vigato, D. E. Fenton and M. Vidali, *Chem. Soc. Rev.*, 1979, **8**, 199.
114. S. E. Groh, *Isr. J. Chem.*, 1976/1977, **15**, 277.

115. D. M. Dooley, R. A. Scott, E. Ellinghaus, E. I. Solomon and H. B. Gray, *Proc. Natl. Acad. Sci. U. S. A.*, 1978, **75**, 3019.
116. D. J. Spira, M. E. Winkler and E. I. Solomon, *Biochem. Biophys. Res. Commun.*, 1982, **107**, 721.
117. C. D. LuBien, M. E. Winkler, T. J. Thamann, R. A. Scott, M. S. Co, K. O. Hodgson and E. I. Solomon, *J. Am. Chem. Soc.*, 1981, **103**, 7014.
118. J. A. Fee and R. G. Briggs, *Biochim. Biophys. Acta*, 1975, **400**, 439.
119. J. A. Fee, *J. Biol. Chem.*, 1973, **248**, 4229.
120. L. Calabrese, D. Cocco and A. Desideri, *FEBS Lett.*, 1979, **106**, 142.
121. E. L. Mutterties, T. N. Rhodin, E. Band, G. F. Brucker and W. R. Pretzer, *Chem. Rev.*, 1979, **79**, 91.
122. E. C. Niederhoffer, J. H. Timmons and A. G. Martell, *Chem. Rev.*, 1984, **84**, 137.
123. P. Cadiot and W. Chodkiewicz in *Chemistry of Acetylenes*, ed. H. G. Viehe, Marcel Dekker, New York, 1969, p.597.
124. A. S. Hay, *J. Org. Chem.*, 1962, **27**, 3320.
125. H. L. Finkbeiner, A. S. Hay and D. M. White in *Polymerisation by Oxidative Coupling*, eds. C. E. Schildnecht and I. Skeist, Interscience, New York, 1977, p. 537-581.
126. C. Glaser, *Ann. Chem. Pharm.*, 1870, **154**, 159.
127. W. G. Nigh in *Oxidation in Organic Chemistry*, Part B, eds. W. S. Trachanovsky, Academic, New York, 1973, Pp.1-96.
128. M. M. Rogic and T. R. Demmin, *J. Am. Chem. Soc.*, 1978, **100**, 5472.
129. W. W. Kaeding, *Hydrocarbon Proc.*, 1964, **43**, 173.
130. W. Brenner, *U. S. Pat. 3*, 1974, **796**,732.
131. E. L. Reilly, *U. S. Pat. 3*, 1976, **987**, 068.
132. K. D. Karlin, Z. Tyeklár, A. Farooq, M. S. Haka, P. Ghosh, R.W. Cruse, Y. Gultneh, J. C. Hayes, P. J. Toscano and J. Zubijeta, *Inorg.Chem.*, 1992, **31**, 1436.
133. W. P. J. Gaykema, W. G. J. Hol, J. M. Vereijken, N. M. Soeter, H. J. Bak and J. J. Beintema, *Nature*, 1984, **309**, 23.

134. K. Lerch, *Life Chem. Reports*, 1987, **5**, 221.
135. L. Casella and L. Rigoni, *J. Chem. Soc. Commun.*, 1985, 1668
136. L. Casella, M. Gullotti, G. Pallanza and L. Rigoni, *J. Am. Chem. Soc.*, 1988, **110**, 4221.
137. K. D. Karlin and J. K. Yandell, *Inorg. Chem.*, 1984, **23**, 1184.
138. S. G. Burton, Ph.D Thesis, Rhodes University, 1993.
139. H. M. J. Hendriks, P. J. M. W. L. Birker, J. van Rijn, G. C. Verschoor and J. Reedjik, *J. Am. Chem. Soc.*, 1982, **104**, 3607.
140. P. S. Bailey and R. E. Erickson, *Org. Synth.*, 1961, **41**, 41.
141. B. S. Furniss, A. J. Hannaford, P. W. G. Smith and A. R. Tatchell, *Vogel's Textbook of Practical Organic Chemistry*, 5<sup>th</sup> ed. 1989, Longman Scientific and Technical, p.1061
142. M. L. Bode, P. T. Kaye and R. George, *J. Chem. Soc., Perkin Trans.*, 1994, 3023.
143. T. N. Sorrell and M. L. Garrity, *Inorg. Chem.*, 1991, **30**, 210.
144. G. F. Smith and W. H. McCurdy Jr., *Anal. Chem.*, 1952, **24**, 371.
145. C. J. Chandler, L. W. Deady and J. A. Reiss, *J. Heterocyclic Chem.*, 1981, **18**, 599.
146. A. D. Baylis and M. E. D. Hillman, *German Patent 2155113 (1972)*.
147. S.E. Drewes and N. D. Emslie, *J. Am. Chem. Soc., Perkin Trans. I*, 1982, 2079.
148. M. L. Bode and P. T. Kaye, *J. Chem. Soc., Perkin Trans.*, 1993, 1809.
149. O. B. FAMILONI, P. T. Kaye and P. J. Klaas, *Chem. Commun.*, 1998, 2563.
150. R. S. Robinson, Ph.D Thesis, Rhodes University, 1997.
151. M. G. B. Drew, C. P. Waters, S. G. McFall and S. M. Nelson, *J. Chem. Res.*, 1979, 360.
152. A. Bencini, A. Bianchi, E. Garcia-Espana, M. Micheloni and P. Paoletti, *Inorg. Chem.*, 1988, **27**, 176.
153. A. Bencini, A. Bianchi, E. Garcia-Espana, S. Mangani, M. Micheloni, P. Orioli and P. Paoletti, *Inorg. Chem.*, 1988, **27**, 1104.
154. R. Menif and A. E. Martell, *J. Chem. Soc., Chem. Commun.*, 1989, 1521.

155. F. Cabral, B. Murphy and J. Nelson, *J. Inorg. Acta.*, 1984, **90**, 169.
156. J. M. Lehn, *Angew. Chem.*, 1988, **100**, 91; *Angew. Chem., Int. Ed. Engl.*, 1988, **27**, 90.
157. H. Jahansouz, Z. Jiang, R. H. Himes, M. P. Hertel and K. B. Mertes, *J. Am. Chem. Soc.*, 1989, **111**, 1409.
158. N. Bergman and F. P. Schmidtchen, *Tetrahedron Lett.*, 1988, **29**, 6235.
159. E. Kimura, Y. Kuramoto, T. Koike, H. Fijioaka and M. Kodama, *J. Org. Chem.*, 1990, **55**, 42.
160. K. E. Krakowiak, J. S. Bradshaw, W. Jiang, N. K. Dalley, G. Wu and R. M. Izatt, *J. Org. Chem.*, 1991, **56**, 2675.
161. K. E. Krakowiak, J. S. Bradshaw, W. Jiang, N. K. Dalley, G. Wu and R. M. Izatt, *J. Org. Chem.*, 1991, **56**, 2675.
162. C. Köllner, B. Pugin and A. Togni, *J. Am. Chem. Soc.*, 1998, **120**, 10274.
163. D. A. Tomalia, A. M. Taylor and W. A. Goddard, *Angew. Chem., Int. Ed. Engl.*, 1990, **29**, 138.
164. D. A. Tomalia, A. M. Taylor and W. A. Goddard, *Angew. Chem.*, 1990, **102**, 119.
165. G. R. Newkome and C. N. Moorefield, *Aldrichchim. Acta.*, 1992, **25**, 31.
166. R. Engel, *Polymer News*, 1992, **17**, 301.
167. H. G. Meikelburger, W. Jaworek and F. Vögtle, *Angew. Chem.*, 1992, **104**, 1609.
168. D. A. Tomalia, *Adv. Mater.*, 1994, **6**, 530.
169. P. Lange, A. Schier and H. Schmidbaur, *Inorg. Chem.*, 1996, **35**, 637.
170. R. Dagani, *Chemical and Engineering News*, 1996, June 3, p. 30.
171. G. R. Newkome, C. N. Moorefield and K. J. Theriot, *J. Am. Chem. Soc.*, 1988, **53**, 5552.
172. X. A. Dominguez, I. C. Lopez and R. Franco, *Notes*, 1961, 1625.
173. P. N. W. Baxter, J. A. Connor, J. D. Wallis, D. C. Povey and A. K. Powell, *J. Chem. Soc., Perkin Trans. 1*, 1992, 1601.
174. W. Paw and R. Eisenberg, *Inorg. Chem.*, 1997, **36**, 2287.
175. C. Hiort, P. Lincoln and B. Nordén, *J. Am. Chem. Soc.*, 1993, **115**, 3448.

176. Y. Singh, R. Sharan and R.N. Kapoor, *Indian Journal of Chemistry*, Sect. A, 1986, **25A**, 771.
177. S. C. Dixit, R. Sharan, and R.N. Kapoor, *J. Organomet. Chem.*, 1987, **332**, 135.
178. A. K. Narula and P. Lukose, *J. Organomet. Chem.*, 1990, **393**, 365.
179. S. P. Datta and B. R. Rabin, *J. Chem. Soc., Faraday Trans.*, 1956, **52**, 1123.
180. S. K. Kim and A. E. Martell, *J. Am. Chem. Soc.*, 1966, **88**, 914.
181. R. B. Martin, M. Chamberlain and J. E. Edsall, *J. Am. Chem. Soc.*, 1960, **82**, 495
182. E. J. Billo and D. W. Margerum, *J. Am. Chem. Soc.*, 1970, **92**, 6811.
183. H. C. Freeman and M. L. Golomb, *J. Chem. Soc., Chem. Commun.*, 1970, 1523.
184. E. B. Wilson and R. B. Martin, *Inorg. Chem.*, 1970, **9**, 528.
185. J. C. Cooper, L. F. Wong and D. W. Margerum, *Inorg. Chem.*, 1978, **17**, 261.
186. D.A. Phillips, *Metals and Metabolism*, Clarendon, Oxford, 1976.
187. R. Williams, *The Metals of Life*, Van Nostrand Reinhold, New York, 1971.
188. A. Massey in *Comprehensive Inorganic Chemistry*, ed. J. C. Bailar, H. J. Emeleus, R. S. Nyholm and A. F. Trotman-Dickinson, Pergamon, Oxford, 1973, vol. 3, p. 1.
189. N. V. Sidgwick in *Comprehensive Coordination Chemistry*, ed. G. Wilkinson, R.D. Gillard and J. A. McCleverty, Pergamon, Oxford, 1987, Vol. 5, p. 535.
190. A. F. Wells in *Comprehensive Coordination Chemistry*, ed. G. Wilkinson, R.D. Gillard and J. A. McCleverty, Pergamon, Oxford, 1987, vol. 5, p 535.
191. J. D. Dunitz and L. E. Orgel, *J. of Phys. Chem. Solids*, 1957, **3**, 20.
192. H. A. Jahn and E. Teller, *Proc. R. Soc. London*, 1937, **161**, 220.
193. F. H. Jardine, *Adv. Inorg. Chem. Radiochem.*, 1975, **17**, 115.
194. W. E. Hatfield and R. Whyman, *Transition Met. Chem.*, 1969, **47**, 5.
195. F. A. Cotton and G. Wilkinson, *Advanced Inorganic Chemistry*, Wiley

- Interscience, New York, 5<sup>th</sup> ed., 1980, Pp757,768.
196. A. D. Cross and R. A. Jones, *An Introduction to Practical Infrared Spectroscopy*, 3<sup>rd</sup> ed. London Butterworths, 1969, p.97.
197. K. Nakamoto and S. J. McCarthy, *Spectroscopy and Structure of Metal Chelate Compounds*, John Wiley and Sons, 1968, p. 265.
198. J. D. Lee, *Concise Inorganic Chemistry*, 4<sup>th</sup> ed., Chapman and Hall, London, 1991, Pp. 783.
199. Reference 203 Pp. 788.
200. Reference 203 Pp. 792.
201. Reference 203 Pp. 796.
202. M. N. Hughes, *The Inorganic Chemistry of Biological Processes*, John Wiley and Sons, London, 1975, p.186.
203. D. E. Fenton, *Biocoordination Chemistry*, Oxford University Press, New York, 1995, Pp. 69, 70.
204. M. N. Hughes, *The Inorganic Chemistry of Biological Processes*, John Wiley and Sons, London, 1975, Pp. 243, 245-250.
205. D. E. Fenton, *Biocoordination Chemistry*, Oxford University Press, New York, 1995, p. 21.
206. G. Mclendon and A. E. Martell, *Coord. Chem. Rev.*, 1976, **19**, 1.
207. R. W. Hay, *Coord. Chem. Rev.*, 1981, **35**, 85.
208. A. Bakac, B. Assink, J. H. Esponson and W. D. Wang, *Inorg. Chem.*, 1996, **35**, 788.
209. J. A. Lee-Thorp, J. E. Rüede and D. A. Thornton, 1978, **50**, 65.
210. D. Nicholls, *Complexes and First Row Transition Elements*, The MacMillan Press, London, 1974, Pp. 96.
211. C. Pariya, S. Ghosh, A. Ghosh, M. Mukherjee, A. K. Mukherjee and N. R. Chaudhuri, *J. Chem. Soc. Dalton Trans.*, 1995, 337
212. F. A. Cotton, G. Wilkinson and P. L. Gaus, *Basic Inorganic Chemistry*, 2<sup>nd</sup> ed. 1987, John Wiley and Sons, New York, p.502-504.
213. D. Volkmer, A. Hörstman, K. Griesar, W. Haase and B. Krebs, *Inorg. Chem.*, 1996, **35**, 1132.

214. Reference 78, Pp.78-80.
215. Reference 194, Pp.186
216. Y. Ihara, Y. Fukuda and K. Sone, *Inorg. Chem.*, 1987, **26**, 3745.
217. Reference 215, Pp.91.
218. Reference 215, Pp.95.
219. Reference 195, Pp.353.
220. Reference 217, Pp.537.
221. N. Farrell, Transition Metal Complexes as Drugs and Chemotherapeutic Agents in *Catalysis by Metal Complexes*, eds B. R. James and R. Ugo, Kluwer Academic Publishers, Dordrecht, 1989, Vol. 11, Pp.46-66
222. C. A. Hunter and J. K. M. Sanders, *J. Am. Chem. Soc.*, 1990, **112**, 5525.
223. M. Van Beusichem and N. Farrell, *Inorg. Chem.*, 1992, **31**, 634.
224. N. L. Alinger, *Adv. Phys. Org. Chem.*, 1976, **13**.1.
225. N. L. Alinger, *J. Am. Chem. Soc.*, 1977, **99**, 8127.
226. D. J. Duchamp, *A. Chem. Soc. Symp. Ser.*, 1979, **112**, 79; M. Geller and D. Shugar, *Drugs Exp. Clin. Res.* 1986, **12**, 595.
227. R. F. Tilton, P. K. Weiner and P. A. Kollman, *Biopolymers*, 1983, **22**, 969.
228. M. R. Snow, *J. Am. Chem. Soc.*, 1970, **92**, 3610.
229. R. B. Hancock, *Prog. Inorg. Chem.*, 1989, **37**, 187.
230. J. C. A. Boeyens, C. C. Fox and R. B. Hancock, *Inorg. Chim. Acta.*, 1984, **87**,1.
231. P. V. Bernhardt and P. Comba, *Helv. Chim. Acta.*, 1991, **74**, 1834; 1992, **75**, 645.
232. M. Yamaguchi, S. Yamamatsu, T. Furusawa, S. Yano, M. Saburi and S. Yoshikawa, *Inorg. Chem.*, 1980, **19**, 2010.
233. R. B. Hancock, P. W. Ngenya, A. Evers, P. W. Wadem and J. C. A. Boeyens, *Inorg. Chem.*, 1990, **29**, 264.
234. N. Oishi, Y. Nishida, K. Ida and S. Kida, *Bull. Chem. Soc. Japan*, 1980, **53**, 2847.
235. E. I. Solomon, *International symposium on oxidases and related redox systems*, 1988, 309.

236. N. Kitajima and Y. Moro-aka, *J. Chem. Soc. Dalton Trans.*, 1993, 2665.
237. A. Bérces, *Inorg. Chem.*, 1997, **36**, 4831.
238. S. Kida, H. Okawa and Y. Nishida in *Copper Coordination Chemistry: Biochemical and Inorganic perspectives*, eds K. D. Karlin and Y. Zubieta, Adenine, Guilderland, New York, 1983, p.425.
239. D. E. Wilcox, A. G. Porras, Y. T. Hwang, K. Lerch, M. E. Winkler and E. I. Solomon, *J. Am. Chem. Soc.*, 1985, **107**, 4015.
240. B. Jung, K. D. Karlin and A. D. Zuberbühler, *J. Am. Chem. Soc.*, 1996, **118**, 3763.
241. D-H Lee, N. Wei, N. N. Murthy, Z. Tyeklár, K. D. Karlin, S. Kaderli, B. Jung and A. D. Zuberbühler, *J. Am. Chem. Soc.*, 1995, **117**, 12498.
242. Z. Tyeklár, R. R. Jacobson, N. Wei, N. N. Murthy, J. Zubieta and K. D. Karlin, *J. Am. Chem. Soc.*, 1993, **115**, 2677.
243. M. Regliér in , *Bioinorganic Chemistry of Copper*, eds. K. D. Karlin and Z. Tyeklár, Chapman and Hall, New York, 1993, p.348.
244. B. W. Rossiter and J. F. Hamilton, *Physical methods of chemistry*, 2<sup>nd</sup> ed. 1986, Vol. 2, Electrochemical methods, Wiley, New York.
245. P. Zanello, S. Tamburini, A. Vigato and G. A. Mazzocchin, *Coord. Chem. Rev.*, 1987, **77**, 165.
246. D. E. Fenton, R. R. Schroeder and R. L. Lintveldt, *J. Am. Chem. Soc.*, 1978, **100**, (6), 1931.
247. R. R. Gagne, R. P. Kreh and J. A. Dodge, *J. Am. Chem. Soc.*, 1979, **101(23)**, 6917.
248. G. Christou, S. P. Perlepes, E. Libby, K. Folting, J. C. Huffmann, R. J. Webb and D. N. Hendrickson, *Inorg. Chem.*, 1990, **29**, 3657.
249. Reference 68, Pp. 371.
250. M. Ali, I. Zilberman, H. Cohen, A. I. Shames and D. Meyerstein, *Inorg. Chem.*, 1996, **35**, 5127.
251. K. J. Oberhausen, R. J. O' Brien, J. F. Richardson and R. M. Buchanan, *Inorg. Chim. Acta.*, 1990, **173**, 145.
252. R. G. Pearson, *Science*, 1966, **151**, 172.

253. J. P. Chyn and F. L. Urbach, *Inorg. Chim. Acta.*, 1991, **189**, 157.
254. K. T. Yasunobu, E. W. Peterson and H. S. Mason, *J. Biol. Chem.*, 1959, **234**, 3291.
255. Passi and M. Nazarro-Porro, *Brit. J. Dermatol.*, 1981, **104**, 659.
256. P. Paul, Z. Tyeklár, R. Jacobson and K. D. Karlin, *J. Am. Chem. Soc.*, 1991, **113**, 5322.
257. K. Kushioka, *J. Org. Chem.*, 1984, **49**, 4456.
258. M. Flinterman and G. Challa, *J. Mol. Catal.*, 1983, **18**, 149.
259. S. Tsuruya, Y. Kishikawa, R. Tanaka and T. Kuse, *J. Catal.*, 1977, **49**, 254.
260. B. Feringa and H. Wynberg, *Bioorg. Chem.*, 1978, **7**, 397.

## 5 APPENDIX

Crystallographic data for cobalt complex **136**.

**Table 1:** Crystal data and structure refinement for cobalt complex **136**.

Identification code	rw6rco_m
Empirical formula	C <sub>21</sub> H <sub>20</sub> Cl <sub>2</sub> Co N <sub>2</sub>
Formula weight	430.24
Temperature	296(2) K
Wavelength	0.71073 Å
Crystal system	Monoclinic
Space group	P(2)/n
Unit cell dimensions	a = 8.7818 (5) Å alpha = 90 deg b = 16.0994 (10) Å beta = 91.8600 (10) deg. c = 13.7265 (8) Å gamma = 90 deg.
Volume Z	1939.7 (2) Å <sup>3</sup>
Density (calculated)	1.892 Mg/m <sup>3</sup>
Absorption coefficient	1.193 mm <sup>-1</sup>
F(000)	1148
Theta range for data collection	1.95 to 28.30 deg.
Limiting indices	-9<=h<=11, -21<=k<=19, -17<=l<=17
Reflections collected / unique	11620
Independent reflections	4349 [R (int) = 0.0386] †
Completeness to theta	28.30, 90.1%
Absorption correction	None
Refinement method	Full-matrix least-squares on F <sup>2</sup>
Data / restraints / parameters	4349 / 0 / 315
Goodness-of-fit on F <sup>2</sup>	1.074
Final R indices [I>2sigma (I)]	R1 = 0.0581, wR2 = 0.1477
R indices (all data)	R1 = 0.0992, wR2 = 0.1730
Largest diff. peak and hole	0.315 and -0.302 e.Å <sup>-3</sup>

**Table 2:** Atomic coordinates ( $\times 10^4$ ) and equivalent isotropic displacement parameters ( $\text{Å}^2 \times 10^3$ ) for cobalt complex **136**.<sup>a,b</sup>  $U(\text{eq})$  is defined as one third of the trace of the orthogonalized  $U_{ij}$  tensor.

	x	y	z	$U(\text{eq})$
Co(1)	2209 (1)	1070 (1)	2078 (1)	46 (1)
Cl(1)	2963 (2)	2060 (1)	3119 (1)	83 (1)
N(1)	4200 (3)	583 (2)	1632 (2)	45 (1)
C(1)	5297 (5)	1115 (3)	1380 (3)	52 (1)
Cl(2)	833 (1)	1373 (1)	715 (1)	65 (1)
N(2)	1283 (3)	41 (2)	2754 (2)	37 (1)
C(2)	6622 (5)	850 (4)	963 (3)	57 (1)
C(3)	6815 (5)	19 (3)	796 (3)	59 (1)
C(4)	5724 (5)	-526 (3)	1092 (3)	52 (1)
C(5)	4408 (4)	-238 (2)	1508 (3)	44 (1)
C(6)	3153 (6)	-815 (3)	1780 (4)	54 (1)
C(7)	2420 (5)	-651 (3)	2758 (3)	48 (1)
C(8)	-154 (4)	-212 (3)	2214 (3)	41 (1)
C(9)	-1205 (4)	-794 (2)	2725 (3)	39 (1)
C(10)	-1405 (5)	-1611 (3)	2395 (3)	48 (1)
C(11)	-2489 (5)	-2118 (3)	2793 (4)	58 (1)
C(12)	-3398 (5)	-1820 (3)	3510 (3)	59 (1)
C(13)	-3216 (5)	-1015 (3)	3849 (3)	52 (1)
C(14)	-2131 (4)	-491 (2)	3460 (3)	41 (1)
C(15)	-1936 (4)	377 (2)	3822 (3)	43 (1)
C(16)	-3205 (5)	840 (3)	4070 (3)	56 (1)
C(17)	-3038 (6)	1627 (3)	4470 (3)	62 (1)
C(18)	-1627 (6)	1949 (3)	4620 (4)	64 (1)
C(19)	-349 (6)	1520 (3)	4360 (3)	54 (1)
C(20)	-480 (4)	719 (2)	3960 (3)	43 (1)
C(21)	933 (4)	209 (3)	3800 (3)	42 (1)

<sup>a</sup> For atom labelling see Figure 36.

<sup>b</sup> Estimated standard deviations in parenthesis.

**Table 3:** Bond lengths [Å] and angles [deg] for cobalt complex **136**.

---

Co(1)-N(1)	2.030(3)
Co(1)-N(2)	2.078(3)
Co(1)-Cl(1)	2.2261(14)
Co(1)-Cl(2)	2.2481(12)
N(1)-C(1)	1.342(5)
N(1)-C(5)	1.345(5)
C(1)-C(2)	1.381(6)
N(2)-C(7)	1.496(5)
N(2)-C(8)	1.499(5)
N(2)-C(21)	1.502(5)
C(2)-C(3)	1.370(7)
C(3)-C(4)	1.370(6)
C(4)-C(5)	1.386(5)
C(5)-C(6)	1.499(6)
C(6)-C(7)	1.530(6)
C(8)-C(9)	1.505(5)
C(9)-C(10)	1.400(5)
C(9)-C(14)	1.404(5)
C(10)-C(11)	1.379(6)
C(11)-C(12)	1.374(7)
C(12)-C(13)	1.385(6)
C(13)-C(14)	1.392(5)
C(14)-C(15)	1.491(5)
C(15)-C(16)	1.391(6)
C(15)-C(20)	1.399(5)
C(16)-C(17)	1.387(6)
C(17)-C(18)	1.353(7)
C(18)-C(19)	1.375(7)
C(19)-C(20)	1.404(6)
C(20)-C(21)	1.510(5)
N(1)-Co(1)-N(2)	100.36(12)
N(1)-Co(1)-Cl(1)	103.21(10)
N(2)-Co(1)-Cl(1)	113.38(9)
N(1)-Co(1)-Cl(2)	106.14(9)
N(2)-Co(1)-Cl(2)	109.74(9)
Cl(1)-Co(1)-Cl(2)	121.30(6)
C(1)-N(1)-C(5)	119.5(3)
C(1)-N(1)-Co(1)	117.6(3)
C(5)-N(1)-Co(1)	122.6(3)
N(1)-C(1)-C(2)	122.1(5)
C(7)-N(2)-C(8)	110.5(3)
C(7)-N(2)-C(21)	106.8(3)
C(8)-N(2)-C(21)	109.1(3)
C(7)-N(2)-Co(1)	109.0(2)
C(8)-N(2)-Co(1)	109.3(2)
C(21)-N(2)-Co(1)	112.2(2)
C(3)-C(2)-C(1)	118.7(5)
C(2)-C(3)-C(4)	119.0(4)
C(3)-C(4)-C(5)	120.5(4)
N(1)-C(5)-C(4)	119.9(4)
N(1)-C(5)-C(6)	118.3(3)

C(4)-C(5)-C(6)	121.6(4)
C(5)-C(6)-C(7)	116.4(4)
N(2)-C(7)-C(6)	115.1(3)
N(2)-C(8)-C(9)	117.2(3)
C(10)-C(9)-C(14)	119.3(4)
C(10)-C(9)-C(8)	120.5(3)
C(14)-C(9)-C(8)	119.8(3)
C(11)-C(10)-C(9)	120.6(4)
C(12)-C(11)-C(10)	120.1(4)
C(11)-C(12)-C(13)	120.3(4)
C(12)-C(13)-C(14)	120.7(4)
C(13)-C(14)-C(9)	119.0(4)
C(13)-C(14)-C(15)	120.8(3)
C(9)-C(14)-C(15)	120.2(3)
C(16)-C(15)-C(20)	119.5(4)
C(16)-C(15)-C(14)	119.9(4)
C(20)-C(15)-C(14)	120.5(3)
C(17)-C(16)-C(15)	120.7(5)
C(18)-C(17)-C(16)	119.7(5)
C(17)-C(18)-C(19)	121.3(5)
C(18)-C(19)-C(20)	120.4(4)
C(15)-C(20)-C(19)	118.5(4)
C(15)-C(20)-C(21)	121.2(3)
C(19)-C(20)-C(21)	119.9(4)
N(2)-C(21)-C(20)	115.6(3)

---

**Table 4:** Anisotropic displacement parameters ( $\text{Å}^2 \times 10^3$ ) for cobalt complex **136**. The anisotropic displacement factor exponent takes the form:  $-2\pi^2 [h^2 a^{*2} U_{11} + \dots + 2 h k a^* b^* U_{12}]$

	U11	U22	U33	U23	U13	U12
Co(1)	40(1)	34(1)	64(1)	6(1)	15(1)	3(1)
Cl(1)	76(1)	53(1)	122(1)	-30(1)	39(1)	-20(1)
N(1)	36(2)	44(2)	54(2)	-4(2)	7(1)	0(1)
C(1)	42(2)	59(3)	56(3)	-5(2)	4(2)	-7(2)
Cl(2)	56(1)	66(1)	74(1)	30(1)	16(1)	18(1)
N(2)	35(2)	36(2)	39(2)	4(1)	3(1)	1(1)
C(2)	37(2)	84(4)	50(3)	-5(2)	3(2)	-8(2)
C(3)	37(2)	89(4)	50(2)	-8(2)	1(2)	12(2)
C(4)	48(2)	60(3)	47(2)	-4(2)	-6(2)	19(2)
C(5)	42(2)	45(2)	45(2)	-2(2)	0(2)	10(2)
C(6)	56(3)	38(2)	69(3)	-6(2)	14(2)	9(2)
C(7)	50(2)	40(2)	53(2)	14(2)	6(2)	6(2)
C(8)	40(2)	46(2)	36(2)	0(2)	-1(2)	1(2)
C(9)	39(2)	42(2)	36(2)	5(2)	-3(2)	-4(2)
C(10)	52(2)	45(2)	48(2)	-1(2)	-3(2)	-1(2)
C(11)	65(3)	40(2)	69(3)	2(2)	-7(2)	-10(2)
C(12)	58(3)	55(3)	65(3)	12(2)	6(2)	-19(2)
C(13)	52(2)	58(3)	48(2)	4(2)	10(2)	-7(2)
C(14)	42(2)	44(2)	36(2)	7(2)	4(2)	-5(2)
C(15)	47(2)	45(2)	38(2)	5(2)	5(2)	-5(2)
C(16)	50(3)	65(3)	54(3)	-2(2)	11(2)	1(2)
C(17)	75(3)	57(3)	55(3)	-4(2)	22(2)	11(3)
C(18)	91(4)	44(3)	59(3)	-6(2)	21(3)	-4(3)
C(19)	70(3)	49(2)	44(2)	-3(2)	8(2)	-13(2)
C(20)	53(2)	46(2)	30(2)	2(2)	7(2)	-3(2)
C(21)	45(2)	43(2)	39(2)	7(2)	-2(2)	-9(2)

**Table 5:** Hydrogen coordinates ( $\times 10^4$ ) and isotropic displacement parameters ( $\text{Å}^2 \times 10^3$ ) for cobalt complex **136**.

	x	y	z	U (eq)
H(1)	5160 (50)	1690 (30)	1470 (30)	63 (13)
H(2)	7310 (60)	1220 (30)	850 (40)	79 (17)
H(3)	7650 (60)	-220 (30)	480 (40)	76 (15)
H(4)	5830 (50)	-1100 (30)	1030 (30)	60 (13)
H(6B)	2310 (50)	-790 (20)	1240 (30)	50 (11)
H(6A)	3510 (60)	-1270 (30)	1780 (30)	73 (16)
H(7B)	2000 (50)	-1150 (30)	3050 (30)	48 (11)
H(7A)	3160 (50)	-490 (30)	3210 (30)	48 (11)
H(8B)	-720 (40)	230 (20)	2100 (30)	37 (10)
H(8A)	130 (40)	-470 (20)	1530 (30)	40 (9)
H(10)	-860 (50)	-1790 (30)	1900 (30)	51 (12)
H(11)	-2600 (50)	-2640 (30)	2520 (30)	57 (12)
H(12)	-4140 (60)	-2150 (30)	3780 (40)	87 (17)
H(13)	-3790 (50)	-790 (30)	4390 (30)	56 (12)
H(16)	-4190 (50)	650 (30)	3920 (30)	49 (11)
H(17)	-3800 (50)	1910 (30)	4640 (30)	53 (12)
H(18)	-1480 (60)	2420 (40)	4850 (40)	82 (17)
H(19)	750 (50)	1720 (30)	4480 (30)	54 (12)
H(21B)	830 (30)	-320 (20)	4090 (20)	22 (8)
H(21A)	1820 (40)	480 (20)	4080 (30)	41 (10)

Crystallographic data for nickel complex **143**.

**Table 1:** Crystal data and structure refinement for nickel complex **143**.

Identification code	newfin
Empirical formula	$C_{21} H_{20} Cl_2 Co N_2$
Formula weight	430.00
Temperature	296(2) K
Wavelength	0.71073 Å
Crystal system	Monoclinic
Space group	$P(2)/n$
Unit cell dimensions	$a = 8.7689 (5) \text{ \AA}$ $\alpha = 90 \text{ deg}$ $b = 15.8377 (10) \text{ \AA}$ $\beta = 91.8760$ $(10) \text{ deg.}$ $c = 13.7979 (8) \text{ \AA}$ $\gamma = 90 \text{ deg.}$
Volume Z	$1915.2 (2) \text{ \AA}^3$
Density (calculated)	$1.491 \text{ Mg/m}^3$
Absorption coefficient	$1.299 \text{ mm}^{-1}$
F(000)	888
Crystal size	$0.20 \times 0.20 \times 0.10 \text{ mm}$
Theta range for data collection	$1.96 \text{ to } 28.28 \text{ deg.}$
Limiting indices	$-11 \leq h \leq 10, -20 \leq k \leq 20, -17 \leq l \leq 16$
Reflections collected / unique	11748
Independent reflections	4317 [R (int) = 0.0328]
Refinement method	Full-matrix least-squares on $F^2$
Data / restraints / parameters	4317 / 0 / 315
Goodness-of-fit on $F^2$	1.087
Final R indices [ $I > 2\sigma(I)$ ]	$R1 = 0.0494, wR2 = 0.0979$
R indices (all data)	$R1 = 0.0714, wR2 = 0.1072$
Largest diff. peak and hole	0.367 and $-0.339 \text{ e.\AA}^{-3}$

**Table 2:** Atomic coordinates ( $\times 10^4$ ) and equivalent isotropic displacement parameters ( $\text{Å}^2 \times 10^3$ ) for nickel complex **143**.<sup>a, b</sup>  $U(\text{eq})$  is defined as one third of the trace of the orthogonalized  $U_{ij}$  tensor.

	x	y	z	$U(\text{eq})$
Ni (1)	2197 (1)	1086 (1)	2108 (1)	41 (1)
Cl (1)	3094 (1)	1985 (1)	3225 (1)	68 (1)
N (1)	4142 (3)	589 (2)	1657 (2)	39 (1)
C (1)	5243 (4)	1134 (2)	1417 (3)	46 (1)
Cl (2)	861 (1)	1315 (1)	718 (1)	56 (1)
C (2)	6558 (4)	879 (3)	991 (3)	51 (1)
N (2)	1270 (3)	46 (2)	2744 (2)	33 (1)
C (3)	6770 (4)	38 (3)	816 (2)	50 (1)
C (4)	5679 (4)	-526 (2)	1082 (2)	46 (1)
C (5)	4344 (4)	-239 (2)	1499 (2)	40 (1)
C (6)	3092 (4)	-831 (2)	1754 (3)	48 (1)
C (7)	2390 (4)	-671 (2)	2734 (2)	42 (1)
C (8)	-192 (3)	-185 (2)	2207 (2)	35 (1)
C (9)	-1226 (3)	-791 (2)	2711 (2)	34 (1)
C (10)	-1432 (4)	-1611 (2)	2366 (2)	42 (1)
C (11)	-2527 (4)	-2130 (2)	2755 (3)	51 (1)
C (12)	-3421 (4)	-1840 (2)	3487 (3)	53 (1)
C (13)	-3223 (4)	-1030 (2)	3839 (3)	47 (1)
C (14)	-2125 (3)	-493 (2)	3459 (2)	36 (1)
C (15)	-1930 (3)	380 (2)	3839 (2)	37 (1)
C (16)	-3192 (4)	858 (2)	4095 (3)	48 (1)
C (17)	-3015 (5)	1644 (2)	4514 (3)	55 (1)
C (18)	-1582 (5)	1973 (2)	4668 (3)	55 (1)
C (19)	-317 (4)	1528 (2)	4391 (2)	47 (1)
C (20)	-465 (4)	728 (2)	3968 (2)	38 (1)
C (21)	932 (4)	202 (2)	3792 (2)	37 (1)

<sup>a</sup> For atom labelling see Figure 46.

<sup>b</sup> Estimated standard deviations in parenthesis.

**Table 3:** Bond lengths [Å] and angles [deg] for nickel complex **143**.

---

Ni(1)-N(1)	1.997(2)
Ni(1)-N(2)	2.047(2)
Ni(1)-Cl(1)	2.2229(11)
Ni(1)-Cl(2)	2.2447(10)
N(1)-C(5)	1.342(4)
N(1)-C(1)	1.344(4)
C(1)-C(2)	1.372(5)
C(2)-C(3)	1.368(5)
N(2)-C(7)	1.501(4)
N(2)-C(8)	1.505(4)
N(2)-C(21)	1.506(4)
C(3)-C(4)	1.368(5)
C(4)-C(5)	1.397(4)
C(5)-C(6)	1.495(5)
C(6)-C(7)	1.525(5)
C(8)-C(9)	1.506(4)
C(9)-C(10)	1.393(4)
C(9)-C(14)	1.401(4)
C(10)-C(11)	1.386(5)
C(11)-C(12)	1.377(5)
C(12)-C(13)	1.381(5)
C(13)-C(14)	1.399(4)
C(14)-C(15)	1.487(4)
C(15)-C(16)	1.395(4)
C(15)-C(20)	1.403(4)
C(16)-C(17)	1.380(5)
C(17)-C(18)	1.370(6)
C(18)-C(19)	1.379(5)
C(19)-C(20)	1.400(5)
C(20)-C(21)	1.508(4)
N(1)-Ni(1)-N(2)	99.87(10)
N(1)-Ni(1)-Cl(1)	100.49(8)
N(2)-Ni(1)-Cl(1)	110.81(7)
N(1)-Ni(1)-Cl(2)	102.97(8)
N(2)-Ni(1)-Cl(2)	107.03(7)
Cl(1)-Ni(1)-Cl(2)	130.68(4)
C(5)-N(1)-C(1)	119.2(3)
C(5)-N(1)-Ni(1)	123.7(2)
C(1)-N(1)-Ni(1)	116.8(2)
N(1)-C(1)-C(2)	122.5(3)
C(3)-C(2)-C(1)	118.9(4)
C(7)-N(2)-C(8)	111.1(2)
C(7)-N(2)-C(21)	106.4(2)
C(8)-N(2)-C(21)	108.8(2)
C(7)-N(2)-Ni(1)	109.6(2)
C(8)-N(2)-Ni(1)	109.2(2)
C(21)-N(2)-Ni(1)	111.8(2)
C(4)-C(3)-C(2)	119.2(3)
C(3)-C(4)-C(5)	120.0(3)
N(1)-C(5)-C(4)	120.1(3)
N(1)-C(5)-C(6)	118.3(3)

C(4)-C(5)-C(6)	121.6(3)
C(5)-C(6)-C(7)	115.1(3)
N(2)-C(7)-C(6)	114.6(3)
N(2)-C(8)-C(9)	116.3(2)
C(10)-C(9)-C(14)	119.7(3)
C(10)-C(9)-C(8)	120.6(3)
C(14)-C(9)-C(8)	119.2(3)
C(11)-C(10)-C(9)	120.3(3)
C(12)-C(11)-C(10)	120.3(3)
C(11)-C(12)-C(13)	120.0(3)
C(12)-C(13)-C(14)	120.9(3)
C(13)-C(14)-C(9)	118.8(3)
C(13)-C(14)-C(15)	120.4(3)
C(9)-C(14)-C(15)	120.8(3)
C(16)-C(15)-C(20)	119.0(3)
C(16)-C(15)-C(14)	120.7(3)
C(20)-C(15)-C(14)	120.2(3)
C(17)-C(16)-C(15)	121.1(4)
C(18)-C(17)-C(16)	119.9(4)
C(17)-C(18)-C(19)	120.3(4)
C(18)-C(19)-C(20)	120.9(3)
C(19)-C(20)-C(15)	118.7(3)
C(19)-C(20)-C(21)	120.2(3)
C(15)-C(20)-C(21)	120.6(3)
N(2)-C(21)-C(20)	115.6(2)

---

**Table 4:** Anisotropic displacement parameters ( $\text{Å}^2 \times 10^3$ ) for nickel complex **143**. The anisotropic displacement factor exponent takes the form:  $-2 \pi^2 [h^2 a^{*2} U_{11} + \dots + 2 h k a^* b^* U_{12}]$

	U11	U22	U33	U23	U13	U12
Ni (1)	36 (1)	31 (1)	56 (1)	4 (1)	13 (1)	3 (1)
Cl (1)	62 (1)	50 (1)	92 (1)	-23 (1)	25 (1)	-16 (1)
N (1)	32 (1)	38 (1)	47 (2)	-2 (1)	7 (1)	0 (1)
C (1)	36 (2)	46 (2)	55 (2)	-7 (2)	4 (1)	-2 (2)
Cl (2)	51 (1)	55 (1)	62 (1)	22 (1)	14 (1)	12 (1)
C (2)	34 (2)	72 (3)	47 (2)	-4 (2)	6 (2)	-8 (2)
N (2)	32 (1)	35 (1)	33 (1)	3 (1)	2 (1)	0 (1)
C (3)	30 (2)	82 (3)	38 (2)	-8 (2)	-1 (1)	11 (2)
C (4)	43 (2)	52 (2)	42 (2)	-8 (2)	-5 (1)	16 (2)
C (5)	37 (2)	44 (2)	39 (2)	-2 (1)	2 (1)	9 (1)
C (6)	51 (2)	34 (2)	61 (2)	-2 (2)	12 (2)	5 (2)
C (7)	42 (2)	36 (2)	47 (2)	10 (1)	5 (2)	4 (1)
C (8)	37 (2)	39 (2)	29 (2)	2 (1)	2 (1)	-3 (1)
C (9)	33 (2)	36 (2)	32 (2)	4 (1)	-2 (1)	-2 (1)
C (10)	42 (2)	38 (2)	44 (2)	0 (1)	1 (1)	1 (1)
C (11)	58 (2)	32 (2)	62 (2)	2 (2)	-7 (2)	-8 (2)
C (12)	51 (2)	50 (2)	60 (2)	11 (2)	9 (2)	-14 (2)
C (13)	45 (2)	52 (2)	45 (2)	3 (2)	10 (2)	-8 (2)
C (14)	35 (2)	40 (2)	34 (2)	5 (1)	2 (1)	-2 (1)
C (15)	43 (2)	41 (2)	29 (2)	5 (1)	5 (1)	-1 (1)
C (16)	45 (2)	50 (2)	48 (2)	2 (2)	10 (2)	1 (2)
C (17)	67 (3)	46 (2)	53 (2)	-3 (2)	18 (2)	10 (2)
C (18)	80 (3)	39 (2)	45 (2)	-3 (2)	17 (2)	-1 (2)
C (19)	58 (2)	45 (2)	37 (2)	0 (1)	5 (2)	-10 (2)
C (20)	49 (2)	40 (2)	25 (2)	5 (1)	6 (1)	-2 (1)
C (21)	38 (2)	42 (2)	32 (2)	4 (1)	-1 (1)	-6 (1)

**Table 5:** Hydrogen coordinates ( $\times 10^4$ ) and isotropic displacement parameters ( $\text{Å}^2 \times 10^3$ ) for nickel complex **143**.

	x	y	z	U(eq)
H(1)	5067(34)	1716(21)	1556(22)	38(8)
H(2)	7228(40)	1250(22)	840(24)	46(10)
H(3)	7615(48)	-155(25)	492(29)	72(12)
H(4)	5757(38)	-1088(21)	961(24)	46(10)
H(6B)	2299(41)	-781(21)	1220(26)	49(10)
H(6A)	3475(41)	-1345(25)	1782(26)	57(11)
H(7A)	1880(38)	-1144(21)	2941(24)	43(9)
H(7A)	3203(39)	-542(22)	3250(25)	49(9)
H(8B)	92(31)	-405(18)	1625(22)	29(7)
H(8A)	-734(35)	327(20)	2108(21)	36(8)
H(10)	-834(36)	-1791(20)	1828(24)	43(9)
H(11)	-2682(38)	-2642(22)	2524(25)	47(9)
H(12)	-4129(41)	-2184(23)	3753(27)	58(11)
H(13)	-3802(41)	-847(21)	4340(26)	52(10)
H(16)	-4145(42)	616(23)	3961(25)	54(10)
H(17)	-3742(48)	1943(26)	4670(30)	71(13)
H(18)	-1465(43)	2458(26)	4976(27)	62(11)
H(19)	639(42)	1756(24)	4493(27)	60(11)
H(21A)	1849(36)	465(20)	4107(22)	41(8)
H(21B)	859(34)	-362(20)	4102(22)	38(8)